ÉCOLE POLYTECHNIQUE DE BRUXELLES
UNIVERSITÉ LIBRE DE BRUXELLES

Witnessing optical nonclassicality and quantum entanglement using multicopy observables

Thèse présentée par Célia GRIFFET
en vue de l'obtention du grade académique de docteure en sciences de l'ingénieur et technologie
Année académique 2022-2023

Sous la direction du Professeur Nicolas CERF, promoteur
Centre for Quantum Information and Communication

Jury de thèse :

Jean-Marc SPARENBERG (Université libre de Bruxelles, Président du jury)
Jérémie ROLAND (Université libre de Bruxelles, Secrétaire du jury)
Stephan DE BIEVRE (Université de Lille, France)
Natalia KOROLKOVA (University of St. Andrews, United Kingdom)
Nicolas CERF (Université libre de Bruxelles)

FREEDOM TO RESEARCH

Célia Griffet
Université libre de Bruxelles
Ecole polytechnique de Bruxelles
50 av. F.D. Roosevelt - CP165/59
1050 Bruxelles
Belgique
Email: celia.griffet@ulb.be

Jury:

Jean-Marc Sparenberg, Président du jury, ULB

Jérémie Roland, Secrétaire du jury, ULB

Stephan De Bièvre, Université de Lille, France

Natalia Korolkova, University of St. Andrews, United Kingdom

Nicolas Cerf, Promoteur, ULB

A papa, à maman,

à Kenzo.

Remerciements - Acknowledgments

Je tiens particulièrement à remercier toutes les personnes qui m'ont soutenue et aidée à la réalisation de cette thèse.

Tout d'abord, merci à Nicolas d'avoir accepté de superviser mon mémoire puis ma thèse et de m'avoir aidée à obtenir un financement. Merci également pour les nombreux échanges scientifiques qui m'ont aidée à progresser dans le domaine ainsi que pour les conférences que tu m'as recommandées.

Merci à Matthieu avec qui j'ai pu découvrir le monde de la recherche et écrire mon premier article. Je n'oublierai pas ma première conférence que tu m'as convaincue de faire et nos vacances en Corse, ainsi que tes passions sur l'archéologie et le whisky. Merci aussi pour tes commentaires précieux sur ma thèse.

Merci à Stephan pour la collaboration et l'invitation à passer quelques jours à Lille pour finaliser notre article.

Je souhaite également remercier Michel Kinnaert et Jérémie pour m'avoir fait confiance afin de donner les séances d'exercices de leur cours. Merci également Jérémie pour ton soutien lors des problèmes informatiques dans le service.

Serge, j'ai d'abord commencé par superviser ton mémoire avant que tu ne commences ta thèse. Je te remercie pour le soutien que tu m'as apporté surtout lors de mes dernières semaines de thèse. Bonne continuation pour ta propre thèse; je suis sure qu'elle se déroulera bien! Enfin, merci pour la relecture de ma thèse.

Thanks Tobi. I really enjoyed working with you on our project. You are a great colleague both scientifically and humanly! Thank you very much for the help during the last weeks of my thesis. Your advices about my manuscript have been really useful.

Atul, merci pour tous les moments partagés, j'ai vraiment apprécié nos nombreuses discussions sur ton apprentissage du Français.

Enea et Timothée, nous avons fait nos études ensemble avant de commencer une thèse au QuIC. Merci d'être toujours là pour discuter.

Merci à Léo de m'avoir accompagnée à ma dernière conférence et d'y avoir mis une bonne ambiance!

Merci à Arne pour la bonne ambiance dans le service depuis ton arrivée. Je me souviendrai longtemps de tes problèmes mathématiques et ton apprentissage des capitales du monde!

Zacharie, Antoine et Marco, nous avons partagé le même bureau. Merci pour la bonne ambiance dans le bureau grâce à vous trois.

Thanks to everyone else at QuIC: Leonardo, Benoît, Ognyan, Hamed, Joseph, Lin-Qing, Julian, Ravi, Shantanav, Chrysoula, Esteban, Raul, Uttam, Siddhartha, Luc, Simon, Nicola. Working at QuIC would not be the same without the people working in it!

Bien entendu, je ne peux pas terminer ces remerciements sans remercier Pascale pour son aide administrative précieuse ainsi que les bons moments passés à discuter.

Enfin, je souhaite remercier Kenzo, mes parents ainsi que tous mes proches, amis et famille, m'ayant soutenue durant ces quatre années de thèse.

Thank you to all the jury members for reading and reviewing this thesis.

Merci au FNRS d'avoir financé ma recherche pendant ces quatre dernières années.

Abstract

The so-called nonclassicality of a single-mode state of light and the entanglement of bipartite photonic states are central quantum phenomena which underlie two of the most essential differences between the classical and the quantum. Since their discovery, these properties have attracted a tremendous, constant interest from the quantum physics community, with the goal of developing protocols that take advantage of them and have no classical counterpart. To take a single example, the entanglement of two photons can be used as a resource to perform quantum cryptography in a device-independent manner, that is, to distribute a secret key in a secure way between two parties who do not even need to trust their quantum devices. In order to exploit these properties and develop optical sources of nonclassical or entangled states, it is crucial to be able to detect whether the state emitted by the source is effectively nonclassical or entangled. Along this way, numerous witnesses (sufficient conditions) for nonclassicality or entanglement have been conceived over the years.

In this thesis, we are especially interested in a hierarchy of criteria that has been developed by Shchukin, Richter, and Vogel in the early 2000s. The most common witness of entanglement is the PPT criterion for "*positive partial transpose*", which states that any separable state must remain physical after undergoing a partial transpose. If this condition is not met, it means that the state is entangled. Based on this, a complete set of criteria was expressed by these authors based on a matrix of moments of the mode (creation and annihilation) operators. Similarly, a set of criteria was built based on a matrix of normally-ordered moments in order to express the non-negativity of the Glauber-Sudarshan P-function, giving rise to a hierarchy of nonclassicality witnesses.

The main difficulty in the practical detection of nonclassicality or entanglement is the measurement of the quantities that are needed to apply these criteria. As a matter of fact, it is often mandatory to resort first to complete quantum state tomography, *i.e.*, reconstructing the density matrix in its entirety, which is a very costly procedure as it requires performing a huge amount of measurements. The various witnesses for nonclassicality or entanglement due to Shchukin, Richter, and Vogel may avoid full tomography but require inefficient sequential measurements for all entries of the matrices. Overcoming this lack of simple practical implementation is the main motivation of this thesis.

For this purpose, we develop a multicopy method inspired from an early work by Brun, in which several identical and independent copies (replicas) of the optical state of interest are processed in a linear interferometer, followed by a bunch of photodetectors with photon-number resolution. First, we apply this method to the above nonclassicality hierarchy. We select some of the most interesting low-order criteria within this hierarchy and analyze their detection capability on test cases, such as squeezed states, Fock states, and Schrödinger cat states. We devise several two- or three-copy optical schemes implementing these criteria and show that the detection power generally scales with the number of copies. It also appears that adding an extra copy sometimes enables making the criterion invariant under displacements in phase space. Further, we highlight an especially efficient four-copy criterion which, if realized, would enable the detection of the nonclassicality of all of the above example states (including displaced states).

Second, we turn to an alternative quantity that has recently been put forward to witness optical nonclassicality, namely the quadrature coherence scale. This quantity measures the scale over which the (x, p) quadrature components of the optical field lose their coherence, indicating nonclassicality as soon as it exceeds some threshold. We design a multicopy measurement scheme of this quantity, which circumvents the need for full state tomography. We prove that its implementation only requires a balanced beam splitter acting on two replicas of the state, followed by photon number measurements and classical postprocessing. Moreover, we generate synthetic data and prove that the shape of the photon number distribution at the output of the interferometer gives us information on the value of the witness and thus on the degree of nonclassicality of the state under scrutiny.

Third, we address the above hierarchy of entanglement witnesses and develop multicopy procedures to measure three selected such witnesses. These procedures consist in using local interferometers on both sides of the bipartite state, followed again by photon number measurements and classical postprocessing. The derivation relies on the Jordan-Schwinger representation of spin observables in terms of multimode operators. We show that these witnesses detect the entanglement of all entangled Gaussian states, and, for the considered 4th-order witnesses, also the entangled Schrödinger cat states and some N00N states. We further analyze the influence of some of the dominant practical imperfections that could hinder these multicopy measurement schemes, namely, imperfect copies (resulting from source fluctuations) and optical losses in the circuit.

As a fourth contribution of this thesis, we devise a new separability criterion for bipartite continuous-variable states that is inspired from the multicopy spin observables associated with the PPT criterion. We compare this criterion to the most common criteria and show that it implies Mancini *et al.*'s criterion, which in turn implies Duan *et al.*'s criterion. It is therefore a necessary and sufficient condition for the entanglement detection of Gaussian entangled states, and hence a strong entanglement witness for arbitrary states based on second-order moments (not even requiring any optimization procedure). Overall, this thesis emphasizes the wide range of applicability of the multicopy technique in quantum optics and continuous-variable quantum information.

Titre

Détection de la non-classicalité optique et de l'intrication quantique à l'aide d'observables multi-copie.

Résumé

La non-classicalité d'un état monomode de la lumière et l'intrication d'états photoniques bipartites sont des phénomènes quantiques centraux composant deux des différences les plus essentielles entre les domaines classique et quantique. Depuis leur découverte, ces propriétés ont suscité un intérêt considérable et constant de la part de la communauté des physiciens, dans le but de développer des protocoles basés sur ces phénomènes et qui n'ont pas d'équivalent classique. Pour prendre un seul exemple, l'intrication de deux photons peut être utilisée comme ressource pour effectuer de la cryptographie quantique, c'est-à-dire pour distribuer une clé secrète de manière sécurisée entre deux parties qui n'ont même pas besoin de faire confiance à leurs dispositifs quantiques. Afin d'exploiter ces propriétés et de développer des sources optiques d'états non-classiques ou intriqués, il est crucial de pouvoir détecter si l'état émis par la source est effectivement non-classique ou intriqué. Dans cette optique, de nombreux témoins (conditions suffisantes) de non-classicalité ou d'intrication ont été conçus au fil des années.

Dans cette thèse, nous nous intéressons particulièrement à une hiérarchie de critères qui a été développée par Shchukin, Richter et Vogel au début des années 2000. Le témoin le plus courant de l'intrication est le critère PPT de "textitpositive partial transpose", qui stipule que tout état séparable doit rester physique après avoir subi une transposition partielle. Si cette condition n'est pas remplie, cela signifie que l'état est intriqué. Sur cette base, un ensemble complet de critères a été exprimé par ces auteurs à partir d'une matrice de moments des opérateurs de mode (création et annihilation). De même, un ensemble de critères a été construit sur la base d'une matrice de moments dans l'ordre normal afin d'exprimer la non-négativité de la fonction P de Glauber, donnant lieu à une hiérarchie de témoins de non-classicalité.

La principale difficulté dans la détection pratique de la non-classicalité ou de l'intrication est la mesure des quantités nécessaires à l'application de ces critères. En effet, il est souvent nécessaire de recourir d'abord à une tomographie complète de l'état quantique, c'est-à-dire de reconstruire la matrice densité dans son intégralité, ce qui est une procédure très coûteuse car elle nécessite d'effectuer un très grand nombre de mesures. Les divers témoins de non-classicalité ou d'intrication de Shchukin, Richter et Vogel peuvent éviter la tomographie complète mais nécessitent des mesures séquentielles inefficaces pour toutes les entrées des matrices. La principale motivation de cette thèse est donc de remédier à ce manque de mise en oeuvre pratique simple.

À cette fin, nous développons une méthode multi-copie inspirée d'un travail de Brun, dans laquelle plusieurs copies identiques et indépendantes (répliques) de l'état optique sont traitées dans un interféromètre linéaire, suivi d'un ensemble de photodétecteurs résolvant le nombre de photons. Nous appliquons tout d'abord cette méthode à la hiérarchie de non-classicalité susmentionnée. Nous sélectionnons certains des critères d'ordre inférieur les plus intéressants au sein de cette hiérarchie et analysons leur capacité de détection sur des cas tests, tels que les états comprimés, les états de Fock et les états-chat de Schrödinger. Nous concevons plusieurs schémas optiques à deux ou trois copies mettant en oeuvre ces critères et montrons que le pouvoir de détection s'échelonne généralement avec le nombre de copies. Il apparaît également que l'ajout d'une copie supplémentaire permet parfois de rendre le critère invariant en cas de déplacements dans l'espace des phases. En outre, nous mettons en évidence un critère à quatre copies particulièrement efficace qui, s'il était implémenté, permettrait la détection de la non-classicalité de tous les états cités en exemple ci-dessus (y compris les états déplacés).

Ensuite, nous nous intéressons à une autre quantité qui a été récemment mise en avant pour témoigner de la non-classicalité optique, à savoir la "quadrature coherence scale". Cette quantité mesure la distance sur laquelle les composantes en quadrature (x, p) du champ optique perdent leur cohérence, indiquant la non-classicalité dès qu'elle dépasse un certain seuil. Nous concevons un schéma de mesure multi-copie de cette quantité, qui contourne le besoin d'une tomographie d'état complète. Nous prouvons que son implémentation ne nécessite qu'un diviseur de faisceau équilibré agissant sur deux répliques de l'état, suivi de mesures du nombre de photons et d'un post-traitement classique. En outre, nous générons des données synthétiques et prouvons que la forme de la distribution du nombre de photons à la sortie de l'interféromètre nous renseigne sur la valeur du témoin et donc sur le degré de non-classicalité de l'état examiné.

Troisièmement, nous abordons la hiérarchie susmentionnée des témoins d'intrication et développons des procédures multi-copie pour mesurer trois témoins particuliers. Ces procédures consistent à utiliser des interféromètres locaux des deux côtés de l'état bipartite, suivis à nouveau par des mesures du nombre de photons et un post-traitement classique. La dérivation repose sur la représentation de Jordan-Schwinger des observables de spin en termes d'opérateurs multimodes. Nous montrons que ces témoins détectent l'intrication de tous les états gaussiens intriqués et, pour les témoins d'ordre 4 considérés, également les états-chat intriqués de Schrödinger et certains états N00N. Nous analysons en outre l'influence de certaines imperfections pratiques importantes qui pourraient entraver ces schémas de mesure multi-copie, à savoir les copies imparfaites (résultant des fluctuations de la source) et les pertes optiques dans le circuit.

Comme quatrième contribution de cette thèse, nous concevons un nouveau critère de séparabilité pour les états bipartites qui s'inspire des observables de spin multi-copie associées au critère PPT. Nous comparons ce critère aux critères les plus courants et montrons qu'il implique le critère de Mancini *et al.*, qui à son tour implique le critère de Duan *et al.*. Il s'agit donc d'une condition nécessaire et suffisante pour la détection d'intrication d'états intriqués gaussiens, et par conséquence d'un témoin d'intrication fort pour des états arbitraires basés sur des moments du second ordre (ne nécessitant même pas de procédure d'optimisation). Dans l'ensemble, cette thèse souligne le large éventail d'applications de la technique multi-copie en optique quantique et en information quantique à variation continue.

List of publications

The present thesis is based on the following publications

Published in peer-reviewed scientific journals

- [6] M. Arnhem, C. Griffet, and N. J. Cerf. Multicopy observables for the detection of optically nonclassical states. *Physical Review A*, 106: 043705, October 2022.

  This article is the subject of Chapter 6.

- [50] C. Griffet, M. Arnhem, S. De Bièvre, and N. J. Cerf. Interferometric measurement of the quadrature coherence scale using two replicas of a quantum optical state. *Physical Review A*, 108: 023730, August 2023.

  This article is the subject of Chapter 7.

- [51] C. Griffet, T. Haas, and N. J. Cerf. Accessing continuous-variable entanglement witnesses with multimode spin observables. *Physical Review A*, 108: 022421, August 2023.

  This article is the subject of Chapter 8.

In preparation

- C. Griffet, T. Haas, and N. J. Cerf. Multicopy entanglement witness for the EPR-covariance matrix. In preparation.

  This article is the subject of Chapter 9.

Publication not related to the present thesis

- [31] S. Deside, M. Arnhem, C. Griffet, and N. J. Cerf. Probabilistic pure state conversion on the majorization lattice. arXiv:2303.10086 [quant-ph]. Submitted to *Physical Review X Quantum*, March 2023.

Contents

List of Figures

List of Tables

Chapter 1

Introduction

Since its inception at the beginning of the twentieth century, quantum theory has attracted an endless curiosity from scientists due to the plethora of new paths that it opens. As is well known, the two phenomena that originated the advent of quantum mechanics are the black-body radiation [120] and the photoelectric effect [35]. Both discoveries hinted to the fact that there exist quanta of energy and thus that all classical theories, implying continuous energy spectra, cannot describe all phenomena at the microscopic scale.

After these two key discoveries, much effort has been devoted, among other things, to unveiling the divergence between the classical and quantum theories. Today, a large number of characteristics have been found to be specific to quantum theory, but the uncertainty principle is probably the most famous one, which is known even to the laymen. This principle was first discovered by Heisenberg [59] before being mathematically formalized by Kennard [80]. In classical physics, one may define exactly the position and momentum of a particle. Instead, in quantum mechanics, uncertainty relations indicate that it is impossible to define simultaneously the position and momentum of a particle with arbitrary precision. The uncertainty principle has far reaching consequences, especially in the rapidly evolving field of quantum information. For example, it provides the ability to perform quantum cryptography [13], which is an important field of research today.

Apart from the uncertainty principle, there are numerous manifestations of what is colloquially called the nonclassicality of a quantum state. In this thesis, we focus on the states of the electromagnetic field of light, which can be described in general as states of a bosonic field or harmonic oscillator in a (countably) infinite-dimensional Hilbert space. In the literature, there exist several definitions for nonclassicality based on the different quasi-probability distributions that can be used to describe the state of light in phase space. We have chosen to focus on what is often called "optical nonclassicality" and has long been advocated by Glauber as a sensible definition of the departure from classical optics. Accordingly, a state of light is said to be nonclassical if its P-function [46, 47, 149] is not a classical probability distribution, *i.e.*, if it is not a non-negative function [151]. Hence, the first strategy one could think of for determining whether a state is nonclassical is to measure its P-function. However, this requires full state tomography, that is, one has to measure the whole density matrix of the state, for which some examples can be found in Refs. [153, 115, 99, 28]. Alternatively, one may turn to nonclassicality witnesses that are easier to access, most prominently Mandel's parameter [100] and the squeezing parameter [2]. In this thesis, we have chosen to consider in particular a complete hierarchy of nonclassicality criteria that has been put forward by Shchukin, Richter and Vogel [142, 140], as well as a more recent notion of quadrature coherence scale [30, 75, 62, 61, 63].

Another striking difference between the classical and the quantum is the phenomenon of entanglement that may be observed between two or more systems. The fact that something unexpected can happen for bipartite systems, from a classical point of view, was first uncovered in 1935 by Einstein, Podolsky and Rosen [36]. Later, a mathematical inequality was constructed by Bell [12], allowing ones to decide whether stronger-than-classical correlations can occur in nature or not. Then, this inequality was reformulated such that the experimental observation of this weird feature, namely nonlocality and its fellow entanglement, was done by Aspect *et al.* in 1982 [9] based on the theoretical work of Clauser *et al.* [27]. The Nobel Prize in Physics was awarded in 2022 to Clauser, Zeilinger, and Aspect, underlying the crucial importance of quantum entanglement in today's physics, where it is the central focus of an entire field of research. It is at the heart of communication protocols such as quantum teleportation [14] or quantum cryptography [37], which could not be realized without it. Hence, assessing whether a state is entangled or not, and hence, if it can be used for some protocols, is of central importance. To that end, so-called entanglement witnesses have been developed for discrete-variable systems [127, 119, 71, 21, 113, 22, 70] as well as for continuous variables [34, 98, 45, 143, 3, 141]. However, many of the powerful entanglement witnesses require state tomography once again.

One of the main objectives of this thesis is to develop a new approach for efficiently measuring some of the witnesses cited above: regarding optical nonclassicality, we consider the hierarchy of Shchukin, Richter, and Vogel [142, 140] as well as the quadrature coherence scale [30, 75, 62, 61, 63], while for entanglement, we consider the hierarchy of Shchukin and Vogel [141]. This approach relies on a early paper by Brun [18] showing that any polynomial function of a state can be measured by using a multicopy observable applied on several independent identical copies. This method has already been widely used in other fields [40, 73, 38, 29, 78, 109, 16, 110, 116], but its use in the area of quantum optics is rather limited (it had been used once before this thesis in connection with uncertainty relations [65]).

Part I focuses on the needed background in order to present the results obtained in this thesis. As they all revolve around quantum optics, we provide a brief overview of the basics of this field in Chapter 2. We start from the quantization of the electromagnetic field and its representation with quasiprobability distributions in phase space. Then, we define the set of quantum states as well as unitaries that are needed for our work. In Chapter 3, we introduce the notion of nonclassicality. In particular, we focus on optical nonclassicality, which is based on the Glauber-Sudarshan P quasiprobability distribution, and discuss the most commonly used witnesses, namely the Mandel and the squeezing parameters. Afterwards, we review the hierarchy of criteria discovered by Shchukin, Richter, and Vogel, as well as the quadrature coherence scale, which are central to our work. Chapter 4 is dedicated to the definition of entanglement as well as to entanglement witnesses, which allow ones to detect if a state is entangled. Particular attention is paid to the separability criteria derived by Shchukin and Vogel in 2005. Finally, we present Brun's multicopy method in Chapter 5. We also discuss some applications of this method, especially the one related to uncertainty relations in quantum optics.

Parts II and III report on the main contributions of this thesis. Part II presents the application of the multicopy method for the detection of nonclassicality, while Part III follows the same approach for the detection of entanglement.

Part II comprises two chapters, each one being associated with a different nonclassicality criterion. In Chapter 6, we show that several criteria belonging to the hierarchy of Shchukin, Richter, and Vogel can be implemented practically with the multicopy method. The advantage of this method is that the witness is accessed by performing simple photon-number measurements after the application of a linear interferometer. We show that stronger witnesses can be obtained if the number of copies involved is increased. For example, we prove that it is sometimes possible to obtain a displacement-invariant criterion simply by adding an extra copy. Furthermore, we highlight a criterion that would allow, if realized, to detect the nonclassicality of the four classes of nonclassical states that we consider (even and odd cat states, squeezed states, and Fock states) while being also displacement invariant. Then, in Chapter 7, we analyze the multicopy measurement of the quadrature coherence scale. To do this, we first apply the method to measure the purity of a quantum state (which is necessary as it appears in the expression of the quadrature coherence scale) before extending this technique to the multicopy measurement of the quadrature coherence scale. We also perform numerical simulations in order to illustrate the feasibily of our method.

Part III is also divided into two chapters following two diametrically opposed approaches. The approach of Chapter 8 is similar to the strategy followed in Part II. Namely, we start from an existing separabilty criterion to which we apply the multicopy method to find an efficient implementation. Here, the implemented criteria are those of Shchukin and Vogel for witnessing the entanglement of a bipartite state. We implement three different criteria, each of which is particularly well-suited for the detection of the entanglement of a certain class of entangled states (Gaussian, Schrödinger cat and N00N states). We also study the effect that two practical imperfections might have on the detection of entanglement, namely optical losses and imperfect copies. Then, in Chapter 9, we follow an opposite approach: starting from a multicopy observable presenting the desired symmetries, we derive a new separability criterion that is quadratic in the mode operators. We compare this new criterion to the similar ones described in the literature, and show that our witness is stronger than most of them.

Finally, we summarize all the main results of this thesis in Chapter 10 and discuss some ideas for future directions.

Part I

Basics of quantum optics in phase space

Chapter 2

Quantum optics

Quantum optics is the quantum description of phenomena involving light. In this field, the energy is quantized and the corresponding quanta are called photons. The original work presented in this thesis lies in the area of quantum optics. Hence, in this chapter, we need to make a brief introduction to this subject.

We start this chapter by quantizing the electromagnetic field, which is the basis of quantum optics. Then, we present the quasi-distributions used to describe quantum states in phase space. After doing that, we introduce the different states we will use in this thesis and present unitary operations that can be used in a quantum circuit. We restrict to the elements that will be useful in the rest of the thesis. This chapter is mainly based on Refs. [2, 93, 94, 101, 157, 43, 159, 17].

2.1 Quantization of the electromagnetic field

Maxwell's equations for an electromagnetic field are given by:

$$\begin{aligned} \vec{\nabla} \times \vec{E} &= \frac{-\partial \vec{B}}{\partial t}, \\ \frac{\vec{\nabla} \times \vec{B}}{\mu_0} &= \epsilon_0 \frac{\partial \vec{E}}{\partial t} + \vec{J}, \\ \epsilon_0 \vec{\nabla} \cdot \vec{E} &= \sigma, \\ \vec{\nabla} \cdot \vec{B} &= 0, \end{aligned} \tag{2.1}$$

where $\vec{E}$ is the electric field, $\vec{B}$ the magnetic field, $\vec{J}$ the current density, ϵ_0 the vacuum permittivity, μ_0 the vacuum permeability and σ the charge density. These equations describe classically the evolution of the electromagnetic field. Solving them allows us to write the electromagnetic field under the form

$$\vec{E}(\vec{r}, t) = \sum_{\vec{k}} \sum_{\lambda=1,2} \vec{e}_{\vec{k},\lambda} i\omega_k \left(A_{\vec{k},\lambda} e^{-i\omega_k t + i\vec{k}.\vec{r}} - A^*_{\vec{k},\lambda} e^{i\omega_k t - i\vec{k}.\vec{r}} \right), \tag{2.2}$$

where $\vec{e}_{\vec{k},\lambda}$ is the polarization vector, ω_k is the mode angular frequency and $\vec{k}$ is the wave vector. For the quantization of the electromagnetic field, the complex amplitudes, $A_{\vec{k},\lambda}$ and $A^*_{\vec{k},\lambda}$, are replaced by operators:

$$\begin{aligned} A_{\vec{k},\lambda} &\to \hat{a}_{\vec{k},\lambda}, \\ A^*_{\vec{k},\lambda} &\to \hat{a}^\dagger_{\vec{k},\lambda}, \end{aligned} \tag{2.3}$$

where $\hat{a}_{\vec{k},\lambda}$ and $\hat{a}^\dagger_{\vec{k},\lambda}$ are the annihilation and creation operators, respectively. They follow the bosonic commutation rules:

$$\begin{aligned} [\hat{a}_{\vec{k},\lambda}, \hat{a}^\dagger_{\vec{k}',\lambda'}] &= \delta_{\vec{k},\vec{k}'} \delta_{\lambda,\lambda'}, \\ [\hat{a}_{\vec{k},\lambda}, \hat{a}_{\vec{k}',\lambda'}] &= 0, \\ [\hat{a}^\dagger_{\vec{k},\lambda}, \hat{a}^\dagger_{\vec{k}',\lambda'}] &= 0, \end{aligned} \tag{2.4}$$

where $[.,.]$ is the commutator between two operators defined as:

$$[\hat{A}, \hat{B}] = \hat{A}\hat{B} - \hat{B}\hat{A}. \tag{2.5}$$

Then, the Hamiltonian of the system can be expressed as

$$\hat{H} = \sum_{\vec{k}} \sum_{\lambda=1,2} \hbar\omega_k \left(\hat{a}^\dagger_{\vec{k},\lambda} \hat{a}_{\vec{k},\lambda} + \frac{1}{2} \right), \tag{2.6}$$

where $\hbar$ is the reduced Planck constant. In the rest of the thesis, we will work with natural units: $\hbar = 1$ and $\omega_k = 1$. Then, introducing the number operator $\hat{n}_{\vec{k},\lambda} = \hat{a}^\dagger_{\vec{k},\lambda} \hat{a}_{\vec{k},\lambda}$, we can rewrite the Hamiltonian

$$\hat{H} = \sum_{\vec{k}} \sum_{\lambda=1,2} \left(\hat{n}_{\vec{k},\lambda} + \frac{1}{2} \right), \tag{2.7}$$

where $\hat{n}_{\vec{k},\lambda}$ is the number of photons in the mode $\vec{k}, \lambda$. For simplicity, in what follows, we will often work with only one mode with a fixed polarization such that we can drop the indices $\vec{k}$ and λ, and also drop vector symbols. It is important to mention that, even if we simplify some notations by restricting ourselves to one mode, everything that will be presented later can generally be extended to several modes quite easily.

In the case of one mode, the operator $\hat{n}_{\vec{k},\lambda}$ is reduced to $\hat{n}$ and is called the number operator. Its eigenstates are the Fock states: $\hat{n}|n\rangle = n|n\rangle$, where n is a non-negative integer, that form an orthonormal basis of the Hilbert space, *i.e.* it can be used to express any state (pure or mixed). Any quantum state can be described by a density operator which is a bounded linear operator presenting three properties: it is Hermitian and non-negative, and it has a unit trace. Using the Fock basis, the density operator of any one mode state can be expressed in this basis as:

$$\hat{\rho} = \sum_{n,n'=0}^{\infty} \rho_{nn'} |n\rangle \langle n'| . \tag{2.8}$$

We will present the Fock states in more detail in Subsection 2.4.2.

Other quantum states are very important in this thesis: the coherent states. The coherent states are defined as the eigenstates of the annihilation operator

$$\hat{a}|\alpha\rangle = \alpha|\alpha\rangle, \tag{2.9}$$

where α is a complex number. Coherent states have two main properties. First, they are not orthogonal to each other. Indeed, their overlap is not equal to zero, since

$$\langle\beta|\alpha\rangle = e^{\frac{-|\alpha-\beta|^2}{2}}. \tag{2.10}$$

Second, the coherent states form an overcomplete basis:

$$\int d^2\alpha\ |\alpha\rangle\langle\alpha| = \pi. \tag{2.11}$$

Those states will be studied in more details in Subsection 2.4.1.

According to Eq. (2.7), we see that the state with the minimal energy has an energy of $\frac{1}{2}$. This state is called the vacuum state, $|0\rangle$, and corresponds to a state with zero photons. The vacuum state is also defined according to the effect of the annihilation operator on it: $\hat{a}|0\rangle = 0$. Hence, it is a particular coherent state.

Using the annihilation and creation operators, it is also possible to define the quadratures of the electromagnetic field:

$$\begin{aligned} \hat{x} &= \frac{1}{\sqrt{2}}(\hat{a} + \hat{a}^\dagger), \\ \hat{p} &= \frac{-i}{\sqrt{2}}(\hat{a} - \hat{a}^\dagger). \end{aligned} \tag{2.12}$$

Interestingly, the Hamiltonian presented in Eq. (2.6) is the same as the Hamiltonian of a free harmonic oscillator. In this case, $\hat{x}$ and $\hat{p}$ correspond to the position and momentum of the oscillator. It is also possible to write the Hamiltonian in terms of $\hat{x}$ and $\hat{p}$:

$$\hat{H} = \frac{1}{2}\left(\hat{x}^2 + \hat{p}^2\right). \tag{2.13}$$

The eigenstates $|x\rangle$ and $|p\rangle$ of the operators $\hat{x}$ and $\hat{p}$,

$$\begin{aligned} \hat{x}|x\rangle &= x|x\rangle, \\ \hat{p}|p\rangle &= p|p\rangle, \end{aligned} \tag{2.14}$$

form two bases (both are complete sets of orthogonal state vectors). However, these states are non-physical as they are non-normalizable. The two bases are connected to each other by a Fourier transform

$$\begin{aligned} |x\rangle &= \frac{1}{2\pi}\int_{-\infty}^{\infty} dp\ e^{ixp}|p\rangle, \\ |p\rangle &= \frac{1}{2\pi}\int_{-\infty}^{\infty} dx\ e^{-ixp}|x\rangle. \end{aligned} \tag{2.15}$$

Using these states, we can also express the state $|\psi\rangle$ in the position basis as a wave function as $\psi(x) = \langle x|\psi\rangle$.

2.2 Uncertainty relations

The quadratures $\hat{x}$ and $\hat{p}$ are canonically conjugated as their commutator $[\hat{x}, \hat{p}]$ is equal to i. This can easily be demonstrated starting from the definitions of the quadratures in terms of the creation/annihilation operators (2.12) and using the bosonic commutation relations (2.4). Any two operators that are canonically conjugated have to follow the Heisenberg uncertainty relation [59]. This means that the following inequality has to be fulfilled for all physical states:

$$\sigma_x^2 \sigma_p^2 \geq \frac{1}{4}, \tag{2.16}$$

where $\sigma_x^2 = \langle \hat{x}^2 \rangle - \langle \hat{x} \rangle^2$ is the variance of $\hat{x}$ and σ_p^2 is the variance of $\hat{p}$, which is defined analogously. This uncertainty relation indicates that it is impossible to perfectly determine the two quadratures simultaneously and is a typical quantum feature. Indeed, in classical physics, we can measure the two quadratures simultaneously.

The first uncertainty relation was uncovered by Heisenberg [59] in 1927 and mathematically formulated by Kennard [80]. However, this relation is only saturated by pure Gaussian states with no correlations between the x and p quadratures (Gaussian states will be presented later in Section 2.4.1). This seminal relation was then generalised, for arbitrary observables $\hat{A}$ and $\hat{B}$ by Robertson [126]. Later, in order to obtain an uncertainty relation that is saturated by all pure Gaussian states, it was also improved by Schrödinger [134] in 1930, by the addition of an anticommutator $\{.,.\}$ to the right-hand-side of the inequality, leading to the well-known Schrödinger-Robertson uncertainty relation:

$$\sigma_A^2 \sigma_B^2 \geq \frac{1}{4} | \langle [\hat{A}, \hat{B}] \rangle |^2 + \frac{1}{4} | \langle \{ \hat{A} - \langle \hat{A} \rangle , \hat{B} - \langle \hat{B} \rangle \} \rangle |^2, \tag{2.17}$$

where the anticommutator between two operators is defined as $\{\hat{A}, \hat{B}\} = \hat{A}\hat{B} + \hat{B}\hat{A}$. In the special case of the quadratures $\hat{x}$ and $\hat{p}$, this last inequality can be written in compact form:

$$\det \gamma \geq \frac{1}{4}, \tag{2.18}$$

where γ is the covariance matrix defined as:

$$\gamma = \begin{pmatrix} \sigma_x^2 & \sigma_{xp} \\ \sigma_{xp} & \sigma_p^2 \end{pmatrix}, \tag{2.19}$$

and σ_{xp} is the covariance between $\hat{x}$ and $\hat{p}$. Compared to the original one, this last uncertainty relation is now saturated by all pure Gaussian states.

2.3 Quasi-probability distributions

Describing the state of a classical particle is easy as we just need to specify its position and momentum. We can therefore represent this state as a single point in the phase space where one axis corresponds to the position while the other one to the momentum for an object moving in one dimension. For a quantum state, this representation is more complicated as this state must satisfy the uncertainty relations like the Robertson-Schrödinger uncertainty relation (Eq. (2.16)). It is then not possible to describe the state of a system by giving its position and its momentum. Instead, in order to describe the state in the phase space, we then use quasi-probability distributions. These are different from probability distributions as they do not obey all the properties of a probability distribution, as we will see in what follows. Three quasi-probability distributions will be presented as they are the most important ones in quantum optics.

2.3.1 Wigner function

We start by presenting the Wigner function [161] as it is the most widely used quasi-probability distribution. This function is defined for a state $\hat{\rho}$ of n-modes ($n \in \mathbb{N}$) as

$$W(\vec{x}, \vec{p}) = \frac{1}{(2\pi)^n} \int_{-\infty}^{\infty} d\vec{y}\, e^{-i\vec{p}\cdot\vec{y}} \,\langle \vec{x} + \frac{\vec{y}}{2} |\, \hat{\rho} | \vec{x} - \frac{\vec{y}}{2} \rangle, \tag{2.20}$$

where $\vec{x} = \{x_1, x_2, ..., x_n\}$ and $\vec{p} = \{p_1, p_2, ..., p_n\}$. It is also possible to express the Wigner function using the momentum representation instead of the position representation:

$$W(\vec{x}, \vec{p}) = \frac{1}{(2\pi)^n} \int_{-\infty}^{\infty} d\vec{q}\, e^{i\vec{x}\cdot\vec{q}} \langle \vec{p} + \frac{\vec{q}}{2} | \hat{\rho} | \vec{p} - \frac{\vec{q}}{2} \rangle. \tag{2.21}$$

The Wigner function of a state sums up to one like every probability distribution

$$\int_{-\infty}^{\infty} d\vec{x} d\vec{p}\, W(\vec{x}, \vec{p}) = 1, \tag{2.22}$$

which is a consequence of the normalization of the state, $\mathrm{Tr}(\hat{\rho}) = 1$ as it will be shown after. Moreover, its values are real, $W(\vec{x}, \vec{p}) = W(\vec{x}, \vec{p})^*$. However, it is a quasi-probability distribution as it can possess negative values.

By integrating the Wigner function over x or p, we obtain the marginal functions $p_x(\vec{x})$ and $p_p(\vec{p})$.These marginals are important as they provide the probability distributions for the position and the momentum:

$$\begin{aligned} p_x(\vec{x}) &= \int_{-\infty}^{\infty} d\vec{p}\, W(\vec{x}, \vec{p}) = \langle \vec{x} | \hat{\rho} | \vec{x} \rangle, \\ p_p(\vec{p}) &= \int_{-\infty}^{\infty} d\vec{x}\, W(\vec{x}, \vec{p}) = \langle \vec{p} | \hat{\rho} | \vec{p} \rangle. \end{aligned} \tag{2.23}$$

Unlike Wigner functions, these distributions fulfill all the properties of a classical probability distribution as they correspond to distributions over measurement outcomes.

The Wigner function has another interesting property: it is the Wigner-Weyl transform of the density operator $\hat{\rho}$ of the state. The Wigner-Weyl transform of an operator $\hat{A}$ is given by

$\tilde{A}(\vec{x},\vec{p})$:

$$\tilde{A}(\vec{x},\vec{p}) = \frac{1}{(2\pi)^n}\int_{-\infty}^{\infty} d\vec{y}\, e^{-i\vec{p}\cdot\vec{y}}\langle\vec{x}+\frac{\vec{y}}{2}|\hat{A}_S|\vec{x}-\frac{\vec{y}}{2}\rangle, \tag{2.24}$$

where $\hat{A}_S$ is the symmetrized form of the operator $\hat{A}$ in terms of the quadrature operators $\hat{x}$ and $\hat{p}$ (for example, if $\hat{A} = \hat{x}\hat{p}$, then, $\hat{A}_S = \frac{\hat{x}\hat{p}+\hat{p}\hat{x}}{2}$). As a consequence of this, the Wigner function is associated with the symmetric order of the operators $\hat{x}$ and $\hat{p}$ (or $\hat{a}^\dagger$ and $\hat{a}$). Hence, looking at the definition of the Wigner function (Eq. (2.20)), it is clear that that the Wigner function is indeed the Wigner-Weyl transform of $\hat{\rho}$. In the rest of this thesis, we will use the Wigner-Weyl transform in Chapter 6. We then list here some basic identities for one-mode system ($n = 1$):

$$\text{Operator } \hat{A} \rightarrow 2\pi\tilde{A}(x,p)$$

$$\begin{aligned} \hat{x} &\rightarrow x \\ \hat{p} &\rightarrow p \\ \hat{x}^2 &\rightarrow x^2 \\ \hat{p}^2 &\rightarrow p^2 \\ \frac{\hat{x}\hat{p}+\hat{p}\hat{x}}{2} &\rightarrow xp \\ \frac{\hat{x}^2\hat{p}^2+\hat{x}\hat{p}\hat{x}\hat{p}+\hat{x}\hat{p}^2\hat{x}+\hat{p}\hat{x}^2\hat{p}+\hat{p}\hat{x}\hat{p}\hat{x}+\hat{p}^2\hat{x}^2}{6} &\rightarrow x^2p^2. \end{aligned} \tag{2.25}$$

The Wigner-Weyl transform of the identity operator $\hat{\mathbb{1}}$ is simply equal to the constant function $1/2\pi$. Note also that the Wigner-Weyl transforms of operators $f(\hat{x})$ and $g(\hat{p})$ are $f(x)/2\pi$ and $g(p)/2\pi$, respectively, where f and g are arbitrary functions.

The Wigner-Weyl transform is mainly used to calculate the overlap between two linear operators $\hat{A}_1$ and $\hat{A}_2$ according to:

$$\text{Tr}(\hat{A}_1\,\hat{A}_2) = (2\pi)^n\int d\vec{x}\,d\vec{p}\,\tilde{A}_1(\vec{x},\vec{p})\,\tilde{A}_2(\vec{x},\vec{p}). \tag{2.26}$$

We will use the overlap formula for one-mode systems ($n = 1$) in Chapter 7 in order to verify some of our results. Moreover, using this formula and the fact that the Wigner function is the Wigner-Weyl transform of the state, we can mention two corollaries to this overlap formula which are often used in quantum optics. First, we can use the Wigner function to calculate the mean value of an operator $\hat{A}$ using the Wigner-Weyl transform:

$$\langle\hat{A}\rangle = \text{Tr}(\hat{A}\hat{\rho}) = (2\pi)^n\int_{-\infty}^{\infty} d\vec{x}d\vec{p}\,W(\vec{x},\vec{p})\tilde{A}(\vec{x},\vec{p}). \tag{2.27}$$

Second, the trace of $\hat{\rho}$ is linked to the integral of the Wigner function:

$$\text{Tr}(\hat{\rho}) = \int d\vec{x}\,d\vec{p}\,W(\vec{x},\vec{p}) = 1, \tag{2.28}$$

which proves that the integral of the Wigner function has to be equal to 1. Another interesting property of the Wigner function is that its value at the origin is proportional to the expectation value of the photon number parity (in the single-mode case): $W(0,0) = \frac{1}{\pi}\mathrm{Tr}(\hat{\rho}(-1)^{\hat{n}})$. To prove this, we need to compute the Wigner-Weyl transform of the parity operator $(-1)^{\hat{n}}/\pi$, namely

$$\frac{1}{2\pi}\int dy\, \langle x-\frac{y}{2}|\frac{(-1)^{\hat{n}}}{\pi}|x+\frac{y}{2}\rangle\, e^{ipy} = \frac{1}{2\pi^2}\int dy\, \langle x-\frac{y}{2}|-x-\frac{y}{2}\rangle\, e^{ipy}. \tag{2.29}$$

Indeed, applying the parity operator on the state $|x+\frac{y}{2}\rangle$ transforms the state in $|-x-\frac{y}{2}\rangle$:

$$\begin{aligned}
(-1)^{\hat{n}}\,|x+\frac{y}{2}\rangle &= e^{i\pi\hat{n}}\,|x+\frac{y}{2}\rangle\,,\\
&= \sum_n e^{i\pi n}\,|n\rangle\,\langle n|x+\frac{y}{2}\rangle,\\
&= \sum_n (-1)^n\,|n\rangle\,\frac{1}{\pi^{\frac{1}{4}}\sqrt{2^n n!}}H_n\left(x+\frac{y}{2}\right)e^{-\frac{1}{2}(x+\frac{y}{2})^2},\\
&= \sum_n |n\rangle\,\frac{1}{\pi^{\frac{1}{4}}\sqrt{2^n n!}}H_n\left(-x-\frac{y}{2}\right)e^{-\frac{1}{2}(-x-\frac{y}{2})^2},\\
&= \sum_n |n\rangle\,\langle n|-x-\frac{y}{2}\rangle,\\
&= |-x-\frac{y}{2}\rangle\,,
\end{aligned} \tag{2.30}$$

where we started by applying the closure relation $\hat{\mathbb{1}} = \sum_n |n\rangle\,\langle n|$. Then, we injected in the equation the wave function of a Fock states (which will be given in Eq. (2.78)) that involves Hermite polynomials of order n H_n. Finally, we used the property of the Hermite polynomials, $(-1)^n H_n(z) = H_n(-z)$, that allows us to find back the closure relation to simplify the expression. The Weyl transform then implies $\langle x-\frac{y}{2}|-x-\frac{y}{2}\rangle$ which is equal to zero unless $x=-x$. We can reformulate this by using a Dirac delta:

$$\langle x-\frac{y}{2}|\frac{(-1)^{\hat{n}}}{\pi}|x+\frac{y}{2}\rangle = \frac{\langle x-\frac{y}{2}|-x-\frac{y}{2}\rangle}{\pi} = \frac{\delta(2x)}{\pi}, \tag{2.31}$$

leading to:

$$\begin{aligned}
\frac{1}{2\pi}\int dy\,\langle x-\frac{y}{2}|\frac{(-1)^{\hat{n}}}{\pi}|x+\frac{y}{2}\rangle\,e^{ipy} &= \frac{\delta(2x)}{2\pi^2}\int dy\,e^{ipy},\\
&= \frac{\delta(x)\delta(p)}{2\pi},
\end{aligned} \tag{2.32}$$

where we have used the identity $\int dy\, e^{ipy} = 2\pi\,\delta(p)$ and $\delta(2x) = \frac{\delta(x)}{2}$. Hence, using the overlap formula (2.26), we get

$$\begin{aligned}
\frac{1}{\pi}\mathrm{Tr}\left(\hat{\rho}\,(-1)^{\hat{n}}\right) &= 2\pi\int dx\,dp\,W(x,p)\,\frac{\delta(x)\delta(p)}{2\pi},\\
&= W(0,0),
\end{aligned} \tag{2.33}$$

as desired. We will use this property in Chapter 7.

2.3.2 Glauber-Sudarshan function

The P function, also called Glauber-Sudarshan function or simply Sudarshan function, can be used to write what is called the "optical equivalence theorem" [46, 47, 149, 84] which is a way of writing the density matrix of a state as a distribution of coherent states

$$\hat{\rho} = \int d^2\alpha \; P(\alpha)|\alpha\rangle\langle\alpha|, \tag{2.34}$$

where α is a coherent state as defined in Eq. (2.9). It is important to note that calling the Glauber-Sudarshan function a "function" is an abuse of language as it is in general a distribution. Moreover, in some special cases, it is so singular that it is not even a distribution. However, this denomination is common in the literature and so we will use it in this thesis. $P(\alpha)$ is a normalized function that can be negative like Wigner functions. However, it often becomes singular, in which case it has to be understood as a distribution with respect to the phase space integral (as mentioned before, sometimes, it does not correspond to a distribution anymore as it is too singular). This quasi-probability function is associated to the normal order where all creation operators are put before the annihilation operators. This order may be written with ": :". The expectation value of a normal ordered term is calculated with the P-Sudarshan function, as [20, 19]

$$\langle \hat{a}^{\dagger k}\hat{a}^l \rangle = \int d^2\alpha \; \alpha^{*k}\alpha^l P(\alpha). \tag{2.35}$$

The P-Sudarshan function can be used to obtain the Wigner function of a state. To do so, we have to convolute the P-function with a Gaussian function having the same width as the vacuum. However, the most important application of the P-function for this thesis is that it can be used to define the optical nonclassicality. Indeed, a quantum state is defined as optically classical if its P-Sudarshan function corresponds to a classical probability distribution function. Hence, a state is classical if its P-function does not present negativities and, intuitively speaking, is not too peaked.

2.3.3 Husimi function

By convoluting the Wigner function of a state with a Gaussian function having the same width as the vacuum, we obtain a smoother quasi-probability distribution: the Husimi Q function [77]. Another definition of the Q function states that it is proportional to the probability distribution of finding the coherent state $|\alpha\rangle$ (defined in Eq. (2.9)), *i.e.*, if the state is given by $\hat{\rho}$, its Husimi distribution is given by:

$$Q(\alpha) = \frac{1}{\pi}\langle\alpha|\hat{\rho}|\alpha\rangle. \tag{2.36}$$

This expression directly follows from Eq. (2.11). The Q function is normalized to one and is always positive unlike the Wigner function. In what follows, we will see that it can also be used to study the nonclassicality of a state. This function is associated to the anti-normal order in terms of the creation and annihilation operator. The anti-normal order means that all the annihilation operators are put before the creation operators. This means that we can use the Husimi function to calculate the mean value of an anti-normally ordered operator

$$\langle \hat{a}^k \hat{a}^{\dagger l} \rangle = \int d^2\alpha \, \alpha^k \alpha^{*l} Q(\alpha). \tag{2.37}$$

The Husimi function can also be obtained from the P-function as:

$$Q(\alpha) = \frac{1}{\pi} \int d\beta^2 \, P(\beta) e^{-|\alpha-\beta|^2}. \tag{2.38}$$

This can be proving by injecting Eq. (2.34) in Eq. (2.36) and by using the overlap of two coherent states, Eq. (2.10).

Finally, we can note that there exists a general way of writing these three quasi-probability distributions by allowing for convolutions with arbitrary widths.

2.4 Quantum states

In quantum optics, states are usually split into two categories: the Gaussian states and the non-Gaussian ones. We start by presenting the Gaussian states as they are very important in quantum optics. Then, we present some non-Gaussian states.

2.4.1 Gaussian states

Gaussian states are defined as states having a Gaussian Wigner function. Interestingly enough, the state is then completely defined by its moments of order one and two. The moment of the first order is the mean value vector (or displacement vector) and is equal to

$$\langle \vec{r} \rangle = \mathrm{Tr}(\vec{r}\hat{\rho}), \tag{2.39}$$

where

$$\vec{r} = \{\hat{x}_1, \hat{p}_1, \hat{x}_2, \hat{p}_2, ..., \hat{x}_n, \hat{p}_n\} \tag{2.40}$$

is the quadrature vector and n the dimension of the state. The second order moment is the covariance matrix of the state

$$\gamma_{ij} = \frac{1}{2}\langle\{\hat{r}_i, \hat{r}_j\}\rangle - \langle\hat{r}_i\rangle\langle\hat{r}_j\rangle. \tag{2.41}$$

In what follows, we will mainly present one mode states so that the covariance matrix reduces to the one presented in Eq. (2.19). It is important to mention that any symmetric matrix is not necessarily a valid covariance matrix. Indeed, the covariance matrix must follow certain rules to describe a physical quantum state. One of these rules is the uncertainty principle as shown in Eq. (2.18). If this condition is not fulfilled, the state can not exist.

For Gaussian states, using only these two moments, we can find back the value of all the other moments as we will do in Chapter 6.

We can also write the Wigner function of the state:

$$W_G(\vec{x}, \vec{p}) = \frac{1}{(2\pi)^n \sqrt{\det \gamma}} e^{-\frac{1}{2}(\vec{r}-\langle\vec{r}\rangle)^T \gamma^{-1} (\vec{r}-\langle\vec{r}\rangle)}, \tag{2.42}$$

where $\vec{x} = \{x_1, x_2, ..., x_n\}$ and $\vec{p} = \{p_1, p_2, ..., p_n\}$. Calculating properties for Gaussian states is easier than for non-Gaussian states. For example, we can calculate the purity of a Gaussian state. The purity of a quantum state is an important quantity as it describes the mixedness of the state. It is equal to 1 if the state is pure, while it is lower than 1 if the state is mixed. It is defined as

$$\mathcal{P}(\hat{\rho}) = \mathrm{Tr}(\hat{\rho}^2), \tag{2.43}$$

which can be calculated by applying Eq. (2.26) for a n-mode system:

$$\mathcal{P}(\hat{\rho}) = (2\pi)^n \int d\vec{x} d\vec{p} \; W^2(\vec{x}, \vec{p}), \tag{2.44}$$

where the Wigner function $W(\vec{x}, \vec{p})$ is the Wigner-Weyl transform of the state $\hat{\rho}$. This finally yields

$$\mathcal{P}(\hat{\rho}) = \frac{1}{2^n \sqrt{\det \gamma}}. \tag{2.45}$$

This value is well known for Gaussian states. In Chapter 7, we will prove this equation by using the multicopy method. Another interesting quantity for Gaussian states that we will use in the same way is the overlap between two Gaussian states. The overlap between two states $\hat{\rho}_A$ and $\hat{\rho}_B$ is defined as $\mathrm{Tr}(\hat{\rho}_A \hat{\rho}_B)$, which can be calculated using Eq. (2.26) and the Wigner functions of the two states, namely

$$\mathrm{Tr}(\hat{\rho}_A \hat{\rho}_B) = (2\pi)^n \int d\vec{x} d\vec{p} \; W_A(\vec{x}, \vec{p}) W_B(\vec{x}, \vec{p}). \tag{2.46}$$

which yields:

$$\mathrm{Tr}(\hat{\rho}_A \hat{\rho}_B) = \frac{1}{\sqrt{\det(\gamma_A + \gamma_B)}}. \tag{2.47}$$

One of the most important example of a one-mode Gaussian state is the vacuum state already mentioned in the last sections. We can write the displacement vector and the covariance matrix of this state:

$$\langle\vec{r}\rangle = \begin{pmatrix} 0 \\ 0 \end{pmatrix}, \tag{2.48}$$

$$\gamma = \begin{pmatrix} \frac{1}{2} & 0 \\ 0 & \frac{1}{2} \end{pmatrix}. \tag{2.49}$$

The vacuum state is very important as we can obtain the other Gaussian states by applying operations on it. These operations will be described in the next section. We first present the different types of Gaussian states.

Coherent states

Coherent states are called coherent as they describe the state emitted by an ideal laser source. They are also often called classical as they exhibit classical properties. We already mentioned that they are defined as they eigenstates of the annihilation operator (Eq. (2.9)). Taking the adjoint of this relation, we have

$$\langle\alpha|\hat{a}^\dagger = \langle\alpha|\alpha^*, \tag{2.50}$$

which will be used later.

Two of their properties were already given before: their non-orthogonality between each other (Eq. (2.10)) and the fact that they form an overcomplete basis (Eq. (2.11)). In addition to those properties, they saturate all uncertainty relations. Indeed, we can calculate the variance of $\hat{x}$ using Eqs. (2.9) and (2.50):

$$\begin{aligned} \sigma_x^2 &= \langle\alpha|(\frac{\hat{a}^\dagger+\hat{a}}{\sqrt{2}})^2|\alpha\rangle - \langle\alpha|(\frac{\hat{a}^\dagger+\hat{a}}{\sqrt{2}})|\alpha\rangle^2, \\ &= \langle\alpha|\frac{\hat{a}^{\dagger 2}+\hat{a}^2+2\hat{a}^\dagger\hat{a}+1}{2}|\alpha\rangle - \langle\alpha|\frac{\alpha+\alpha^*}{\sqrt{2}}|\alpha\rangle^2, \\ &= \frac{\alpha^{*2}+\alpha^2+2\alpha^*\alpha+1}{2} - \frac{\alpha^{*2}+\alpha^2+2\alpha^*\alpha}{2}, \\ &= \frac{1}{2}, \end{aligned} \tag{2.51}$$

where we used the bosonic commutation relations between the first and second line. Analogous calculations lead to $\sigma_p^2 = \frac{1}{2}$ such that, for coherent states, we obtain the expression

$$\sigma_x^2\sigma_p^2 = \frac{1}{4}, \tag{2.52}$$

which shows that inequality (2.16) is indeed saturated for coherent states.

Using the values obtained for the variances and doing the same kind of calculation to obtain the covariance, we can write the covariance matrix of a coherent state

$$\gamma = \begin{pmatrix} \frac{1}{2} & 0 \\ 0 & \frac{1}{2} \end{pmatrix}, \tag{2.53}$$

and we can also calculate its mean value vector

$$\langle\vec{r}\rangle = \begin{pmatrix} \sqrt{2}\,\Re(\alpha) \\ \sqrt{2}\,\Im(\alpha) \end{pmatrix}. \tag{2.54}$$

Using these informations, we can represent a coherent state $|\alpha\rangle$ in the phase space as done in

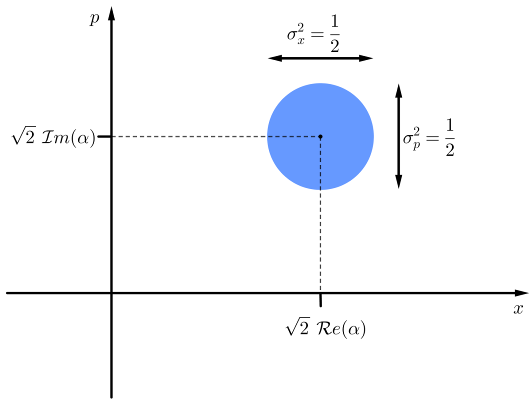

Figure 2.1: Phase space representation of a coherent state.

Fig. 2.1. It is interesting to notice that the vacuum state is just a particular case of a coherent state where $\alpha = 0$. It is also possible to decompose the coherent state in the Fock basis

$$|\alpha\rangle = e^{\frac{-|\alpha|^2}{2}} \sum_{n=0}^{\infty} \frac{\alpha^n}{\sqrt{n!}} |n\rangle. \tag{2.55}$$

Using this expression, we can calculate the photon number distribution of a coherent state

$$p(n) = |\langle n|\alpha\rangle|^2 = e^{-|\alpha|^2} \frac{|\alpha|^{2n}}{n!}, \tag{2.56}$$

which is a Poisson distribution with its mean and variance equal to $|\alpha|^2$. This distribution will be used in Chapter 7 to prove differently a known property of the so-called quadrature coherence scale [30, 75, 62, 61, 63].

Squeezed states

Squeezed states are Gaussian states whose variances in both quadratures are not the same anymore. Indeed, squeezed states have been compressed along a direction and stretched along the perpendicular direction. This phenomenon is represented in the phase space in Fig. 2.2 in the particular case of a squeezing along the x-axis ($\phi = 0$). Squeezed states are defined with a complex squeezing parameter $\xi = re^{i\phi}$, where $\phi \in [0, 2\pi[$ is the squeezing angle and $r \in [0, +\infty[$ the squeezing intensity.

As for coherent states, squeezed states can also be decomposed in the Fock basis,

$$|\xi\rangle = \frac{1}{\sqrt{\cosh(r)}} \sum_{n=0}^{\infty} e^{in\phi} \frac{\sqrt{(2n)!}}{2^n n!} \tanh^n(r) |2n\rangle, \tag{2.57}$$

where we notice that the sum only involves terms with an even number of photons. This property will be used in Chapter 6 to calculate the elements of some matrix.

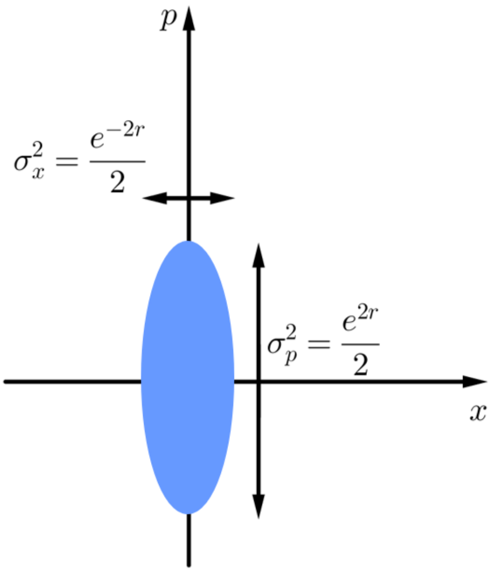

Figure 2.2: Phase space representation of a squeezed vacuum state.

In the special case $\phi = 0$, we can give the mean value vector and the covariance matrix of a squeezed state. This state is still centered in phase space so that its mean value vector is equal to $\vec{0}$

$$\langle \vec{r} \rangle = \begin{pmatrix} 0 \\ 0 \end{pmatrix}. \tag{2.58}$$

The covariance matrix shows that one quadrature is compressed and the other one stretched:

$$\begin{pmatrix} \frac{e^{-2r}}{2} & 0 \\ 0 & \frac{e^{2r}}{2} \end{pmatrix}. \tag{2.59}$$

We see that squeezed states also saturate the uncertainty relation (2.18).

Thermal states

Thermal states are mixed Gaussian states. Like coherent states, the two variances are equal but this time, they are greater than $\frac{1}{2}$. We can represent them in phase space as done in Fig. 2.3. They are defined in the Fock basis with one parameter q as

$$\hat{\rho}_q = (1-q) \sum_{n=0}^{\infty} q^n |n\rangle\langle n|, \tag{2.60}$$

Using this expression, we can compute the mean number of photons in the state, namely:

$$\langle \hat{n} \rangle_q = \frac{q}{1-q}. \tag{2.61}$$

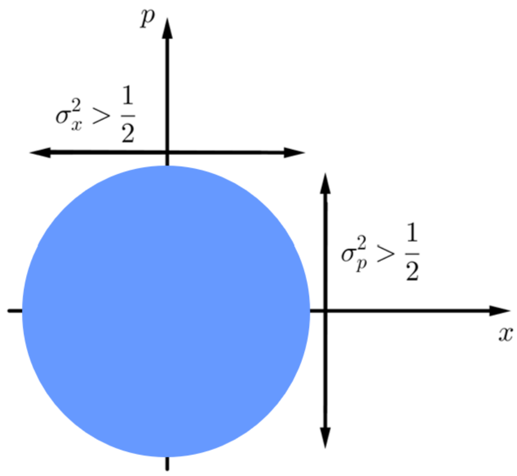

Figure 2.3: Phase space representation of a thermal state.

The states can then be expressed using this mean number as

$$\hat{\rho}_q = \sum_{n=0}^{\infty} \frac{\langle \hat{n} \rangle_q^n}{(1 + \langle \hat{n} \rangle_q)^{n+1}} |n\rangle\langle n|. \tag{2.62}$$

The mean value vector of a thermal state is a zero-vector as the state is centered in the phase space and the covariance matrix is given by:

$$\gamma = \begin{pmatrix} \langle \hat{n} \rangle_q + \frac{1}{2} & 0 \\ 0 & \langle \hat{n} \rangle_q + \frac{1}{2} \end{pmatrix}. \tag{2.63}$$

We can mention that the thermal states do not saturate the uncertainty relation (2.18) for non-zero temperature.

EPR states

Finally, a well-known two-mode Gaussian state in quantum optics is the two-mode squeezed vacuum state (TMSV). This state is also often called the EPR state (for Einstein-Podolski-Rosen [36]) and can be written in the Fock basis:

$$|\mathrm{EPR}\rangle = \frac{1}{\cosh r} \sum_{n=0}^{\infty} (\tanh r)^n |n,\, n\rangle. \tag{2.64}$$

In some reference books, the parameter r is not the one used to write the state and it is instead expressed as a function of $\lambda = \tanh r$:

$$|\mathrm{EPR}\rangle = \sqrt{1-\lambda^2} \sum_{n=0}^{\infty} \lambda^n |n,\, n\rangle. \tag{2.65}$$

In the limit of infinite squeezing ($r \to \infty$), the state is a maximally entangled state which is one reason for its importance. The other reason is that it is a joint eigenstate of the commuting operators $\hat{x}_1 - \hat{x}_2$ and $\hat{p}_1 + \hat{p}_2$, where 1 and 2 denote the first and the second mode, respectively. The covariance matrix of the EPR state is given by

$$\gamma = \frac{1}{2}\begin{pmatrix} \cosh(2r) & 0 & \sinh(2r) & 0 \\ 0 & \cosh(2r) & 0 & -\sinh(2r) \\ \sinh(2r) & 0 & \cosh(2r) & 0 \\ 0 & -\sinh(2r) & 0 & \cosh(2r) \end{pmatrix}. \tag{2.66}$$

Note that one way to obtain a TMSV state is to send two squeezed vacuum states with perpendicular squeezing in a balanced beam splitter. This can also be performed by using parametric processes such as over-threshold parametric amplification. In Chapter 8, we will use these entangled states as references to analyze our multicopy entanglement criteria.

2.4.2 Non-Gaussian states

Cat states

Cat states are named after the well-known thought experiment of Schrödinger [135] where a cat is simultaneously in two very different macroscopic states (dead and alive). Therefore, cat states are defined as an equal superposition of two opposed coherent states. These states can be split into two categories, the even and odd cat states

$$|c_\pm\rangle = \frac{1}{\sqrt{N_\pm}}(|\alpha\rangle \pm |-\alpha\rangle), \tag{2.67}$$

where the subscript $+$ corresponds to the even cat state and the subscript $-$ to the odd cat state and where $N_\pm$ are the normalization constants

$$N_\pm = 2\left(1 \pm e^{-2|\alpha|^2}\right). \tag{2.68}$$

Cat states enjoy two interesting properties that will be exploited in Chapter 6. First, the even and odd cat states are orthogonal to each other. This can easily be demonstrated using the properties of the coherent states

$$\begin{aligned} \langle c_-|c_+\rangle &= \frac{1}{\sqrt{N_- N_+}}(\langle\alpha| - \langle-\alpha|)(|\alpha\rangle + |-\alpha\rangle), \\ &= \frac{1}{\sqrt{N_- N_+}}(\langle\alpha|\alpha\rangle + \langle\alpha|-\alpha\rangle - \langle-\alpha|\alpha\rangle - \langle-\alpha|-\alpha\rangle), \\ &= \frac{1}{\sqrt{N_- N_+}}(1 + e^{\frac{-|-\alpha-\alpha|^2}{2}} - e^{\frac{-|\alpha+\alpha|^2}{2}} - 1), \\ &= 0. \end{aligned} \tag{2.69}$$

The second interesting property is that applying an annihilation operator to an even cat state gives a state proportional to an odd cat state and vice versa

$$
\begin{aligned}
\hat{a}|c_\pm\rangle &= \hat{a}\frac{1}{\sqrt{N_\pm}}(|\alpha\rangle \pm |-\alpha\rangle), \\
&= \frac{1}{\sqrt{N_\pm}}\frac{\sqrt{N_\mp}}{\sqrt{N_\mp}}(\alpha|\alpha\rangle \mp \alpha|-\alpha\rangle), \\
&= \frac{\alpha\sqrt{N_\mp}}{\sqrt{N_\pm}}|c_\mp\rangle.
\end{aligned}
\tag{2.70}
$$

Taking the adjoint, we have also $\langle c_\pm|\hat{a}^\dagger = \langle c_\mp|\frac{\alpha^*\sqrt{N_\mp}}{\sqrt{N_\pm}}$. All these properties will be used in Chapter 6.

It is also possible to generalize the cat states to a two-mode state. This corresponds to the state:

$$
\begin{aligned}
\hat{\rho} = N(\alpha,\beta,z)\Big[&|\alpha,\beta\rangle\langle\alpha,\beta| + |-\alpha,-\beta\rangle\langle-\alpha,-\beta| \\
&- (1-z)\left(|\alpha,\beta\rangle\langle-\alpha,-\beta| + |-\alpha,-\beta\rangle\langle\alpha,\beta|\right)\Big],
\end{aligned}
\tag{2.71}
$$

with a mixing parameter $z \in [0,1]$ and a normalization constant

$$
N(\alpha,\beta,z) = \frac{\left(1-(1-z)e^{-2(|\alpha^2|+|\beta|^2)}\right)^{-1}}{2},
\tag{2.72}
$$

with $\alpha, \beta \in \mathbb{C}$. This state is an entangled state except when $z = 1$ and $\alpha = \beta = 0$.

Fock states

As said before, the Fock states are the eigenstates of the number operator:

$$
\hat{n}|n\rangle = n|n\rangle.
\tag{2.73}
$$

They are often used in quantum optics as they form a complete basis, namely they are orthonormal

$$
\langle n'|n\rangle = \delta_{n',n},
\tag{2.74}
$$

where δ is the Kronecker delta. The Fock state $|0\rangle$ is nothing else than the vacuum state. The application of the creation/annihilation operator to a Fock state gives another Fock state with one photon more/less:

$$
\begin{aligned}
\hat{a}|n\rangle &= \sqrt{n}|n-1\rangle, \\
\hat{a}^\dagger|n\rangle &= \sqrt{n+1}|n+1\rangle.
\end{aligned}
\tag{2.75}
$$

Hence, any Fock state can be obtained by applying several times the creation operator to the vacuum state:

$$
|n\rangle = \frac{\hat{a}^{\dagger n}}{\sqrt{n!}}|0\rangle.
\tag{2.76}
$$

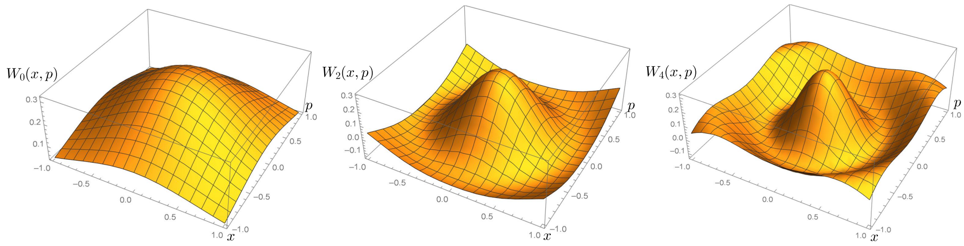

Figure 2.4: Wigner function of a Fock state $|n\rangle$ with $n = 0, 2, 4$. We see that the Wigner function possesses negative values for $n = 2, 4$.

We can give the Wigner function of a Fock state

$$W_n(x,p) = \frac{(-1)^n}{\pi} e^{-x^2-p^2} L_n(2(x^2+p^2)), \tag{2.77}$$

where L_n is the Laguerre polynomial of order n. An important property of the Fock state is that its Wigner function is negative in some regions (except for $|0\rangle$), which was not the case for a Gaussian state. This effect can be seen in Fig. 2.4.

We can also give its wave function (which was already used in Eq. (2.30)):

$$\psi_n(x) = \langle x|n\rangle = \frac{1}{\pi^{\frac{1}{4}}\sqrt{2^n n!}} H_n(x) e^{-\frac{x^2}{2}}, \tag{2.78}$$

where H_n is the Hermite polynomial of order n.

N00N states

These states are pure bipartite states with arbitrary complex amplitudes defined as [131]:

$$|\psi\rangle = \alpha\,|n,0\rangle + \beta\,|0,n\rangle\,, \tag{2.79}$$

with integer $n \geq 1$ and $|\alpha|^2 + |\beta|^2 = 1$.

This class of non-Gaussian states includes two well-known states: the first Bell state $n = 1, \alpha = \beta = 1/\sqrt{2}$, as well as the Hong-Ou-Mandel state $n = 2, \alpha = -\beta = 1/\sqrt{2}$ [69]. Moreover, these N00N states are entangled states for the whole range of the parameter n.

2.5 Quantum operations

In the last section, we presented the different kinds of states that will be used in this thesis. The objective of the thesis is to design quantum circuits allowing to measure certain properties of states, like nonclassicality. To design such circuits, we introduce quantum operations to transform states. Here, we present Gaussian unitaries that can be implemented in a circuit. Moreover, the unitaries we present allow us to create the Gaussian states presented before starting from the vacuum state.

The unitaries that we present are called Gaussian because, if the state entering the unitary is Gaussian, then the output state is Gaussian too. The operations can also be classified as active or passive. An active operation is an operation that does not conserve the number of photons in the state while a passive one conserves the mean photon number. Finally, the unitaries can also be classified depending on the number of modes involved. Indeed, some operations involve only one mode while others make an interaction between several modes. We separate the operations according to this property (single-mode/two-mode interactions) in the rest of this section. Before doing that, we give some generalities about Gaussian unitaries and how they change states and their quadratures. The transformations will be written $\hat{U}$. $\hat{U}$ is unitary, which means that $\hat{U}^\dagger \hat{U} = \hat{U}\hat{U}^\dagger = \mathbb{1}$ and hence $\hat{U}^\dagger = \hat{U}^{-1}$. Applying such a transformation to a state $\hat{\rho}$ gives a new state $\hat{\rho}'$

$$\hat{\rho} \to \hat{\rho}' = \hat{U}\hat{\rho}\hat{U}^\dagger. \tag{2.80}$$

If the unitary is Gaussian, it can be generated as $\hat{U} = e^{-i\hat{H}}$ by a Hamiltonian $\hat{H}$ having the property that it is a polynomial of second order in the creation and annihilation operators. Since the Hamiltonian is hermitian, $\hat{H} = \hat{H}^\dagger$, the operator $\hat{U}$ is indeed unitary:

$$\hat{U}^\dagger \hat{U} = e^{i\hat{H}} e^{-i\hat{H}} = \mathbb{1}. \tag{2.81}$$

A Hamiltonian of second order in the creation and annihilation operators can be written under the general form

$$\hat{H} = i(\vec{a}^\dagger \vec{\alpha} + \vec{a}^\dagger F \vec{a} + \vec{a}^\dagger G \vec{a}^{\dagger T}) + \text{H.c.}, \tag{2.82}$$

where $\vec{a}$ is the vector of the annihilation operators ($\vec{a} = \{\hat{a}_1, \hat{a}_2, ..., \hat{a}_n\}$), $\vec{a}^\dagger$ is the vector of the creation operators, $\vec{\alpha}$ is a complex vector of dimension n, F and G are $n \times n$ complex matrices and H.c. stands for Hermitian conjugate.

We can analyze the effect of such an operation in terms of the transformation of the annihilation operators and creation operators or in terms of its action on the quadratures. The annihilation operators are transformed following a linear unitary Bogoliubov transformation:

$$\vec{a} \to \hat{U}^\dagger \vec{a} \hat{U} = A\vec{a} + B\vec{a}^\dagger + \vec{\alpha}, \tag{2.83}$$

where A and B are $n \times n$ complex matrices satisfying $AB^T = BA^T$ and $AA^\dagger = BB^\dagger + \mathbb{1}$. The values of the matrices A and B depend on the values of the matrices F and G following lengthy calculations which are not detailed here. These calculations are simplified when dealing with particular examples. The description of the modification of the quadratures is easier as it is given by an affine map:

$$\vec{r} \to \mathcal{S}\vec{r} + \vec{d}, \tag{2.84}$$

where $\vec{r}$ is the vector of dimension $2n$ already defined in Eq. (2.40), $\vec{d}$ is a real vector of dimension $2n$ and $\mathcal{S}$ is a real symplectic matrix of dimension $2n$ which can also be derived from A and B by doing long calculations. A symplectic matrix is a matrix satisfying [136]

$$\mathcal{S}\Omega\mathcal{S}^T = \Omega, \tag{2.85}$$

where Ω is the symplectic form

$$\Omega = \bigoplus_{k=1}^{n} \omega,\ \omega = \begin{pmatrix} 0 & 1 \\ -1 & 0 \end{pmatrix}. \tag{2.86}$$

This matrix has to be symplectic to preserve the commutation relations between the quadratures. Finally, as Gaussian states are completely defined by their displacement vector and their covariance matrix, it is interesting to write the effect of the unitary operation on them:

$$\langle\vec{r}\rangle \to \mathcal{S}\langle\vec{r}\rangle + \vec{d},\ \gamma \to \mathcal{S}\gamma\mathcal{S}^T. \tag{2.87}$$

2.5.1 Single mode operations

Displacement

The displacement unitary is a single-mode active Gaussian unitary. Its effect in phase space is to displace the state. An example is shown in Fig. 2.5 a). In a quantum optics circuit, we can represent a displacement operation as a circle, see Fig. 2.5 a).

The unitary is defined with a complex parameter α:

$$\hat{D}(\alpha) = e^{\alpha\hat{a}^\dagger - \alpha^*\hat{a}}. \tag{2.88}$$

The inverse operation is also a displacement, this time with a parameter $-\alpha$:

$$\hat{D}^{-1}(\alpha) = \hat{D}(-\alpha). \tag{2.89}$$

Coherent states can be created by applying a displacement operator on the vacuum state

$$|\alpha\rangle = \hat{D}(\alpha)|0\rangle. \tag{2.90}$$

This constitutes an alternative definition of a coherent state: a coherent state $|\alpha\rangle$ is a state obtained by displacing the vacuum of α in phase space.

The effect of the displacement on the creation and annihilation operators is given by

$$\begin{aligned} \hat{D}^\dagger(\alpha)\hat{a}\hat{D}(\alpha) &= \hat{a} + \alpha, \\ \hat{D}^\dagger(\alpha)\hat{a}^\dagger\hat{D}(\alpha) &= \hat{a}^\dagger + \alpha^*, \end{aligned} \tag{2.91}$$

while the quadratures change as

$$\begin{aligned}\hat{D}^{\dagger}(\alpha)\hat{x}\hat{D}(\alpha) &= \hat{x} + \sqrt{2}\mathcal{R}e(\alpha),\\ \hat{D}^{\dagger}(\alpha)\hat{p}\hat{D}(\alpha) &= \hat{p} + \sqrt{2}\mathcal{I}m(\alpha).\end{aligned} \tag{2.92}$$

Phase shift

A phase shift can also be called a rotation as its action rotates the distribution in phase space (see Fig. 2.5 b)). Moreover, this unitary corresponds to the free evolution of a harmonic oscillator. It is a passive operation as it conserves the number of photons. In the rest of the thesis, the phase-shift operation will be represented in quantum optics circuits as a square, see Fig. 2.5 b).

The unitary is

$$\hat{R}(\phi) = e^{-i\phi\hat{a}^{\dagger}\hat{a}} = e^{-i\phi\hat{n}}, \tag{2.93}$$

where we see that we can express it using the number operator. The annihilation and creation operators are transformed by multiplying them with a phase:

$$\begin{aligned}\hat{R}^{\dagger}(\phi)\hat{a}\hat{R}(\phi) &= \hat{a}e^{-i\phi},\\ \hat{R}^{\dagger}(\phi)\hat{a}^{\dagger}\hat{R}(\phi) &= \hat{a}^{\dagger}e^{i\phi}.\end{aligned} \tag{2.94}$$

We can write the symplectic matrix associated to a rotation as

$$\mathcal{R}(\phi) = \begin{pmatrix}\cos\phi & \sin\phi\\ -\sin\phi & \cos\phi\end{pmatrix}, \tag{2.95}$$

which is nothing but a rotation matrix. Using this symplectic matrix, we can find the transformed quadratures:

$$\begin{pmatrix}\hat{x}\\ \hat{p}\end{pmatrix} \to \mathcal{R}(\phi)\begin{pmatrix}\hat{x}\\ \hat{p}\end{pmatrix} = \begin{pmatrix}\cos\phi\ \hat{x} + \sin\phi\ \hat{p}\\ -\sin\phi\ \hat{x} + \cos\phi\ \hat{p}\end{pmatrix}. \tag{2.96}$$

Squeezing

The operation of squeezing is an active operation and its unitary is given by

$$\hat{S}(\xi) = e^{\frac{1}{2}(\xi\hat{a}^{\dagger 2} - \xi^{*}\hat{a}^{2})}, \tag{2.97}$$

where $\xi = re^{i\phi}$ is a complex number, r is the squeezing parameter and ϕ is the squeezing angle. $\hat{S}(\xi)$ is a unitary operator and its inverse corresponds to a squeezing with a parameter $-\xi$:

$$\hat{S}^{-1}(\xi) = \hat{S}^{\dagger}(\xi) = \hat{S}(-\xi). \tag{2.98}$$

Using this operator, we can give an alternative definition for squeezed states: a squeezed state is a state obtained after the application of the squeezing operator on the vacuum state $|\xi\rangle = \hat{S}(\xi)|0\rangle$. This is presented in Fig. 2.5 c). Finally, in this thesis, a squeezer will be represented in a circuit as an oval, see Fig. 2.5 c).

Applying a squeezing to the creation and annihilation operators transforms them as the following Bogoliubov transformations

$$\begin{aligned} \hat{S}^\dagger(\xi)\hat{a}\hat{S}(\xi) &= \cosh r\, \hat{a} - e^{i\phi}\sinh r\, \hat{a}^\dagger, \\ \hat{S}^\dagger(\xi)\hat{a}^\dagger\hat{S}(\xi) &= \cosh r\, \hat{a}^\dagger - e^{-i\phi}\sinh r\, \hat{a}. \end{aligned} \tag{2.99}$$

A state with a non-zero squeezing angle ϕ can also be obtained by squeezing along the x axis followed by a rotation using a phase-shifter. Hence, we will in the rest of this paragraph study the particular case $\phi = 0, \xi = r$. In this case, the symplectic matrix associated to a squeezing is

$$\mathcal{S}(r) = \begin{pmatrix} e^{-r} & 0 \\ 0 & e^{r} \end{pmatrix}. \tag{2.100}$$

With this symplectic matrix, the quadratures evolve as

$$\begin{aligned} \hat{x} &\to e^{-r}\hat{x}, \\ \hat{p} &\to e^{r}\hat{p}. \end{aligned} \tag{2.101}$$

General one-mode Gaussian operation

It is possible to define a general unitary such that, applied to the vacuum state, it can generate any one-mode Gaussian state. To do so, we have to combine a displacement, a rotation and a squeezing along the quadrature $\hat{x}$

$$|\alpha, \phi, r\rangle = \hat{D}(\alpha)\hat{R}(\phi)\hat{S}(r)|0\rangle. \tag{2.102}$$

It is important to note that the order of the application of the unitaries is important as they do not commute $\hat{D}(\alpha)\hat{S}(\xi) \neq \hat{S}(\xi)\hat{D}(\alpha)$. However, it is possible to obtain the same Gaussian state by applying the operation in another order with the parameters α, ϕ and r adapted.

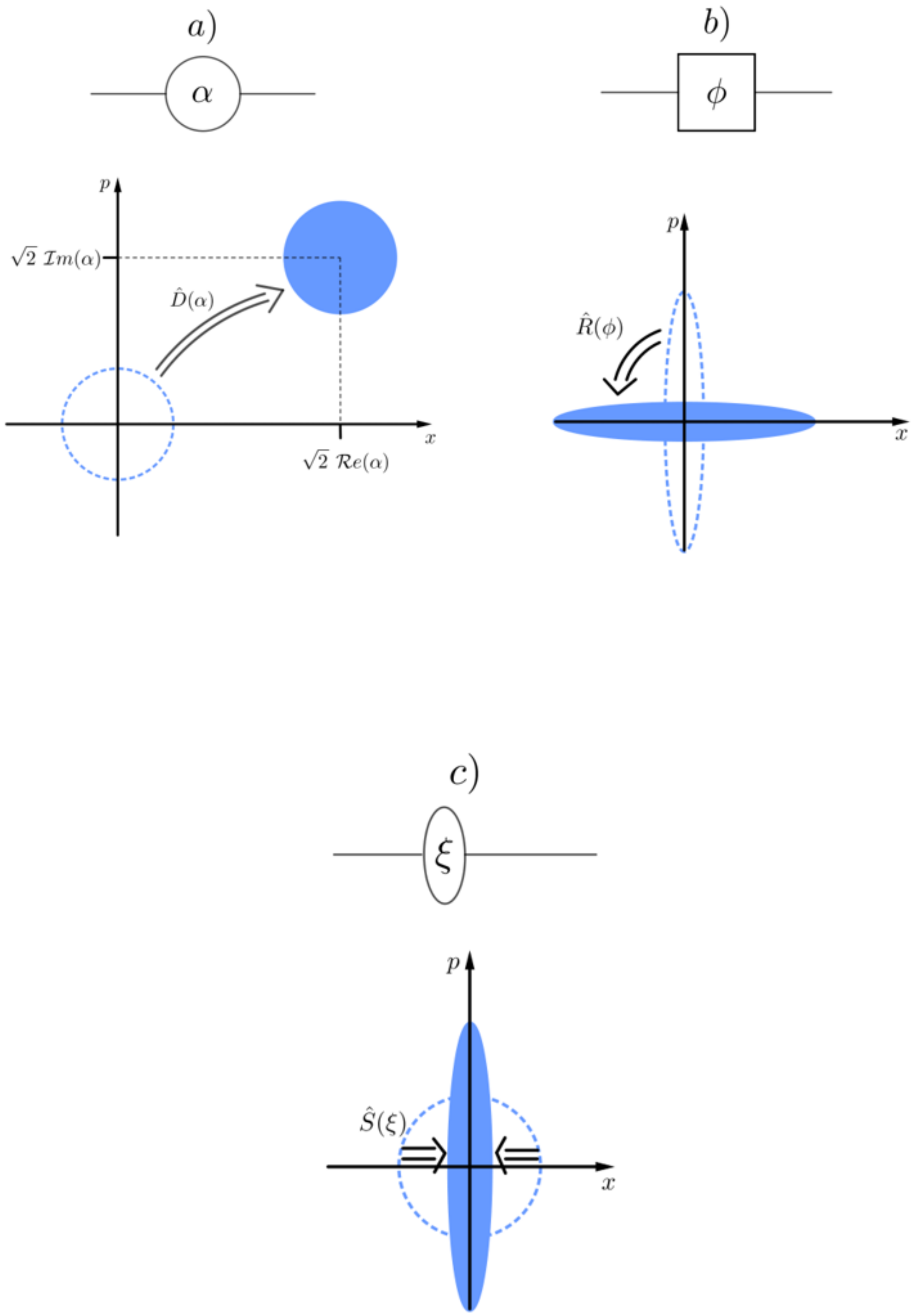

Figure 2.5: Representation of one-mode Gaussian unitaries and their effect in quantum phase-space: a) displacement operation, b) phase-shift operation, c) single-mode squeezing.

2.5.2 Two-mode operations

Beam splitter

The beam splitter is one of the most important two-mode Gaussian unitaries. It constitutes the simplest example of an interferometer and we will represent it in circuits as in Fig. 2.6 a). The unitary is defined by

$$\hat{B}(\theta) = e^{\theta(\hat{a}^\dagger \hat{b} - \hat{a}\hat{b}^\dagger)}, \tag{2.103}$$

where $\hat{a}$ and $\hat{b}$ are the annihilation operators corresponding to the two modes and θ is a parameter that describe the transmittivity of the beam splitter. Indeed, the transmittivity is given by

$$\tau = \cos^2(\theta). \tag{2.104}$$

If this transmittivity is equal to $\frac{1}{2}$, we call this a 50:50 beam splitter or balanced beam splitter. The reflectivity of the beam splitter can be deduced from the transmittivity, $r = 1 - \tau$. The annihilation operators of the two modes are transformed as

$$\begin{aligned} \hat{B}^\dagger(\tau)\hat{a}\hat{B}(\tau) &= \sqrt{\tau}\hat{a} + \sqrt{1-\tau}\hat{b}, \\ \hat{B}^\dagger(\tau)\hat{b}\hat{B}(\tau) &= -\sqrt{1-\tau}\hat{a} + \sqrt{\tau}\hat{b}. \end{aligned} \tag{2.105}$$

We can find the transformations of the creation operators by taking the adjoints of these expressions. The symplectic matrix associated to a beam splitter is given by

$$\mathcal{B}(\tau) = \begin{pmatrix} \sqrt{\tau} & 0 & \sqrt{1-\tau} & 0 \\ 0 & \sqrt{\tau} & 0 & \sqrt{1-\tau} \\ -\sqrt{1-\tau} & 0 & \sqrt{\tau} & 0 \\ 0 & -\sqrt{1-\tau} & 0 & \sqrt{\tau} \end{pmatrix}, \tag{2.106}$$

and the quadratures transform then as

$$\begin{pmatrix} \hat{x}_1 \\ \hat{p}_1 \\ \hat{x}_2 \\ \hat{p}_2 \end{pmatrix} \to \mathcal{B}(\tau) \begin{pmatrix} \hat{x}_1 \\ \hat{p}_1 \\ \hat{x}_2 \\ \hat{p}_2 \end{pmatrix}. \tag{2.107}$$

A property of the beam splitter that we will use in what follows is that if the two inputs are identical centered Gaussian states, the beam splitter does not change the states, *i.e.*, the output is the same as the input.

Note that, here, we used the general convention for the definition of the beam splitter. However, sometimes it is more convenient to define the action of the beam splitter as:

$$\begin{pmatrix} \hat{a}' \\ \hat{b}' \end{pmatrix} = \begin{pmatrix} \sqrt{\tau} & \sqrt{1-\tau} \\ \sqrt{1-\tau} & -\sqrt{\tau} \end{pmatrix} \begin{pmatrix} \hat{a} \\ \hat{b} \end{pmatrix}. \tag{2.108}$$

In the result chapters, we will always precise which convention is used before using it.

Two-mode squeezing

The Gaussian unitary associated to a two-mode squeezer is

$$\hat{S}_2(r) = e^{\frac{r}{2}(\hat{a}\hat{b} - \hat{a}^\dagger \hat{b}^\dagger)}, \tag{2.109}$$

where r is a parameter quantifying the two-mode squeezing. This operation is not a new one as it can be obtained by using two balanced beam splitters and two one-mode squeezers with opposite parameters (ξ and $-\xi$). This is presented in Fig. 2.6 b). First, the two modes interact in a 50:50 beam splitter then one mode is squeezed while the other mode is anti-squeezed. Finally, they interact again in a balanced beam splitter. Knowing this decomposition, we can find the symplectic matrix associated to the two-mode squeezer:

$$\begin{aligned} \mathcal{S}_2(r) &= \mathcal{B}\left(\frac{1}{2}\right)^T (\mathcal{S}(-r) \otimes \mathcal{S}(r))\, \mathcal{B}\left(\frac{1}{2}\right), \\ &= \begin{pmatrix} \cosh r & 0 & \sinh r & 0 \\ 0 & \cosh r & 0 & -\sinh r \\ \sinh r & 0 & \cosh r & 0 \\ 0 & -\sinh r & 0 & \cosh r \end{pmatrix}. \end{aligned} \tag{2.110}$$

The quadratures are then transformed as:

$$\begin{pmatrix} \hat{x}_1 \\ \hat{p}_1 \\ \hat{x}_2 \\ \hat{p}_2 \end{pmatrix} \rightarrow \mathcal{S}_2(r) \begin{pmatrix} \hat{x}_1 \\ \hat{p}_1 \\ \hat{x}_2 \\ \hat{p}_2 \end{pmatrix}. \tag{2.111}$$

Interestingly enough, applying this two-mode squeezer to a two-mode vacuum state generates an EPR state.

$$|\text{EPR}\rangle = \mathcal{S}_2(r)|00\rangle. \tag{2.112}$$

Finally, starting from the EPR state, we can obtain a thermal state with a parameter $\bar{n} = \sinh^2 r$ by tracing out the second mode:

$$\hat{\rho}_q = \text{Tr}_2(|\text{EPR}\rangle\langle\text{EPR}|). \tag{2.113}$$

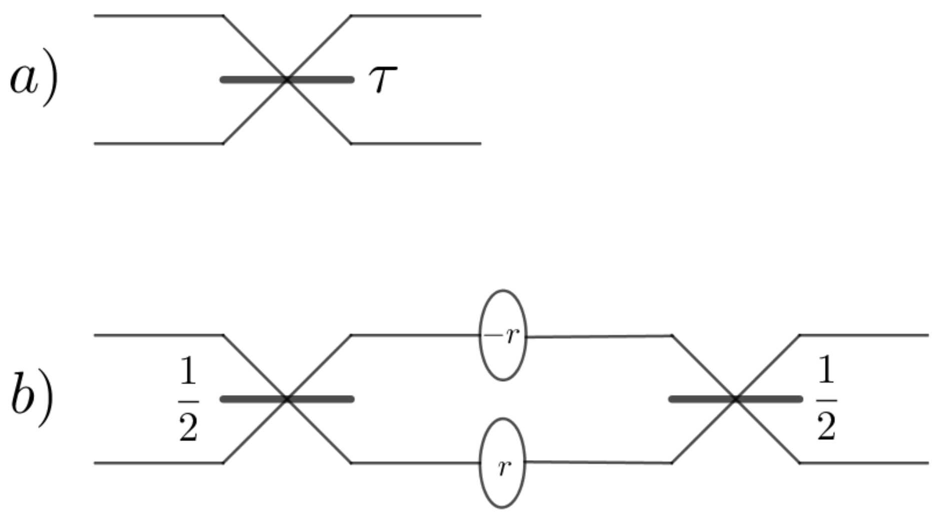

Figure 2.6: Representation of two-mode Gaussian unitaries and their effect in quantum phase-space: a) beam splitter and b) two-mode squeezer.

Chapter 3

Notion of nonclassicality and nonclassicality witnesses

Quantum states can be divided in two categories: classical and nonclassical states. As its name indicates, a classical state is a state presenting all the common properties that are expected from states described by classical theories. On the other side, a nonclassical state is a state that presents properties that cannot be described by classical theories. Such states are very important in quantum optics as their nonclassical properties can be seen as resources for quantum information protocols. The use of nonclassical states is at the origin of quantum advantages in areas such as quantum computation but we can also mention distributed quantum computing, quantum networks, quantum boson sampling, quantum metrology or quantum communication [114, 145, 85, 139, 162, 138, 88, 44, 123]. Moreover, it has been proven that nonclassicality is a necessary condition to create entanglement with a beam splitter and entanglement is one of the biggest features that differentiates classical and quantum theory [83]. Given its importance in quantum information, entanglement will be treated separately in Chapter 4.

Knowing the importance of the nonclassical states, it is necessary to have a clear definition of what a nonclassical state is and how to detect it. In this chapter, we start by defining when a state is considered as nonclassical and then we review some of the criteria whose violation signals nonclassicality. Among the nonclassicality criteria, two are very important in this thesis: the Shchukin, Richter and Vogel criteria and the quadrature coherence scale. Indeed, Chapters 6 and 7 focus on how to measure these criteria by using a multicopy measurement technique. Finally, we shortly outline the link between nonclassicality and entanglement.

3.1 Definition of optical nonclassicality

The definition of optical nonclassicality is based on the P-Sudarshan function defined in Subsection 2.3.2. However, we must mention that there exist several definitions of nonclassicality.

In this thesis, we focus on the optical nonclassicality (based on the P-Sudarshan function) but it is also possible to study the nonclassicality of a state based on the negativity of its Wigner function [23] (where the nonclassicality of the state is witnessed by the negativity of the Wigner function) or based on the zeros of its Husimi function [97]. With these definitions, the ensemble of nonclassical states is not the same as the one for optical nonclassicality. Hence, these other definitions will not be used in this thesis; we will only define the nonclassicality of a state based on its P-Sudarshan function.

As a reminder, every state can be expressed using the P-Sudarshan distribution as

$$\hat{\rho} = \int d^2\alpha \; P(\alpha)|\alpha\rangle\langle\alpha|. \tag{3.1}$$

As presented is Subsection 2.3.2, the P-Sudarshan function can have negative values and can be ill-behaved (it can contain derivative of Dirac delta distributions). This is at the basis of the definition of a nonclassical state: if the P-Sudarshan function is not a probability distribution, the state is nonclassical [151]. Conversely, if the P-function of a state can be identified as a classical probability distribution, the state is said to be classical. If P is a probability distribution function, it means that it is positive everywhere and at most proportional to the Dirac delta function (but not its derivative). The Dirac delta distribution ($P(\alpha) = \delta(\alpha - \alpha')$) corresponds to the P-function of a coherent state:

$$\hat{\rho} = \int d^2\alpha' \; \delta(\alpha - \alpha')|\alpha'\rangle\langle\alpha'| = |\alpha\rangle\langle\alpha|. \tag{3.2}$$

This is logical as we already mentioned the fact that the coherent states are also often called classical states. All other classical states can always be written as convex mixtures of coherent states. For example, thermal states fulfill this condition and are hence classical.

The whole study in this thesis is based on the fact that coherent states are classical states. We must mention that all scientists do not agree on this definition. Indeed, some people consider that coherent states are nonclassical states as they are used in some quantum protocols such as for example continuous-variable quantum key distribution [53]. However, according to the definition of optical nonclassicality, coherent states are classical states and it is thus the convention we use in this thesis.

Among the states studied in Chapter 2, the squeezed states, the cat states and the Fock states do not have P-functions which correspond to proper probability distributions (their expressions involve derivatives of Dirac delta-functions) and are thus nonclassical (see Chapter 6).

The definition of optical nonclassicality is based on the P-Sudarshan function. Hence, to identify nonclassical states, the first idea one could have would be to analyze the P-function of a given state. However, determining the P-function of a given state requires full tomography and is often unfeasible. Therefore, one instead prefers nonclassicality witnesses which correspond to conditions on expectation values of suitably chosen hermitian operators fulfilled by classical states. Thus, nonclassicality is demonstrated when such a condition is violated. In what follows, we describe some of the well-known witnesses for nonclassicality.

3.2 Witnesses for detecting nonclassicality

3.2.1 Mandel parameter

This witness is due to Mandel [100]. He noticed that the coherent states have a Poissonian photon number distribution as shown in Eq. (2.56). According to the definition, a state is classical if it can be expressed as a convex mixture of coherent states. This implies that the photon number distribution of a classical state can only be wider than a Poissonian distribution. Mandel thus stated that if the photon number distribution of a state is narrower than a Poissonian distribution, then it is nonclassical. Such distributions are called sub-Poissonian distributions.

To express this mathematically, we introduce the Mandel parameter Q_M:

$$Q_M = \frac{\langle (\hat{a}^\dagger \hat{a})^2 \rangle - \langle \hat{a}^\dagger \hat{a} \rangle^2 - \langle \hat{a}^\dagger \hat{a} \rangle}{\langle \hat{a}^\dagger \hat{a} \rangle} = \frac{\sigma_n^2}{\langle \hat{a}^\dagger \hat{a} \rangle} - 1, \tag{3.3}$$

where σ_n^2 is the variance of the photon number $\hat{n} = \hat{a}^\dagger \hat{a}$. Coherent states have Poissonian photon number distributions and therefore, the variance of their number of photons is equal to the mean number of photons, resulting in $Q_M = 0$. If the distribution is narrower, then the variance is lower than the mean and thus $Q_M < 0$, which is an evidence of nonclassicality. Otherwise, if $Q_M \geq 0$, the witness is inconclusive; we can not conclude if the state is nonclassical or not.

It is possible to prove rigorously that Mandel parameter can only become negative for nonclassical states. To do so, we have to analyze the numerator of Eq. (3.3) (the denominator is always non-negative):

$$\langle (\hat{a}^\dagger \hat{a})^2 \rangle - \langle \hat{a}^\dagger \hat{a} \rangle^2 - \langle \hat{a}^\dagger \hat{a} \rangle = \langle \hat{a}^{\dagger 2} \hat{a}^2 \rangle - \langle \hat{a}^\dagger \hat{a} \rangle^2, \tag{3.4}$$

by using the bosonic commutation relations. Then, we express the two remaining terms by using the P-Sudarshan function (Eq. (2.35)):

$$\begin{aligned} \langle \hat{a}^{\dagger 2} \hat{a}^2 \rangle &= \int d^2\alpha \, P(\alpha) \alpha^{*2} \alpha^2, \\ \langle \hat{a}^\dagger \hat{a} \rangle &= \int d^2\alpha \, P(\alpha) \alpha^* \alpha, \end{aligned} \tag{3.5}$$

leading to

$$\langle (\hat{a}^\dagger \hat{a})^2 \rangle - \langle \hat{a}^\dagger \hat{a} \rangle^2 - \langle \hat{a}^\dagger \hat{a} \rangle = \int d^2\alpha \, P(\alpha) (\alpha^* \alpha - \langle \alpha^* \alpha \rangle_P)^2. \tag{3.6}$$

As the value of "$(\alpha^* \alpha - \langle \alpha^* \alpha \rangle_P)^2$" in the integral is always positive, the integral can only be negative if the P-Sudarshan function shows negative values. Hence, $Q_M < 0$ only if the state is nonclassical.

This criterion detects the nonclassicality of Fock states, in which case $Q_M = -1$. However, some nonclassical states such as the squeezed states lead to positive values of the Mandel parameter and are therefore not identified as nonclassical by this criterion. There is a need to develop other criteria.

3.2.2 Squeezing parameter

This witness is based on a rotated quadrature:

$$\hat{x}_\theta = \frac{\hat{a}e^{-i\theta} + \hat{a}^\dagger e^{i\theta}}{\sqrt{2}}, \tag{3.7}$$

where $\theta \in [0, 2\pi[$ describes the angle of the quadrature. For example, $\theta = 0$ corresponds to the usual quadrature $\hat{x}$ while $\theta = \frac{\pi}{2}$ is the p-quadrature. The squeezing parameter is given by:

$$S_\theta = \langle : \hat{x}_\theta^2 : \rangle - \langle \hat{x}_\theta \rangle^2, \tag{3.8}$$

where : : corresponds to the normal order. By developing the first term and putting it in normal order, we can reexpress the squeezing parameter as

$$S_\theta = \left\langle \frac{\hat{a}^2 e^{-2i\theta} + \hat{a}^{\dagger 2} e^{2i\theta} + 2\hat{a}^\dagger \hat{a}}{2} \right\rangle - \left\langle \frac{\hat{a}e^{-i\theta} + \hat{a}^\dagger e^{i\theta}}{\sqrt{2}} \right\rangle^2. \tag{3.9}$$

Once again, this parameter is equal to 0 for coherent states. Indeed, we have

$$\begin{aligned} S_\theta &= \langle \alpha | \frac{\hat{a}^2 e^{-2i\theta} + \hat{a}^{\dagger 2} e^{2i\theta} + 2\hat{a}^\dagger \hat{a}}{2} | \alpha \rangle - \langle \alpha | \frac{\hat{a}e^{-i\theta} + \hat{a}^\dagger e^{i\theta}}{\sqrt{2}} | \alpha \rangle^2, \\ &= \frac{\alpha^2 e^{-2i\theta} + \alpha^{*2} e^{2i\theta} + 2\alpha^{*\dagger}\alpha}{2} - \left(\frac{\alpha e^{-i\theta} + \alpha^* e^{i\theta}}{\sqrt{2}} \right)^2, \\ &= 0. \end{aligned} \tag{3.10}$$

It can be proven that the squeezing parameter can be negative only if the state is nonclassical. To prove this, the same method as the proof for the Mandel parameter is used: the parameter is expressed as a function of the P-Sudarshan function using Eq. (2.35), then we obtain an integral that can be negative only if the P-function takes negative values.

Similarly to the Mandel parameter, the squeezing parameter is only a sufficient criterion. It is not able to detect the nonclassicality of all the nonclassical states; for example, the squeezing parameter is positive for Fock states. This time, however, it is negative for squeezed states. In this sense, it is complementary to the Mandel parameter. We thus still need other witnesses. Note that more details can be found on the squeezing witness in the case of mixed states in Ref. [2].

3.2.3 Shchukin, Richter and Vogel matrix of moments

A part of this section is based on the following paper that I published together with Matthieu Arnhem and Nicolas Cerf:

M. Arnhem, C. Griffet and N. J. Cerf. Multicopy observables for the detection of optically nonclassical states. Physical Review A, 106: 043705, October 2022. [6]

One of the two most important witnesses of this thesis is based on a matrix of moments. This was first presented in Ref. [142, 140] by Shchukin, Richter and Vogel. We present here the development leading to this witness and give some of its properties.

As shown in Subsection 2.3.2, the expectation value of a normally-ordered function of the annihilation $\hat{a}$ and creation $\hat{a}^\dagger$ operators can be expressed using the P-function as it is the quasi-probability distribution associated with the normal order. We can then express the expectation value of any normally-ordered operator function $:\hat{g}(\hat{a},\hat{a}^\dagger):$ as

$$\langle :\hat{g}(\hat{a},\hat{a}^\dagger): \rangle = \int d^2\alpha \, P(\alpha) \, g(\alpha,\alpha^*). \tag{3.11}$$

Hence, if the P function $P(\alpha)$ admits negative values, then Eq. (3.11) can become negative for some well chosen function $\hat{g}(\hat{a},\hat{a}^\dagger)$. These negative values are a clear evidence of the nonclassicality of the state $\hat{\rho}$ as indicated by the definition of nonclassicality (see Section 3.1). This suggests a close connection between the expectation value of normally-ordered functions and the nonclassical character of the P function: as observed in Ref. [140], any normally-ordered Hermitian operator of the form $:\hat{f}^\dagger\hat{f}:$ can be used to detect nonclassicality. As shown in Ref. [142], these witnesses of nonclassicality can be constructed for three different sets of operators $(\hat{a},\hat{a}^\dagger)$, $(\hat{x}_\phi,\hat{p}_\phi)$ and $(\hat{x}_\phi,\hat{n})$. Note that the operators used for the construction do not need to be conjugate variables (as shown by the last set of operators considered by the authors, $(\hat{x}_\phi,\hat{n})$). In this thesis, we only consider the set $(\hat{a},\hat{a}^\dagger)$. In this case, one exploits the fact that any operator $\hat{f}$ can be expressed as a (normally-ordered) Taylor series

$$\hat{f}(\hat{a},\hat{a}^\dagger) = \sum_{k=0}^{\infty}\sum_{l=0}^{\infty} c_{kl}\, \hat{a}^{\dagger k}\, \hat{a}^l. \tag{3.12}$$

The expectation value of $:\hat{f}^\dagger\hat{f}:$ can then be written in terms of the P function following Eq. (3.11) as

$$\langle :\hat{f}^\dagger\hat{f}: \rangle = \int d^2\alpha \, P(\alpha) \, |f(\alpha)|^2, \tag{3.13}$$

where $f(\alpha) = \sum_{k=0}^{\infty}\sum_{l=0}^{\infty} c_{kl}\, \alpha^{*k}\, \alpha^l$. This expression is always positive for any $f(\alpha)$ provided $P(\alpha)$ is a classical probability distribution $P_{cl}(\alpha)$ as it is then positive everywhere. Hence, for any nonclassical state $\hat{\rho}$ there exists an appropriate operator $\hat{f}$, such that this state is witnessed, *i.e.*

$$\forall \text{ nonclassical } \hat{\rho} \; \exists \hat{f} \qquad \text{s.t.} \qquad \langle :\hat{f}^\dagger \hat{f}: \rangle < 0. \tag{3.14}$$

Furthermore, as shown in Ref. [140], these nonclassicality criteria can be reformulated in terms of an infinite countable set of inequalities, which involve the principal minors of an infinite-dimensional matrix of moments. The infinite set of inequalities completely characterizes the nonclassicality of the quantum state under study.

To obtain this set of inequalities, we first express the necessary and sufficient criterion for classicality by injecting the expression of $\hat{f}$ (Eq. (3.12)) in Eq. (3.14):

$$\langle :\hat{f}^\dagger \hat{f}: \rangle = \sum_{k,m=0}^{\infty} \sum_{l,n=0}^{\infty} c_{mn}^* c_{kl} \, \langle \hat{a}^{\dagger(k+n)} \, \hat{a}^{l+m} \rangle \geq 0, \;\; \forall \hat{f}, \tag{3.15}$$

for any complex coefficients c_{ij}'s. To go further, the authors use Sylvester's criterion which is a necessary and sufficient condition to determine if a Hermitian matrix is positive-definite. The Hermitian matrix considered here is the matrix D_∞ which is an infinite matrix associated with the quadratic form, Eq. (3.15). Then, Sylvester's criterion states that the matrix if positive-definite (and thus that the state is classical) if all the determinants of the matrix of moments D_N are non-negative. These submatrices D_N are defined as

$$D_N = \begin{pmatrix} 1 & \langle \hat{a} \rangle & \langle \hat{a}^\dagger \rangle & \langle \hat{a}^2 \rangle & \langle \hat{a}^\dagger \hat{a} \rangle & \langle \hat{a}^{\dagger 2} \rangle & \dots \\ \langle \hat{a}^\dagger \rangle & \langle \hat{a}^\dagger \hat{a} \rangle & \langle \hat{a}^{\dagger 2} \rangle & \langle \hat{a}^\dagger \hat{a}^2 \rangle & \langle \hat{a}^{\dagger 2} \hat{a} \rangle & \langle \hat{a}^{\dagger 3} \rangle & \dots \\ \langle \hat{a} \rangle & \langle \hat{a}^2 \rangle & \langle \hat{a}^\dagger \hat{a} \rangle & \langle \hat{a}^3 \rangle & \langle \hat{a}^\dagger \hat{a}^2 \rangle & \langle \hat{a}^{\dagger 2} \hat{a} \rangle & \dots \\ \langle \hat{a}^{\dagger 2} \rangle & \langle \hat{a}^{\dagger 2} \hat{a} \rangle & \langle \hat{a}^{\dagger 3} \rangle & \langle \hat{a}^{\dagger 2} \hat{a}^2 \rangle & \langle \hat{a}^{\dagger 3} \hat{a} \rangle & \langle \hat{a}^{\dagger 4} \rangle & \dots \\ \langle \hat{a}^\dagger \hat{a} \rangle & \langle \hat{a}^\dagger \hat{a}^2 \rangle & \langle \hat{a}^{\dagger 2} \hat{a} \rangle & \langle \hat{a}^\dagger \hat{a}^3 \rangle & \langle \hat{a}^{\dagger 2} \hat{a}^2 \rangle & \langle \hat{a}^{\dagger 3} \hat{a} \rangle & \dots \\ \langle \hat{a}^2 \rangle & \langle \hat{a}^3 \rangle & \langle \hat{a}^\dagger \hat{a}^2 \rangle & \langle \hat{a}^4 \rangle & \langle \hat{a}^\dagger \hat{a}^3 \rangle & \langle \hat{a}^{\dagger 2} \hat{a}^2 \rangle & \dots \\ \vdots & \vdots & \vdots & \vdots & \vdots & \vdots & \ddots \end{pmatrix}, \tag{3.16}$$

and contain all normally-ordered moments of $\hat{a}$ and $\hat{a}^\dagger$. The matrix of moments D_N, where N is the size of the matrix, can be defined for any dimension $N \times N$ and its determinant will be written $d_{1\cdots N} = \det(D_N)$ in the rest of this thesis, where the index of d means that all rows and columns of D_N are kept in the range from 1 to N. Remarkably, as a consequence of Bochner's theorem, the classicality criteria become necessary and sufficient when the determinants are positive for all orders [142], that is, $\hat{\rho}$ is classical if and only if

$$d_{1\dots N} \geq 0, \; \forall N. \tag{3.17}$$

The determinants $d_{1\dots N}$ are the so-called dominant principal minors of matrix D_N, *i.e.*, the determinants of the matrices constructed by taking all rows and columns in the upper-left corner of the matrix. Hence, the negativity of any single determinant $d_{1\dots N}$ of order N is a sufficient condition for nonclassicality.

One property is that one can construct various matrices of moments having similar properties and nonclassicality detection power. In this thesis, we focus on the principal minors of the matrix of moments D_N, which are built by selecting some rows and corresponding columns and then taking the determinant of the resulting matrix. For example, if rows and columns i, j, and k are selected, the associated principal minor is written d_{ijk}. Interestingly, any principal minor such as d_{ijk} provides a sufficient criterion for nonclassicality: if $d_{ijk} < 0$, then the state $\hat{\rho}$ is nonclassical. Some examples of principal minors that are not dominant are $d_{14}, d_{15}, d_{124}, d_{134}$, and d_{145}, while examples of dominant principal minors are $d_{12}, d_{123}, d_{1234}$, and d_{1235}. Note that we adopt a slightly relaxed definition of a dominant principal minor: it is associated with the upper left submatrix but assuming the order of rows and columns is irrelevant within a given block (the block structure of the matrix of moments D_N will be described in Chapter 6). For example, d_{1235} is understood as a dominant principal minor although the fourth row and column are omitted. Each of these minors might have a distinct physical interpretation and hence, detect the nonclassicality of different types of nonclassical states (see Ref. [105] for a review of nonclassicality criteria).

To measure these witnesses, Shchukin and Vogel designed circuits in Ref. [142]. However, their circuits are designed to measure each moment of the matrix one by one. This means that to calculate one determinant, we need to make one measure for each element. One of the objective of this thesis is to find a less costly protocol to measure these determinants by using a multicopy technique. This is done in Chapter 6.

3.2.4 Quadrature coherence scale

A part of this section is based on the following paper that I published together with Matthieu Arnhem, Stephan De Bièvre and Nicolas Cerf:

C. Griffet, M. Arnhem, S. De Bièvre, and N. J. Cerf. Interferometric measurement of the quadrature coherence scale using two replicas of a quantum optical state. Physical Review A, 108: 023730, August 2023. [50]

In this section, we focus on a witness of optical nonclassicality called the quadrature coherence scale (QCS), introduced in Ref. [30] and further studied in Refs. [75, 62, 61, 63]. When it was first defined [30], the QCS was called the ordering sensitivity as it was linked to the change in the s-ordered entropy that is defined in that paper. Later, it was renamed QCS [62] as it can be proven to be linked to the coherences with respect to the quadratures of the state.

The QCS of the state $\hat{\rho}$ of n bosonic modes is denoted as $\mathcal{C}(\hat{\rho})$. There exist several definitions of the QCS but the most common one is the following [30, 62]:

$$\mathcal{C}^2(\hat{\rho}) = \frac{1}{2n\,\mathcal{P}(\hat{\rho})} \left(\sum_{j=1}^{2n} \mathrm{Tr}\,\left([\hat{\rho}, \hat{r}_j][\hat{r}_j, \hat{\rho}] \right) \right), \tag{3.18}$$

where $\hat{\mathbf{r}} = (\hat{x}_1, \hat{p}_1, \cdots, \hat{x}_n, \hat{p}_n)$ is the vector of position and momentum quadratures, and $\mathcal{P}(\hat{\rho}) = \mathrm{Tr}(\hat{\rho}^2)$ is the purity of the state $\hat{\rho}$ that was already defined in Eq. (2.43). It was shown in Ref. [30] that the QCS is a witness of optical nonclassicality: if $\mathcal{C}(\hat{\rho}) > 1$, then the state $\hat{\rho}$ is nonclassical. Since the converse is not true, this witness is not faithful, *i.e.* not necessary and sufficient. It nevertheless provides both an upper and lower bound on some suitably defined distance from the set of optically classical states $\mathcal{C}_{\mathrm{cl}}$ and, as such, it defines an optical nonclassicality measure [30]:

$$\mathcal{C}(\hat{\rho}) - 1 \leq d(\hat{\rho}, \mathcal{C}_{\mathrm{cl}}) \leq \mathcal{C}(\hat{\rho}), \tag{3.19}$$

where $d(\hat{\rho}, \mathcal{C}_{\mathrm{cl}})$ is the distance to the classical set of states. In particular, the larger the QCS, the farther the state is from $\mathcal{C}_{\mathrm{cl}}$. In addition, $\mathcal{C}^2(\hat{\rho})$ has a direct physical interpretation as being inversely proportional to the decoherence time of $\hat{\rho}$ [62].

Another expression of the QCS presented in Ref. [30] will be used in this thesis:

$$\mathcal{C}^2(\hat{\rho}) = \frac{1}{4} \frac{\|\nabla_\alpha W\|_2^2}{\|W\|_2^2}, \tag{3.20}$$

where W is the Wigner function of the state and $\|\cdot\|_2$ stands for the L^2-norm, such that for example $\|W\|_2^2 := \int d^2\alpha \, |W(\alpha)|^2$ and $\nabla_\alpha = (\partial_{\alpha_1}, \partial_{\alpha_2})$. Intuitively, this means that if the Wigner function of the state oscillates a lot, then the QCS is bigger. Comparing the Wigner functions of different states can lead to an intuition about the QCS of these states. For example, in Ref. [30], the authors compare two families of states:

$$\hat{\rho}_{2M} = \frac{1}{2M} \sum_{n=1}^{2M} |n\rangle\langle n|, \quad \hat{\rho}_{\mathrm{even},M} = \frac{1}{M} \sum_{n=1}^{M} |2n\rangle\langle 2n|. \tag{3.21}$$

with $M \geq 1$. The purity and QCS of these states are given in Ref. [30]:

$$\mathcal{P}(\hat{\rho}_{2M}) = \frac{1}{2M}, \quad \mathcal{P}(\hat{\rho}_{\mathrm{even},M}) = \frac{1}{M}, \tag{3.22}$$

and

$$\mathcal{C}^2(\hat{\rho}_{2M}) = 1 + \frac{1}{M}, \quad \mathcal{C}^2(\hat{\rho}_{\mathrm{even},M}) = 1 + 2(M+1). \tag{3.23}$$

We see that the QCS of the two states are bigger than 1, showing the nonclassicality of these families of states. It also appears that the QCS of $\hat{\rho}_{\mathrm{even},M}$ increases proportionally to M while for the other class of states, there is no such increase. This can be linked to the fact that the Wigner function of $\hat{\rho}_{\mathrm{even},M}$ shows deeper fluctuations as can be seen in Fig. 3.1.

The evaluation of the QCS on large families of benchmark states has confirmed its efficiency as an optical nonclassicality measure [30, 75, 62, 61, 63]. One important example is the case of a Gaussian state. It was proven in Ref. [61] that the QCS is then given by

$$\mathcal{C}^2(\hat{\rho}_G) = \frac{\mathrm{Tr}\gamma^{-1}}{4n}, \tag{3.24}$$

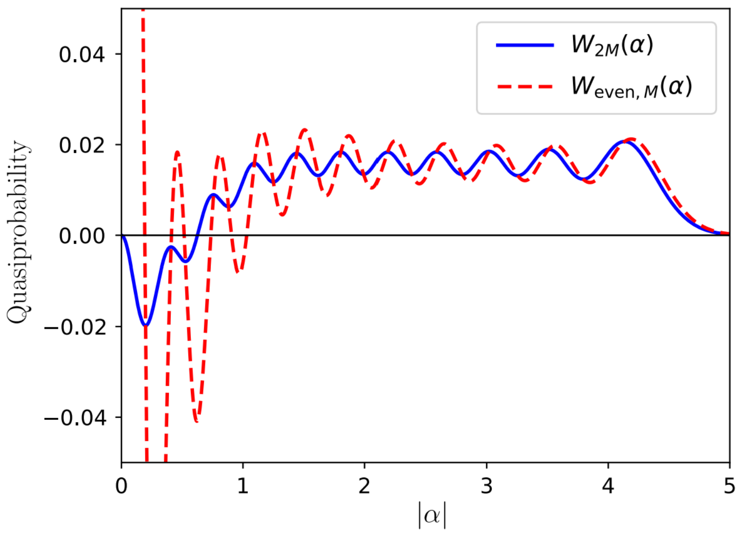

Figure 3.1: Wigner function of $\hat{\rho}_{2M}$ and $\hat{\rho}_{\mathrm{even},M}$ for $M = 10$. For larger fluctuations around the mean of the Wigner function, the QCS increases. (Figure taken from Ref. [30]).

where γ is the covariance matrix of the state. We will prove again this expression using the formalism developed in Chapter 7.

The values of the QCS for two particular Gaussian states are of interest in this thesis as we will use them in Chapter 7: the values for the squeezed states and the value for the thermal states,

$$\begin{aligned} \mathcal{C}^2(|\xi\rangle) &= \cosh(2r), \\ \mathcal{C}^2(\hat{\rho}_q) &= \frac{1}{1 + 2\langle \hat{n} \rangle_q}, \end{aligned} \tag{3.25}$$

respectively. In Ref. [49], the authors calculated the values of the QCS in the case of lossy squeezed states or thermal states. They represent the losses by a beam splitter of transmittance η where one entry is the state and the other one is the vacuum. The QCS for these states is then given by

$$\begin{aligned} \mathcal{C}^2(|\xi\rangle;\eta) &= \frac{1}{1 + (1-2\eta)\frac{\eta\cosh(2r)-\eta}{\eta\cosh(2r)-\eta+1}}, \\ \mathcal{C}^2(\hat{\rho}_q;\eta) &= \frac{1}{1 + 2\eta\langle \hat{n} \rangle_q}, \end{aligned} \tag{3.26}$$

which reduces to Eq. (3.25) in the special case of $\eta = 1$, *i.e.* when there are no losses.

3.3 Nonclassicality and entanglement

It has been proven in 2002 that there exists a close connection between nonclassicality and entanglement [83]. Entangled states are multipartite states presenting features that can not be described with classical theories. The well-known case of bipartite entangled states will be presented in detail in the next chapter (Chapter 4). However, we can already mention that they are very important for quantum communication protocols and are thus essential in the field.

Kim *et al.* (Ref. [83]) proved that nonclassicality is needed in order to produce entanglement when using a simple beam splitter. The setup presented in Ref. [83] is the following: the authors use a 50:50 beam splitter where the two inputs are two independent states (*i.e.*, two states that are not entangled). Then, the authors analyze the output to see if the state is entangled or not depending on the input modes.

First, the authors investigate two different kinds of input states: Fock states and squeezed states. It is well known that in these two particular cases, it is possible to produce entanglement. Indeed, inputting one single photon in each input, $|1\rangle\,|1\rangle$, the output state is the famous Hong-Ou-Mandel state (Ref. [69]):

$$|\mathrm{HOM}\rangle = \frac{|2,0\rangle - |0,2\rangle}{\sqrt{2}}, \tag{3.27}$$

which is an entangled state. For squeezed states, we already mentioned that it is possible to obtain a TMSV states which is a maximally entangled state in the limit of an infinite squeezing.

After that, the authors study what happens if the two input states are general mixed Gaussian states. In this case, it is proven that if the two input states are classical, then the output state is not entangled. In conclusion, nonclassicality is then a necessary condition for the creation of entanglement through a 50:50 beam splitter.

Chapter 4

Notion of entanglement and separability criteria

One of the most important features of bipartite states in quantum information is certainly entanglement. Bipartite states are states shared between two parties A and B (often called Alice and Bob). These states can present a particular property called entanglement which is a property that can not be described classically. Entanglement is one of the most important discoveries in quantum optics as it leads to new perspectives for communications that do not exist when considering only classical mechanics. Nowadays, entanglement is at the basis of many quantum communication protocols like quantum teleportation [14] or quantum cryptography [37].

The notion of entanglement arose in 1935 after a paper by Einstein, Podolsky and Rosen [36] who wanted to prove that the quantum theory was not complete. In what follows, we will call this paper EPR after the names of its authors. The term "entanglement" itself was first used by Schrödinger in one of his letters to Einstein. In the EPR paper, the authors propose a thought experiment to prove that there should be a classical theory based on hidden variables that could justify the results of a thought experiment. Later, it was proven that quantum theory is not incomplete and that the results were due to entanglement. Still today, the state that was used for this argument is very important as it corresponds to a maximally entangled state that we call EPR-state (this state was already introduced in Chapter 2).

Since entanglement is very important, it is also crucial to be able to determine whether a state is entangled or not. If the state is not entangled, we call it separable. To do so, separability criteria and entanglement witnesses are defined. In this chapter, we start by giving the definition of an entangled state. After that, we review some entanglement witnesses and in particular, Shchukin-Vogel witnesses (Ref. [141]) that will be used in Chapter 8. Reviews about entanglement can be found in Refs. [58, 74]; many of the definitions presented in this chapter are taken from these two references.

4.1 Definition of entanglement and separability criteria

Defining an entangled state is done by defining what it is not. Indeed, we rather define a separable state (*i.e.*, a state that is not entangled) and then say that a state is entangled if and only if it can not be expressed under this form. Here, we start by the simplest case: the case of a pure state.

A pure state is separable if and only if it can be written under the form of a tensor product between two states:

$$|\psi_{AB}\rangle = |\psi_A\rangle \otimes |\psi_B\rangle = |\psi_A\rangle\,|\psi_B\rangle\,, \tag{4.1}$$

where $|\psi_A\rangle$ (respectively $|\psi_B\rangle$) is a state living in the Hilbert space $\mathcal{H}_A$ (respectively $\mathcal{H}_B$) and $|\psi_{AB}\rangle$ is a state living in the tensor product of the two Hilbert spaces $\mathcal{H}_A \otimes \mathcal{H}_B$. If the state can not be expressed under this form, it is entangled. Usually, for pure states, we will drop the $\otimes$ symbol for simplicity as it is done in the last equality of Eq. (4.1).

In the case of mixed states, there exists a particular case of a separable state: the product state. A product state has the following form

$$\hat{\rho}_{AB} = \hat{\rho}_A \otimes \hat{\rho}_B, \tag{4.2}$$

which means that it corresponds to a tensor product between two monopartite states. One of these states belongs to Alice, $\hat{\rho}_A$, while the second one belongs to Bob, $\hat{\rho}_B$. According to this expression, it is clear that Alice (or Bob) can apply any local unitary transformation to her system or make any measurement on it and that this won't affect Bob's state. A general separable mixed state is defined as a state $\hat{\rho}_{AB}$ that can be put under the form of a convex mixture of product states; namely,

$$\hat{\rho}_{AB} = \sum_i p_i \left(\hat{\rho}^i_A \otimes \hat{\rho}^i_B\right), \tag{4.3}$$

where $p_i \geq 0\ \forall i$ and $\sum_i p_i = 1$. If a mixed state can not be put under this form, it is entangled.

Finding if a state is entangled based on this definition is proven to be a NP-hard problem [74]. Hence, two simpler tools have been developed: separability criteria and entanglement witnesses. Separability criteria are mathematical conditions which give necessary and sometimes even sufficient criteria for separability. However, often, the knowledge of the state, *i.e.* its full density matrix, is required to use these criteria. Hence, we need to perform full tomography of the state, which is very costly [153, 115, 99, 28]. In contrast, entanglement witnesses are observables, $\hat{W}$, that can be measured. The result of the measurement of a witness gives a negative value, $\mathrm{Tr}(\hat{\rho}\hat{W}) < 0$, only if the state is entangled. However, if the result is positive, $\mathrm{Tr}(\hat{\rho}\hat{W}) \geq 0$, then we can not say if the state is entangled or separable. Witnesses are easier to use as they do not require full tomography. Moreover, for every entangled state, there exists an entanglement witness that can detect it [71]. Sometimes, separability criteria can be stated as entanglement witnesses. Hence, in many cases, the names "separability criterion" and "entanglement witness" are used as synonyms. In the rest of the sections, we describe separability criteria and entanglement witnesses starting from the discrete-variable case before turning to the continuous-variable case.

Notice that the definitions given in this section are restricted to bipartite entanglement as we will only consider bipartite systems in the rest of this thesis. However, there also exist separability criteria and entanglement witnesses for multipartite systems with more than two parties. Details can be found in Ref. [58].

4.2 Discrete-variable separability criteria

4.2.1 Criteria based on the Schmidt decomposition

Detecting entanglement in the particular case of discrete pure states is an easy task when using the Schmidt decomposition of a state [112]. Indeed, each pure bipartite state can be decomposed as

$$|\psi_{AB}\rangle = \sum_i \lambda_i |i_A\rangle |i_B\rangle, \tag{4.4}$$

where $\sum_i \lambda_i^2 = 1$ and $|i_A\rangle$ (respectively $|i_B\rangle$) is an orthonormal basis of $\mathcal{H}_A$ (respectively $\mathcal{H}_B$). The λ_i^2's are the Schmidt coefficients. The Schmidt rank of the state $|\psi_{AB}\rangle$ is defined as the number of λ_i strictly positive. For pure states, this Schmidt rank is necessary and sufficient to determine if the state is entangled: a pure bipartite state is separable if and only if its Schmidt rank is equal to 1.

Note that the fact that the state is entangled implies that the two subsystems obtained when tracing out one of the two modes (either A or B) are mixed. Indeed, we can show that the subsystem of Alice obtained by tracing out the mode B is given by

$$\hat{\rho}_A = \mathrm{Tr}_B(\hat{\rho}_{AB}) = \sum_i \lambda_i^2 |i_A\rangle\langle i_A|. \tag{4.5}$$

Hence, if more than one Schmidt coefficient is non-zero, then $\hat{\rho}_A$ is mixed. This is a signature of the fact that the total state $|\psi_{AB}\rangle$ is entangled. This can be reformulated using the von Neumann entropy [154] defined for a quantum state $\hat{\rho}$ as $S(\hat{\rho}) = -\mathrm{Tr}\,(\hat{\rho}\log_2\hat{\rho})$. The von Neumann entropy can also be formulated in terms of the eigenvalues μ_i of $\hat{\rho}$ as $S(\hat{\rho}) = -\sum_i \mu_i \log_2 \mu_i$. In the case of the state presented in Eq. (4.5), this reduces to

$$S(\hat{\rho}_A) = -\mathrm{Tr}\left(\lambda_i^2 \log_2 \lambda_i^2\right). \tag{4.6}$$

It appears that if the Schmidt rank is equal to 1, $S(\hat{\rho}_A) = 0$. This means that if the von Neumann entropy of any of the two subsystems is equal to zero, we can conclude that the bipartite state is separable.

For mixed states, the detection of entanglement becomes more complicated. There exists a generalization of this criterion for mixed states that is called the computable cross-norm criterion. This criterion is due to Rudolph [127]. To define this criterion, we use a generalized Schmidt decomposition that is valid for mixed states: the operator Schmidt (OS) decomposition, which allows to write, for a mixed quantum state $\hat{\rho}$ as

$$\hat{\rho} = \sum_i \lambda_i^{\mathrm{OS}} \left(\hat{A}_i \otimes \hat{B}_i\right), \tag{4.7}$$

where the operators $\hat{A}_i$'s (respectively $\hat{B}_i$'s) form an orthonormal basis of the operator space of subsystem A (respectively B), in the sense that

$$\mathrm{Tr}\left(\hat{A}_i^\dagger \hat{A}_j\right) = \delta_{ij}, \tag{4.8}$$

and the same for $\hat{B}_i$.

Using this operator Schmidt decomposition, the cross-norm criterion can be stated as follows: if the state $\hat{\rho}$ is separable, then $\sum_i \lambda_i^{OS} \leq 1$. Conversely, if $\sum_i \lambda_i^{OS} > 1$, then it means that the state is entangled.

4.2.2 Positive partial transpose

One of the most important separability criteria is the positive partial transpose criterion (PPT). It is very important as many of the criteria developed after it are based on it or are reformulations of it. PPT was first developed by Peres [119] as a necessary criterion for separability. Peres stated that if the state $\hat{\rho}_{AB}$ is separable, then $(\hat{\rho}_{AB})^{T_B} \geq 0$, where T_B is the partial transpose applied to the subsystem B. It means that the density matrix of the state after application of the partial transposition on subsystem B should remain non-negative or, in other words, that the density matrix has to remain physical under partial transposition. Note that, here, we apply the partial transposition on subsystem B but equivalent results are obtained if this transposition is done on subsystem A. In general, this condition is only a necessary condition, but Horodecki *et al.* showed in Ref. [71] that the condition becomes also sufficient when considering systems of dimensions 2x2 or 2x3: in such systems, $\hat{\rho}_{AB}$ is separable if and only if $(\hat{\rho}_{AB})^{T_B} \geq 0$. We can write the mathematical form of this criterion by decomposing the density matrix of the state in a well-chosen product basis as:

$$\hat{\rho}_{AB} = \sum_{i,j}^{N} \sum_{k,l}^{M} \rho_{ij,kl} \left|i\right\rangle \left\langle j\right| \otimes \left|k\right\rangle \left\langle l\right| \text{ is separable} \Rightarrow (\hat{\rho}_{AB})^{T_B} = \sum_{i,j}^{N} \sum_{k,l}^{M} \rho_{ij,kl} \left|i\right\rangle \left\langle j\right| \otimes \left|l\right\rangle \left\langle k\right| \geq 0. \tag{4.9}$$

In systems of dimension higher than 2x2 or 2x3, the PPT criterion is not sufficient, and hence, even if the density matrix of the partially-transpose state possesses only positive values, we can not conclude whether the state is entangled or not. The states whose entanglement is not detected by PPT are called bound entangled states [72] and other criteria are needed to detect their entanglement, for example the cross-norm criterion of Subsection 4.2.1.

4.2.3 Entropies and majorization criteria

Other criteria based on the von Neumann entropy have been developed in Refs. [71, 21] and are based on the joint von Neumann entropy:

$$S(\hat{\rho}_{AB}) = -\mathrm{Tr}(\hat{\rho}_{AB}\log_2\hat{\rho}_{AB}). \tag{4.10}$$

References [71, 21] state that if $\hat{\rho}_{AB}$ is separable then $S(\hat{\rho}_{AB}) \geq S(\hat{\rho}_A)$ and $S(\hat{\rho}_{AB}) \geq S(\hat{\rho}_B)$. This can also be rewritten using conditional von Neumann entropies as $S(A|B) = S(\hat{\rho}_{AB}) - S(\hat{\rho}_B) \geq 0$ and $S(B|A) = S(\hat{\rho}_{AB}) - S(\hat{\rho}_A) \geq 0$.

These entropy criteria are in fact implied by another criterion based on majorization theory: the criterion of Nielsen and Kempe (Ref. [113]). The authors prove that if $\hat{\rho}_{AB}$ is separable then

$$\lambda_{\rho_{AB}} \prec \lambda_{\rho_A} \text{ and } \lambda_{\rho_{AB}} \prec \lambda_{\rho_B}, \tag{4.11}$$

where the λ_ρ's are the eigenvalues of the state $\hat{\rho}$ and $\lambda \prec \eta$ means that η majorizes λ. Interested readers can found more information about majorization theory in Ref. [104]. In general, majorization relations between two probability distributions imply inequalities on Schur-concave and Schur-convex functions. Since the von Neumann entropy is an example of a Schur-concave function, we can easily prove that the separability criteria presented above (Refs. [71, 21]) are implied by Nielsen and Kempe's criterion.

4.2.4 Other witnesses: reduction map and faithful entanglement

There exist many other criteria for discrete variables systems that can be found for example in the review of Gühne and Tóth [58]. We mention two of them here. The first one is the reduction criterion [22, 70] that is based on a reduction map

$$\Lambda : \hat{\rho}_{AB} \to \mathbb{1}_A \otimes \hat{\rho}_B - \hat{\rho}_{AB}. \tag{4.12}$$

If a state is separable, then one has $\Lambda(\hat{\rho}_{AB}) \geq 0$.

Another witness often used is a witness based on the fidelity of the state we want to analyze with a known entangled state. If the fidelity is high, it means that the two states are close to each other. This kind of witness is written as

$$\hat{W} = \alpha\mathbb{1} - |\psi\rangle\langle\psi|, \tag{4.13}$$

where α is a constant and $|\psi\rangle$ is an entangled state. Usually, $|\psi\rangle$ is taken to be a maximally entangled state. We say that the state is entangled if $\mathrm{Tr}(\hat{\rho}\hat{W}) < 0$. Such states are called faithful entangled states. More details about the geometry of faithful entanglement can be found in Ref. [57].

4.3 Continuous-variable separability criteria

4.3.1 Duan, MGVT and Simon criteria

Based on the PPT criterion, it is possible to derive several criteria involving moments of the quadratures. When limiting ourselves to moments of second order, we can find three famous witnesses due to Duan *et al.* [34], Simon [143] and Mancini *et al.* [98, 45].

The PPT criterion has initially been expressed for discrete variables; it is then needed to see what is the effect of a partial transposition on a continuous-variable system. This was done in Simon's paper [143]. He proved that applying a partial transpose on a continuous-variable system reduces to a local mirror reflection in the phase space. Indeed, starting from the definition of the Wigner function, he showed that the Wigner function of a bipartite state is transformed under a partial transposition as

$$W(x_1, x_2, p_1, p_2) \xrightarrow{T_B} W(x_1, x_2, p_1, -p_2). \tag{4.14}$$

Applying a partial transpose on the second subsystem is then reduced to the change of sign of the momentum of this subsystem, $\hat{p}_2 \to -\hat{p}_2$. The three following separability criteria can be demonstrated by using this simple change.

We start with EPR-like operators defined as

$$\begin{aligned} \hat{x}_\pm &= |r|\hat{x}_1 \pm \frac{1}{r}\hat{x}_2, \\ \hat{p}_\pm &= |r|\hat{p}_1 \pm \frac{1}{r}\hat{p}_2, \end{aligned} \tag{4.15}$$

where r is non-zero and real.

Then, replacing the observables $\hat{A}$ and $\hat{B}$ in the Robertson-Schrödinger uncertainty relation Eq. (2.17) by the EPR-like quadratures given in Eq. (4.15), $\hat{x}_\pm$ and $\hat{p}_\pm$, gives:

$$\sigma^2_{x_\pm}\sigma^2_{p_\pm} \geq \frac{1}{4}|\langle[\hat{x}_\pm, \hat{p}_\pm]\rangle|^2 + \frac{1}{4}|\langle\{\hat{x}_\pm - \langle\hat{x}_\pm\rangle, \hat{p}_\pm - \langle\hat{p}_\pm\rangle\}\rangle|^2. \tag{4.16}$$

In the right-hand side, we will only take into account the first term (the second one is always positive so we can remove it and keep a valid inequality). Calculating the commutator then gives:

$$\sigma^2_{x_\pm}\sigma^2_{p_\pm} \geq \frac{1}{4}\left(|r|^2 + \frac{1}{r^2}\right)^2. \tag{4.17}$$

Developing the simple inequality $(\sigma_{x_\pm} - \sigma_{p_\pm})^2 \geq 0$, we can rewrite

$$\sigma_{x_\pm}^2 + \sigma_{p_\pm}^2 \geq 2\sigma_{x_\pm}\sigma_{p_\pm}. \tag{4.18}$$

Using then Eq. (4.17), we obtain

$$\sigma_{x_\pm}^2 + \sigma_{p_\pm}^2 \geq 2\sigma_{x_\pm}\sigma_{p_\pm} \geq \left(|r|^2 + \frac{1}{r^2}\right). \tag{4.19}$$

This expression can be separated into two different uncertainty relations

$$\begin{aligned} \sigma_{x_\pm}^2 + \sigma_{p_\pm}^2 &\geq \left(|r|^2 + \frac{1}{r^2}\right), \\ \sigma_{x_\pm}^2 \sigma_{p_\pm}^2 &\geq \frac{1}{4}\left(|r|^2 + \frac{1}{r^2}\right)^2. \end{aligned} \tag{4.20}$$

Using the PPT criterion, we can obtain separability criteria by applying the partial transposition to the state in these inequalities. Note that a partial transposition will change the sign of $\hat{p}_2$ as mentioned before, therefore transforming $\hat{p}_\pm$ into $\hat{p}_\mp$, but it won't affect $\hat{x}_\pm$ as it can be seen from the definitions of $\hat{x}_\pm$ and $\hat{p}_\pm$, Eqs. (4.15). The two separability criteria obtained are

$$\sigma_{x_\pm}^2 + \sigma_{p_\mp}^2 \geq |r|^2 + \frac{1}{r^2}. \tag{4.21}$$

$$\sigma_{x_\pm}^2 \sigma_{p_\mp}^2 \geq \frac{1}{4}\left(|r|^2 + \frac{1}{r^2}\right)^2. \tag{4.22}$$

where the first one (presented in Eq. (4.21)) is nothing else than the criterion of Duan *et al.* (note that the initial proof of Duan *et al.* is completely different from the one presented here). The second separability criterion we just proved simultaneously is the criterion by Mancini *et al.* [98, 45]. We can already note that this criterion is stronger than the one of Duan. This is obvious when looking at Eq. (4.19). Usually, this criterion is named MGVT after the authors' names.

The last criterion of order two has been proposed by Simon [143] and is based on the formulation of the uncertainty principle proved in his paper [144]. In this paper, he showed the following uncertainty relation:

$$\gamma + \frac{i}{2}\Omega \geq 0, \tag{4.23}$$

where γ is the 4x4 covariance matrix of the bipartite state and Ω is the symplectic form defined in Eq. (2.86). By applying the partial transpose to this relation, Simon obtained the following separability criterion

$$\gamma^{T_B} + \frac{i}{2}\Omega \geq 0. \tag{4.24}$$

Simon's criterion is stronger than the one of Duan *et al.* and Mancini *et al.* Indeed, it can be reformulated under the form of a sum of the variances of two observables that are more general than the EPR-like quadratures. A schematic representation of the states whose entanglement can be detected by these three witnesses is shown in Fig. 4.1. In this figure, we represent the convex set of separable states inside the convex set of all states. Then, we add a line in blue for each of the three criteria. The states whose entanglement is detected by a criterion are on the right of the associated line while the undetected entangled states are on the left of it.

When considering Gaussian states, the three aforementioned criteria all become equal. Moreover, for Gaussian states, the criteria are proved to be necessary and sufficient for separability which explains why the Gaussian entangled states are on the right of every line in Fig. 4.1. This is done for example in Duan *et al.* paper [34] where it is shown that a bipartite Gaussian state can be transformed without changing the entanglement of the state into the standard form

$$\gamma^G = \begin{pmatrix} n_1 & 0 & c_1 & 0 \\ 0 & n_2 & 0 & c_2 \\ c_1 & 0 & m_1 & 0 \\ 0 & c_2 & 0 & m_2 \end{pmatrix}, \tag{4.25}$$

where

$$\frac{n_1 - 1}{m_1 - 1} = \frac{n_2 - 1}{m_2 - 1} \tag{4.26}$$

and

$$|c_1| - |c_2| = \sqrt{(n_1 - 1)(m_1 - 1)} - \sqrt{(n_2 - 1)(m_2 - 1)}. \tag{4.27}$$

By using this form, the authors prove that if the Gaussian state is entangled, then the witness is necessary and sufficient. Later, it has been proved that all three criteria can be extended and are necessary and sufficient when considering $1 \times N$ Gaussian states (this means that Alice possesses one mode and Bob N modes) [160] or $N \times M$ bisymmetric Gaussian states [137].

Finally, these three separability criteria were improved in 2016 by taking into account the degree of Gaussianity [64]. This allows the detection of the entanglement of some non-Gaussian states that could not be detected by any of the former second-moment criteria.

4.3.2 Higher-order criteria: Shchukin-Vogel hierarchy

A part of this section is based on the following paper that I published together with Tobias Haas and Nicolas Cerf:

C. Griffet, T. Haas, and N. J. Cerf. Accessing continuous-variable entanglement witnesses with multimode spin observables. Physical Review A, 108: 022421, August 2023. [51]

All the criteria presented in the previous section are limited to moments of the quadratures of order two. This is shown to give necessary and sufficient conditions when considering Gaussian states. However, for non-Gaussian states these criteria are not necessary and sufficient but only necessary separability criteria. Hence, many non-Gaussian entangled states are not detected. To improve this, one possibility is to derive new witnesses based on higher order of the quadratures. This is sketched in Fig. 4.1; where we can see that states whose entanglement was not detected by second order criteria can be detected by a higher order cri-

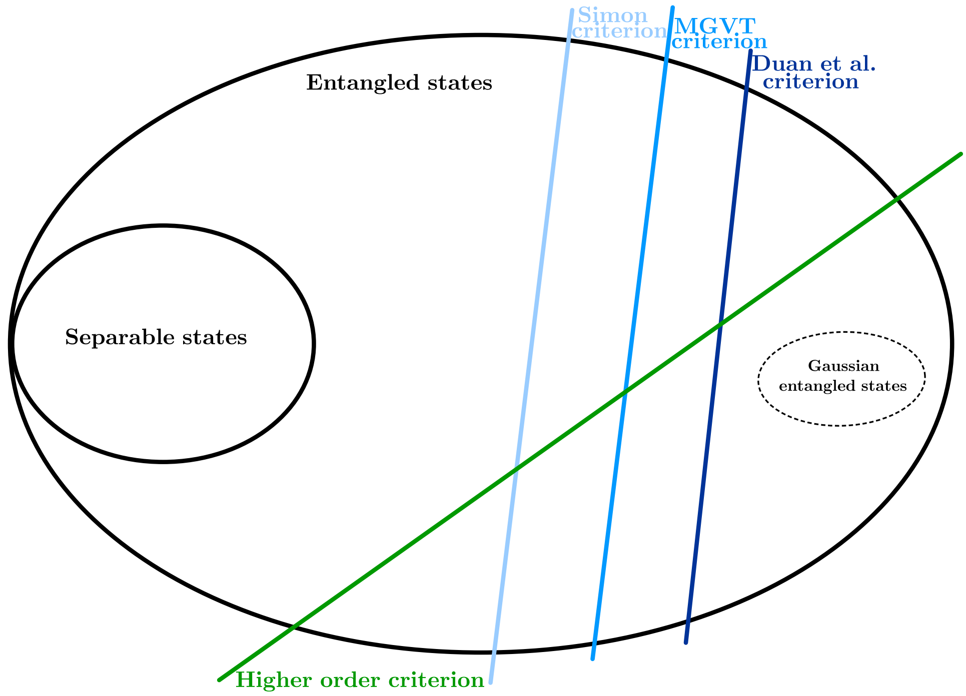

Figure 4.1: Representation of the convex set of separable states inside the set of all the states. Each line corresponds to an entanglement witness which detects the entanglement of the states on the right of the line. The blue lines correspond to second order criteria (from the weaker to the stronger one: Duan *et al.*, MGVT and Simon criteria). The green line corresponds to a fictive higher order criterion. Gaussian entangled states do not constitute a convex set of states, emphasized by the dashed lines.

terion. Moreover, such witnesses are incomparable to the ones of order two presented before: it is possible to find states that are detected by *e.g.* Duan *et al.*'s criterion but that will not be detected by a higher order criterion.

One example of such criterion is the witness of Agarwal [3] which involves fourth order terms. Since this witness is important for our results on multicopy observables to detect entanglement, it will be analyzed in Chapter 8 where we will showcase a class of non-Gaussian entangled states that can be detected as entangled states. We will also devise an implementation allowing us to efficiently measure this witness.

In 2005, a complete hierarchy of criteria was developed by Shchukin and Vogel [141]. These criteria involve arbitrarily high moments of the quadratures. We describe this hierarchy in more detail here as it will be at the basis of the results presented in Chapter 8. Note that this result was further analyzed in a comment [106] and in a paper by Miranowicz *et al.* [107]. To develop the hierarchy, Shchukin and Vogel use the fact that the non-negativity of the partial transpose $\hat{\rho}^{T_B}$ can be assessed in full generality by demanding that for all normally-ordered operators

$$\hat{f} = \sum_{n,m,k,l} c_{nmkl}\, \hat{a}^{\dagger n} \hat{a}^{m} \hat{b}^{\dagger k} \hat{b}^{l}, \tag{4.28}$$

with complex-valued c's, the inequality

$$\mathrm{Tr}\left(\hat{\rho}^{T_B}\hat{f}^\dagger\hat{f}\right) \geq 0, \tag{4.29}$$

is fulfilled. Indeed, the mean value of $\hat{f}^\dagger\hat{f}$, with $\hat{f}$ being any operator of the form given in Eq. (4.28), must be non-negative:

$$\mathrm{Tr}\left(\hat{\rho}\hat{f}^\dagger\hat{f}\right) \geq 0. \tag{4.30}$$

Then, applying the PPT criterion (taking the partial transpose on the second mode) leads to Eq. (4.29). Using the matrix of moments $D_{pqrs,nmkl} = \langle \hat{a}^{\dagger q}\hat{a}^p\hat{a}^{\dagger n}\hat{a}^m\hat{b}^{\dagger s}\hat{b}^r\hat{b}^{\dagger k}\hat{b}^l\rangle$, this inequality can then be expressed as a bilinear form in c as

$$\sum_{\substack{n,m,k,l\\p,q,r,s}} c^*_{pqrs}\, c_{nmkl}\, D^{T_B}_{pqrs,nmkl} \geq 0, \tag{4.31}$$

for all complex-valued c's. By Sylvester's criterion, the latter inequality holds true for all c's if and only if all principal minors of the matrix D^{T_B} are non-negative. Since $D^{T_B}_{pqrs,nmkl} = D_{pqkl,nmrs}$ due to the form of the matrix of moments, the authors obtain that $\hat{\rho}^{T_B}$ is non-negative if and only if all determinants

$$d = |D^{T_B}| = \begin{vmatrix} 1 & \langle\hat{a}\rangle & \langle\hat{a}^\dagger\rangle & \langle\hat{b}^\dagger\rangle & \langle\hat{b}\rangle & \cdots \\ \langle\hat{a}^\dagger\rangle & \langle\hat{a}^\dagger\hat{a}\rangle & \langle\hat{a}^{\dagger 2}\rangle & \langle\hat{a}^\dagger\hat{b}^\dagger\rangle & \langle\hat{a}^\dagger\hat{b}\rangle & \cdots \\ \langle\hat{a}\rangle & \langle\hat{a}^2\rangle & \langle\hat{a}\hat{a}^\dagger\rangle & \langle\hat{a}\hat{b}^\dagger\rangle & \langle\hat{a}\hat{b}\rangle & \cdots \\ \langle\hat{b}\rangle & \langle\hat{a}\hat{b}\rangle & \langle\hat{a}^\dagger\hat{b}\rangle & \langle\hat{b}^\dagger\hat{b}\rangle & \langle\hat{b}^2\rangle & \cdots \\ \langle\hat{b}^\dagger\rangle & \langle\hat{a}\hat{b}^\dagger\rangle & \langle\hat{a}^\dagger\hat{b}^\dagger\rangle & \langle\hat{b}^{\dagger 2}\rangle & \langle\hat{b}\hat{b}^\dagger\rangle & \cdots \\ \vdots & \vdots & \vdots & \vdots & \vdots & \ddots \end{vmatrix}, \tag{4.32}$$

are non-negative. This proves that the negativity of any minor of matrix D^{T_B} provides an entanglement witness. It can also be proven that the principal minors of this matrix also lead to valid entanglement witnesses. Indeed, taking a specific choice for $\hat{f}$ where for example, we cancel some of the coefficients c leads to a smaller matrix. In fact, this smaller matrix corresponds to the matrix D^{T_B} where we only keep a subset of rows and corresponding columns. In Chapter 8, we will focus on three submatrices: $d_{1,2,4}$, $d_{1,4,9}$, and $d_{1,9,13}$. The notation $d_{1,2,4}$ indicates that we look at the determinant of the matrix consisting of the first, second, and fourth rows and columns of D^{T_B}. The interest of these matrices will be presented in detail in Chapter 8.

In order to better show the process leading to these criteria based on submatrices, we develop here how we can obtain the criterion based on $d_{1,2,4}$. We start by taking the following function $\hat{f}_{1,2,4}$:

$$\hat{f}_{1,2,4} = c_1 + c_2\hat{a} + c_3\hat{b}, \tag{4.33}$$

then we can express the partial transpose of the mean value of $\hat{f}^\dagger\hat{f}$ as

$$\langle\hat{f}^\dagger_{1,2,4}\hat{f}_{1,2,4}\rangle^{T_B} = \langle(c_1^* + c_2^*\hat{a}^\dagger + c_3^*\hat{b}^\dagger)(c_1 + c_2\hat{a} + c_3\hat{b})\rangle^{T_B}. \tag{4.34}$$

Rewriting this expression as a bilinear form for c, we have

$$\langle \hat{f}_{1,2,4}^{\dagger} \hat{f}_{1,2,4} \rangle^{T_B} = \begin{pmatrix} c_1^* & c_2^* & c_3^* \end{pmatrix} \langle \begin{pmatrix} 1 & \hat{a} & \hat{b} \\ \hat{a}^{\dagger} & \hat{a}^{\dagger}\hat{a} & \hat{a}^{\dagger}\hat{b} \\ \hat{b}^{\dagger} & \hat{b}^{\dagger}\hat{a} & \hat{b}^{\dagger}\hat{b} \end{pmatrix} \rangle^{T_B} \begin{pmatrix} c_1 \\ c_2 \\ c_3 \end{pmatrix}. \tag{4.35}$$

To obtain the determinant we are looking for, we still need to apply the partial transpose on the matrix we just obtained. We know that applying a partial transposition corresponds to the sign flip of $\hat{p}_2$ which corresponds to the transformation:

$$\begin{aligned} \hat{b} &\longrightarrow \hat{b}^{\dagger}, \\ \hat{b}^{\dagger} &\longrightarrow \hat{b}, \\ \hat{b}^{\dagger}\hat{b} &\longrightarrow (\hat{b}^{\dagger}\hat{b})^{T_B} = (\hat{b}^{T_B}\hat{b}^{\dagger T_B}) = \hat{b}^{\dagger}\hat{b}. \end{aligned} \tag{4.36}$$

The a-mode operators are not affected, leading to the expression:

$$\langle \hat{f}_{1,2,4}^{\dagger} \hat{f}_{1,2,4} \rangle^{T_B} = \begin{pmatrix} c_1^* & c_2^* & c_3^* \end{pmatrix} \langle \begin{pmatrix} 1 & \hat{a} & \hat{b}^{\dagger} \\ \hat{a}^{\dagger} & \hat{a}^{\dagger}\hat{a} & \hat{a}^{\dagger}\hat{b}^{\dagger} \\ \hat{b} & \hat{a}\hat{b} & \hat{b}^{\dagger}\hat{b} \end{pmatrix} \rangle \begin{pmatrix} c_1 \\ c_2 \\ c_3 \end{pmatrix}. \tag{4.37}$$

Using Sylvester's criteria, this expression is non-negative if and only if

$$d_{1,2,4} = \begin{vmatrix} 1 & \langle \hat{a} \rangle & \langle \hat{b}^{\dagger} \rangle \\ \langle \hat{a}^{\dagger} \rangle & \langle \hat{a}^{\dagger}\hat{a} \rangle & \langle \hat{a}^{\dagger}\hat{b}^{\dagger} \rangle \\ \langle \hat{b} \rangle & \langle \hat{a}\hat{b} \rangle & \langle \hat{b}^{\dagger}\hat{b} \rangle \end{vmatrix} \geq 0. \tag{4.38}$$

We can then verify that it indeed corresponds to taking the rows and columns 1, 2, and 4 in Shchukin-Vogel's matrix (4.32).

Interestingly, Shchukin and Vogel demonstrated that some well-known criteria are particular cases of their matrix. For example, Simon's criterion is deduced from $d_{1,2,3,4,5} \geq 0$.

We also note that all principal subdeterminants of (4.32) are invariant under arbitrary local rotations $\hat{a} \to e^{-i\theta_a}\hat{a}$ and $\hat{b} \to e^{-i\theta_b}\hat{b}$ (with the definitions of rotations coming from Section 2.5.1). Indeed, in every term of these determinants, local annihilation and creation operators appear equally often so that all phases cancel termwise. This property implies that the entanglement witnesses are invariant if Alice or Bob applies a local phase shift. The same is *not* true for arbitrary local displacements in general, $\hat{a} \to \hat{a} + \alpha$ and $\hat{b} \to \hat{b} + \beta$, which can be seen by considering for example the subdeterminant $d_{2,3}$. Indeed, $d_{2,3}$ is equal to

$$d_{2,3} = \begin{vmatrix} \langle \hat{a}^{\dagger}\hat{a} \rangle & \langle \hat{a}^{\dagger 2} \rangle \\ \langle \hat{a}^2 \rangle & \langle \hat{a}\hat{a}^{\dagger} \rangle \end{vmatrix}, \tag{4.39}$$

while its displaced version is given by

$$d_{2,3}^{\text{displaced}} = \begin{vmatrix} \langle(\hat{a}^\dagger + \alpha^*)(\hat{a} + \alpha)\rangle & \langle(\hat{a}^\dagger + \alpha^*)^2\rangle \\ \langle(\hat{a} + \alpha)^2\rangle & \langle(\hat{a} + \alpha)(\hat{a}^\dagger + \alpha^*)\rangle \end{vmatrix}. \tag{4.40}$$

When developing the two determinants, we can easily prove that $d_{2,3} \neq d_{2,3}^{\text{displaced}}$. However, for some specific subdeterminants, this symmetry is restored, as we will see in Chapter 8.

4.3.3 Other criteria: entropic based criteria, realignement criteria and criteria based on Q-distribution

There exist many other criteria but as they are not used in this thesis, we will not present them in detail here. Among them, we can however cite the fact that the cross-norm criterion presented in Subsection 4.2.1 can be reformulated under a new form that is more adapted to continuous-variables systems. This was done by Chen *et al.* in 2003 [25] and is called the realignment criterion as it is based on a realignment map. The realignment criterion was also reexpressed in another form [164], while a weaker form that gives similar results for some states and is easier to measure has been proposed [60]. Criteria based on the entropy have also been developed by applying the PPT criterion to continuous-variable uncertainty relations formulated in terms of entropies [156, 155, 130, 150, 132, 133]. Finally, new criteria based on the Husimi Q-distribution have also been expressed [42, 41, 55, 54, 56]. These are, again, derived from the PPT criterion.

Many entanglement criteria have already been implemented in practice. Indeed, for example, entanglement was certified experimentally in the context of quantum optics [33, 133, 7, 122, 108] and in cold atom experiments [52, 148, 118, 39, 87, 89, 86]. However, new technological advances demand for new physical implementation of criteria.

Chapter 5

Multicopy measurement method

The main theme in this thesis, the multicopy method was first introduced by Brun in 2004 [18]. This method allows to access polynomial functions of a quantum state by performing measurements on several replicas of the state. In the next chapters, we will use it to measure different witnesses of nonclassicality and entanglement. Here, we first present the multicopy method and then show recent results in the context of quantum optics [65].

5.1 Measurement of a polynomial function of the state

5.1.1 Objective

In quantum information, many witnesses and important quantities can be written in the form of a polynomial function of a state $\hat{\rho}$

$$f(\hat{\rho}) = \sum_{i_1,j_1,\ldots,i_m,j_m} c_{i_1 j_1 \ldots i_m j_m} \rho_{i_1,j_1} \rho_{i_2,j_2} \ldots \rho_{i_m j_m} + \ldots \sum_{i_1,j_1} c_{i_1 j_1} \rho_{i_1,j_1} + c, \tag{5.1}$$

where the c's are complex constants and the $\rho_{i,j}$ are the matrix elements involved in the expression of the density operator in the basis $\{|i\rangle\}$:

$$\hat{\rho} = \sum_{i,j=0}^{d-1} \rho_{i,j} |i\rangle\langle j|. \tag{5.2}$$

Using the normalization of the state, $\mathrm{Tr}\hat{\rho} = 1$, this expression can be reduced to an expression involving only terms of the order m:

$$f(\hat{\rho}) = \sum_{i_1,j_1,\ldots,i_m,j_m} c_{i_1 j_1 \ldots i_m j_m} \rho_{i_1,j_1} \rho_{i_2,j_2} \ldots \rho_{i_m,j_m}. \tag{5.3}$$

Usually, quantities expressed in such a form can only be measured by doing full tomography of the state, which is a complicated process. Some examples of this full tomography process are presented in [153, 115, 99, 28]. In order to overcome this difficulty, Brun presented in Ref. [18] an alternative measurement method that involves several copies of a state.

5.1.2 Multicopy measurement method

Brun defined a multicopy observable $\hat{A}_f$ that has to be applied to m identical copies of a quantum state $\hat{\rho}$ if the objective is to measure a polynomial function of order m:

$$f(\hat{\rho}) = \mathrm{Tr}(\hat{A}_f \hat{\rho}^{\otimes m}). \tag{5.4}$$

In order to determine this observable $\hat{A}_f$, Brun defines the operators

$$\hat{A}_{i_1 j_1 \ldots i_m j_m} = |j_1\rangle\langle i_1| \otimes \ldots \otimes |j_m\rangle\langle i_m|, \tag{5.5}$$

such that

$$\mathrm{Tr}(\hat{A}_{i_1 j_1 \ldots i_m j_m} \hat{\rho}^{\otimes m}) = \rho_{i_1, j_1} \ldots \rho_{i_m, j_m}. \tag{5.6}$$

Then, using these operators, it is possible to obtain $\hat{A}_f$ as

$$\hat{A}_f = \sum_{i_1, j_1, \ldots, i_m, j_m} c_{i_1 j_1 \ldots i_m j_m} \hat{A}_{i_1 j_1 \ldots i_m j_m}, \tag{5.7}$$

such that, by measuring the mean value of this observable on m identical copies of the state, we obtain the desired value of the function $f(\hat{\rho})$. However, such operator is not always Hermitian ($\hat{A}_f \neq \hat{A}_f^\dagger$) and hence, it is not always directly measurable. In such cases, it is needed to define two new operators that will be observable and that we can measure to obtain the value of the function:

$$\begin{aligned} \hat{O}_f &= \tfrac{1}{2}(\hat{A}_f + \hat{A}_f^\dagger), \\ \hat{O}'_f &= \tfrac{-i}{2}(\hat{A}_f - \hat{A}_f^\dagger). \end{aligned} \tag{5.8}$$

Using these observables, we can express $\hat{A}_f$:

$$\hat{A}_f = \hat{O}_f + i\hat{O}'_f. \tag{5.9}$$

The function is then given by $f(\hat{\rho}) = \mathrm{Tr}(\hat{\rho}^{\otimes m}(\hat{O}_f + i\hat{O}'_f))$.

Once the observables are found, it is still needed to find an implementable circuit to apply the measurement. This last step is not trivial and there exists no general algorithm to do it. If the circuit exists and is simple, we obtain a way of measuring the desired function that is substantially simpler than doing full tomography. Hence, we are mainly concerned with finding expressions and corresponding implementations of multicopy observables which implement witnesses for the detection of nonclassicality and entanglement.

5.2 Application of the method

Since the publication of Brun's paper, some applications of this multicopy measurement technique have been proposed. In this section, we start by the analysis of a simple function as an example: the purity. We then make a brief analysis of the main applications of multicopy measurements in the literature. Finally, we present the only known application of the multicopy technique in quantum optics.

5.2.1 Multicopy observable for the measure of the purity

As said before, the purity of a quantum state is an important quantity in quantum optics. Its expression is given in Eq. (2.43). Apart from the fact that the purity is useful to describe a quantum state, the purity is even more important for this thesis as it appears in the expression of the quadrature coherence scale (QCS), see Eq. (3.18). Since one of the results of this thesis is a multicopy observable to measure the QCS, we also have, as a subroutine, a multicopy implementation for the measurement of the purity.

Looking at Eq. (2.43), we see that the purity consists of a function of the density operator of the form of Eq. (5.3). The order of the polynomial involved is two which means that we need two copies to implement the multicopy version. The multicopy version of the purity can be found in Ref. [18]:

$$\mathcal{P}(\hat{\rho}) = \mathrm{Tr}(\hat{\rho}^{\otimes 2}\hat{S}), \tag{5.10}$$

where $\hat{S}$ is the swap operator. This expression will be proved again in Chapter 7 when we will be interested in the measurement of the quadrature coherence scale.

The swap operator for the measurement of the purity has already been implemented in the context of many-body Bose-Hubbard systems [29, 78]. We will demonstrate again the implementation of the swap operator in a quantum optics context in Chapter 7.

The multicopy measurement technique has also been used to measure fidelity, overlap and purity using discrete circuits involving phase-shifts [40, 73, 38]. Experimental implementations can also be found in Refs. [109, 16, 110, 116].

5.2.2 Application of the method in quantum optics

Prior to this thesis original work, there was only one application of the multicopy measurement technique in the field of quantum optics [65]. During this thesis, the technique has been applied to other quantum optics examples. It is thus interesting to study in more details Ref. [65]. Its objective was to use a multicopy setup in order to find an (entropic) uncertainty relation invariant under all Gaussian transformations. Indeed, as mentioned earlier, the invariance under symplectic transformations of the uncertainty relation is a desired property because then all pure Gaussian states saturate the inequality. This was not fulfilled in the first uncertainty relations of Heisenberg and Kennard [59, 80] but was satisfied for the relation of Robertson and Schrödinger, Eq. (2.18) [134, 126]. For entropies, such a relation has only been conjectured (see Ref. [152]).

In Ref. [65], the authors want to find back this uncertainty relation but also the circuit to measure it. The first step is to find a two-copy observable such that its variance is equal to $\sigma_x^2\sigma_p^2$. To do so, there exist several observables but the authors impose that the observable must be invariant by rotation. This leads to the following observable:

$$\begin{aligned}\hat{L}_y &= \tfrac{i}{2}(\hat{a}_1\hat{a}_2^\dagger - \hat{a}_1^\dagger\hat{a}_2),\\ &= \tfrac{1}{2}(\hat{x}_1\hat{p}_2 - \hat{p}_1\hat{x}_2),\end{aligned} \tag{5.11}$$

which is such that its mean value is equal to 0, $\langle\langle\hat{L}_y\rangle\rangle = 0$. This observable is called $\hat{L}_y$ as it can be obtained by applying the Jordan-Schwinger map on the y-Pauli matrix as we will show later in this thesis and the notation $\langle\langle...\rangle\rangle$ represents the mean value of the observable for two identical copies $\langle\langle...\rangle\rangle = \mathrm{Tr}\,(...\,\hat{\rho}\otimes\hat{\rho})$. The variance of $\hat{L}_y$ is given by:

$$\sigma^2_{\hat{L}_y} = \langle\langle\hat{L}_z^2\rangle\rangle = \frac{1}{2}\left(\det\gamma_c + \frac{1}{4}\langle[\hat{x},\hat{p}]\rangle^2\right), \tag{5.12}$$

where γ_c stands for the covariance matrix of a centered state:

$$\gamma_c = \begin{pmatrix} \langle\hat{x}^2\rangle & \frac{1}{2}\langle\{\hat{x},\hat{p}\}\rangle \\ \frac{1}{2}\langle\{\hat{x},\hat{p}\}\rangle & \langle\hat{p}^2\rangle \end{pmatrix}. \tag{5.13}$$

By definition, the variance of an observable has to be bigger than zero:

$$\det\gamma_c \geq -\frac{1}{4}\langle[\hat{x},\hat{p}]\rangle^2. \tag{5.14}$$

This inequality is nothing but the Robertson-Schrödinger uncertainty relation for centered states: $\det\gamma_c \geq \frac{1}{4}$. Moreover, the authors designed a circuit to measure the observable $\hat{L}_y$ (see Fig. 5.1). To measure this observable, the second copy of the state is first rotated by an angle of $\frac{\pi}{2}$, then the two modes are sent in a 50:50 beam splitter and finally, the photon numbers in both outputs are measured. After the application of such circuit, the observable is equal to:

$$\hat{L}_y = \frac{1}{2}(\hat{n}_1' - \hat{n}_2'), \tag{5.15}$$

which means that the observable is linked to the number of photons in each output.

To summarize, the authors have found a multicopy observable which has a variance linked to the uncertainty relation. However, this observable is only invariant under rotation and not under displacement, so it needs to be improved. For that, it appears that increasing the number of copies leads to a better result. Indeed, the authors managed to find a 3-copy observable

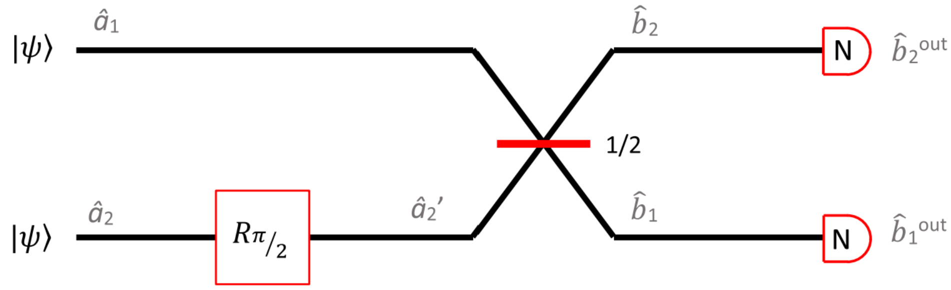

Figure 5.1: Circuit for the measurement of $\hat{L}_y$ (Figure taken from Ref. [65]).

presenting all the wanted invariances.

To express it, we define the observable $\hat{L}_y^{ij}$ acting on the modes i and j:

$$\hat{L}_y^{ij} = \frac{1}{2}(\hat{x}_i\hat{p}_j - \hat{p}_i\hat{x}_j), \tag{5.16}$$

then the 3-copy observable is given by:

$$\hat{M} = \frac{1}{\sqrt{3}}(\hat{L}_y^{12} + \hat{L}_y^{23} + \hat{L}_y^{31}). \tag{5.17}$$

As for the 2-copy observable, its mean value for three identical copies is equal to zero:

$$\langle\langle\langle \hat{M} \rangle\rangle\rangle = 0, \tag{5.18}$$

while its variance is given by:

$$\sigma_{\hat{M}}^2 = \langle\langle\langle \hat{M}^2 \rangle\rangle\rangle = \frac{1}{2}(\det\gamma + \frac{1}{4}\langle[\hat{x},\hat{p}]\rangle^2), \tag{5.19}$$

where the notation $\langle\langle\langle ... \rangle\rangle\rangle$ corresponds to the expectation value on three identical copies: $\mathrm{Tr}\,(...\,\hat{\rho}\otimes\hat{\rho}\otimes\hat{\rho})$. Since this variance is also bigger than zero by definition, it gives:

$$\det\gamma \geq -\frac{1}{4}\langle[\hat{x},\hat{p}]\rangle^2. \tag{5.20}$$

This final inequality is nothing else than the Robertson-Schrödinger uncertainty relation of Eq. 2.18. Thus, the authors managed to find a 3-copy observable leading to uncertainty relations presenting the right invariances. Moreover, the circuit implementing $\hat{M}$ is found in the paper (see Fig. 5.2).

Based on this observable, it is also possible to write an entropic uncertainty relation:

$$H(\hat{M})_\rho \geq 0. \tag{5.21}$$

Analyzing these results, we can draw some conclusions that were useful in obtaining

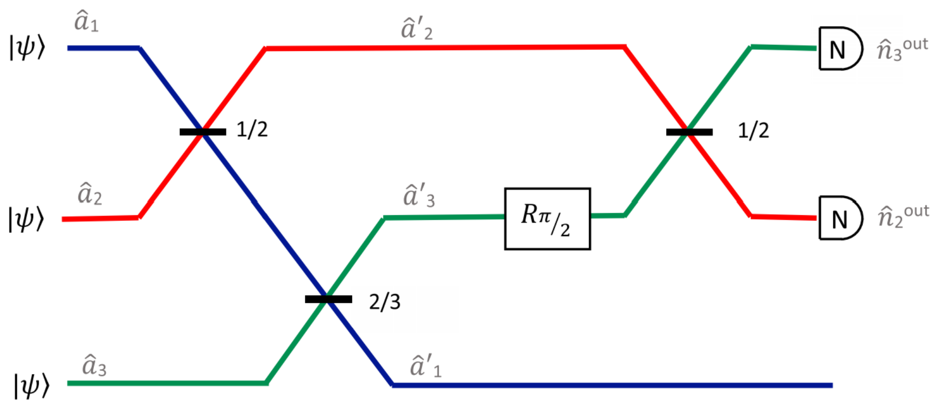

Figure 5.2: Circuit for the measurement of $\hat{M}$ (Figure taken from Ref. [65]).

the results of this thesis. Indeed, we see the importance of the invariance under symplectic transformations. It also appears that increasing the numbers of copies improves the results, as in this case, it allows them to consider non-centered states. Finally, the authors implement a multicopy version of the determinant of the covariance matrix. The form of a determinant suits very well the multicopy method as we can find a multicopy observable by assigning to each row a copy. These remarks lead us to investigate the multicopy implementation of witnesses that are put under the form of a determinant. This is exactly what we do in Chapters 6 and 8.

On the mathematical side, the authors are using an observable $\hat{L}_y$ which is a component of the angular momentum $\hat{L}$. In what follows, we will still use this observable but also the other components x and z of the same angular momentum. We will also show that they can be obtained using the so-called Jordan Schwinger map.

Part II

Multicopy criteria for nonclassicality detection

Chapter 6

Multicopy observables for the detection of optically nonclassical states

This chapter is based on the following paper that I published together with Matthieu Arnhem and Nicolas Cerf:

M. Arnhem, C. Griffet and N. J. Cerf. Multicopy observables for the detection of optically nonclassical states. Physical Review A, 106: 043705, October 2022. [6]

6.1 Introduction

Determining whether a quantum optical state admits nonclassical properties or not is an ubiquitous question in the theory of quantum optics as well as in the development of quantum technologies. Numerous proposals for identifying quantum states displaying nonclassicality have been discussed in the literature, see *e.g.* [4, 97, 124, 125, 128, 30, 61] or see [105] for a review of different criteria. We focus here on a possible definition of optical nonclassicality as introduced by Glauber and Sudarshan [46, 47, 149], starting from the assertion that classical states are those that are expressible as convex mixtures of coherent states. Accordingly, when the Glauber-Sudarshan P function of a state is incompatible with a true probability distribution (*i.e.*, when it admits negative values in phase space or is not well-behaved in the sense that it cannot be expressed as a regular function), the state is said to be optically nonclassical. A straightforward operational meaning of optical nonclassicality is that it is a necessary condition in order to produce entanglement with a beam splitter [76, 117, 48] (see Section 3.3). More generally, being able to identify and characterize such nonclassical optical states is essential since nonclassical features are often taken as resources for quantum information tasks [114, 145] such as quantum computation [85], distributed quantum computing [139], quantum networks [162], quantum boson sampling [138], quantum metrology [88, 44] or quantum communication [123].

Various implementation methods have been proposed for identifying nonclassical states, exploiting measurements ranging from single-photon detection [146, 10] to continuous-variable measurements such as homodyne detection [142] or heterodyne detection [15]. In this chapter, we introduce a technique that uses multiple replicas (*i.e.*, identical copies) of a quantum state in order to construct a nonclassicality observable. The relevance of multicopy observables in quantum optics has recently been explored in the context of uncertainty relations [65]. It relies on the observation that polynomial functions of the elements of a density matrix can be expressed by defining an observable acting on several replicas of the state, avoiding the need for quantum tomography [18]. In the present chapter, we consider the nonclassicality criteria resulting from the matrix of moments of the optical field as introduced in [140, 142]. In the simplest cases at hand, the multicopy observables enable an original implementation of nonclassicality witnesses through linear interferometry and photon number detectors.

This chapter is constructed as follows. In Section 6.2, we review the properties of the matrix of moments defined in Eq. (3.16) that can be used when designing the implementation of the criteria. In Section 6.3, we benchmark the performances of the nonclassicality criteria derived from the determinant of these matrices [142, 140]. We consider a variety of states that are known to be nonclassical (Fock states, squeezed states, cat states, squeezed thermal states) in order to identify which criteria do detect their nonclassicality. This is useful to guide our search for designing multicopy nonclassicality observables, as carried out in Section 6.4. There, we focus on the most interesting criteria based on a few selected principal minors of the matrix of moments as identified in Section 6.3 and provide a physical implementation whenever possible. Finally, in Section 6.5, we give our conclusions and discuss further perspectives.

6.2 Optical nonclassicality of quantum states

In Section 6.3, we will study all the principal minors of the matrix of moment D_N of dimension 5×5, which is helpful to determine which of them are good candidates for constructing a multicopy observable (as will then be addressed in Section 6.4). Before coming to this, it is relevant to list the important properties of the matrix of moments D_N and its determinants:

- The matrix of moment D_N presents a block structure. Indeed, the matrix of moments D_N is defined in Eq. (3.16). By inspection, we see that the entry $m_{i,j}$ of row i and column j results from the (expectation value of the) product of the first entries in the same row and same column taken in normal order, namely

$$m_{i,j} = \langle \hat{m}_{i,j} \rangle = \langle : \hat{m}_{i,1}\, \hat{m}_{1,j} : \rangle = \langle : \hat{m}^{\dagger}_{1,i}\, \hat{m}_{1,j} : \rangle, \tag{6.1}$$

where the entries of the first row are defined as

$$\hat{m}_{1,j} = \hat{a}^{\dagger l}\hat{a}^{n-l}. \tag{6.2}$$

In this expression, the index j is decomposed into two indices n and l via

$$j = \frac{n(n+1)}{2} + l + 1, \tag{6.3}$$

which can be understood from the block structure of the matrix D_N as illustrated in Fig. 6.1. The index n stands for the block index and goes from 0 to infinity (when $N \to \infty$). It corresponds to the total order in $\hat{a}$ and $\hat{a}^\dagger$ of the block, while l goes from 0 to n corresponds to the order in $\hat{a}^\dagger$ (the order in $\hat{a}$ being of course $n-l$) within the nth block.

- The matrix of moment D_N is Hermitian. Hence, its determinant as well as all its principal minors are real-valued. This is easily seen from Eq. (6.1) since $m_{i,j} = \langle : \hat{m}_{1,i}^\dagger \hat{m}_{1,j} : \rangle = \langle : (\hat{m}_{1,j}^\dagger \hat{m}_{1,i})^\dagger : \rangle = m_{j,i}^*$.

- All principal minors of matrix D_N vanish for coherent states $|\alpha\rangle$. This property is consistent with the fact that the coherent states are on the boundary of the convex set of classical states. Any statistical mixture of coherent states is classical and can only give a higher value of all principal minors. Conversely, a slight deviation from a coherent state to a nonclassical state may induce some principal minor to have a negative value. The nonclassicality of coherent states is of course not detected by all nonclassicality criteria since they are classical, but they come with a vanishing value for all principal

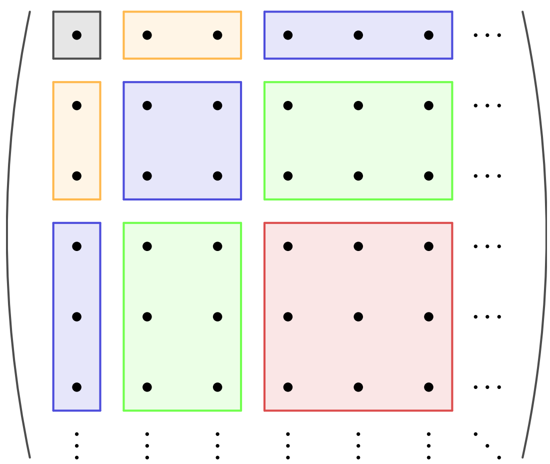

Figure 6.1: Block structure of the matrix of moments. The blocks of the same color are composed of entries having the same total power in $\hat{a}$ and $\hat{a}^\dagger$. Each element can be either defined with respect to its row i and column j, either with the number of its block n and its position j in the block (vertically and horizontally). The link between these two notations is given by Eq. (6.3).

minors (dominant or not) of the matrix of moment, which is consistent with extremality. For example, using $\hat{a}|\alpha\rangle = \alpha|\alpha\rangle$ and $\langle\alpha|\hat{a}^\dagger = \langle\alpha|\alpha^*$, the matrix of moments D_{123} can be written as

$$D_{123}^{|\alpha\rangle} = \begin{pmatrix} 1 & \alpha & \alpha^* \\ \alpha^* & \alpha^*\alpha & \alpha^{*2} \\ \alpha & \alpha^2 & \alpha^*\alpha \end{pmatrix}. \tag{6.4}$$

One may see that $D_{123}^{|\alpha\rangle}$ is a rank-one matrix since it can be written as the outer product $\vec{\alpha} \otimes \vec{\alpha}^\dagger$, where $\vec{\alpha} = (1, \alpha, \alpha^*)^\dagger$. Hence, its determinant $d_{123}^{|\alpha\rangle}$ is equal to 0. In view of the form of the matrix of moments, this argument holds for all principal minors (of order strictly greater than one) which are therefore equal to 0 for coherent states. This shows the special role played by coherent states in the sense that they saturate all inequalities in Eq. (3.17).

- All principal minors of matrix D_N are invariant under rotations in phase space. Hence, all corresponding nonclassicality criteria are invariant under rotations in phase space. This property is consistent with the fact that nonclassicality is a feature that is unaffected by such rotations. This simplifies the calculations since all phase terms can be given arbitrary values and will typically be set to zero. The invariance of $d_{1\cdots N} = \det(D_N)$ under rotations is easy to prove. Indeed, applying a rotation transforms the operator $\hat{a}$ into $e^{i\theta}\hat{a}$ and $\hat{a}^\dagger$ into $e^{-i\theta}\hat{a}^\dagger$. Since each term in the development of the determinant of D_N always involves the same power in $\hat{a}$ and $\hat{a}^\dagger$, the factors $e^{i\theta}$ and $e^{-i\theta}$ cancel each other out. Hence, the observable is not affected by phase shifts and the criterion is invariant under rotations. For example, we have

$$\begin{aligned} d_{123}^{\theta} &= \begin{vmatrix} 1 & \langle\hat{a}e^{-i\theta}\rangle & \langle\hat{a}^\dagger e^{i\theta}\rangle \\ \langle\hat{a}^\dagger e^{i\theta}\rangle & \langle\hat{a}^\dagger e^{i\theta}\hat{a}e^{-i\theta}\rangle & \langle\hat{a}^{\dagger 2}e^{2i\theta}\rangle \\ \langle\hat{a}e^{-i\theta}\rangle & \langle\hat{a}^2 e^{-2i\theta}\rangle & \langle\hat{a}^\dagger e^{i\theta}\hat{a}e^{-i\theta}\rangle \end{vmatrix}, \\ &= \langle\hat{a}^\dagger\hat{a}\rangle^2 - \langle\hat{a}^{\dagger 2}\rangle\langle\hat{a}^2\rangle - 2\langle\hat{a}^\dagger\rangle\langle\hat{a}\rangle\langle\hat{a}^\dagger\hat{a}\rangle + \langle\hat{a}^{\dagger 2}\rangle\langle\hat{a}\rangle^2 + \langle\hat{a}^\dagger\rangle^2\langle\hat{a}^2\rangle, \\ &= d_{123}, \end{aligned} \tag{6.5}$$

where the superscript θ means that the state has been rotated by an angle θ. In view of the form of D_N, it is clear that this rotation invariance also holds for all principal minors (and not just dominant principal minors).

- All *dominant* principal minors of matrix D_N are invariant under displacements in phase space. This property is consistent with the fact that nonclassicality is unaffected by such displacements. Hence, we can simplify our calculations by considering states that are centered in phase space. Note that, unfortunately, the *nondominant* principal minors do not enjoy this invariance property. In Section 6.4.1, we will consider the effect of displacements on some non-dominant principal minors and illustrate how it affects the detection capability of the corresponding criteria. The invariance under displacements of the dominant principal minors $d_{1\cdots N} = \det(D_N)$ of the matrix of moments can be understood from the simple example of d_{123}. It exploits a property of the determinant, namely that adding to a column (or row) a linear combination of any other columns (or rows) does not change the value of the determinant. By using this property recursively to d_{123}, we show that it is equal to d^{α}_{123} where the superscript α means that the state has been transformed by the displacement operator $\hat{D}(\alpha) = \exp\left(\alpha\hat{a}^{\dagger} - \alpha^{*}\hat{a}\right)$, which transforms the operator $\hat{a}$ into $\hat{a} + \alpha$ and $\hat{a}^{\dagger}$ into $\hat{a}^{\dagger} + \alpha^{*}$.

$$
\begin{aligned}
d_{123} &= \begin{vmatrix} 1 & \langle\hat{a}\rangle & \langle\hat{a}^{\dagger}\rangle \\ \langle\hat{a}^{\dagger}\rangle & \langle\hat{a}^{\dagger}\hat{a}\rangle & \langle\hat{a}^{\dagger 2}\rangle \\ \langle\hat{a}\rangle & \langle\hat{a}^{2}\rangle & \langle\hat{a}^{\dagger}\hat{a}\rangle \end{vmatrix}, \\
&= \begin{vmatrix} 1 & \langle\hat{a}\rangle + \alpha & \langle\hat{a}^{\dagger}\rangle + \alpha^{*} \\ \langle\hat{a}^{\dagger}\rangle & \langle\hat{a}^{\dagger}\hat{a}\rangle + \alpha\langle\hat{a}^{\dagger}\rangle & \langle\hat{a}^{\dagger 2}\rangle + \alpha^{*}\langle\hat{a}^{\dagger}\rangle \\ \langle\hat{a}\rangle & \langle\hat{a}^{2}\rangle + \alpha\langle\hat{a}\rangle & \langle\hat{a}^{\dagger}\hat{a}\rangle + \alpha^{*}\langle\hat{a}\rangle \end{vmatrix}, \\
&= \begin{vmatrix} 1 & \langle\hat{a}\rangle + \alpha & \langle\hat{a}^{\dagger}\rangle + \alpha^{*} \\ \langle\hat{a}^{\dagger}\rangle + \alpha^{*} & \langle\hat{a}^{\dagger}\hat{a}\rangle + \alpha\langle\hat{a}^{\dagger}\rangle + \alpha^{*}(\langle\hat{a}\rangle + \alpha) & \langle\hat{a}^{\dagger 2}\rangle + \alpha^{*}\langle\hat{a}^{\dagger}\rangle + \alpha^{*}(\langle\hat{a}^{\dagger}\rangle + \alpha^{*}) \\ \langle\hat{a}\rangle + \alpha & \langle\hat{a}^{2}\rangle + \alpha\langle\hat{a}\rangle + \alpha(\langle\hat{a}\rangle + \alpha) & \langle\hat{a}^{\dagger}\hat{a}\rangle + \alpha^{*}\langle\hat{a}\rangle + \alpha(\langle\hat{a}^{\dagger}\rangle + \alpha^{*}) \end{vmatrix}, \\
&= \begin{vmatrix} 1 & \langle\hat{a} + \alpha\rangle & \langle\hat{a}^{\dagger} + \alpha^{*}\rangle \\ \langle\hat{a}^{\dagger} + \alpha^{*}\rangle & \langle(\hat{a}^{\dagger} + \alpha^{*})(\hat{a} + \alpha)\rangle & \langle(\hat{a}^{\dagger} + \alpha^{*})^{2}\rangle \\ \langle\hat{a} + \alpha\rangle & \langle(\hat{a} + \alpha)^{2}\rangle & \langle(\hat{a}^{\dagger} + \alpha^{*})(\hat{a} + \alpha)\rangle \end{vmatrix}, \\
&= d^{\alpha}_{123}.
\end{aligned}
\tag{6.6}
$$

This proof holds for any dominant principal minors d_N but not for the other principal minors of the matrix of moments D_N. Remember that we adopt a slightly relaxed definition of dominant principal minors, which means that we must exhaust all rows and columns of a block before moving to the next block but the order of rows and columns is irrelevant within a given block.

6.3 Nonclassicality criteria based on the matrix of moments

Let us benchmark the performance of the nonclassicality criteria derived from the principal submatrices of the matrix of moments D_N (up to $N = 5$) in terms of their ability to detect the nonclassicality of various nonclassical states. We express the corresponding principal minors for common classes of nonclassical pure states, such as Fock states, squeezed states, or cat states (note that all these states are centered in phase space). All values are listed in Table 6.1, where negative values imply the actual detection of nonclassicality (see entries with gray background). We then study the performance of the criteria when applied to Gaussian (pure or mixed) states and determine that d_{123} is a necessary and sufficient nonclassicality criterion for these states. Overall, our observations lead us to focus on d_{15}, d_{23}, d_{123} and d_{1235} when constructing multicopy nonclassicality observables in Section 6.4.

6.3.1 Nonclassical pure states

Fock states

Fock states $|n\rangle$ (except for the vacuum state $|0\rangle$) are common nonclassical states, which can be identified as nonclassical states by criteria such as d_{15}, d_{125}, d_{135}, d_{145}, or d_{1235}, as can be seen in Table 6.1 (see Subsection 2.4.2 for the definition of a Fock state). In a nutshell, the nonclassicality of the Fock states is only detected when an odd number of off-diagonal entries of the type $\langle \hat{a}^{\dagger k} \hat{a}^{k} \rangle$ appear in the principal submatrix of the matrix of moments D_N. This explains why Fock states' nonclassicality is only detected in Table 6.1 for criteria that involve the fifth row or column since the first non-zero off-diagonal element of D_5 is $(D_5)_{1,5} = (D_5)_{5,1}$. For completeness, we list all nonzero moments (entries of matrix D_5) in Table 6.2.

Squeezed states

Squeezed states are nonclassical quantum states (see Subsection 2.4.1 for the definition of a squeezed state) which can be used, for instance, to enhance the sensitivity of the LIGO experiment [1, 26] by improving a detector such that it can go beyond the quantum noise limit. In order to check which principal minors detect them as nonclassical states, we need to evaluate the entries of the matrix of moments D_5. First, we observe that all moments $\langle \hat{a}^{\dagger k} \hat{a}^{l} \rangle$ of odd order $k + l$ vanish since squeezed states can be decomposed into even Fock states [159], that is

$$|S_r\rangle = \frac{1}{\sqrt{\cosh r}} \sum_{k=0}^{\infty} (-e^{i\phi} \tanh r)^k \frac{\sqrt{2k!}}{2^k k!} |2k\rangle, \tag{6.7}$$

where r is the squeezing factor and ϕ is the squeezing angle.

The non-vanishing low-order moments are listed in Table 6.2 (as a consequence of the rotation invariance, we may assume $\phi = 0$ without loss of generality). These expressions allow us to easily calculate the different determinants of principal submatrices from the matrix of moments D_5 for squeezed states (see Table 6.1). The nonclassicality of squeezed states is detected, for example, by d_{23}, d_{123}, d_{234}, d_{235}, or d_{1235}.

Size	Principal minor	Fock states	Squeezed states	Odd cat states	Even cat states
2	$d_{12} = d_{13}$	n	$\sinh^2(r)$	$\lvert\beta\rvert^2 \frac{N_+}{N_-}$	$\lvert\beta\rvert^2 \frac{N_-}{N_+}$
2	$d_{14} = d_{16}$	$n(n-1)$	$2\sinh^4(r)$	0	0
2	d_{15}	$-n$	$\cosh(2r)\sinh^2(r)$	$\lvert\beta\rvert^4(1 - \frac{N_+^2}{N_-^2})$	$\lvert\beta\rvert^4(1 - \frac{N_-^2}{N_+^2})$
2	d_{23}	n^2	$-\sinh^2(r)$	$\lvert\beta\rvert^4(\frac{N_+^2}{N_-^2} - 1)$	$\lvert\beta\rvert^4(\frac{N_-^2}{N_+^2} - 1)$
2	$d_{24} = d_{26} = d_{34} = d_{36}$	$n^2(n-1)$	$\sinh^4(r)(\cosh^2(r) + 2\sinh^2(r))$	$\lvert\beta\rvert^6 \frac{N_+}{N_-}$	$\lvert\beta\rvert^6 \frac{N_-}{N_+}$
2	$d_{25} = d_{35}$	$n^2(n-1)$	$\sinh^4(r)(\cosh^2(r) + 2\sinh^2(r))$	$\lvert\beta\rvert^6 \frac{N_+}{N_-}$	$\lvert\beta\rvert^6 \frac{N_-}{N_+}$
2	$d_{45} = d_{56}$	$n^2(n-1)^2$	$\frac{1}{2}(5 - 3\cosh(2r))\sinh^4(r)$	$\lvert\beta\rvert^8(1 - \frac{N_+^2}{N_-^2})$	$\lvert\beta\rvert^8(1 - \frac{N_-^2}{N_+^2})$
2	d_{46}	$n^2(n-1)^2$	$-2(1 + 3\cosh(2r))\sinh^4(r)$	0	0
3	d_{123}	n^2	$-\sinh^2(r)$	$\lvert\beta\rvert^4(\frac{N_+^2}{N_-^2} - 1)$	$\lvert\beta\rvert^4(\frac{N_-^2}{N_+^2} - 1)$
3	$d_{124} = d_{126} = d_{134} = d_{136}$	$n^2(n-1)$	$2\sinh^6(r)$	0	0
3	$d_{125} = d_{135}$	$-n^2$	$\sinh^4(r)\cosh(2r)$	$\lvert\beta\rvert^6 \frac{N_+}{N_-}(1 - \frac{N_+^2}{N_-^2})$	$\lvert\beta\rvert^6 \frac{N_-}{N_+}(1 - \frac{N_-^2}{N_+^2})$
3	$d_{145} = d_{156}$	$-n^2(n-1)$	$-2\sinh^6(r)$	0	0
3	d_{146}	$n^2(n-1)^2$	$-4\cosh(2r)\sinh^4(r)$	0	0
3	$d_{234} = d_{236}$	$n^3(n-1)$	$\frac{1}{2}(1 - 3\cosh(2r))\sinh(r)^4$	$\lvert\beta\rvert^8(\frac{N_+^2}{N_-^2} - 1)$	$\lvert\beta\rvert^8(\frac{N_-^2}{N_+^2} - 1)$
3	d_{235}	$n^3(n-1)$	$-\sinh(r)^4(\cosh(r)^2 + 2\sinh(r)^2)$	$\lvert\beta\rvert^8(\frac{N_+^2}{N_-^2} - 1)$	$\lvert\beta\rvert^8(\frac{N_-^2}{N_+^2} - 1)$
3	$d_{245} = d_{256} = d_{345} = d_{356}$	$n^3(n-1)^2$	$\frac{1}{2}(5 - 3\cosh(2r))\sinh^6(r)$	$\lvert\beta\rvert^{10} \frac{N_+}{N_-}(1 - \frac{N_+^2}{N_-^2})$	$\lvert\beta\rvert^{10} \frac{N_-}{N_+}(1 - \frac{N_-^2}{N_+^2})$
3	$d_{246} = d_{346}$	$n^3(n-1)^2$	$-2(1 + 3\cosh(2r))\sinh^6(r)$	0	0
3	d_{456}	$n^3(n-1)^3$	$-8\sinh^6(r)$	0	0
4	d_{1234}	$n^3(n-1)$	$-2\sinh^6(r)$	0	0
4	d_{1235}	$-n^3$	$-\cosh(2r)\sinh^4(r)$	$-\lvert\beta\rvert^8(\frac{N_+^2}{N_-^2} - 1)^2$	$-\lvert\beta\rvert^8(\frac{N_-^2}{N_+^2} - 1)^2$
4	d_{1456}	$-n^3(n-1)^2$	$-4\sinh^6(r)$	0	0
5	d_{12345}	$-n^4(n-1)$	$2\sinh^8(r)$	0	0

Table 6.1: Principal minors of the matrix of moments (3.16) up to dimension N=5 evaluated for different classes of nonclassical (centered) pure states, namely Fock states $\lvert n\rangle$, squeezed states $\lvert S_r\rangle$ of squeezing parameter r, and even or odd cat states $\lvert c_{\pm}^{\beta}\rangle$ of complex amplitude β. A light gray background corresponds to states that are detected as nonclassical since the determinant is always negative, while a dark gray background corresponds to states that are only detected as nonclassical above a certain threshold value of the squeezing parameter r. The smallest minor that detects the nonclassicality of Fock states (and odd cat states) is d_{15}, while the smallest minor that detects the nonclassicality of squeezed states (and even cat states) is d_{23}. The minor d_{123} is equal to d_{23} for centered states, but, in addition, is invariant under displacements (not visible in the table). The minor d_{1235} yields the strongest criterion in this table since it detects the nonclassicality of Fock, squeezed, and (even and odd) cat states. It is worth mentioning that the minors $d_{24} = d_{26} = d_{34} = d_{36}$ and $d_{25} = d_{35}$ are positive (implying no detection of nonclassicality) for all states for which the moments of odd total order in $\hat{a}$ and $\hat{a}^\dagger$ are zero.

Moment	Fock	Squeezed	Cat	Thermal squeezed states
$\langle \hat{a}^\dagger \hat{a} \rangle$	n	$\sinh^2(r)$	$\lvert\beta\rvert^2 \frac{N_\mp}{N_\pm}$	$(\overline{n}+\frac{1}{2})\cosh(2r)-\frac{1}{2}$
$\langle \hat{a}^2 \rangle = \langle \hat{a}^{\dagger 2} \rangle^*$	0	$-\sinh(r)\cosh(r)$	β^2	$-(\overline{n}+\frac{1}{2})\sinh(2r)$
$\langle \hat{a}^{\dagger 2}\hat{a}^2 \rangle$	$n(n-1)$	$\sinh^2(r)\left[\cosh^2(r)+2\sinh^2(r)\right]$	$\lvert\beta\rvert^4$	$\frac{1}{2}(\overline{n}+\frac{1}{2})^2[3\cosh(4r)+1]-2(\overline{n}+\frac{1}{2})\cosh(2r)+\frac{1}{2}$
$\langle \hat{a}^\dagger \hat{a}^3 \rangle = \langle \hat{a}^{\dagger 3}\hat{a} \rangle^*$	0	$-3\sinh^3(r)\cosh(r)$	$\beta^2\lvert\beta\rvert^2\frac{N_\mp}{N_\pm}$	$-\frac{3}{2}(\overline{n}+\frac{1}{2})^2\sinh(4r)+\frac{3}{2}(\overline{n}+\frac{1}{2})\sinh(2r)$
$\langle \hat{a}^4 \rangle = \langle \hat{a}^{\dagger 4} \rangle^*$	0	$3\sinh^2(r)\cosh^2(r)$	β^4	$\frac{3}{2}(\overline{n}+\frac{1}{2})^2[\cosh(4r)-1]$

Table 6.2: Non-zero moments (entries of the matrix D_5) evaluated for different classes of nonclassical (centered) states, namely Fock states $|n\rangle$, squeezed states $|S_r\rangle$ of squeezing parameter r, even or odd cat states $|c_\pm^\beta\rangle$ of complex amplitude β, and Gaussian mixed states (for these, we may consider with no loss of generality a thermal state of mean photon number $\overline{n}$ that is squeezed with a squeezing parameter r). All these moments are used to evaluate the nonclassicality criteria based on the minors of the matrix of moments (3.16) as shown in Tables 6.1 and 6.3.

Cat states

Another archetype of nonclassical states consists of the even and odd optical cat states, written $|c_+\rangle$ and $|c_-\rangle$ respectively. These states were defined in Subsection 2.4.2. However, we remind here their definition: they are defined as superpositions of coherent states of opposite phases $|\beta\rangle$ and $|-\beta\rangle$, namely

$$|c_\pm^\beta\rangle = \frac{1}{\sqrt{N_\pm}}(|\beta\rangle \pm |-\beta\rangle), \tag{6.8}$$

where β is a complex amplitude and N_+ and N_- are normalization constants defined as $N_\pm = 2\left(1 \pm e^{-2|\beta|^2}\right)$. Remember that even cat states and odd cat states are orthogonal to each other, *i.e.*, $\langle c_\pm^\alpha | c_\mp^\beta\rangle = 0$, while applying the annihilation operator to an odd cat state results in a state proportional to an even cat state and vice-versa:

$$\hat{a}\ |c_\pm^\beta\rangle = \beta\sqrt{\frac{N_\mp}{N_\pm}}\ |c_\mp^\beta\rangle\,. \tag{6.9}$$

As the even cat state is orthogonal to the odd cat state, many moments appearing in the matrix will vanish and be equal to zero. As an example, we can calculate $\langle c_\pm^\beta|\ \hat{a}\ |c_\pm^\beta\rangle$:

$$\langle c_\pm^\beta|\ \hat{a}\ |c_\pm^\beta\rangle = \langle c_\pm^\beta|\ \beta\sqrt{\frac{N_\mp}{N_\pm}}\ |c_\mp^\beta\rangle = \beta\sqrt{\frac{N_\mp}{N_\pm}}\ \langle c_\pm^\beta|c_\mp^\beta\rangle = 0. \tag{6.10}$$

Using this logic, the only non-zero entries in the matrix of moments D_N are those of form $\langle \hat{a}^{\dagger k}\hat{a}^l\rangle$ where $k+l$ is even, as shown in Table 6.2 up to $k+l=4$. This allows us to calculate the different determinants of principal submatrices from the matrix of moments D_5 for even and odd cat states (see Table 6.1).

Observations

From Table 6.1, we can make the following observations (limited to the matrix of moments up to dimension 5) :

- Increasing the dimension of the matrix of moments does not necessarily lead to a stronger criterion. For example, d_{12345} does not detect the nonclassicality of more states than d_{1234} while being of higher order.
- Some criteria seem to be complementary in the sense that if the nonclassicality of a state is detected by one criterion, it will not be detected by the complementary criterion and vice-versa. This is, for instance, the case of d_{15} (detecting the nonclassicality of Fock states but not squeezed states) and d_{23} (detecting the nonclassicality of squeezed states but not Fock states). Furthermore, it is often the case that a criterion detecting the nonclassicality of Fock states such as d_{15} also detects the nonclassicality of odd cat

states (similarly, a criterion detecting squeezed states as nonclassical such as d_{23} often detects even cat states as nonclassical).

- The strongest criterion seems to be based on d_{1235} since it is the lowest order determinant that detects the nonclassicality of Fock states, squeezed, and (even and odd) cat states.

These observations motivate the rest of this chapter, in which we will mostly focus on the multicopy observables for determinants d_{15}, d_{23}, d_{123} and d_{1235}.

6.3.2 Nonclassical mixed states

The nonclassicality of mixed states has been studied, for example, in Refs. [82, 96, 75] and many other papers. We consider here the simplest case of Gaussian mixed states, for which the limit of nonclassicality is well known: a state is nonclassical if the smallest quadrature variance is smaller than the vacuum noise variance [82]. The relevant Gaussian mixed states here are the squeezed thermal states, since a displacement does not affect nonclassicality. It is also sufficient to consider squeezing of the x-quadrature since all considered criteria are invariant under rotations. The covariance matrix of these states is written as

$$\gamma^G = (\overline{n} + \frac{1}{2}) \begin{pmatrix} e^{-2r} & 0 \\ 0 & e^{2r} \end{pmatrix}, \tag{6.11}$$

where $\overline{n}$ is the mean photon number of the thermal state that is squeezed and r is the squeezing parameter.

In order to calculate the principal minors of interest (d_{15}, d_{23}, d_{123}, and d_{1235}), we take advantage of the fact that, for Gaussian states, the moments of order higher than two can be expressed as a function of the first- and second-order moments only. Given that squeezed thermal states are centered states, all elements of the matrix of moments D_N can thus be expressed from the covariance matrix γ^G. For example, the fourth-order moment $\langle \hat{a}^{\dagger 2} \hat{a}^2 \rangle$ can be calculated from the Wigner function $W(x, p)$ of the state $\hat{\rho}$ by using the overlap formula

$$\langle \hat{A} \rangle = \mathrm{Tr}(\hat{A}\hat{\rho}) = \int dx\, dp\, W(x, p)\, \bar{A}(x, p), \tag{6.12}$$

where $\bar{A}(x, p)$ is the Weyl transform of $\hat{A}$. The latter can be obtained by exploiting the commutation relation $[\hat{a}, \hat{a}^\dagger] = 1$ in such a way as to write $\hat{A} = \hat{a}^{\dagger 2} \hat{a}^2$ in terms of symmetrically-ordered operators only, namely

$$\hat{A} = S(\hat{a}^{\dagger 2} \hat{a}^2) - 2\, S(\hat{a}^\dagger \hat{a}) + \frac{1}{2}, \tag{6.13}$$

	Squeezed thermal states
d_{15}	$\frac{1}{4}[1-2(1+2\overline{n})\cosh(2r)+(1+2\overline{n})^2\cosh(4r)]$
$d_{123}=d_{23}$	$\frac{1}{2}+\overline{n}+\overline{n}^2-\frac{1}{2}(1+2\overline{n})\cosh(2r)$
d_{1235}	$d_{15}\,d_{23}$

Table 6.3: Principal minors of the matrix of moments D_5 evaluated for centered Gaussian states (*i.e.*, squeezed thermal states).

where $S(\cdot)$ denotes symmetric ordering and

$$\begin{aligned} S(\hat{a}^{\dagger 2}\hat{a}^2) &= \frac{1}{6}(\hat{a}^{\dagger 2}\hat{a}^2+\hat{a}^\dagger\hat{a}\hat{a}^\dagger\hat{a}+\hat{a}^\dagger\hat{a}^2\hat{a}^\dagger+\hat{a}\hat{a}^\dagger\hat{a}\hat{a}^\dagger+\hat{a}\hat{a}^{\dagger 2}\hat{a}+\hat{a}^2\hat{a}^{\dagger 2}), \\ S(\hat{a}^\dagger\hat{a}) &= \frac{1}{2}(\hat{a}^\dagger\hat{a}+\hat{a}\hat{a}^\dagger). \end{aligned} \tag{6.14}$$

Hence, $\hat{A}$ can be reexpressed in terms of the $\hat{x}$ and $\hat{p}$ quadrature operators as

$$\hat{A}=\frac{1}{12}(\hat{x}^2\hat{p}^2+\hat{p}^2\hat{x}^2+\hat{x}\hat{p}\hat{x}\hat{p}+\hat{x}\hat{p}^2\hat{x}+\hat{p}\hat{x}^2\hat{p}+\hat{p}\hat{x}\hat{p}\hat{x})+\frac{1}{4}(\hat{x}^4+\hat{p}^4)-(\hat{x}^2+\hat{p}^2)+\frac{1}{2}. \tag{6.15}$$

The Weyl transform of this expression yields

$$\bar{A}(x,p)=\frac{1}{2}x^2p^2+\frac{1}{4}(x^4+p^4)-(x^2+p^2)+\frac{1}{2}, \tag{6.16}$$

so that the mean value of $\hat{A}$ can be written as

$$\langle\hat{A}\rangle=\frac{1}{2}\langle x^2p^2\rangle+\frac{1}{4}\left(\langle x^4\rangle+\langle p^4\rangle\right)-\left(\langle x^2\rangle+\langle p^2\rangle\right)+\frac{1}{2}. \tag{6.17}$$

For a Gaussian distribution, we have

$$\begin{aligned} \langle x^4\rangle &= 3\,\Delta x^4 = 3\left(\overline{n}+\frac{1}{2}\right)^2 e^{-4r}, \\ \langle x^2p^2\rangle &= \Delta x^2\Delta p^2 = \left(\overline{n}+\frac{1}{2}\right)^2, \\ \langle p^4\rangle &= 3\,\Delta p^4 = 3\left(\overline{n}+\frac{1}{2}\right)^2 e^{4r}, \end{aligned} \tag{6.18}$$

so that we get the expression of $\langle\hat{a}^{\dagger 2}\hat{a}^2\rangle$ that is displayed in Table 6.2 for Gaussian states. By using the same method to calculate the other nonzero moments (also displayed in Table 6.2), we finally obtain the corresponding values of the principal minors shown in Table 6.3.

We see that d_{15} is always positive for any values of parameters $\overline{n}$ and r, so it does not yield a criterion. In contrast, d_{23} is interesting as it can be negative for some values of $\overline{n}$ and r. Of course, when the mean number of thermal photons $\overline{n}=0$, we recover the result for squeezed states and $d_{23}=-\sinh^2(r)$ is negative for all values of the squeezing parameter $r>0$. However, when $\overline{n}>0$, the determinant becomes positive below some threshold value of r. From Ref. [82], we know that a necessary and sufficient condition for a squeezed thermal state with covariance matrix γ^G to be nonclassical is

$$(\overline{n}+\frac{1}{2})\,e^{-2r}<\frac{1}{2}. \tag{6.19}$$

It is easy to check that this precisely corresponds to the condition $d_{23}<0$, so the criterion based on the sign of d_{23} is necessary and sufficient for squeezed thermal states. Note that d_{23} is not invariant under displacements, so that this criterion loses its power when applied to an arbitrary Gaussian state (*i.e.*, a displaced squeezed thermal state). However, the determinant d_{123} can be used instead since it is invariant under displacements and coincides with d_{23} for centered states. Thus, $d_{123}<0$ provides a necessary and sufficient nonclassicality criterion for Gaussian states.

Note finally that for the special case of centered Gaussian states (squeezed thermal states), d_{1235} is equal to the product of d_{15} and d_{23} since all entries of odd order in the annihilation and creation operators in the matrix of moments D_5 vanish. Since d_{15} is always positive for Gaussian states, d_{1235} has thus the same detection power as d_{23}. Furthermore, since it is invariant under displacements, d_{1235} has the same detection power as d_{123} for arbitrary Gaussian states. Yet, going beyond Gaussian states, we have seen that d_{1235} actually surpasses d_{123} in the sense that it also detects the nonclassicality of (displaced) Fock states.

This is also true for non-Gaussian mixed states. For example, we may consider a restricted class of non-Gaussian mixed states that are nonclassical as a result of photon addition or subtraction from a Gaussian state. Such states are viewed as essential for quantum computing, see *e.g.* Refs. [24, 158]. Interestingly, all the moments appearing in the matrix of moments D_N for these states can be deduced from the moments of the corresponding Gaussian states as displayed in Table 6.2. Indeed, for the photon-subtracted Gaussian states, the moments are

$$\begin{aligned}\langle\hat{a}^{\dagger k}\hat{a}^{l}\rangle &= \mathrm{Tr}(\hat{a}^{\dagger k}\hat{a}^{l}\hat{a}\rho^{G}\hat{a}^{\dagger}) = \mathrm{Tr}(\hat{a}^{\dagger(k+1)}\hat{a}^{(l+1)}\rho^{G}),\\ &= \langle\hat{a}^{\dagger(k+1)}\hat{a}^{(l+1)}\rangle_{G},\end{aligned} \tag{6.20}$$

where we have used the cyclic invariance property of the trace. For the photon-added Gaussian states, it can be shown that

$$\begin{aligned}\langle\hat{a}^{\dagger k}\hat{a}^{l}\rangle &= \mathrm{Tr}(\hat{a}^{\dagger k}\hat{a}^{l}\hat{a}^{\dagger}\rho^{G}\hat{a}),\\ &= \mathrm{Tr}((\hat{a}^{\dagger(k+1)}\hat{a}^{(l+1)}+(l+k+1)\hat{a}^{\dagger k}\hat{a}^{l}+kl\hat{a}^{\dagger(k-1)}\hat{a}^{(l-1)})\rho^{G}),\\ &= \langle\hat{a}^{\dagger(k+1)}\hat{a}^{(l+1)}\rangle_{G}+(l+k+1)\,\langle\hat{a}^{\dagger k}\hat{a}^{l}\rangle_{G}+kl\,\langle\hat{a}^{\dagger(k-1)}\hat{a}^{(l-1)}\rangle_{G}.\end{aligned} \tag{6.21}$$

Hence, we can easily derive the principal minors for photon-added and photon-subtracted Gaussian states directly from the matrix of moments calculated for the corresponding Gaussian states. It is worth noticing that even the simpler criterion based on d_{15} can detect the nonclassicality of photon-subtracted Gaussian states for small values of $\overline{n}$ and r, while it is useless in the case of Gaussian states. The parameter ranges of the Gaussian photon-substracted states for which d_{15} detects the nonclassicality is presented on Fig. 6.2.

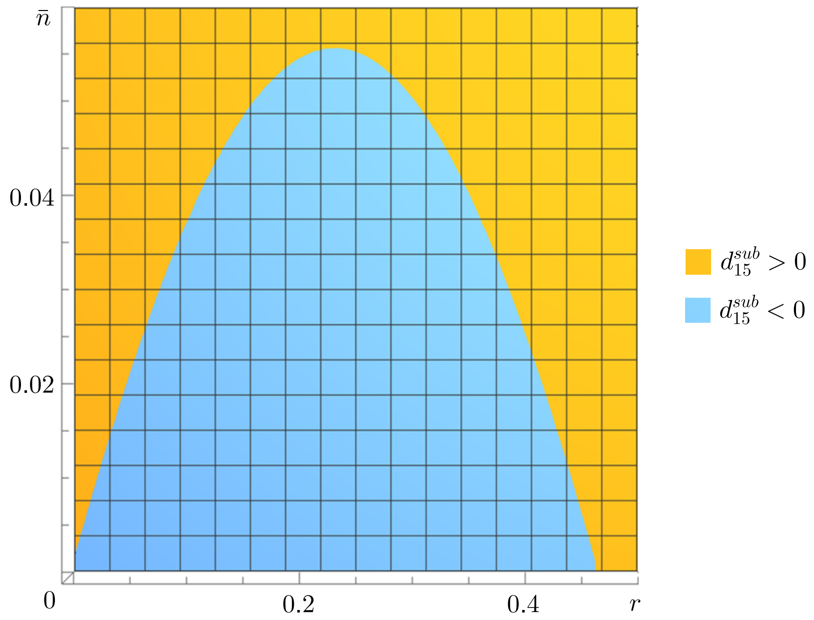

Figure 6.2: Value of d_{15} for Gaussian photon-substracted states. The blue region shows the values of the parameters for which the nonclassicality of the state is detected by d_{15}.

6.4 Multicopy nonclassicality observables

Potential implementations of nonclassicality criteria based on the matrix of moments D_N have been considered in Ref. [142], but the idea was to experimentally evaluate each individual entry of the matrix before calculating its determinant. Instead, in the present work, we look for an optical implementation that makes it possible to directly access the value of the determinant by measuring the expectation value of some nonclassicality observable. Since the principal minors discussed in Section 6.3 (especially d_{15}, d_{23}, d_{123}, and d_{1235}) are polynomial functions of the matrix elements of $\hat{\rho}$, we turn to multicopy observables as defined in Ref. [18]. This method appears to be well adapted here since the nonclassicality criteria involve determinants (a similar technique has been successfully applied for accessing determinants of other matrices of moments connected to uncertainty relations, see Ref. [65]).

We start by detailing the design of two-copy observables for accessing the determinants d_{12} and d_{14}, used as examples to introduce the method, followed by d_{23} and d_{15}. Then, we increase the number of copies and consider the 3-copy nonclassicality observable for d_{123} and 4-copy nonclassicality observable for d_{1235}. We also discuss the optical implementation of these observables whenever possible. In what follows, when we present a circuit, it is implicit that we put identical copies of a state in each input of the circuit.

6.4.1 Two-copy observables

Instructive examples: d_{12} and d_{14}

The determinant d_{12}, which is expressed as

$$d_{12} = \begin{vmatrix} 1 & \langle \hat{a} \rangle \\ \langle \hat{a}^\dagger \rangle & \langle \hat{a}^\dagger \hat{a} \rangle \end{vmatrix} = \langle \hat{a}^\dagger \hat{a} \rangle - \langle \hat{a} \rangle \langle \hat{a}^\dagger \rangle, \tag{6.22}$$

is useless for nonclassicality detection in the sense that it is positive for all (classical or non-classical) states. Indeed, d_{12} is simply the thermal (or chaotic) photon number, *i.e.*, the total photon number minus the coherent photon number $\langle \hat{a} \rangle \langle \hat{a}^\dagger \rangle$. Since d_{12} is invariant under displacements, centering the state on the origin in phase space simply results in $d_{12} = \langle \hat{a}^\dagger \hat{a} \rangle \geq 0$.

Nevertheless, it is instructive to illustrate the multicopy observable technique with this simple example, where we need two copies of the original state $\hat{\rho}$. We consider a 2×2 operator matrix mimicking the matrix of moments D_2 except that we remove all expectation values. Then, we associate the first row of this operator matrix with the first copy (mode 1) and the second row with the second copy (mode 2). In a last step, we average over all permutations $\sigma \in S_2$ on the mode indices in order to ensure the Hermiticity of the resulting multicopy observable, that is,

$$\begin{aligned} \hat{B}_{12} &= \frac{1}{|S_2|} \sum_{\sigma \in S_2} \begin{vmatrix} 1 & \hat{a}_{\sigma(1)} \\ \hat{a}^\dagger_{\sigma(2)} & \hat{a}^\dagger_{\sigma(2)} \hat{a}_{\sigma(2)} \end{vmatrix}, \\ &= \frac{1}{2} (\hat{a}_2^\dagger \hat{a}_2 + \hat{a}_1^\dagger \hat{a}_1 - \hat{a}_1 \hat{a}_2^\dagger - \hat{a}_2 \hat{a}_1^\dagger), \end{aligned} \tag{6.23}$$

where $|S_2| = 2!$ is the order of the symmetric group S_2.

Note that the method used above to obtain the multicopy observable will be used again several times in this thesis. The different steps to obtain the observable starting from a determinant that we want to measure are always the same. First, we drop the mean value in the determinant so that the determinant now contains operators. Then, we assign to each row of the determinant a copy index and finally, we sum on all the permutations of the indices so that the obtained operator is Hermitian. This method will always work when dealing with matrices that are Hermitian (which is the case in this chapter and will be the case in Chapter 8) by construction. In this case, this method gives us an easier way to obtain multicopy observables than the method presented by Brun in Ref. [18].

The value of the determinant d_{12} is obtained by measuring the expectation value of this observable on two copies of the same state $\hat{\rho}$, namely $\langle\langle \hat{B}_{12} \rangle\rangle \equiv \mathrm{Tr}[(\hat{\rho} \otimes \hat{\rho})\, \hat{B}_{12}]$. Indeed, we have

$$\begin{aligned}
\langle\langle \hat{B}_{12} \rangle\rangle &= \frac{1}{2} \langle\langle\, \hat{a}_2^\dagger \hat{a}_2 + \hat{a}_1^\dagger \hat{a}_1 - \hat{a}_1 \hat{a}_2^\dagger - \hat{a}_2 \hat{a}_1^\dagger \,\rangle\rangle, \\
&= \frac{1}{2} (\langle \hat{a}_2^\dagger \hat{a}_2 \rangle + \langle \hat{a}_1^\dagger \hat{a}_1 \rangle - \langle \hat{a}_1 \rangle \langle \hat{a}_2^\dagger \rangle - \langle \hat{a}_2 \rangle \langle \hat{a}_1^\dagger \rangle), \\
&= \langle \hat{a}^\dagger \hat{a} \rangle - \langle \hat{a} \rangle \langle \hat{a}^\dagger \rangle = d_{12},
\end{aligned} \tag{6.24}$$

where $\langle \cdot \rangle \equiv \mathrm{Tr}[\hat{\rho}\,\cdot]$.

Finally, we look for an optical implementation of observable $\hat{B}_{12}$ by means of linear optics and photon-number resolving detectors. Although it is not immediately obvious from Eq. (6.23), we can exploit the Jordan-Schwinger representation of angular momenta in terms of bosonic annihilation and creation operators. The Jordan-Schwinger representation of the SU(2) algebra connects the angular momentum operators with the bosonic mode operators of two modes $\hat{a}_1$ and $\hat{a}_2$ as follows

$$\hat{L}_j = \frac{1}{2} \hat{A}^\dagger \sigma_j \hat{A}, \tag{6.25}$$

where $\hat{A} = (\hat{a}_1\, \hat{a}_2)^T$ and σ_j are the three Pauli matrices with $j = x, y, z$. The fourth associated operator is denoted as

$$\hat{L}_0 = \frac{1}{2} \hat{A}^\dagger \sigma_0 \hat{A}, \tag{6.26}$$

where $\sigma_0 = \mathbf{1}$ is the 2×2 identity matrix, and it is linked to the Casimir operator $\hat{L}_x^2 + \hat{L}_y^2 + \hat{L}_z^2 = \hat{L}_0(\hat{L}_0 + 1)$. We get a representation of angular momenta as we recover the usual commutation relations $[\hat{L}_j, \hat{L}_k] = i\, \epsilon_{j,k,l}\, \hat{L}_l$ with $\epsilon_{j,k,l}$ being the Levi-Civita symbol, as well as $[\hat{L}_j, \hat{L}_0] = 0, \forall j$.

The three components of the angular momentum $\hat{L}$ can then be expressed as

$$\hat{L}_x = \frac{1}{2} (\hat{a}_2^\dagger \hat{a}_1 + \hat{a}_1^\dagger \hat{a}_2), \tag{6.27}$$

$$\hat{L}_y = \frac{i}{2} (\hat{a}_2^\dagger \hat{a}_1 - \hat{a}_1^\dagger \hat{a}_2), \tag{6.28}$$

$$\hat{L}_z = \frac{1}{2} (\hat{a}_1^\dagger \hat{a}_1 - \hat{a}_2^\dagger \hat{a}_2). \tag{6.29}$$

Hence, we can express $\hat{B}_{12}$ as the difference between $\hat{L}_0$ (*i.e.*, half the total photon number) and the x-component of the angular momentum operator, namely,

$$\hat{B}_{12} = \hat{L}_0 - \hat{L}_x. \tag{6.30}$$

In order to find the optical implementation of $\hat{B}_{12}$, let us derive the effect of linear optics transformations on the angular momentum operators. When applying a beam splitter of transmittance τ, the angular momentum operators transform as

$$\begin{aligned}
&\hat{L}_0 \to \hat{L}_0, \\
&\hat{L}_x \to (1-2\tau)\,\hat{L}_x + 2\sqrt{\tau(1-\tau)}\,\hat{L}_z, \\
&\hat{L}_y \to -\hat{L}_y, \\
&\hat{L}_z \to (2\tau-1)\,\hat{L}_z + 2\sqrt{\tau(1-\tau)}\,\hat{L}_x.
\end{aligned} \tag{6.31}$$

When applying a phase shifter of phase ϕ on the second mode, the angular momentum operators transforms as

$$\begin{aligned}
&\hat{L}_0 \to \hat{L}_0, \\
&\hat{L}_x \to \cos(\phi)\,\hat{L}_x - \sin(\phi)\,\hat{L}_y, \\
&\hat{L}_y \to \cos(\phi)\,\hat{L}_y + \sin(\phi)\,\hat{L}_x, \\
&\hat{L}_z \to \hat{L}_z.
\end{aligned} \tag{6.32}$$

These expressions are useful in order to find optical schemes for measuring the multicopy observables of interest. For example, we see that $\hat{L}_y$ transforms into $\hat{L}_x$ under a phase shift of $\pi/2$, while $\hat{L}_x$ transforms into $\hat{L}_z$ and vice versa under a 50:50 beam splitter transformation. This allows us to reexpress the multicopy observables of interest in such a way that they only depend on $\hat{L}_0$ and $\hat{L}_z$ operators (hence they are accessible via photon number measurement). Since the application of any linear optics (passive) transformation does not change the total photon number, $\hat{L}_0$ is unaffected by such a transformation which can de seen in Eqs. 6.31 and 6.32. In contrast, $\hat{L}_x$ can be turned by a 50:50 beam splitter into $\hat{L}_z$, which corresponds to the difference of the photon numbers between the two modes. This transformation has already been used in Ref. [65]. We can prove this by studying the transformation of the operators: applying a 50:50 beam splitter transforms the mode operators according to

$$\hat{a}'_1 = \frac{\hat{a}_1 + \hat{a}_2}{\sqrt{2}}, \qquad \hat{a}'_2 = \frac{\hat{a}_1 - \hat{a}_2}{\sqrt{2}}, \tag{6.33}$$

so that $\hat{L}_x$ transforms into $\hat{L}'_z = \frac{1}{2}(\hat{a}'^{\dagger}_1\hat{a}'_1 - \hat{a}'^{\dagger}_2\hat{a}'_2)$, where the primes refer to mode operators after the beam splitter. Hence, the operator $\hat{B}_{12}$ is transformed into

$$\hat{B}_{12} = \hat{L}_0 - \hat{L}'_z = \frac{1}{2}(\hat{n}'_1 + \hat{n}'_2 - \hat{n}'_1 + \hat{n}'_2) = \hat{n}'_2, \tag{6.34}$$

where $\hat{n}'_1 = \hat{a}'^{\dagger}_1\hat{a}'_1$ and $\hat{n}'_2 = \hat{a}'^{\dagger}_2\hat{a}'_2$.

This implies that measuring the mean photon number in the second mode after the beam splitter transformation of Fig. 6.3 gives the value of the determinant

$$d_{12} = \langle\langle \hat{B}_{12} \rangle\rangle = \langle \hat{n}'_2 \rangle. \tag{6.35}$$

Obviously, we have $d_{12} \geq 0$, so that d_{12} does not yield a useful criterion to detect nonclassical states. It is trivial to understand from Eq. (6.33) that this scheme gives access to the thermal

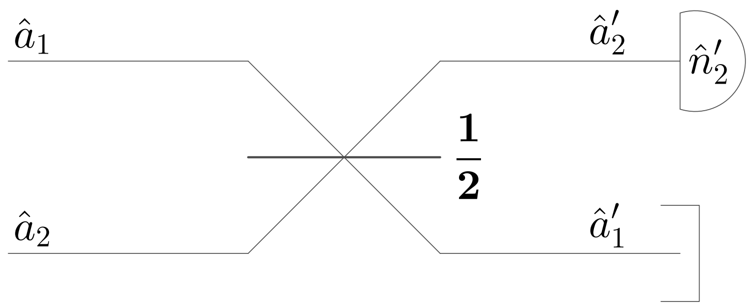

Figure 6.3: Implementation of the measurement of d_{12}. We first apply a 50:50 beam-splitter and then use a photon-number resolving detector on the second mode (*i.e.*, the mode where the coherent fields of the two identical input states interfere destructively), yielding n_2'.

(or chaotic) photon number since the coherent component of the two identical input states is concentrated on the first output mode $\hat{a}_1'$, while the mean field vanishes in the second output mode $\hat{a}_2'$. The latter is then only populated by the thermal photons.

Before moving to principal minors that are actually useful to detect nonclassicality, let us briefly consider the next case in Table 6.1, namely,

$$d_{14} = \begin{vmatrix} 1 & \langle \hat{a}^2 \rangle \\ \langle \hat{a}^{\dagger 2} \rangle & \langle \hat{a}^{\dagger 2}\hat{a}^2 \rangle \end{vmatrix} = \langle \hat{a}^{\dagger 2}\hat{a}^2 \rangle - \langle \hat{a}^2 \rangle \langle \hat{a}^{\dagger 2} \rangle. \tag{6.36}$$

By building the corresponding two-copy observable, it is straightforward to check that $d_{14} \geq 0$ so it is useless for nonclassicality detection. Indeed, we have

$$\begin{aligned} \hat{B}_{14} &= \frac{1}{|S_2|} \sum_{\sigma \in S_2} \begin{vmatrix} 1 & \hat{a}^2_{\sigma(1)} \\ \hat{a}^{\dagger 2}_{\sigma(2)} & \hat{a}^{\dagger 2}_{\sigma(2)}\hat{a}^2_{\sigma(2)} \end{vmatrix}, \\ &= \frac{1}{2}(\hat{a}_2^{\dagger 2}\hat{a}_2^2 + \hat{a}_1^{\dagger 2}\hat{a}_1^2 - \hat{a}_1^2\hat{a}_2^{\dagger 2} - \hat{a}_2^2\hat{a}_1^{\dagger 2}), \end{aligned} \tag{6.37}$$

In analogy with $\hat{B}_{12}$, this two-copy observable can be reexpressed in terms of angular momentum operators, namely,

$$\hat{B}_{14} = 2\,(\hat{L}_0^2 - \hat{L}_x^2). \tag{6.38}$$

As before, we may transform $\hat{L}_x$ into $\hat{L}_z'$ by using a 50:50 beam splitter as described in Eq. (6.33), which gives

$$\hat{B}_{14} = 2\,(\hat{L}_0^2 - \hat{L}_z'^2) = 2\,\hat{n}_1'\hat{n}_2'. \tag{6.39}$$

Thus, this determinant can be accessed by applying a 50:50 beam splitter on two identical copies as in Fig. 6.3 but then measuring the mean value of the product of the photon numbers, that is

$$d_{14} = \langle\langle \hat{B}_{14} \rangle\rangle = 2\,\langle \hat{n}_1'\hat{n}_2' \rangle \geq 0. \tag{6.40}$$

In the following, we apply the same technique to determinants that enable the detection of nonclassicality. The calculations follow exactly the same path: we assign a mode to each row of the operator matrix and then symmetrize it as in Eq. (6.23) or (6.37). Finally, whenever possible, we find a linear optics transformation such that the observable can be measured by means of photon number resolving detectors. Since the difficulty of this procedure increases with the number of copies, we limit our search to principal submatrices of D_5 up to dimension 4×4.

Detection of squeezed states: d_{23}

As shown in Table 6.1, the two most interesting principal submatrices of dimension 2×2 for detecting nonclassical states are d_{15} and d_{23}. We start with d_{23}, expressed as

$$d_{23} = \begin{vmatrix} \langle \hat{a}^\dagger \hat{a} \rangle & \langle \hat{a}^{\dagger 2} \rangle \\ \langle \hat{a}^2 \rangle & \langle \hat{a}^\dagger \hat{a} \rangle \end{vmatrix} = \langle \hat{a}^\dagger \hat{a} \rangle^2 - \langle \hat{a}^2 \rangle \langle \hat{a}^{\dagger 2} \rangle. \tag{6.41}$$

The criterion derived from d_{23} detects the nonclassicality of squeezed states and even cat states (it does not detect the nonclassicality of Fock states and odd cat states). Note that d_{23} is not invariant under displacements (as we shall see, this invariance can be enforced by considering d_{123} instead). Following the procedure described in Section 6.4.1, we obtain the multicopy observable

$$\begin{aligned} \hat{B}_{23} &= \frac{1}{|S_2|} \sum_{\sigma \in S_2} \begin{vmatrix} \hat{a}^\dagger_{\sigma(1)} \hat{a}_{\sigma(1)} & \hat{a}^{\dagger 2}_{\sigma(1)} \\ \hat{a}^2_{\sigma(2)} & \hat{a}^\dagger_{\sigma(2)} \hat{a}_{\sigma(2)} \end{vmatrix}, \\ &= \hat{a}_1^\dagger \hat{a}_1 \hat{a}_2^\dagger \hat{a}_2 - \frac{1}{2} \left(\hat{a}_1^{\dagger 2} \hat{a}_2^2 + \hat{a}_2^{\dagger 2} \hat{a}_1^2 \right). \end{aligned} \tag{6.42}$$

Similarly as for $\hat{B}_{12}$ or $\hat{B}_{14}$, we can express $\hat{B}_{23}$ in terms of angular momentum operators, namely,

$$\hat{B}_{23} = 2\, \hat{L}_y^2 - \hat{L}_0. \tag{6.43}$$

It must be noted that Eq. (6.43) can also be reexpressed more concisely as a normally ordered operator, namely,

$$\hat{B}_{23} = 2\ {:}\hat{L}_y^2{:}\,, \tag{6.44}$$

where the normal ordering symbol must be understood term by term, that is, we must expand $\hat{L}_y^2$ in powers of $\hat{a}$ and $\hat{a}^\dagger$ and then normally order each term separately.

Using Eq. (6.43), we may design a linear interferometer in order to measure $\hat{B}_{23}$ with photon-number resolving detectors. We consider the same interferometer as considered in Ref. [65], which is composed of a $\pi/2$ phase shifter on the second mode followed by a 50:50 beam splitter as shown in Fig. 6.4. Under the $\pi/2$ local phase shift, the second mode operator

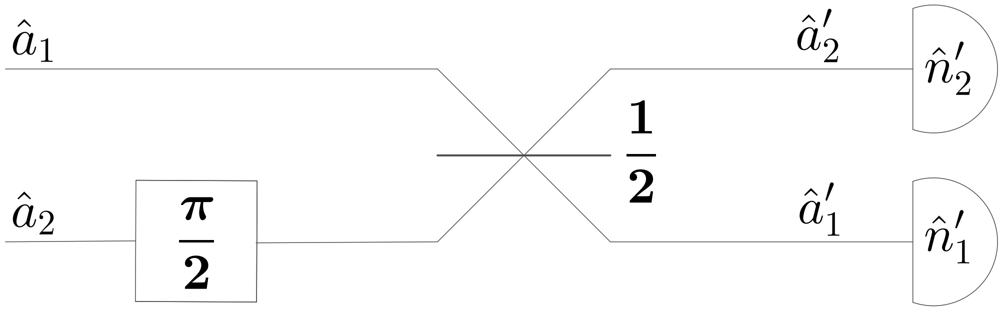

Figure 6.4: Implementation of the measurement of d_{23}. We first apply a phase shift of phase $\pi/2$ on the second mode, followed by a 50:50 beam splitter. Then, the value of d_{23} is accessed by measuring the number of photons in both output modes and computing Eq. (6.47).

transforms according to

$$\hat{a}'_2 = -i\,\hat{a}_2, \tag{6.45}$$

while the 50:50 beam splitter transformation is described in Eq. (6.33). The operator $\hat{L}_0$ is again invariant under these operations, but $\hat{L}_y$ transforms into $\hat{L}'_x$ following the phase shifter on the second mode and then transforms into $\hat{L}'_z$ after the 50:50 beam splitter. Hence, after applying the interferometer shown in Fig. 6.4, the nonclassicality observable takes the form

$$\begin{aligned}\hat{B}_{23} &= 2\ :\hat{L}'^2_z:\,, \\ &= 2\,\hat{L}'^2_z - \hat{L}_0, \\ &= \frac{1}{2}(\hat{n}'_1 - \hat{n}'_2)^2 - \frac{1}{2}(\hat{n}'_1 + \hat{n}'_2),\end{aligned} \tag{6.46}$$

and its expectation value yields

$$\begin{aligned}d_{23} &= \langle\langle \hat{B}_{23} \rangle\rangle, \\ &= \frac{1}{2}\left\langle (\hat{n}'_1 - \hat{n}'_2)^2 - (\hat{n}'_1 + \hat{n}'_2) \right\rangle.\end{aligned} \tag{6.47}$$

As a consequence, the principal minor d_{23} can be evaluated simply by accessing the joint photon number statistics on the two output modes $\hat{a}'_1$ and $\hat{a}'_2$.

It is instructive to understand how the nonclassicality of a squeezed state is detected by Eq. (6.47). Two copies of a squeezed state are transformed through the interferometer of Fig. 6.4 as follows. The phase shift rotates the second squeezed states by $\pi/2$, and the 50:50 beam splitter produces (from the two orthogonal squeezed states) a two-mode squeezed vacuum state, $(\cosh r)^{-1} \sum_{n=0}^{\infty} (\tanh r)^n\, |n, n\rangle$. This state exhibits a perfect photon-number correlation. Hence, the squared photon-number difference in Eq. (6.47) vanishes while the second term, which is proportional to the sum of photon numbers, comes with a negative sign. Thus, squeezed states are detected as nonclassical with $d_{23} < 0$ as soon as $r > 0$.

Note that Eq. (6.47) can also be reformulated as

$$d_{23} = \frac{1}{2}\left(Q_1'\langle\hat{n}_1'\rangle + Q_2'\langle\hat{n}_2'\rangle + \langle\hat{n}_1'\rangle^2 + \langle\hat{n}_2'\rangle^2 - 2\langle\hat{n}_1'\hat{n}_2'\rangle\right), \tag{6.48}$$

where Q_1' and Q_2' denote the Mandel Q parameters of the output states occupying modes $\hat{a}_1'$ and $\hat{a}_2'$. The Q parameter is defined as

$$Q = \frac{(\Delta\hat{n})^2 - \langle\hat{n}\rangle}{\langle\hat{n}\rangle}, \tag{6.49}$$

and measures the deviation from “Poissonianity” of the state (it vanishes for a coherent state, associated with a Poisson distribution). If the input state is a product of two identical coherent states, it is transformed under the interferometer of Fig. 6.4 into a product of two coherent states, hence $Q_1' = Q_2' = 0$. Further, $\langle\hat{n}_1'\rangle^2 = \langle\hat{n}_2'\rangle^2 = \langle\hat{n}_1'\hat{n}_2'\rangle$ since the two output coherent states are independent and have equal squared amplitudes. This confirms that $d_{23} = 0$ for coherent states.

Detection of Fock states: d_{15}

The criterion based on d_{15} is complementary to the one based on d_{23} as it detects the nonclassicality of Fock states and odd cat states (it does not detect the nonclassicality of squeezed states and even cat states). It is defined as

$$d_{15} = \begin{vmatrix} 1 & \langle\hat{a}^\dagger\hat{a}\rangle \\ \langle\hat{a}^\dagger\hat{a}\rangle & \langle\hat{a}^{\dagger 2}\hat{a}^2\rangle \end{vmatrix} = \langle\hat{a}^{\dagger 2}\hat{a}^2\rangle - \langle\hat{a}^\dagger\hat{a}\rangle^2, \tag{6.50}$$

and is not invariant under displacements (just as d_{23}). It can be rewritten as

$$d_{15} = \langle\hat{n}^2\rangle - \langle\hat{n}\rangle^2 - \langle\hat{n}\rangle = (\Delta\hat{n})^2 - \langle\hat{n}\rangle, \tag{6.51}$$

and can thus be reexpressed in terms of the Mandel Q parameter of the input state as

$$d_{15} = Q\,\langle\hat{n}\rangle, \tag{6.52}$$

so that the nonclassicality criterion based on d_{15} is simply a witness of the sub-Poissonian statistics ($Q < 0$) of the state. Obviously, we have $d_{15} = 0$ for coherent states while $d_{15} > 0$ for (classical) thermal states, as expected.

The procedure described in Section 6.4.1 yields the following two-copy nonclassicality observable

$$\hat{B}_{15} = \frac{1}{2}(\hat{n}_1 - \hat{n}_2)^2 - \frac{1}{2}(\hat{n}_1 + \hat{n}_2), \tag{6.53}$$

whose expectation value is written as

$$d_{15} = \frac{1}{2}\left\langle(\hat{n}_1 - \hat{n}_2)^2 - (\hat{n}_1 + \hat{n}_2)\right\rangle. \tag{6.54}$$

Interestingly, d_{15} involves the same observable as the one used to measure d_{23} [see Eq. (6.47)]

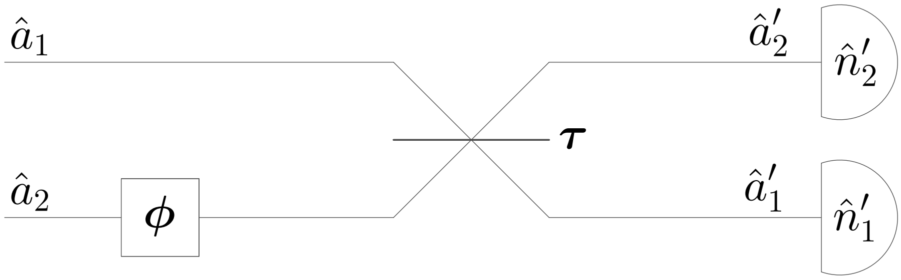

Figure 6.5: Extended circuit that interpolates between the measurement of d_{15} and d_{23}. We need a phase shifter of phase ϕ followed by a beam splitter of transmittance τ, and then we measure the photon number on both output modes in order to access the expectation value of the observable of Eq. (6.56).

except that we do not need the prior interferometer. This similarity will be exploited in the next section. It also implies that d_{15} can be expressed in terms of Mandel Q parameters of the input states, namely

$$d_{15} = \frac{1}{2}\left(Q_1\langle\hat{n}_1\rangle + Q_2\langle\hat{n}_2\rangle + (\langle\hat{n}_1\rangle - \langle\hat{n}_2\rangle)^2\right), \tag{6.55}$$

which resembles Eq. (6.48) where we have used $\langle\hat{n}_1\hat{n}_2\rangle = \langle\hat{n}_1\rangle\langle\hat{n}_2\rangle$ since the inputs are in a product state. Of course, for two identical inputs, this reduces to Eq. (6.52).

Interpolation between d_{15} and d_{23}

As we observe in Table 6.1, the criteria d_{15} and d_{23} taken together detect the nonclassicality of the four considered kinds of pure states. Given the similarity between Eqs. (6.47) and (6.54), it is tempting to construct a common multicopy observable that interpolates between d_{15} and d_{23}. It is based on a linear optical interferometer composed of a phase shifter of phase ϕ and a beam splitter of transmittance τ (see Fig. 6.5), followed by the measurement of the observable

$$\hat{B}_{15,23} = \frac{1}{2}(\hat{n}'_1 - \hat{n}'_2)^2 - \frac{1}{2}(\hat{n}'_1 + \hat{n}'_2), \tag{6.56}$$

where the primes refer to output modes. By applying the interferometer of Fig. 6.5 backwards on Eq. (6.56), we may reexpress it as a function of the input mode operators, namely

$$\hat{B}_{15,23} = \frac{1}{2} : [(\hat{a}_2^\dagger\hat{a}_1\, e^{-i\phi} + \hat{a}_1^\dagger\hat{a}_2\, e^{i\phi})\, 2\sqrt{(1-\tau)\tau} + (\hat{a}_1^\dagger\hat{a}_1 - \hat{a}_2^\dagger\hat{a}_2)\,(-1+2\tau)]^2 : . \tag{6.57}$$

This observable clearly interpolates between $\hat{B}_{15}$ ($\tau = 1$) and $\hat{B}_{23}$ ($\phi = \pi/2$ and $\tau = 1/2$). Since Eq. (6.57) is the square of a Hermitian operator, $\hat{B}_{15,23}$ can be written under the form $:\hat{f}^\dagger\hat{f}:$ and is indeed a valid observable for witnessing nonclassicality.

We start by setting the phase shift to $\phi = \pi/2$ as it does not play any role in $\hat{B}_{15}$ and study the detection of the different types of nonclassical states as a function of the transmittance

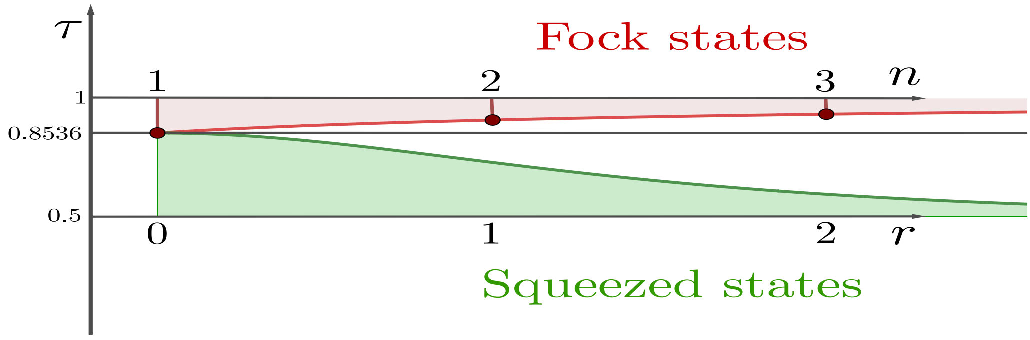

Figure 6.6: Detection limit on the parameter (n or r) characterizing the input state for several values of the transmittance τ (the phase is set to $\phi = \pi/2$). The red area corresponds to the values of n where the nonclassicality of the Fock states are detected (their nonclassicality is detected for $\tau = 1$, reducing to d_{15}), while the green region corresponds to the values of r where the nonclassicality of the squeezed states is detected (their nonclassicality is detected for $\tau = 1/2$, reducing to d_{23}). Unfortunately, at the threshold value $\tau^* \approx 0.8536$, all Fock states and squeezed states are left undetected.

τ (with $1/2 \leq \tau \leq 1$), see Fig. 6.6. It appears that the nonclassicality of Fock states $|n\rangle$ with $n \geq 1$ may only be detected when the transmittance is above a threshold value $\tau^* = (2+\sqrt{2})/4 \approx 0.8536$, while the nonclassicality of squeezed states with $r > 0$ may only be detected for values of the transmittance lower than this threshold τ^*. The value of τ^* is such that the coefficients of the two operator terms in Eq. (6.57) are equal. Moreover, it is possible to show that the nonclassicality of odd cat states may only be detected when $\tau > \tau^*$ while the nonclassicality of even cat states may only be detected when $\tau < \tau^*$. This means that there is no value of the transmittance enabling the detection of the four classes of nonclassical states considered in Table 6.1. Unfortunately, changing the value of the phase shift ϕ does not change the situation, so we cannot find a single two-copy observable that detects all four classes of nonclassical states.

Note that the criteria based on d_{15} and d_{23} can be viewed as complementary: if one of them detects a nonclassical state, *i.e.*, its value is negative, then the other one is necessarily positive for that state (of course, they can be both positive as, for example, for classical states). Indeed, we have

$$d_{23} + d_{15} = d_{14} \geq 0, \tag{6.58}$$

where the inequality comes from Eq. (6.40). Hence, the witnesses d_{15} and d_{23} cannot both simultaneously detect nonclassicality for a given state.

This can also be observed in Table 6.1 and Fig. 6.6: d_{15} and d_{23} play complementary roles in the detection of nonclassical states. In order to illustrate this fact, we study an arbitrary superposition of Fock states $|0\rangle$, $|1\rangle$, and $|2\rangle$ with real amplitudes a, b, and c, namely,

$$|\psi_{012}\rangle = a|0\rangle + b|1\rangle + c|2\rangle, \tag{6.59}$$

where $a^2 + b^2 + c^2 = 1$. First, by setting $c = 0$ in Eq. (6.59), *i.e.*, for a superposition of $|0\rangle$ and $|1\rangle$ Fock states, we see that the determinant d_{23} is always positive since $\langle \hat{a}^{\dagger 2}\rangle = \langle \hat{a}^2\rangle = 0$, so the nonclassicality is not detected. In contrast, d_{15} is always negative for all superpositions of $|0\rangle$ and $|1\rangle$ (this is expected since d_{15} detects the nonclassicality of $|1\rangle$). For this special case, the values of d_{23} and d_{15} are plotted in Fig. 6.9. Second, by setting $b = 0.1$ in Eq. (6.59), the situation is a bit more complicated but it confirms the complementarity of d_{23} and d_{15}, as shown in Fig. 6.7.

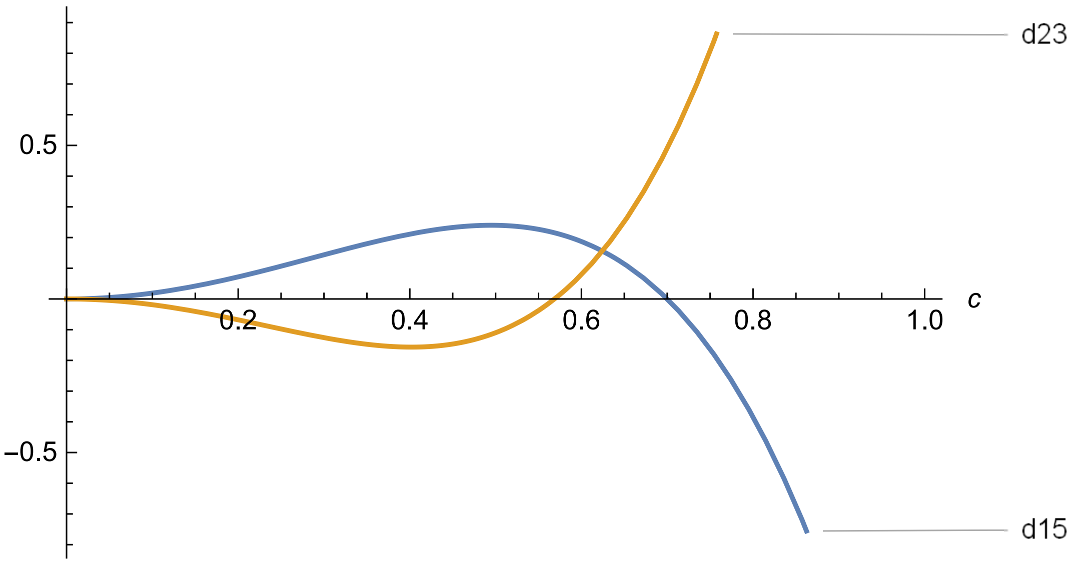

Figure 6.7: Comparison of the values of d_{15} and d_{23} for a ternary superposition of $|0\rangle$, $|1\rangle$, and $|2\rangle$ Fock states (with $b = 0.1$). The criteria d_{15} and d_{23} are complementary in the sense that they do not simultaneously detect nonclassicality.

Effect of a displacement on d_{15} and d_{23}

In general, we expect that the nonclassical character of a quantum state will be harder to detect when the state is moved away from the origin in phase space. As we shall see, this is often (but not always) the case. We can calculate the difference Δ^α between the determinant (d_{15} or d_{23}) when the state is displaced by $\hat{D}(\alpha)$ with $\alpha = |\alpha|e^{i\theta_\alpha}$ and the same determinant when the state is centered. The differences Δ^α in the case of d_{15} are presented in Table 6.4 for the considered states.

For Fock states as well as odd cat states, the effect of a displacement on d_{15} is given by an extra positive factor $\Delta^\alpha > 0$, so that displacements always deteriorate the detection. For squeezed states as well as even cat states, the result of a displacement on d_{15} is that it can either enhance ($\Delta^\alpha < 0$) or deteriorate ($\Delta^\alpha > 0$) the detection of nonclassicality. Indeed, the

State	$\Delta^\alpha = d_{15}^\alpha - d_{15}$
Fock	$\Delta^\alpha = 2n\|\alpha\|^2$
Squeezed	$\Delta^\alpha = 2\sinh(r)\|\alpha\|^2(\cosh(r)\cos(2\theta_\alpha - \psi) + \sinh(r))$
Odd cat	$\Delta^\alpha = 2\|\alpha\|^2\|\beta\|^2(\cos(2\theta_\alpha - 2\theta_\beta) + \frac{N_+}{N_-})$
Even cat	$\Delta^\alpha = 2\|\alpha\|^2\|\beta\|^2(\frac{N_-}{N_+} - \cos(2\theta_\alpha - 2\theta_\beta))$

Table 6.4: Effect of the displacement $\hat{D}(\alpha)$ on the determinant d_{15}. The table shows the difference between the determinant when the state is displaced and when it is centered (so that $\Delta^\alpha < 0$ implies an enhanced detection capability).

sign of Δ^α depends on the difference between the angle of squeezing ψ (or the angle of the cat state θ_β) and the angle of the displacement θ_α.

6.4.2 Three-copy observable

As we have observed in Section 6.4.1, the two-mode criteria d_{23} and d_{15} are not invariant under displacements. This comes with the fact that some nonclassical states become undetected if they are displaced in phase space. In order to overcome this effect of displacements, we build an observable involving a third replica of the input state following a similar reasoning as in Ref. [65]. We focus on the three-copy observable $\hat{B}_{123}$, which can be obtained by extending the procedure described in Section 6.4.1. From the explicit form of the principal minor

$$\begin{aligned} d_{123} &= \begin{vmatrix} 1 & \langle \hat{a} \rangle & \langle \hat{a}^\dagger \rangle \\ \langle \hat{a}^\dagger \rangle & \langle \hat{a}^\dagger \hat{a} \rangle & \langle \hat{a}^{\dagger 2} \rangle \\ \langle \hat{a} \rangle & \langle \hat{a}^2 \rangle & \langle \hat{a}^\dagger \hat{a} \rangle \end{vmatrix}, \\ &= \langle \hat{a}^\dagger \hat{a} \rangle^2 - \langle \hat{a}^{\dagger 2} \rangle \langle \hat{a}^2 \rangle - 2\langle \hat{a}^\dagger \rangle \langle \hat{a} \rangle \langle \hat{a}^\dagger \hat{a} \rangle + \langle \hat{a}^{\dagger 2} \rangle \langle \hat{a} \rangle^2 + \langle \hat{a}^\dagger \rangle^2 \langle \hat{a}^2 \rangle, \end{aligned} \tag{6.60}$$

we get the corresponding nonclassicality observable

$$\begin{aligned} \hat{B}_{123} &= \frac{1}{|S_3|} \sum_{\sigma \in S_3} \begin{vmatrix} 1 & \hat{a}_{\sigma(1)} & \hat{a}^\dagger_{\sigma(1)} \\ \hat{a}^\dagger_{\sigma(2)} & \hat{a}^\dagger_{\sigma(2)} \hat{a}_{\sigma(2)} & \hat{a}^{\dagger 2}_{\sigma(2)} \\ \hat{a}_{\sigma(3)} & \hat{a}^2_{\sigma(3)} & \hat{a}^\dagger_{\sigma(3)} \hat{a}_{\sigma(3)} \end{vmatrix}, \\ &= \frac{1}{3}\left(\hat{a}_2^\dagger \hat{a}_2 \hat{a}_3^\dagger \hat{a}_3 + \hat{a}_1^\dagger \hat{a}_1 \hat{a}_3^\dagger \hat{a}_3 + \hat{a}_1^\dagger \hat{a}_1 \hat{a}_2^\dagger \hat{a}_2 \right) \\ &- \frac{1}{6}(\hat{a}_2^{\dagger 2} \hat{a}_3^2 + \hat{a}_2^2 \hat{a}_3^{\dagger 2} + \hat{a}_1^{\dagger 2} \hat{a}_3^2 + \hat{a}_1^2 \hat{a}_3^{\dagger 2} + \hat{a}_1^{\dagger 2} \hat{a}_2^2 + \hat{a}_1^2 \hat{a}_2^{\dagger 2}) \\ &- \frac{1}{3}(\hat{a}_1^\dagger \hat{a}_1 \hat{a}_2^\dagger \hat{a}_3 + \hat{a}_1^\dagger \hat{a}_1 \hat{a}_2 \hat{a}_3^\dagger + \hat{a}_1 \hat{a}_2^\dagger \hat{a}_2 \hat{a}_3^\dagger + \hat{a}_1^\dagger \hat{a}_2^\dagger \hat{a}_2 \hat{a}_3 + \hat{a}_1 \hat{a}_2^\dagger \hat{a}_3^\dagger \hat{a}_3 + \hat{a}_1^\dagger \hat{a}_2 \hat{a}_3^\dagger \hat{a}_3) \\ &+ \frac{1}{3}\left(\hat{a}_1^{\dagger 2} \hat{a}_2 \hat{a}_3 + \hat{a}_1 \hat{a}_2^{\dagger 2} \hat{a}_3 + \hat{a}_1 \hat{a}_2 \hat{a}_3^{\dagger 2} \right) \\ &+ \frac{1}{3}\left(\hat{a}_1^2 \hat{a}_2^\dagger \hat{a}_3^\dagger + \hat{a}_1^\dagger \hat{a}_2^2 \hat{a}_3^\dagger + \hat{a}_1^\dagger \hat{a}_2^\dagger \hat{a}_3^2 \right), \end{aligned} \tag{6.61}$$

where $|S_3| = 3!$. It is straightforward to check that the mean value of this observable (6.61) over three identical copies gives $\langle\langle\langle \hat{B}_{123} \rangle\rangle\rangle = d_{123}$.

Similarly to $\hat{B}_{23}$, the nonclassicality observable $\hat{B}_{123}$ can be written in a much more compact form in terms of a normally-ordered expression

$$\hat{B}_{123} = \frac{2}{3} : \left(\hat{L}_y^{12} + \hat{L}_y^{23} + \hat{L}_y^{31}\right)^2 : , \tag{6.62}$$

where $\hat{L}_y^{kl} = \frac{i}{2}(\hat{a}_l^\dagger \hat{a}_k - \hat{a}_k^\dagger \hat{a}_l)$. Here, the superscript of the angular momentum component $\hat{L}_y$ stands for the two modes that are involved in the definition (6.28). The observable $\hat{B}_{123}$ can be accessed by first applying a linear optics transformation corresponding to the first two beam splitters in Fig. 6.8, which effects the rotation

$$\begin{aligned}
\hat{a}_1' &= \frac{1}{\sqrt{3}}(\hat{a}_1 + \hat{a}_2 + \hat{a}_3), \\
\hat{a}_2' &= \frac{1}{\sqrt{2}}(\hat{a}_1 - \hat{a}_2), \\
\hat{a}_3' &= \frac{1}{\sqrt{6}}(\hat{a}_1 + \hat{a}_2 - 2\hat{a}_3),
\end{aligned} \tag{6.63}$$

on the mode operators. Interestingly, this induces the same rotation of the angular momentum y-components,

$$\begin{aligned}
\hat{L}_y^{23\prime} &= \frac{1}{\sqrt{3}}(\hat{L}_y^{23} + \hat{L}_y^{31} + \hat{L}_y^{12}), \\
\hat{L}_y^{31\prime} &= \frac{1}{\sqrt{2}}(\hat{L}_y^{23} - \hat{L}_y^{31}), \\
\hat{L}_y^{12\prime} &= \frac{1}{\sqrt{6}}(\hat{L}_y^{23} + \hat{L}_y^{31} - 2\hat{L}_y^{12}).
\end{aligned} \tag{6.64}$$

In other words, the two vectors $(\hat{a}_1, \hat{a}_2, \hat{a}_3)^T$ and $(\hat{L}_y^{23}, \hat{L}_y^{31}, \hat{L}_y^{12})^T$ undergo the exact same orthogonal transformation. Note that, in contrast, the vectors $(\hat{L}_x^{23}, \hat{L}_x^{31}, \hat{L}_x^{12})^T$ and $(\hat{L}_z^{23}, \hat{L}_z^{31}, \hat{L}_z^{12})^T$ undergo different linear transformations which are mixing their components. By using Eq. (6.64), we can reexpress Eq. (6.62) in terms of output angular momentum variables as

$$\hat{B}_{123} = 2 : \left(\hat{L}_y^{23\prime}\right)^2 : , \tag{6.65}$$

which resembles Eq. (6.44) except that it acts on modes 2 and 3. Hence, in analogy with what we did for $\hat{B}_{23}$, we can access $\hat{B}_{123}$ with a subsequent linear optical transformation applied onto modes 2 and 3, corresponding to the phase shifter and last beam splitter in Fig. 6.8. This converts the angular momentum y-component associated with modes 2 and 3 into the corresponding z-component, so we have

$$\begin{aligned}
\hat{B}_{123} &= 2 : \left(\hat{L}_z^{23\prime\prime}\right)^2 : , \\
&= 2 \left(\hat{L}_z^{23\prime\prime}\right)^2 - \hat{L}_0^{23},
\end{aligned} \tag{6.66}$$

where the double primes refer to the output of the full circuit of Fig. 6.8. Here $\hat{L}_z^{kl} = \frac{1}{2}(\hat{a}_k^\dagger \hat{a}_k - \hat{a}_l^\dagger \hat{a}_l)$ and $\hat{L}_0^{kl} = \frac{1}{2}(\hat{a}_k^\dagger \hat{a}_k + \hat{a}_l^\dagger \hat{a}_l)$. Thus, after applying this circuit, the observable

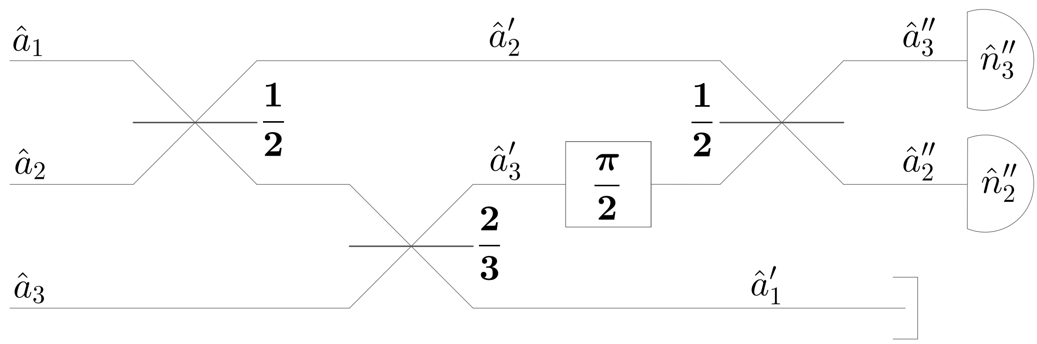

Figure 6.8: Three-mode circuit for accessing the nonclassicality witness d_{123}. We recognize the circuit for measuring d_{23} applied on modes 2 and 3, preceded by two beam splitters of transmittance $1/2$ and $2/3$ corresponding to the transformation of Eq. (6.63). The role of these two beam splitters is to concentrate the coherent field of the three replicas into mode 1, which is left unmeasured.

$\hat{B}_{123}$ transforms into

$$\hat{B}_{123} = \frac{1}{2}(\hat{n}_2'' - \hat{n}_3'')^2 - \frac{1}{2}(\hat{n}_2'' + \hat{n}_3''), \tag{6.67}$$

which is analogous to Eq. (6.46). Its expectation value yields

$$\begin{aligned} d_{123} &= \langle\langle\langle \hat{B}_{123} \rangle\rangle\rangle\,, \\ &= \frac{1}{2}\left\langle (\hat{n}_2'' - \hat{n}_3'')^2 - (\hat{n}_2'' + \hat{n}_3'') \right\rangle. \end{aligned} \tag{6.68}$$

The intuition behind this circuit follows from Ref. [65]. With the first two beam splitters in Fig. 6.8, we apply a transformation that concentrates the coherent component of the three identical input states in the first mode, which is traced out. The second and third modes thus have a vanishing mean field, so we can apply the same scheme as for measuring $\hat{B}_{23}$ but on these two modes, which leads to $\hat{B}_{123}$. Up to a mode relabelling, the operator in Eq. (6.67) is indeed the same as the one used for evaluating d_{23}, see Eq. (6.47). Notably, the circuit for evaluating d_{123} as shown in Fig. 6.8 is the same circuit as the one used in Ref. [65] in order to measure an uncertainty observable; the key difference is that the observable $(\hat{n}_2'' - \hat{n}_3'')^2/4$ must be measured instead at the output of the circuit in order to evaluate the uncertainty.

It must be noted that the circuit of Fig. 6.8 is not unique. Another option to access $\hat{B}_{123}$ is to apply the circuit of a three-dimensional discrete Fourier transform on the three input modes. This circuit is actually equivalent to the circuit of Fig. 6.8 up to $\pm\pi/6$ phase shifters on modes 2 and 3, which do not play a role since we measure photon numbers. Hence, this leads to the same observable.

We stress that in addition of being the displacement-invariant version of d_{23}, the criterion based on d_{123} is also superior in that it is able to detect the nonclassicality of states that are different from displaced states detected by d_{23}. A simple example is the superposition of the two Fock states $|0\rangle$ and $|1\rangle$, see Eq. (6.59) with $c = 0$. The values of d_{23} and d_{123} are plotted in Fig. 6.9. We see that while d_{23} never detects any superposition of the first two Fock

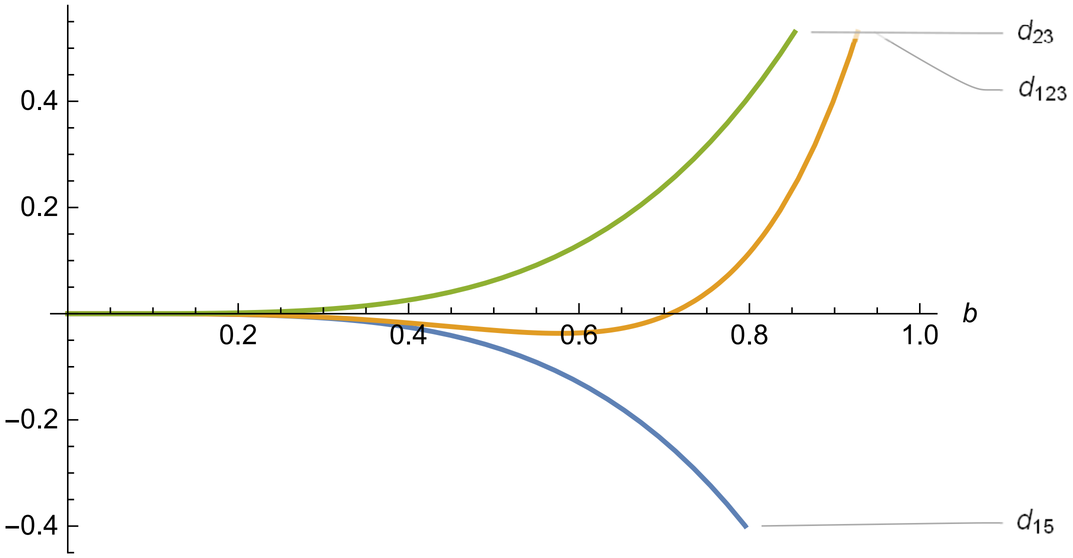

Figure 6.9: Comparison of the values of d_{123} and d_{23} for a superposition of $|0\rangle$ and $|1\rangle$ Fock states $|\psi_{01}\rangle = a|0\rangle + b|1\rangle$. While d_{23} never detects any such superposition as nonclassical, d_{123} detects them up to $b = 0.7$. Moreover, d_{15} always detects these superposition states as nonclassical.

states, d_{123} detects such superpositions up to $b = 0.7$. Note that d_{15} is always negative, which confirms that these superpositions are always nonclassical.

6.4.3 Four-copy observable

By adding a fourth replica of the input state, it is possible to further improve the detection capability of nonclassicality observables. The most interesting nonclassicality criterion derived from a 4×4 matrix is d_{1235} since it detects the nonclassicality of all squeezed, Fock, and even or odd cat states (see Table 6.1). It is written as

$$d_{1235} = \begin{vmatrix} 1 & \langle \hat{a} \rangle & \langle \hat{a}^\dagger \rangle & \langle \hat{a}^\dagger \hat{a} \rangle \\ \langle \hat{a}^\dagger \rangle & \langle \hat{a}^\dagger \hat{a} \rangle & \langle \hat{a}^{\dagger 2} \rangle & \langle \hat{a}^{\dagger 2} \hat{a} \rangle \\ \langle \hat{a} \rangle & \langle \hat{a}^2 \rangle & \langle \hat{a}^\dagger \hat{a} \rangle & \langle \hat{a}^\dagger \hat{a}^2 \rangle \\ \langle \hat{a}^\dagger \hat{a} \rangle & \langle \hat{a}^\dagger \hat{a}^2 \rangle & \langle \hat{a}^{\dagger 2} \hat{a} \rangle & \langle \hat{a}^{\dagger 2} \hat{a}^2 \rangle \end{vmatrix}. \tag{6.69}$$

As before, its associated four-copy observable $\hat{B}_{1235}$ can be obtained by assigning a different mode to each row and averaging over all $|S_4| = 4!$ permutations, namely

$$\hat{B}_{1235} = \frac{1}{|S_4|} \sum_{\sigma \in S_4} \begin{vmatrix} 1 & \hat{a}_{\sigma(1)} & \hat{a}^\dagger_{\sigma(1)} & \hat{a}^\dagger_{\sigma(1)} \hat{a}_{\sigma(1)} \\ \hat{a}^\dagger_{\sigma(2)} & \hat{a}^\dagger_{\sigma(2)} \hat{a}_{\sigma(2)} & \hat{a}^{\dagger 2}_{\sigma(2)} & \hat{a}^{\dagger 2}_{\sigma(2)} \hat{a}_{\sigma(2)} \\ \hat{a}_{\sigma(3)} & \hat{a}^2_{\sigma(3)} & \hat{a}^\dagger_{\sigma(3)} \hat{a}_{\sigma(3)} & \hat{a}^\dagger_{\sigma(3)} \hat{a}^2_{\sigma(3)} \\ \hat{a}^\dagger_{\sigma(4)} \hat{a}_{\sigma(4)} & \hat{a}^\dagger_{\sigma(4)} \hat{a}^2_{\sigma(4)} & \hat{a}^{\dagger 2}_{\sigma(4)} \hat{a}_{\sigma(4)} & \hat{a}^{\dagger 2}_{\sigma(4)} \hat{a}^2_{\sigma(4)} \end{vmatrix}. \tag{6.70}$$

This expression of $\hat{B}_{1235}$ is lengthy but we know that calculating its mean value $\langle\langle\langle\langle\hat{B}_{1235}\rangle\rangle\rangle\rangle$ yields d_{1235}. Since it is an Hermitian operator, $\hat{B}_{1235}$ may be rewritten as $\hat{B}_{1235} = :\hat{f}_{1235}^{\dagger}\hat{f}_{1235}:$, where $\hat{f}_{1235}$ is Hermitian too and is defined as

$$\begin{aligned}
\hat{f}_{1235} = \frac{-i}{2\sqrt{6}}(&\hat{a}_1^\dagger\hat{a}_1\hat{a}_2^\dagger\hat{a}_3 - \hat{a}_1^\dagger\hat{a}_2^\dagger\hat{a}_2\hat{a}_3 - \hat{a}_1^\dagger\hat{a}_1\hat{a}_2\hat{a}_3^\dagger + \hat{a}_1\hat{a}_2^\dagger\hat{a}_2\hat{a}_3^\dagger + \hat{a}_1^\dagger\hat{a}_2\hat{a}_3^\dagger\hat{a}_3 - \hat{a}_1\hat{a}_2^\dagger\hat{a}_3^\dagger\hat{a}_3 \\
&- \hat{a}_1^\dagger\hat{a}_1\hat{a}_2^\dagger\hat{a}_4 + \hat{a}_1^\dagger\hat{a}_2^\dagger\hat{a}_2\hat{a}_4 + \hat{a}_1^\dagger\hat{a}_1\hat{a}_3^\dagger\hat{a}_4 - \hat{a}_2^\dagger\hat{a}_2\hat{a}_3^\dagger\hat{a}_4 - \hat{a}_1^\dagger\hat{a}_3^\dagger\hat{a}_3\hat{a}_4 + \hat{a}_2^\dagger\hat{a}_3^\dagger\hat{a}_3\hat{a}_4 \\
&+ \hat{a}_1^\dagger\hat{a}_1\hat{a}_2\hat{a}_4^\dagger - \hat{a}_1\hat{a}_2^\dagger\hat{a}_2\hat{a}_4^\dagger - \hat{a}_1^\dagger\hat{a}_1\hat{a}_3\hat{a}_4^\dagger + \hat{a}_2^\dagger\hat{a}_2\hat{a}_3\hat{a}_4^\dagger + \hat{a}_1\hat{a}_3^\dagger\hat{a}_3\hat{a}_4^\dagger - \hat{a}_2\hat{a}_3^\dagger\hat{a}_3\hat{a}_4^\dagger \\
&- \hat{a}_1^\dagger\hat{a}_2\hat{a}_4^\dagger\hat{a}_4 + \hat{a}_1\hat{a}_2^\dagger\hat{a}_4^\dagger\hat{a}_4 + \hat{a}_1^\dagger\hat{a}_3\hat{a}_4^\dagger\hat{a}_4 - \hat{a}_2^\dagger\hat{a}_3\hat{a}_4^\dagger\hat{a}_4 - \hat{a}_1\hat{a}_3^\dagger\hat{a}_4^\dagger\hat{a}_4 + \hat{a}_2\hat{a}_3^\dagger\hat{a}_4^\dagger\hat{a}_4), \\
= \frac{2}{\sqrt{6}}(&\hat{L}_z^{12}\hat{L}_y^{34} + \hat{L}_z^{13}\hat{L}_y^{42} + \hat{L}_z^{14}\hat{L}_y^{23} + \hat{L}_y^{12}\hat{L}_z^{34} + \hat{L}_y^{13}\hat{L}_z^{42} + \hat{L}_y^{14}\hat{L}_z^{23}), \\
= \frac{1}{\sqrt{6}}&\sum_{\sigma\in P_4}\hat{L}_z^{\sigma(1)\sigma(2)}\hat{L}_y^{\sigma(3)\sigma(4)},
\end{aligned} \tag{6.71}$$

where P_4 is the group of even permutations. The expression of $\hat{f}_{1235}$ can be further simplified if we apply some linear optics transformation on the four modes. In analogy with the three-mode observable, we apply an orthogonal transformation on the mode operators that has the property of concentrating the coherent component of the four identical input states onto the first mode. By choosing the tensor product of two two-dimensional discrete Fourier transforms (realized with 50:50 beam splitters),

$$\begin{aligned}
\hat{a}_1' &= \frac{1}{2}(\hat{a}_1 + \hat{a}_2 + \hat{a}_3 + \hat{a}_4), \\
\hat{a}_2' &= \frac{1}{2}(\hat{a}_1 - \hat{a}_2 + \hat{a}_3 - \hat{a}_4), \\
\hat{a}_3' &= \frac{1}{2}(\hat{a}_1 + \hat{a}_2 - \hat{a}_3 - \hat{a}_4), \\
\hat{a}_4' &= \frac{1}{2}(\hat{a}_1 - \hat{a}_2 - \hat{a}_3 + \hat{a}_4),
\end{aligned} \tag{6.72}$$

we obtain the simpler expression

$$\hat{f}_{1235} = -\sqrt{\frac{2}{3}}(\hat{L}_x^{23'}\hat{L}_y^{23'} + \hat{L}_x^{34'}\hat{L}_y^{34'} + \hat{L}_x^{42'}\hat{L}_y^{42'}), \tag{6.73}$$

which only depends on modes 2, 3, and 4 as expected since $\hat{B}_{1235}$ is invariant under displacements. Thus, $\hat{f}_{1235}$ is simply proportional to the scalar product between vectors $(\hat{L}_x^{23'}, \hat{L}_x^{34'}, \hat{L}_x^{42'})^T$ and $(\hat{L}_y^{23'}, \hat{L}_y^{34'}, \hat{L}_y^{42'})^T$. However, we have not found a way to further simplify this expression and bring it to an experimental scheme. The problem is that $\hat{f}_{1235}$ is made of products of non-commuting operators $\hat{L}_x^{kl}$ and $\hat{L}_y^{kl}$, which, in addition, do not transform similarly when the mode operators undergo an orthogonal transformation. Unfortunately, applying local phase shifts and beam splitters does not help in reducing to an expression involving $\hat{L}_z^{kl}$ and $\hat{L}_0^{kl}$ only, as we were able to do for all previous multicopy observables.

Note that the issue does not seem to be related to the fact that we consider a four-copy observable. Indeed, while it is useless for nonclassicality detection, the principal minor d_{25} can be expressed as the expectation value of the two-copy observable

$$\hat{B}_{25} = :(\hat{L}_0 - \hat{L}_x)(\hat{L}_0^2 - \hat{L}_z^2):, \tag{6.74}$$

which also cannot be accessed using only linear optics and photon number measurements.

Let us stress that the criterion based on d_{1235} is in general stronger than those based on d_{23} and d_{15}. In the special case of centered states, that is $\langle \hat{a} \rangle = \langle \hat{a}^\dagger \rangle = 0$, we can show that d_{1235} can be negative even if d_{15} and d_{23} are both positive.

In this case, the determinant d_{1235} can be written as

$$d_{1235} = \begin{vmatrix} 1 & 0 & 0 & \langle \hat{a}^\dagger \hat{a} \rangle \\ 0 & \langle \hat{a}^\dagger \hat{a} \rangle & \langle \hat{a}^{\dagger 2} \rangle & \langle \hat{a}^{\dagger 2} \hat{a} \rangle \\ 0 & \langle \hat{a}^2 \rangle & \langle \hat{a}^\dagger \hat{a} \rangle & \langle \hat{a}^\dagger \hat{a}^2 \rangle \\ \langle \hat{a}^\dagger \hat{a} \rangle & \langle \hat{a}^\dagger \hat{a}^2 \rangle & \langle \hat{a}^{\dagger 2} \hat{a} \rangle & \langle \hat{a}^{\dagger 2} \hat{a}^2 \rangle \end{vmatrix}, \tag{6.75}$$

which, by using the method of cofactors, simplifies to

$$d_{1235} = d_{235} - \langle \hat{a}^\dagger \hat{a} \rangle^2 d_{23}. \tag{6.76}$$

We may factorize the determinant d_{235} by using the following property of determinants of block matrices. If A and D are square matrices and if A^{-1} exists, then

$$\det \begin{pmatrix} A & B \\ C & D \end{pmatrix} = \det(A)\ \det(D - CA^{-1}B). \tag{6.77}$$

Hence, assuming the extra constraint that D_{23} is invertible, we get

$$d_{235} = d_{23} \left(\langle \hat{a}^{\dagger 2} \hat{a}^2 \rangle - \begin{pmatrix} \langle \hat{a}^\dagger \hat{a}^2 \rangle & \langle \hat{a}^{\dagger 2} \hat{a} \rangle \end{pmatrix} D_{23}^{-1} \begin{pmatrix} \langle \hat{a}^{\dagger 2} \hat{a} \rangle \\ \langle \hat{a}^\dagger \hat{a}^2 \rangle \end{pmatrix} \right). \tag{6.78}$$

By plugging Eq. (6.78) into Eq. (6.76), we rewrite d_{1235} in a factorized form as

$$d_{1235} = d_{23} \left(d_{15} - \begin{pmatrix} \langle \hat{a}^\dagger \hat{a}^2 \rangle & \langle \hat{a}^{\dagger 2} \hat{a} \rangle \end{pmatrix} D_{23}^{-1} \begin{pmatrix} \langle \hat{a}^{\dagger 2} \hat{a} \rangle \\ \langle \hat{a}^\dagger \hat{a}^2 \rangle \end{pmatrix} \right). \tag{6.79}$$

In particular, under the assumption that D_{23} is positive definite (and hence $d_{23} > 0$) and that $d_{15} < 0$, then $d_{1235} < 0$ and nonclassicality can be detected for sure. Moreover, we see that d_{1235} is stronger than d_{23} and d_{15} since even if d_{15} is positive but smaller than the second term in the right-hand side of Eq. (6.79), then d_{1235} will detect the state as nonclassical.

An alternate decomposition of d_{1235} can be obtained by exchanging the role of d_{15} and

d_{23}, which results in

$$\begin{aligned} d_{1235} &= d_{23}\ \det\left(D_{15} - \frac{1}{d_{23}}\begin{pmatrix} 0 & 0 \\ 0 & x \end{pmatrix}\right), \\ &= d_{23}\, d_{15} - x. \end{aligned} \tag{6.80}$$

with $x = 2\langle \hat{a}^\dagger \hat{a}\rangle \langle \hat{a}^{\dagger 2}\hat{a}\rangle \langle \hat{a}^\dagger \hat{a}^2\rangle - \langle \hat{a}^{\dagger 2}\rangle \langle \hat{a}^\dagger \hat{a}^2\rangle^2 - \langle \hat{a}^2\rangle \langle \hat{a}^{\dagger 2}\hat{a}\rangle^2$. In this case again, we see that d_{1235} is stronger than d_{15} and d_{23} as it can be negative even if d_{15} and d_{23} are both positive.

If we further assume that $\langle \hat{a}^{\dagger 2}\hat{a}\rangle = \langle \hat{a}^\dagger \hat{a}^2\rangle = 0$, then we simply have

$$d_{1235} = d_{15} d_{23}, \tag{6.81}$$

in which case a separate implementation of the d_{15} and d_{23} circuits becomes sufficient to obtain the value of d_{1235} and there is no need for a four-copy observable. This is the case for Fock, squeezed, and cat states.

6.5 Conclusion and perspectives

In summary, we have analyzed a family of nonclassicality criteria based on the matrix of moments of the optical field and (restricting ourselves to dimension $N = 5$) have benchmarked their ability to detect nonclassical states, such as Fock states, squeezed states, and cat states. We have then developed a multicopy technique that allowed us to access these criteria by considering several identical replicas of the state and measuring the expectation value of some appropriate observables. For two- and three-copy nonclassicality observables, we have found a physical implementation that relies on linear optics and photodetectors with single-photon resolution. The main advantage of this multicopy technique is that it overcomes the need for full state tomography in order to detect nonclassicality. Furthermore, higher-order moments of the considered state can be accessed by measuring only lower-order moments such as the photon number on several replicas. The price to pay is of course the need to ensure interferometric stability on the replicas over which a joint observable is measured.

Specifically, we have found that the criteria based on d_{23} and d_{15} are detecting well-known nonclassical features such as squeezing (for d_{23}) and sub-Poissonian photon number statistics (for d_{15}). These criteria can be accessed with a simple linear optics circuit applied on two replicas of the state, followed by photon number measurement. Then, we have found a stronger criterion based on d_{123}, which is invariant under displacements but keeps the same detection performance as d_{23}. This criterion can be associated with a three-copy nonclassicality observable $\hat{B}_{123}$, which can again be accessed with interferometry and photon number measurements. Further, it also leads to a necessary and sufficient condition for the detection of nonclassicality in the entire set of Gaussian (pure and mixed) states.

Finally, we have identified the criterion based on d_{1235} as the most remarkable of all criteria built from the minors of the matrix of moments of dimension $N = 5$. It detects the nonclassicality of all states that are detected by d_{15} and d_{123} but also the nonclassicality of many more states that cannot be detected by either of them. We have found a simple expression for its associated four-copy nonclassicality observable $\hat{B}_{1235}$, but have unfortunately not been able to find a corresponding physical implementation in terms of a linear interferometer and photon number detectors. Finding an implementation (involving probably a more complex circuit or higher-order measurements) is left as a challenging open problem. The difficulty arises because of the much higher order in mode operators of the observable $\hat{B}_{1235}$. Since we deal with three modes in Eq. (6.73) rather than two modes as in Eq. (6.65), a possible approach could be to exploit the adjoint representation formed by 3×3 matrices instead of the fundamental representation of SU(2) (*i.e.*, the set of 2×2 Pauli matrices), written in terms of mode operators. Even though d_{1235} only gives a sufficient (not necessary) condition for nonclassicality, it is expected to detect a wide range of nonclassical states, so that finding a feasible optical implementation of d_{1235} would be highly valuable. Of course, in order to avoid false positives, one would have to assess the robustness of this nonclassicality condition against slightly different replicas, which will necessarily be the case in practice.

Another promising direction that is left for further work would be to extend our technique for detecting the nonclassicality of multimode optical states. We should be able to develop multicopy multimode observables, where each replica is made of several modes. Overall, this could result in an experimentally-friendly procedure to certify optical nonclassicality.

Chapter 7

Two-copy measurement of the quadrature coherence scale

This chapter is based on the following paper that I published together with Matthieu Arnhem, Stephan De Bièvre and Nicolas Cerf:

C. Griffet, M. Arnhem, S. De Bièvre, and N. J. Cerf. Interferometric measurement of the quadrature coherence scale using two replicas of a quantum optical state. Physical Review A, 108: 023730, August 2023. [50]

7.1 Introduction

In quantum optics, a state $\hat{\rho}$ is said to be optically classical provided its Glauber-Sudarshan P function is non-negative [151]. In other words, an optically classical state is a statistical mixture of coherent states. Detecting the optical nonclassicality of a given state $\hat{\rho}$ using this definition is, unfortunately, very difficult since the P function can be singular and hence hard to determine both theoretically and experimentally. Further, it is impractical to rule out the existence of a convex mixture of coherent states realizing $\hat{\rho}$ by checking all realizations of $\hat{\rho}$. Instead, one is usually forced to resort to so-called witnesses, which only provide a necessary condition on the non-negativity of $P(z)$, hence a sufficient condition on nonclassicality. Following this line, a large variety of witnesses and measures of optical nonclassicality have been proposed over the last decades in order to detect and quantify nonclassicality, see, *e.g.*, Refs. [4, 97, 124, 128, 30, 162, 88, 15, 66, 11, 67, 68, 90, 91, 32, 103, 79, 8, 147, 81, 5, 111, 129, 163, 95].

In this chapter, we focus on a witness of optical nonclassicality called the quadrature coherence scale (QCS) that we presented in Section 3.2.4. The difficulty with measuring the QCS (or many other nonclassicality witnesses) of an arbitrary state $\hat{\rho}$ arises from the fact that it is a nonlinear function of $\hat{\rho}$, as is obvious from Eq. (3.18). At first sight, it therefore seems that the task of experimentally accessing $\mathcal{C}(\hat{\rho})$ imposes one to carry out an exhaustive state tomography of $\hat{\rho}$ before computing Eq. (3.18). Here, we contradict this statement and exhibit an elegant solution that bypasses state tomography and only requires two replicas (independent and identical copies) of $\hat{\rho}$ in order to measure $\mathcal{C}(\hat{\rho})$. The fact that nonlinear functions of a state may be estimated by quantum interferometry using several replicas of the state has long been known [38, 109]. Specifically, the evaluation of any polynomial in the matrix elements of $\hat{\rho}$ can be reduced to the measurement of a joint observable over several replicas of $\hat{\rho}$ (the order of the polynomial translates into the number of replicas) [18]. This multicopy interferometric technique has, for example, been used to witness qubit entanglement by coupling two identical pairs of polarization-entangled photons with beam splitters [16]. It was also shown to give direct access to the purity and entanglement of atomic qubits in an optical lattice by coupling the atoms pairwise via beam-splitter operations [110, 116]. Notably, this method has been exploited for experimentally accessing the entanglement in a many-body Bose-Hubbard system [29, 78]. In particular, the purity of ultracold bosonic atoms in an optical lattice was accessed in Ref. [78] by probing the average parity at the output of a 50:50 beam splitter (realized by controlled tunneling).

Nonetheless, this multicopy technique has not yet been much exploited in continuous-variable quantum information theory and quantum optics. An exception is the recent derivation of symplectic-invariant entropic uncertainty relations in phase-space by using a multicopy uncertainty observable [65]. In a related work, it was also shown that nonclassicality witnesses based on matrices of moments of the optical field could be expressed as multicopy observables, resulting in possible experimental schemes to detect nonclassicality [6]. Here, we use similar ideas and show that the QCS of a state can be experimentally accessed by performing an interferometric measurement involving only two replicas of the state impinging on a 50:50 beam splitter. We thereby establish an interesting connection between the nonclassicality of a state and the resulting photon-number distribution at the output of the beam splitter, which can be viewed as an extension of the Hong-Ou-Mandel effect.

The chapter is organized as follows. In Section 7.2, we describe the aforementioned two-copy interferometric circuit and show how it enables measuring the purity of a single-mode state, which constitutes the denominator of the QCS. Then, in Section 7.3, we show how to use the same measurement to determine the numerator of the QCS, thereby establishing our central result. In Section 7.4, we illustrate our two-copy expression of the QCS [Eq. (7.21)] by applying it on several families of benchmark states. As a by-product of our analysis, we provide in Section 7.5 an alternative expression for the QCS that exploits the phase-space formulation of quantum optics and is of interest in its own right. In the process, we show that the same interferometric circuit can be used to compute the overlap between two distinct single-mode states. For notational convenience, we limit ourselves to the state of a single bosonic mode in Secs. 7.2, 7.3, 7.4, and 7.5, but we then show in Section 7.6 how to extend our results to multimode states. Finally, we conclude in Section 7.7.

7.2 Two-copy observable for measuring the purity

As is well known, directly accessing the purity $\mathcal{P}(\hat{\rho}) = \mathrm{Tr}(\hat{\rho}^2)$ of a quantum state $\hat{\rho}$ as the expectation value of some observable is impossible since it is nonlinear in $\hat{\rho}$. However, as is also well known and readily checked, it can be reexpressed as the expectation value of the so-called *swap* operator $\hat{S}$ taken over two replicas of the state, that is [38, 109]

$$\mathcal{P}(\hat{\rho}) = \mathrm{Tr}\left((\hat{\rho} \otimes \hat{\rho})\, \hat{S}\right), \tag{7.1}$$

where $\hat{S}$ is defined as $\hat{S}|\varphi\rangle|\psi\rangle = |\psi\rangle|\varphi\rangle, \forall\, |\varphi\rangle, |\psi\rangle$. Note that $\hat{S}$ is a unitary operator that is also Hermitian, so that it can be viewed as an observable. The fact that we need two replicas here is of course simply related to the fact that $\mathcal{P}(\hat{\rho})$ is quadratic in $\hat{\rho}$.

To find the actual measurement scheme, we proceed as in Refs. [29, 78]. The swap operator $\hat{S}$ naturally extends to the infinite-dimensional Fock space of a bosonic mode (or harmonic oscillator), in which case it is convenient to express it in terms of mode operators $\hat{a}$ and $\hat{b}$, namely,

$$\hat{S} = e^{i\frac{\pi}{2}(\hat{a}^\dagger - \hat{b}^\dagger)(\hat{a} - \hat{b})}. \tag{7.2}$$

To prove this equation, we introduce the Hamiltonian $\hat{H} = -(\hat{a}^\dagger - \hat{b}^\dagger)(\hat{a} - \hat{b})$ and write the Heisenberg evolution of $\hat{a}$ and $\hat{b}$, namely,

$$\begin{aligned} \hat{a}(t) &= \exp(it\hat{H})\, \hat{a}\, \exp(-it\hat{H}), \\ \hat{b}(t) &= \exp(it\hat{H})\, \hat{b}\, \exp(-it\hat{H}). \end{aligned} \tag{7.3}$$

Hence,

$$\begin{aligned} i\,\frac{d\hat{a}(t)}{dt} &= [\hat{a}(t), \hat{H}] = -\hat{a}(t) + \hat{b}(t), \\ i\,\frac{d\hat{b}(t)}{dt} &= [\hat{b}(t), \hat{H}] = -\hat{b}(t) + \hat{a}(t), \end{aligned} \tag{7.4}$$

resulting in the solution

$$\begin{aligned} \hat{a}(t) &= \frac{1 + e^{2it}}{2}\,\hat{a} + \frac{1 - e^{2it}}{2}\,\hat{b}, \\ \hat{b}(t) &= \frac{1 - e^{2it}}{2}\,\hat{a} + \frac{1 + e^{2it}}{2}\,\hat{b}. \end{aligned} \tag{7.5}$$

Setting $t = \pi/2$, we obtain

$$\hat{a}(\pi/2) = \hat{b}, \qquad \hat{b}(\pi/2) = \hat{a}, \tag{7.6}$$

effecting a swap of the two modes. This implies that $\hat{S} = e^{-i\frac{\pi}{2}\hat{H}}$, which proves Eq. (7.2).

In order to measure $\hat{S}$, we can simply use a 50:50 (balanced) beam splitter. The latter corresponds to the Gaussian unitary [159]

$$\hat{U}_{BS} = e^{\frac{\pi}{4}(\hat{a}^\dagger \hat{b} - \hat{a}\hat{b}^\dagger)}, \tag{7.7}$$

and, in the Heisenberg picture, it transforms the mode operators $\hat{a}$ and $\hat{b}$ as

$$\begin{aligned} \hat{c} &:= \hat{U}_{BS}^\dagger \, \hat{a} \, \hat{U}_{BS} = (\hat{a} + \hat{b})/\sqrt{2}, \\ \hat{d} &:= \hat{U}_{BS}^\dagger \, \hat{b} \, \hat{U}_{BS} = (-\hat{a} + \hat{b})/\sqrt{2}, \end{aligned} \tag{7.8}$$

where $\hat{c}$ and $\hat{d}$ denote the corresponding output mode operators. Hence, Eq. (7.2) can be reexpressed as

$$\hat{S} = e^{i\pi \, \hat{d}^\dagger \hat{d}} = (-1)^{\hat{n}_d}, \tag{7.9}$$

where $\hat{n}_d = \hat{d}^\dagger \hat{d}$ is the photon number in mode $\hat{d}$. Here, $\hat{d}$ stands for the "difference" mode, that is, it exhibits destructive interference if we feed the beam splitter with two identical coherent states. From Eq. (7.9), it thus appears that the measurement of the purity of a state can be achieved by measuring the average parity of the photon number in the "difference" mode at the output of a 50:50 beam splitter after having sent two identical copies of the state at its input. Indeed, Eq. (7.1) reduces to

$$\begin{aligned} \mathcal{P}(\hat{\rho}) &= \mathrm{Tr}\left((\hat{\rho} \otimes \hat{\rho}) \, (-1)^{\hat{n}_d}\right), \\ &= \mathrm{Tr}\left(\hat{U}_{\mathrm{BS}}(\hat{\rho} \otimes \hat{\rho}) \hat{U}_{\mathrm{BS}}^\dagger \, (-1)^{\hat{n}_b}\right), \end{aligned} \tag{7.10}$$

where the first (second) line corresponds to the Heisenberg (Schrödinger) picture. An analogous expression can be found in Refs. [29, 78]. Using the unitary $\hat{U}_{BS}$ corresponding to a 50:50 beam splitter as defined in Eq. (7.7), we can also express the swap operator (7.2) in the Heisenberg picture as

$$\hat{S} = \hat{U}_{BS}^\dagger \, e^{i\pi \, \hat{b}^\dagger \hat{b}} \, \hat{U}_{BS}. \tag{7.11}$$

Hence, the swap operator can be implemented by processing the two modes (forwards) through a 50:50 beam splitter, acting with a π-phase shift in the second mode, and then processing again the two modes (backwards) through a 50:50 beam splitter. As we could expect, $\hat{S}$ is simply the Gaussian unitary that corresponds to a Mach-Zehnder interferometer with a π-phase in one of the two arms, effecting a swap between the two modes.

As an illustration, let us check the effect of $\hat{S}$ on two coherent states $|\alpha\rangle$ and $|\beta\rangle$. We have

$$\begin{aligned} \hat{S} \, |\alpha\rangle \otimes |\beta\rangle &= \hat{U}_{BS}^\dagger \, e^{i\pi \, \hat{b}^\dagger \hat{b}} \, \hat{U}_{BS} \, |\alpha\rangle \otimes |\beta\rangle, \\ &= \hat{U}_{BS}^\dagger \, e^{i\pi \, \hat{b}^\dagger \hat{b}} \, \left|\frac{\alpha + \beta}{\sqrt{2}}\right\rangle \left|\frac{-\alpha + \beta}{\sqrt{2}}\right\rangle, \\ &= \hat{U}_{BS}^\dagger \, \left|\frac{\alpha + \beta}{\sqrt{2}}\right\rangle \left|\frac{\alpha - \beta}{\sqrt{2}}\right\rangle, \\ &= \left|\frac{(\alpha + \beta) - (\alpha - \beta)}{2}\right\rangle \left|\frac{(\alpha + \beta) + (\alpha - \beta)}{2}\right\rangle, \\ &= |\beta\rangle \otimes |\alpha\rangle, \end{aligned} \tag{7.12}$$

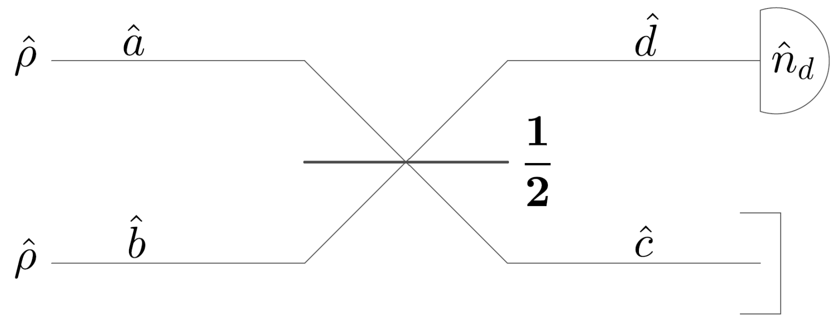

Figure 7.1: Two-copy circuit implementing the measurement of the purity $\mathcal{P}(\hat{\rho})$ as well as quadrature coherence scale $\mathcal{C}(\hat{\rho})$ of a bosonic state $\hat{\rho}$. Two identical copies of the state are sent on a 50:50 beam splitter and the photon number statistics is measured in the output mode d (associated with destructive interference). The mean photon number parity yields the purity, while the numerator and denominator of Eq. (7.21) can be accessed separately in order to determine the QCS.

where we have used the fact that a product of coherent states $|\alpha\rangle \otimes |\beta\rangle$ results under $\hat{U}_{BS}$ into another product of coherent states $|(\alpha+\beta)/\sqrt{2}\rangle \otimes |(-\alpha+\beta)/\sqrt{2}\rangle$. Alternatively, we can simply check that $\hat{S}\,|\alpha\rangle \otimes |\beta\rangle$ is a common eigenstate of $\hat{a}$ and $\hat{b}$ with respective eigenvalues β and α (note the interchange). Indeed, we have

$$\begin{aligned} \hat{a}\,(\hat{S}\,|\alpha\rangle \otimes |\beta\rangle) &= \hat{S}\,(\hat{S}^\dagger\,\hat{a}\,\hat{S})\,|\alpha\rangle \otimes |\beta\rangle, \\ &= \hat{S}\,\hat{b}\,|\alpha\rangle \otimes |\beta\rangle, \\ &= \beta\,(\hat{S}\,|\alpha\rangle \otimes |\beta\rangle), \end{aligned} \tag{7.13}$$

and a similar equation holds for $\hat{b}\,(\hat{S}\,|\alpha\rangle \otimes |\beta\rangle)$.

To sum up, the two-copy interferometric procedure in order to measure the purity of a state $\hat{\rho}$ is represented in Fig. 7.1. One must send two identical copies of $\hat{\rho}$ on a 50:50 beam splitter, which results in the output state $\hat{U}_{\mathrm{BS}}\,(\hat{\rho} \otimes \hat{\rho})\,\hat{U}^\dagger_{\mathrm{BS}}$, and then measure the number of photons with a photon-number resolving detector in the output that is associated with destructive interference. The purity is simply equal to the expectation value of the parity of the photon number in the reduced state $\hat{\rho}_d = \mathrm{Tr}_c(\hat{\rho} \otimes \hat{\rho})$ of mode $\hat{d}$, namely,

$$\mathcal{P}(\hat{\rho}) = \mathrm{Tr}_d\left(\hat{\rho}_d\,(-1)^{\hat{n}_d}\right). \tag{7.14}$$

This means that two identical copies have to be sent into a balanced beam splitter. At the output d of the beam splitter, we measure the number of photons. This experience is reproduced several times and we then calculate the mean value of the parity of the number of photons measured. This gives the purity of the input state. It makes sense that the output mode $\hat{d}$ is solely involved here because we expect the purity to be invariant under displacements of $\hat{\rho}$ in phase space. Indeed, mode $\hat{c}$ must be disregarded since its state depends on the mean field of the input state $\hat{\rho}$ (in contrast, the mean field of $\hat{\rho}_d$ always vanishes, regardless of the mean field of $\hat{\rho}$). Furthermore, we easily understand that Eq. (7.14) only shows a dependence in the photon number $\hat{n}_d$ in mode $\hat{d}$ since the purity is also invariant under rotations of $\hat{\rho}$ in phase space (remember that a rotation of $\hat{\rho}$ induces a rotation of $\hat{\rho}_d$ since the beam splitter unitary $\hat{U}_{BS}$ is covariant with respect to a pair of identical rotations).

7.3 Two-copy observable for measuring the QCS

The central result of this chapter is a two-copy interferometric procedure for measuring the QCS of a state. In the case of a single-mode state $\hat{\rho}$, Eq. (3.18) reduces to

$$\mathcal{C}^2(\hat{\rho}) = -\frac{1}{2\,\mathcal{P}(\hat{\rho})}\,\mathrm{Tr}\left([\hat{\rho},\hat{x}]^2 + [\hat{\rho},\hat{p}]^2\right), \tag{7.15}$$

where the purity $\mathcal{P}(\hat{\rho})$ appears in the denominator. The latter can be accessed by applying the multicopy technique as explained in Section 7.2 [see Eq. (7.14)], so we only need to focus on the numerator $\mathcal{N}(\hat{\rho})$. Writing

$$\mathcal{C}^2(\hat{\rho}) = \frac{\mathcal{N}(\hat{\rho})}{\mathcal{P}(\hat{\rho})}, \tag{7.16}$$

the numerator can be rewritten as

$$\begin{aligned}
\mathcal{N}(\hat{\rho}) &= -\frac{1}{2}\,\mathrm{Tr}\left([\hat{\rho},\hat{x}]^2 + [\hat{\rho},\hat{p}]^2\right), \\
&= \frac{1}{2}\bigg(\int (x-x')^2\,|\langle x|\hat{\rho}|x'\rangle|^2\,\mathrm{d}x\,\mathrm{d}x' \\
&\qquad + \int (p-p')^2\,|\langle p|\hat{\rho}|p'\rangle|^2\,\mathrm{d}p\,\mathrm{d}p'\bigg), \\
&= \frac{1}{2}\bigg(\int (x-x')^2\,\langle x,x'|\hat{\rho}\otimes\hat{\rho}|x',x\rangle\,\mathrm{d}x\,\mathrm{d}x' \\
&\qquad + \int (p-p')^2\,\langle p,p'|\hat{\rho}\otimes\hat{\rho}|p',p\rangle\,\mathrm{d}p\,\mathrm{d}p'\bigg),
\end{aligned} \tag{7.17}$$

where we have expanded the first and second terms of the right-hand side in the position and momentum basis, respectively.

In order to access $\mathcal{N}(\hat{\rho})$ from two copies of $\hat{\rho}$, we proceed along the same line as for the purity $\mathcal{P}(\hat{\rho})$. It is easy to recognize the two-copy observable $\hat{N}$ that appears in Eq. (7.17), that is,

$$\mathcal{N}(\hat{\rho}) = \mathrm{Tr}\left((\hat{\rho}\otimes\hat{\rho})\,\hat{N}\right), \tag{7.18}$$

where

$$\hat{N} = \frac{1}{2}\left[(\hat{x}_a-\hat{x}_b)^2 + (\hat{p}_a-\hat{p}_b)^2\right]\,\hat{S}, \tag{7.19}$$

with $\hat{x}_a$ ($\hat{p}_a$) and $\hat{x}_b$ ($\hat{p}_b$) denoting the position (momentum) quadratures of modes $\hat{a}$ and $\hat{b}$. The terms involving these quadratures can be simplified by using the quadratures $(\hat{x}_d, \hat{p}_d)$ of the difference mode $\hat{d}$, that is,

$$\hat{N} = (\hat{x}_d^2 + \hat{p}_d^2)\,\hat{S} = (1 + 2\,\hat{n}_d)\,\hat{S}. \tag{7.20}$$

The observable $\hat{N}$ plays the same role here as the swap operator $\hat{S}$ in Eq. (7.1). Note that the two factors in $\hat{N}$ are commuting Hermitians, which implies that $\hat{N}$ is itself Hermitian, as expected. Remarkably, we see that $\hat{N}$ is measurable with the same circuit as the one used for the purity in Fig. 7.1. Indeed, putting together Eqs. (7.9) and (7.20), we obtain the two-copy expression for the QCS,

$$\mathcal{C}^2(\hat{\rho}) = \frac{\mathrm{Tr}_d\left(\hat{\rho}_d\,(-1)^{\hat{n}_d}\,(1+2\,\hat{n}_d)\right)}{\mathrm{Tr}_d\left(\hat{\rho}_d\,(-1)^{\hat{n}_d}\right)}, \tag{7.21}$$

which is our main result. We again need to send two replicas of $\hat{\rho}$ on a 50:50 beam splitter and measure the photon number $\hat{n}_d$ of the state $\hat{\rho}_d$ in the "difference" mode $\hat{d}$. From the measured statistics of $\hat{n}_d$, we can compute both the numerator and denominator of Eq. (7.21).

Similarly as before, only the state of mode $\hat{d}$ is involved in Eq. (7.21), which was expected since the QCS is invariant under displacements in phase space. Further, Eq. (7.21) only depends on the photon number $\hat{n}_d$ in mode $\hat{d}$, which ensures that the QCS is, in addition, invariant under rotations in phase space.

7.4 Applications

Let us discuss some applications of this new expression of the QCS as a two-copy observable, Eq. (7.21). First, we emphasize that it gives a better grasp on the reason why it detects optical nonclassicality than the one-copy expression, Eq. (7.15). Indeed, we will show that it can be used to prove quite easily that $\mathcal{C}^2 \leq 1$ for any classical state (mixture of coherent states). In contrast with the proof of Ref. [30], the physical interpretation is straightforward. Sending two identical coherent states $|\alpha\rangle \otimes |\alpha\rangle$ in the 50:50 beam splitter of Fig. 7.1 results in a coherent state $|\sqrt{2}\,\alpha\rangle$ in mode $\hat{c}$ and the vacuum state $|0\rangle$ in mode $\hat{d}$. Hence, the measured value of $\hat{n}_d$ always vanishes and it is immediate that $\mathcal{C}^2(|\alpha\rangle\langle\alpha|) = 1$ for any coherent state $|\alpha\rangle$. Then, a simple calculation exploiting the Poisson distribution of the photon number in a coherent state is enough to prove that $\mathcal{C}^2$ can only decrease when mixing coherent states. Indeed, all classical states are mixtures of coherent states $\hat{\rho} = \int P(\alpha)\,|\alpha\rangle\langle\alpha|\,\mathrm{d}^2\alpha$. To measure the QCS, we inject two identical copies of state $\hat{\rho}$ in the circuit of Fig. 7.1, so the input state is

$$\hat{\rho}\otimes\hat{\rho} = \int P(\alpha)\,P(\beta)\,|\alpha\rangle\langle\alpha| \otimes |\beta\rangle\langle\beta|\,\mathrm{d}^2\alpha\,\mathrm{d}^2\beta, \tag{7.22}$$

with $\int P(\alpha)\,\mathrm{d}^2\alpha = 1$ and $P(\alpha) \geq 0, \forall\alpha$. Each product term $|\alpha\rangle \otimes |\beta\rangle$ of this mixture results, at the output of the 50:50 beam splitter, into another product of coherent states $|(\alpha+\beta)/\sqrt{2}\rangle \otimes |(-\alpha+\beta)/\sqrt{2}\rangle$. We only care here about the reduced output state in mode $\hat{d}$, that is

$$\hat{\rho}_d = \int P_d(\gamma)\,|\gamma\rangle\langle\gamma|\,\mathrm{d}^2\gamma, \tag{7.23}$$

where we have made the change of variables $\delta = (\alpha+\beta)/\sqrt{2}$ and $\gamma = (-\alpha+\beta)/\sqrt{2}$, and then have integrated over variable δ. Here, $P_d(\gamma)$ of course depends on $P(\alpha)$ but its explicit expression is irrelevant for the proof; we only note that $P_d(\gamma) \geq 0, \forall\gamma$, since it is a probability density, so that $\hat{\rho}_d$ is a classical state too.

We are left with having to compute the mean values of $(-1)^{\hat{n}_d}$ and $(-1)^{\hat{n}_d}(1+2\hat{n}_d)$ based on the distribution of the photon number n_d in state $\hat{\rho}_d$. Using the probability distribution of the photon number in a coherent state $|\gamma\rangle$,

$$p_\gamma(n) = e^{-|\gamma|^2}\frac{|\gamma|^{2n}}{n!}, \tag{7.24}$$

we obtain the following expressions

$$\sum_{n_d=0}^{\infty}(-1)^{n_d}\, p_\gamma(n_d) \;=\; e^{-|\gamma|^2}, \tag{7.25}$$

$$\sum_{n_d=0}^{\infty}(-1)^{n_d}\,(1+2n_d)\, p_\gamma(n_d) \;=\; e^{-|\gamma|^2}(1-|\gamma|^2). \tag{7.26}$$

Hence, taking the average over γ, we obtain the simple expression for the QCS:

$$\mathcal{C}^2(\rho) = \frac{\int P_d(\gamma)\, e^{-|\gamma|^2}(1-|\gamma|^2)\, \mathrm{d}^2\gamma}{\int P_d(\gamma)\, e^{-|\gamma|^2}\, \mathrm{d}^2\gamma}, \tag{7.27}$$

$$= 1 - \frac{\int P_d(\gamma)\, e^{-|\gamma|^2}|\gamma|^2\, \mathrm{d}^2\gamma}{\int P_d(\gamma)\, e^{-|\gamma|^2}\, \mathrm{d}^2\gamma}. \tag{7.28}$$

Since the second term in this expression is always positive, the QCS can only be smaller than or equal to 1 for classical states.

Second, we note that the definition of the QCS as given by Eq. (3.18) [or Eq. (7.15) for a single mode] is not convenient for computing its value. A number of alternative expressions have been derived in Refs. [30, 75, 62, 61] that are more suitable for this purpose in various situations. For example, if the Wigner function of state $\hat{\rho}$ is known, one can use Eq. (3.20), see below. Simple expressions also exist when the state $\hat{\rho}$ is pure [30] or Gaussian [62, 61]. In what follows, we analyze the new expression, Eq. (7.21), and illustrate its merits. We start by rewriting the expression of the purity, Eq. (7.10), as

$$\mathcal{P}(\hat{\rho}) = \sum_{n=0}^{\infty} p_n\,(-1)^n, \tag{7.29}$$

where

$$p_n = \langle n|\hat{\rho}_{\mathrm{out},b}|n\rangle, \tag{7.30}$$

is the probability of finding n photons in state

$$\hat{\rho}_{\mathrm{out},b} = \mathrm{Tr}_a\left(\hat{U}_{\mathrm{BS}}(\hat{\rho}\otimes\hat{\rho})\hat{U}_{\mathrm{BS}}^{\dagger}\right) \tag{7.31}$$

at the measured output of the beam splitter. Similarly,

$$\mathcal{N}(\hat{\rho}) = \sum_{n=0}^{\infty} p_n \,(-1)^n \,(1+2n)\,, \tag{7.32}$$

so that Eq. (7.21) can be rewritten as

$$\mathcal{C}^2(\hat{\rho}) = 1 + 2\,\frac{\sum_n n\,(-1)^n p_n}{\sum_n (-1)^n p_n}. \tag{7.33}$$

Whereas it looks simple, Eq. (7.33) yields a convenient method to compute the QCS theoretically only when the p_n's can be easily calculated. Still, the main message of our chapter is that, provided the p_n's can be experimentally measured using the above interferometric scheme, we get access to $\mathcal{C}^2(\hat{\rho})$ from Eq. (7.33).

Interestingly, we may suggestively rewrite $\mathcal{C}^2(\hat{\rho})$ in terms of some peculiar average. Let

$$\pi_n = \frac{(-1)^n \, p_n}{\sum_n (-1)^n \, p_n} \tag{7.34}$$

be the quasi-probability distribution associated with p_n (with $\sum_n \pi_n = 1$ but $\pi_n \ngeq 0$). Then, Eq. (7.33) becomes

$$\mathcal{C}^2(\hat{\rho}) = 1 + 2\,\langle n\,\rangle_\pi, \tag{7.35}$$

where $\langle\cdot\rangle_\pi$ denotes the average with respect to π_n. Hence, $\langle n\rangle_\pi > 0$ is equivalent to $\mathcal{C}^2(\hat{\rho}) > 1$ as a sufficient condition for optical nonclassicality.

At this point, it is instructive to consider what happens when $\hat{\rho} = |\psi\rangle\langle\psi|$ is a pure state, so that

$$\mathcal{P}(|\psi\rangle\langle\psi|) = \sum_n (-1)^n p_n = 1. \tag{7.36}$$

Since $\sum_n p_n = 1$, this implies that only even values of n can be observed at the output of the 50:50 beam splitter ($p_n = 0$ if n is odd), which can be viewed as the manifestation of an extended Hong-Ou-Mandel effect. In this case $\pi_n = p_n$ becomes a genuine probability distribution and the QCS is simply given by

$$\mathcal{C}^2(|\psi\rangle\langle\psi|) = 1 + 2\,\bar{n}, \tag{7.37}$$

where $\bar{n} = \sum_n n\,p_n$ is the average photon number in the measured output mode of the beam splitter. We see here that the QCS always exceeds one unless the pure state $|\psi\rangle$ is a coherent state, in which case $p_n = \delta_{n,0}$ and $\bar{n} = 0$. This is consistent with the fact that the only classical pure states are coherent states. The value of the QCS for all other pure states is very easy to find since $\bar{n} = \langle\hat{a}^\dagger\hat{a}\rangle_\psi - \langle\hat{a}\rangle_\psi \langle\hat{a}^\dagger\rangle_\psi$, where $\langle\cdot\rangle_\psi = \langle\psi|\cdot|\psi\rangle$ denotes the expectation value in the input pure state $|\psi\rangle$. This is sometimes also called the number of thermal (non-coherent) photons of $|\psi\rangle$. Furthermore, it is just equal to the average photon number $\bar{n} = \langle\hat{a}^\dagger\hat{a}\rangle_\psi$ of the input state if the latter state is centered on the origin (if the mean field vanishes). We then immediately recover the known expressions of the QCS for a vacuum squeezed state or a Fock state [30], namely,

$$\mathcal{C}^2(|\xi\rangle\langle\,\xi|) = \cosh(2r), \quad \mathcal{C}^2(|n\rangle\langle n|) = 1 + 2n. \tag{7.38}$$

Let us turn to examples of mixed states $\hat{\rho}$ and illustrate how the behavior of distribution of the p_n's yields a qualitative idea on the value of the QCS. For this purpose, we consider the following two families of states (these states were already presented in Section 3.2.4 but we give back their purity and QCS here as we will use it):

$$\hat{\rho}_{2M} = \frac{1}{2M}\sum_{n=1}^{2M}|n\rangle\langle n|, \quad \hat{\rho}_{\mathrm{even},M} = \frac{1}{M}\sum_{n=1}^{M}|2n\rangle\langle 2n|. \tag{7.39}$$

with $M \geq 1$. It was shown in Ref. [30] that

$$\mathcal{P}(\hat{\rho}_{2M}) = \frac{1}{2M}, \quad \mathcal{P}(\hat{\rho}_{\mathrm{even},M}) = \frac{1}{M}, \tag{7.40}$$

and

$$\mathcal{C}^2(\hat{\rho}_{2M}) = 1 + \frac{1}{M}, \quad \mathcal{C}^2(\hat{\rho}_{\mathrm{even},M}) = 1 + 2(M+1). \tag{7.41}$$

In other words, as M increases, both states are increasingly mixed, but, whereas this goes with a lower nonclassicality for $\hat{\rho}_{2M}$, the nonclassicality of $\hat{\rho}_{\mathrm{even},M}$ gets higher. As shown in Ref. [30], this corresponds to increasingly fast oscillations in the Wigner function of the $\hat{\rho}_{\mathrm{even},M}$, which are absent for the $\hat{\rho}_{2M}$.

These two families of states are phase-invariant. For those states, we can evaluate numerically the p_n to show that they can give information about the QCS. To find the p_n for phase-invariant states, let us first derive the photon number probability at the output if we put N photons in mode $\hat{a}$ and N' photons in mode $\hat{b}$. Then the initial state is given by:

$$|NN'\rangle_{a,b} = \frac{\hat{a}^{\dagger N}}{\sqrt{N!}}\frac{\hat{b}^{\dagger N'}}{\sqrt{N'!}}|00\rangle_{a,b}. \tag{7.42}$$

Expanding this state on the number bases associated to the c and d modes yields:

$$|NN'\rangle_{a,b} = \frac{(-\hat{c}^\dagger + \hat{d}^\dagger)^N}{\sqrt{2^N N!}}\frac{(\hat{c}^\dagger + \hat{d}^\dagger)^{N'}}{\sqrt{2^{N'}N'!}}|00\rangle_{a,b}, \tag{7.43}$$

$$= \sum_{n=0}^{N+N'}\sum_{n'=0}^{N'} c(n,n',N,N')|N+N'-n,n\rangle_{c,d}, \tag{7.44}$$

where

$$c(n,n',N,N') = \frac{(-1)^{N-n+n'}\sqrt{N!N'!(N+N'-n)!n!}}{\sqrt{2^{N+N'}}(n-n')!n'!(N-n+n')!(N'-n')!}. \tag{7.45}$$

Consequently, the photon probability distribution in mode $\hat{d}$ is equal to:

$$p_n^{N,N'} = \Big(\sum_{n'=0}^{N'} c(n,n',N,N')\Big)^2. \tag{7.46}$$

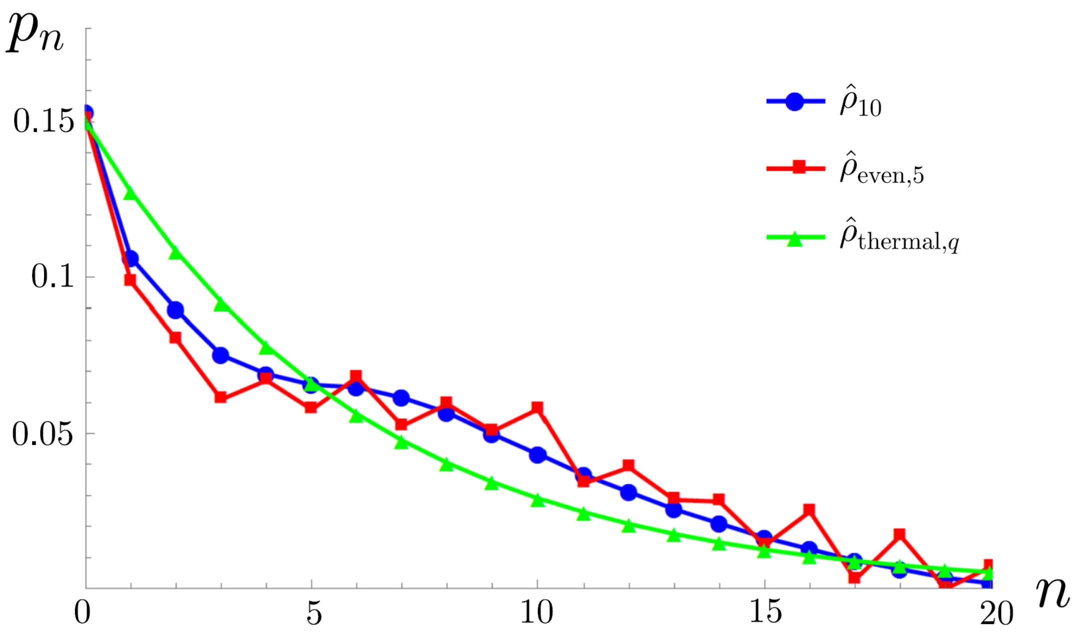

Figure 7.2: Graphs of p_n as defined in Eq. (7.30) for the states $\hat{\rho}_{2M}$ and $\hat{\rho}_{\text{even},M}$ with $M = 5$, as well as for $\hat{\rho}_{\text{thermal},q}$ with $q = 0.85$. The value of q is chosen so that $\langle \hat{n} \rangle_{0.85} = 5.7$ is close to the mean photon number in $\hat{\rho}_{10}$ and $\hat{\rho}_{\text{even},5}$, namely, 5.5 and 6. The purities of these states are given, respectively, by $\mathcal{P}(\hat{\rho}_{10}) = 1/10$, $\mathcal{P}(\hat{\rho}_{\text{even},5}) = 1/5$, and $\mathcal{P}(\hat{\rho}_{\text{thermal},q}) = 0.08$, while their QCS are given by $\mathcal{C}^2(\hat{\rho}_{10}) = 6/5$, $\mathcal{C}^2(\hat{\rho}_{\text{even},5}) = 13$, and $\mathcal{C}^2(\hat{\rho}_{\text{thermal},q}) = 0.08$.

If the state is $\hat{\rho} = \sum_m \lambda_m |m\rangle\langle m|$, then as input state, we have:

$$\hat{\rho} \otimes \hat{\rho} = \sum_m \sum_{m'} \lambda_m \lambda_{m'} |m\rangle\langle m| \otimes |m'\rangle\langle m'|, \tag{7.47}$$

and the probability distribution is given by:

$$p_n = \sum_m \sum_{m'} \lambda_m \lambda_{m'} p_n^{m,m'}. \tag{7.48}$$

These expressions are readily evaluated numerically and are used to produce the plots in Fig. 7.2 representing the numerically obtained values of p_n for both states for $M = 5$. It is also clear that these expressions are not a convenient starting point to compute the QCS of the state $\hat{\rho}$. One observes on these graphs that the p_n's evolve more smoothly as a function of n for $\hat{\rho}_{10}$ than for $\hat{\rho}_{\text{even},5}$. Since for both states $\mathcal{P}(\hat{\rho}) = \sum_{k=0}^{10}(p_{2k} - p_{2k+1})$, this immediately explains the lower value of the purity for $\hat{\rho}_{10}$ than for $\hat{\rho}_{\text{even},5}$. In general, it is clear that if the p_n's evolve slowly with n, the value of the purity will tend to be smaller. If, on the other hand, they change sharply with successive n (with higher values for even n than for odd n), the purity will tend to be larger. This effect is accentuated in the numerator of the QCS because of the extra n factor. This qualitatively explains the large value of the QCS for $\hat{\rho}_{\text{even},5}$ as a consequence of the sharp variations in the corresponding p_n's as observed in Fig. 7.2.

To further corroborate this picture, we compute the QCS for thermal states (defined in

Subsection 2.4.1)

$$\hat{\rho}_q = (1-q)\sum_n q^n |n\rangle\langle n|, \qquad 0 \leq q < 1, \tag{7.49}$$

with a mean photon number $\langle \hat{n} \rangle_q = q/(1-q)$. Since sending two identical thermal states at a beam splitter results into the same product of thermal states at the output [159], we simply have $p_n = (1-q)\,q^n$. The graph of p_n for $q = 0.85$ is shown in Fig. 7.2 and one sees that it is indeed very smooth as a function of n, without fast oscillations as expected since thermal states are well known to be classical. Using Eq. (7.29) and (7.32), we have

$$\mathcal{P}(\hat{\rho}_q) = (1-q)\sum_{n=0}^{\infty}(-1)^n q^n = \frac{1-q}{1+q}, \tag{7.50}$$

$$\mathcal{N}(\hat{\rho}_q) = (1-q)\sum_{n=0}^{\infty}(-1)^n q^n (1+2n) = \frac{(1-q)^2}{(1+q)^2}, \tag{7.51}$$

so that Eq. (7.33) yields

$$\mathcal{C}^2(\hat{\rho}_q) = \frac{1-q}{1+q} = \frac{1}{1+2\langle \hat{n} \rangle_q} < 1. \tag{7.52}$$

We can also represent the influence of the value of the parameter M or q. Indeed, for the states $\hat{\rho}_{2M}$, we know that the QCS decreases when M increases. This appears clearly when representing the p_n for different values of M (see Fig. 7.3). Indeed, for greater values of M, we see that p_n is smoother and thus that the differences $(p_{2k} - p_{2k+1})$ are smaller. As these differences are involved in the calculation of the numerator of the QCS weighted by n, if they are smaller, the QCS will be smaller which corresponds to the theory expectation.

For $\hat{\rho}_{\text{even},M}$, the effect is the opposite. Indeed, for these states, the QCS depends linearly on M and thus increases when M increases. In Fig. 7.4, we see that p_n is oscillating for any value of M with local minima for n odd. However, when M is bigger, the oscillations extend to higher n's. This is expected since for M bigger, we input more photons in the circuit. However, this explains why the QCS increases with the value of M. Indeed, the numerator of the QCS is weighted by n; hence, the oscillations for high n leads to a bigger value for the QCS.

Finally, thermal states are classical states which means that their QCS is smaller than one for any value of the parameter q. We thus expect that p_n will be very smooth for any value of the parameter. This is what we represent in Fig. 7.5 and indeed, all the distributions are very smooth.

In summary, when the p_n's can be determined, experimentally or otherwise, an inspection of their behavior as a function of n gives a good indication on whether the QCS is large or small. More precisely, one expects that when the p_n's evolve slowly with n, the state has a small QCS, whereas sharp variations in the p_n's indicate a large QCS, hence a nonclassical state. Note that these variations can be viewed as a consequence of quantum interference, so that we see here again that large interference effects are associated to a large degree of non-

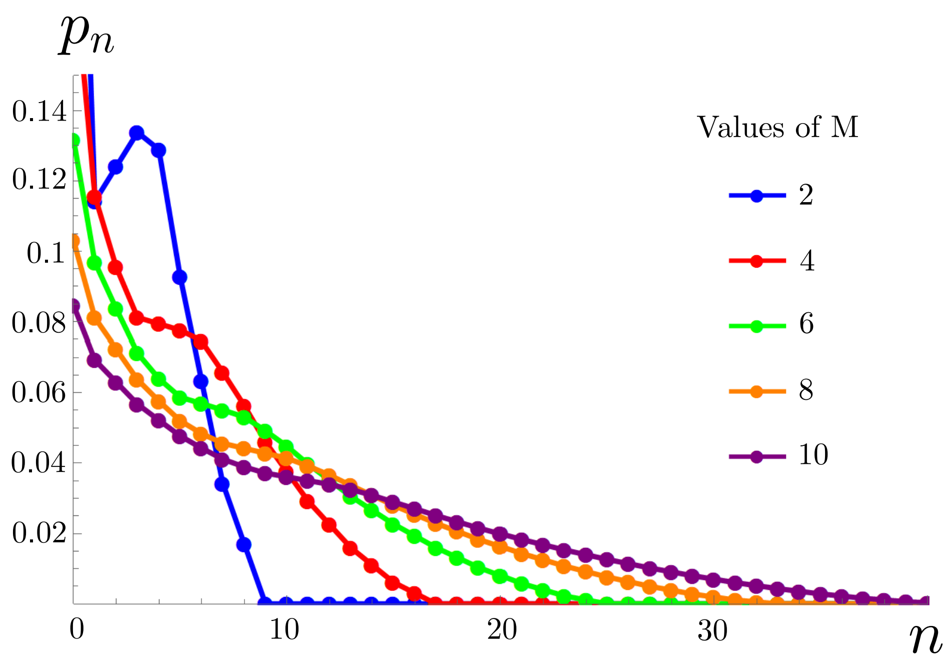

Figure 7.3: Graphs of p_n as defined in Eq. (7.30) for states $\hat{\rho}_{2M}$ for $M = 2, 4, 6, 8$ and 10.

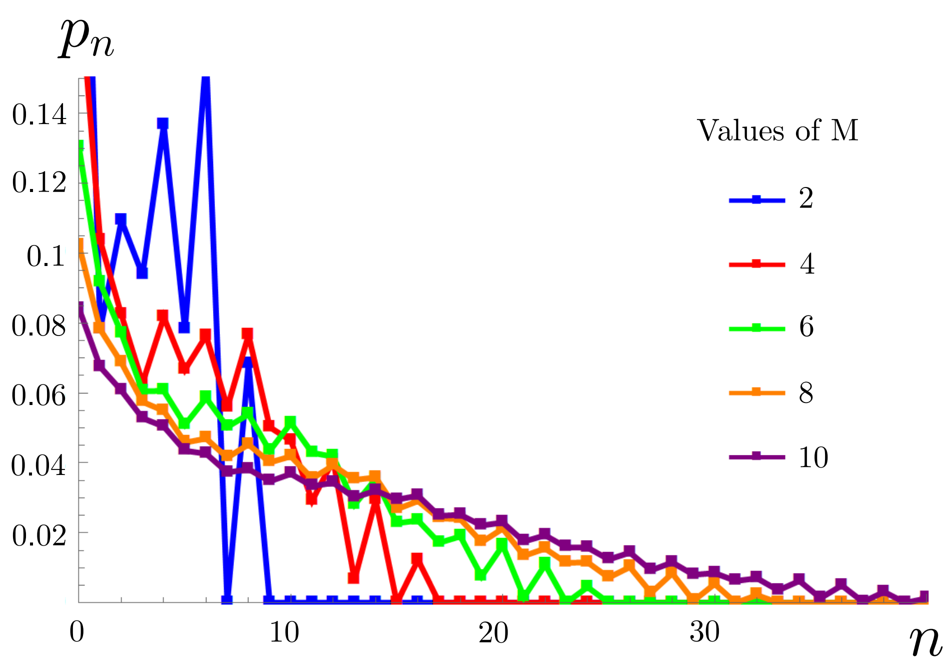

Figure 7.4: Graphs of p_n as defined in Eq. (7.30) for states $\hat{\rho}_{\text{even},M}$ for $M = 2, 4, 6, 8$ and 10.

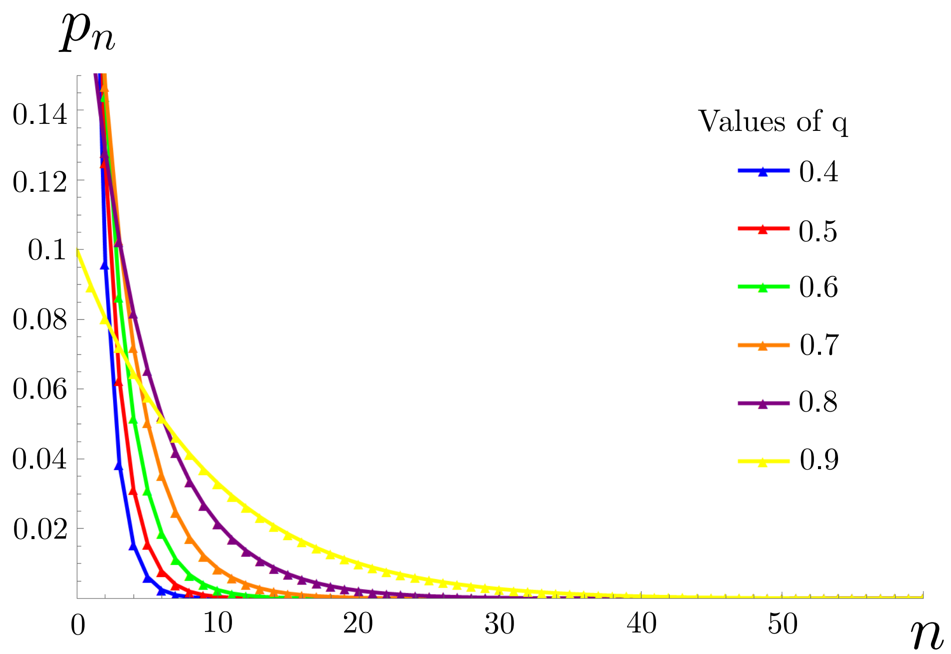

Figure 7.5: Graphs of p_n as defined in Eq. (7.30) for states $\hat{\rho}_q$ for $q = 0.4,\ 0.5,\ 0.6,\ 0.7,\ 0.8$ and 0.9.

classicality. When the state is pure (except for coherent states), the full sequence p_n exhibits clear oscillations since all odd terms vanish (extended Hong-Ou-Mandel effect). When the state is mixed, the fluctuations may remain, but are less pronounced. Eq. (7.33) suggests that the QCS is a measure of the intensity of these fluctuations.

7.5 Phase-space interpretation

Combining the results of the previous sections with phase-space formalism, we can express the purity and QCS of a state $\hat{\rho}$ in terms of the Wigner function of the output state $\hat{\rho}_d$ that is found in the output mode $\hat{d}$ (associated with destructive interference). This in turn yields expressions of the purity and QCS in terms of the Wigner function of state $\hat{\rho}$. We refer to Subsection 2.3.1 for the basics of Wigner functions and the conventions we use here.

It is instructive to consider the purity as a special case of the overlap of two input states $\hat{\rho}_a$ and $\hat{\rho}_b$ impinging on the 50:50 beam splitter in Fig. 7.1. If their respective Wigner functions are denoted by $W_a(x,p)$ and $W_b(x,p)$, then the Wigner function of the state on mode $\hat{d}$,

$$\hat{\rho}_d = \mathrm{Tr}_c(\hat{\rho}_a \otimes \hat{\rho}_b) = \mathrm{Tr}_a\left(\hat{U}_{\mathrm{BS}}(\hat{\rho}_a \otimes \hat{\rho}_b)\hat{U}_{\mathrm{BS}}^{\dagger}\right), \tag{7.53}$$

is given by the (scaled) convolution [92]

$$W_d(x,p) = 2\int W_a(x',p')\, W_b(x'+\sqrt{2}x, p'+\sqrt{2}p)\, \mathrm{d}x'\, \mathrm{d}p'. \tag{7.54}$$

Its value at the origin in phase-space is thus

$$W_d(0,0) \quad = \quad 2\int W_a(x',p')\,W_b(x',p')\,dx'\,dp'. \tag{7.55}$$

Note that $W_d(x,p) \geq 0, \forall x,p$, at the output of a 50:50 beam splitter with arbitrary input states $\hat{\rho}_a$ and $\hat{\rho}_b$ [152], which is consistent with the fact that the overlap $\mathrm{Tr}(\hat{\rho}_a\,\hat{\rho}_b)$ is non-negative. Hence, using the overlap formula Eq. (2.26), we have

$$\mathrm{Tr}(\hat{\rho}_a\,\hat{\rho}_b) = \pi\,W_d(0,0). \tag{7.56}$$

Then, using the well-known property that the value of a Wigner function evaluated at the origin is proportional to the expectation value of the photon number parity, [see Subsection 2.3.1, Eq. (2.33)], we conclude that [29, 78]

$$\mathrm{Tr}(\hat{\rho}_a\,\hat{\rho}_b) = \pi\,W_d(0,0) = \mathrm{Tr}_d\left(\hat{\rho}_d\,(-1)^{\hat{n}_d}\right). \tag{7.57}$$

This implies that the overlap between states $\hat{\rho}_a$ and $\hat{\rho}_b$ can be accessed by measuring the expectation value of the photon number parity on the output mode $\hat{d}$ (associated with destructive interference) of a 50:50 beam splitter using the scheme of Fig. 7.1 but with input states $\hat{\rho}_a$ and $\hat{\rho}_b$. Of course, the purity corresponds to the special case where $\hat{\rho}_a$ and $\hat{\rho}_b$ are both equal to $\hat{\rho}$ in which case, Eq. (7.57) reduces to Eq. (7.14).

We will now use Eq. (7.21) to express the QCS in terms of the Wigner function of the state $\hat{\rho}_d$ and its derivatives evaluated at the origin. For the denominator, the desired expression results from Eq. (7.57) where $\hat{\rho}_a = \hat{\rho}_b$, that is,

$$\begin{aligned}
\mathcal{P}(\hat{\rho}) &= \mathrm{Tr}\left[(\hat{\rho}\otimes\hat{\rho})\,\hat{S}\right], \\
&= \mathrm{Tr}_d\left[\hat{\rho}_d\,(-1)^{\hat{n}_d}\right], \\
&= \pi\,W_d(0,0).
\end{aligned} \tag{7.58}$$

For the numerator $\mathcal{N}(\hat{\rho})$, we can write

$$\begin{aligned}
\mathcal{N}(\hat{\rho}) &= \mathrm{Tr}\left[(\hat{\rho}\otimes\hat{\rho})\,\hat{N}\right], \\
&= \mathrm{Tr}_d\left[\hat{\rho}_d\,(\hat{x}_d^2+\hat{p}_d^2)\,(-1)^{\hat{n}_d}\right].
\end{aligned} \tag{7.59}$$

In order to express the QCS in terms of the Wigner function of state $\hat{\rho}_d$, we then need to compute the Weyl transform of the operator $(\hat{x}^2+\hat{p}^2)\,(-1)^{\hat{n}}/\pi$ and then apply the overlap formula. We first calculate the Weyl transform of $\hat{x}^2\,(-1)^{\hat{n}}/\pi$, namely

$$
\begin{aligned}
&\frac{1}{2\pi}\int \langle x-\frac{y}{2}|\frac{\hat{x}^2\,(-1)^{\hat{n}}}{\pi}|x+\frac{y}{2}\rangle\, e^{ipy}\,dy \\
&= \frac{1}{2\pi^2}\int \left(x-\frac{y}{2}\right)^2 \langle x-\frac{y}{2}|-x-\frac{y}{2}\rangle\, e^{ipy}\,dy, \\
&= \frac{\delta(2x)}{8\pi^2}\int y^2\, e^{ipy}\,dy, \\
&= -\frac{\delta(x)\,\delta''(p)}{8\pi},
\end{aligned} \tag{7.60}
$$

where we have used the identity $\int y^2\, e^{ipy}\,dy = -2\pi\,\delta''(p)$. Using the overlap formula, we then obtain

$$
\begin{aligned}
\frac{1}{\pi}\mathrm{Tr}\left(\hat{\rho}\,\hat{x}^2\,(-1)^{\hat{n}}\right) &= -2\pi\int W(x,p)\,\frac{\delta(x)\,\delta''(p)}{8\pi}\,dx\,dp, \\
&= -\frac{1}{4}\frac{\partial^2 W}{\partial p^2}\bigg|_{x=0,p=0},
\end{aligned} \tag{7.61}
$$

where we have used the identity $\int f(x)\,\delta''(x)\,dx = f''(0)$. Similarly, we have

$$
\frac{1}{\pi}\mathrm{Tr}\left(\hat{\rho}\,\hat{p}^2\,(-1)^{\hat{n}}\right) = -\frac{1}{4}\frac{\partial^2 W}{\partial x^2}\bigg|_{x=0,p=0}, \tag{7.62}
$$

so that

$$
\frac{1}{\pi}\mathrm{Tr}\left(\hat{\rho}\,(\hat{x}^2+\hat{p}^2)\,(-1)^{\hat{n}}\right) = -\frac{1}{4}\Delta W\bigg|_{x=0,p=0}, \tag{7.63}
$$

where Δ stands for the Laplacian. The numerator of the QCS can then be expressed as

$$
\mathcal{N}(\hat{\rho}) = -\frac{\pi}{4}\Delta W_d\bigg|_{x=0,p=0}. \tag{7.64}
$$

As a result, we obtain

$$
\mathcal{C}^2(\hat{\rho}) = \frac{\mathcal{N}(\hat{\rho})}{\mathcal{P}(\hat{\rho})} = -\frac{1}{4}\frac{\Delta W_d}{W_d}\bigg|_{x=0,p=0}. \tag{7.65}
$$

Finally, we can express $\mathcal{C}^2(\hat{\rho})$ in terms of the Wigner function of the state $\hat{\rho}$ itself (instead of $\hat{\rho}_d$). From Eq. (7.54) with $W_a = W_b = W$ and partial integration, one readily sees that

$$
\Delta W_d(0,0) = 4\int W(x',p')\,\Delta W(x',p')\,\mathrm{d}x'\,\mathrm{d}p', \tag{7.66}
$$

$$
= -\|\nabla_\alpha W\|^2. \tag{7.67}
$$

Using this together with Eq. (7.55) for $W_a = W_b = W$, Eq. (7.65) can be reexpressed as

$$
\mathcal{C}^2(\hat{\rho}) = \frac{1}{4}\frac{\|\nabla_\alpha W\|_2^2}{\|W\|_2^2}, \tag{7.68}
$$

which is nothing else than the formula already known (Eq. (3.20)).

Using these results, one can easily recover the well-known formula for Gaussian purity, overlap and QCS. To do this, we start from the expression of the Wigner function of a Gaussian state centered at origin given by Eq. (2.42). It is sufficient to consider a centered state here since the purity and QCS are both invariant under displacements in phase-space (and displacements are easy to account for in the overlap between two states).

Purity We can recover the expression of the purity by using Eq. (7.56). If $\hat{\rho}$ is a Gaussian state centered at origin, then $\hat{\rho}_d = \hat{\rho}$ because the product of two identical Gaussian states impinging on a beam splitter remains unchanged [159]. Thus, $W_d(0,0) = 1/(2\pi\sqrt{\det\gamma})$ according to Eq. (2.42), so that we have, from Eq. (7.56),

$$\mathrm{Tr}\left(\hat{\rho}^2\right) = \pi\, W_d(0,0) = \frac{1}{2\sqrt{\det\gamma}}, \tag{7.69}$$

which is indeed the usual formula for the purity of a Gaussian state Eq.(2.45) ([159]).

Interestingly enough, it then follows from Eq. (7.14) that, for a centered Gaussian state,

$$\mathrm{Tr}\left(\hat{\rho}^2\right) = \mathrm{Tr}\left(\hat{\rho}\,(-1)^{\hat{n}}\right).$$

Overlap We now use Eq. (7.56) in the special case where $\hat{\rho}_a$ and $\hat{\rho}_b$ are two Gaussian states (both assumed to be centered for simplicity). First note that, if $\hat{\rho}_a$ ($\hat{\rho}_b$) is characterized by the covariance matrix γ_a (γ_b), then the output state $\hat{\rho}_d$ of the 50:50 beam splitter is a centered Gaussian state with covariance matrix $\gamma_d = (\gamma_a + \gamma_b)/2$ [159]. Its Wigner function as given by Eq. (2.42) admits the value at origin

$$W_d(0,0) = \frac{1}{2\pi\sqrt{\det\gamma_d}} = \frac{1}{\pi\sqrt{\det(\gamma_a+\gamma_b)}}. \tag{7.70}$$

Using Eq. (7.56), we then find

$$\mathrm{Tr}(\hat{\rho}_a\,\hat{\rho}_b) = \frac{1}{\sqrt{\det(\gamma_a+\gamma_b)}}, \tag{7.71}$$

which is the well-known formula (Eq. (2.47)) for the overlap between two centered Gaussian states [102].

Quadrature coherence scale If the input state is Gaussian, then W_d is simply equal to the Wigner function of the input state and has the form of Eq. (2.42). In that case, the Laplacian at origin is easily expressed as:

$$\Delta W_d\big|_{x=0,p=0} = -\frac{\mathrm{Tr}(\gamma^{-1})}{2\pi\sqrt{\det\gamma}}, \tag{7.72}$$

while $W_d(0,0) = 1/(2\pi\sqrt{\det\gamma})$, so that we conclude that the QCS of a Gaussian state of covariance matrix γ is

$$\mathcal{C}^2(\hat{\rho}) = -\frac{1}{4}\frac{\Delta W_d}{W_d}\bigg|_{x=0,p=0} = \frac{1}{4}\,\mathrm{Tr}(\gamma^{-1}), \tag{7.73}$$

in agreement with the expression proven in Ref. [62] (Eq. (3.24)).

7.6 Multimode case

The extension of the multicopy interferometric method to the measurement of the QCS and purity of a n-mode state is immediate. Note first that the swap operator can be written as

$$\hat{S} = e^{i\frac{\pi}{2}\sum_{k=1}^{N}(\hat{a}_k^\dagger - \hat{b}_k^\dagger)(\hat{a}_k - \hat{b}_k)}, \tag{7.74}$$

where k is the mode index. Coupling the set of $\hat{a}$ and $\hat{b}$ modes pairwise is done with stack of N beam splitter (see Fig. 7.6), each of them effecting the unitary

$$\hat{U}_{BS_k} = e^{\frac{\pi}{4}(\hat{a}_k^\dagger\hat{b}_k - \hat{a}_k\hat{b}_k^\dagger)}. \tag{7.75}$$

Defining $\hat{c}_k$ and $\hat{d}_k$ as in Eq. (7.8), one finds:

$$\hat{S} = \prod_{k=1}^{N} e^{i\pi\hat{d}_k^\dagger\hat{d}_k} = (-1)^{\sum_{k=1}^{N}\hat{n}_{d_k}}. \tag{7.76}$$

Hence, the multimode purity is expressible as before,

$$\mathcal{P}(\hat{\rho}) = \mathrm{Tr}\left((\hat{\rho}\otimes\hat{\rho})\hat{S}\right) = \mathrm{Tr}\left(\hat{\rho}_d(-1)^{\sum_k \hat{n}_{d_k}}\right), \tag{7.77}$$

where

$$\hat{\rho}_d = \mathrm{Tr}_c(\rho\otimes\rho).$$

Again, the same circuit can be used to measure the multimode version of the QCS with

$$\mathcal{C}^2(\hat{\rho}) = \frac{\mathrm{Tr}\left(\hat{\rho}_d\sum_{k'}(-1)^{\sum_k \hat{n}_{d_k}}(1+2\hat{n}_{d_{k'}})\right)}{n\ \mathrm{Tr}\left(\hat{\rho}_d(-1)^{\sum_k \hat{n}_{d_k}}\right)}. \tag{7.78}$$

7.7 Conclusion

The quadrature coherence scale is an efficient nonclassicality witness and measure, which can be expressed through several equivalent formulas, making it relatively easy to compute for a large variety of states [30, 75, 62, 61]. It has a clear physical interpretation, notably because

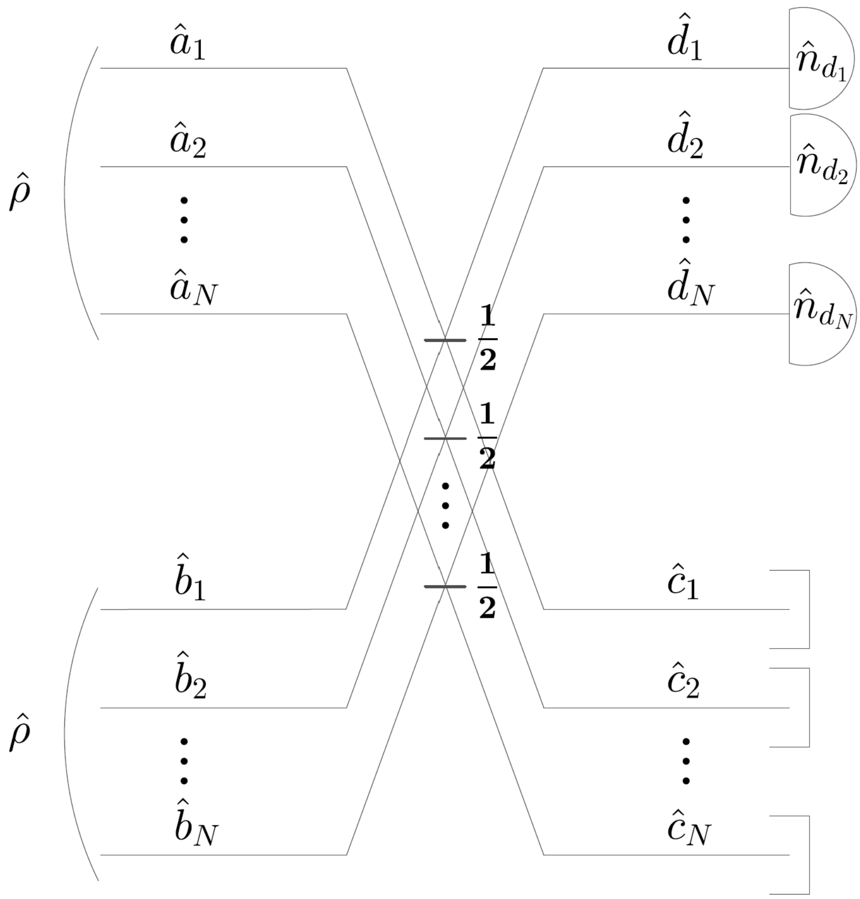

Figure 7.6: Circuit implementing the measurement of the purity and QCS for a N-mode state $\hat{\rho}$. Here, two identical copies of the state are sent in a stack of 50:50 beam splitters and the photon number statistics is measured in the output modes $\hat{d}_k$, with $k = 1, \cdots N$.

it is inversely proportional to the decoherence time of the state [62]. Nevertheless, since it is a nonlinear function of the density matrix, its measurement would *a priori* seem to require a complete state tomography. We have shown that this problem can be avoided through the use of a simple two-copy interferometric measurement scheme using a 50:50 beam splitter associated with photon counting. The method can easily be adapted to multimode systems, in which case one needs to couple the modes pairwise using a stack of 50:50 beam splitters. The downside of this procedure is of course the need to ensure the interferometric stability of the joint measurement of the two replicas, as well as the need for photon-number resolving detectors.

The underlying multicopy technique used here was put forward in the 2000s [18, 38, 109] and was more recently applied to bosonic atoms in optical lattices [29, 78] as well as continuous-variable quantum optical systems [65, 6]. The present work further extends the range of applicability of this set of techniques in quantum optics. Recently, our scheme has been implemented in Ref. [49] proving that it is indeed implementable. In this paper, the authors implement our scheme to measure the QCS of squeezed states using the Xanadu's machine Borealis. They prove that the value of the QCS obtained by performing the ex-

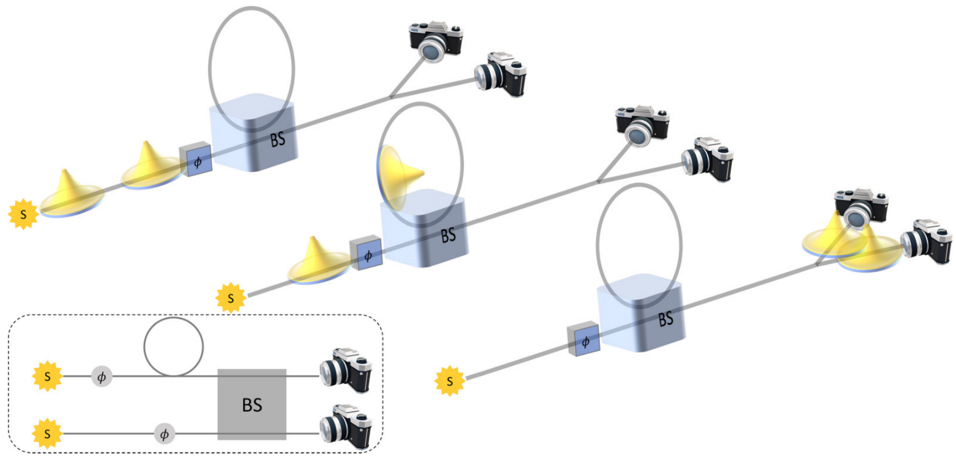

Figure 7.7: Experimental implementation of our scheme to measure the QCS of a squeezed state (Figure taken from Ref. [49]).

periment matches with the expected theoretical value up to some practical imperfections. A scheme showing the experiment is shown in Fig. 7.7 where two pulsed identical squeezed states are put into the circuit. The two states then interact into a balanced beam splitter and the output photon numbers are measured. The statistics of the number of photons obtained is then used to obtain the value of the QCS which is in agreement with the theory.

Part III

Multicopy criteria for entanglement detection

Chapter 8

Multicopy observables for the detection of continuous-variable entanglement

This chapter is based on the following paper that I published together with Tobias Haas and Nicolas Cerf:

C. Griffet, T. Haas, and N. J. Cerf. Accessing continuous-variable entanglement witnesses with multimode spin observables. Physical Review A, 108: 022421, August 2023. [51]

8.1 Introduction

Entanglement is, without doubt, one of the most important properties in quantum mechanics. Over the last two decades, plenty of methods for characterizing entanglement theoretically as well as experimentally have been put forward [121, 74, 58]. A common strategy relies on demonstrating entanglement by violating a set of experimentally accessible conditions fulfilled by all separable states and violated by a few entangled ones. This includes the prominent Peres-Horodecki (PPT) criterion [119, 71], which states that bipartite entanglement can be certified when the partially transposed density operator exhibits a negative eigenvalue.

Conditions implied by this PPT criterion have been studied extensively in the framework of continuous variable quantum systems [17, 159, 136], where entanglement detection is further complicated by the infinite dimensional Hilbert space. This encompasses formulations based on uncertainty relations for second moments [34, 143, 98, 45, 64], fourth-order moments [3], entropies over canonical variables [156, 155, 130, 150, 132], as well as entropic quantities based on the Husimi Q-distribution [42, 41, 55, 54, 56]. With these approaches, entanglement could be certified experimentally in the context of quantum optics [33, 133, 7, 122, 108] and with cold atoms [52, 148, 118, 39, 87, 89, 86].

Although all of the aforementioned criteria are implied by the PPT criterion, they are generally weaker in the sense that they can not detect entanglement for a few entangled states that have a negative partial transpose. A complete hierarchy of conditions in terms of moments of the bosonic mode operators, being sufficient *and* necessary for the negativity of the partial transpose, has been put forward by Shchukin and Vogel in [141], and was further developed in Refs. [106, 107]. While this approach settled the quest for faithfully evaluating the negativity of the partially transposed state, efficient methods for accessing the most important low-order conditions have until now remained elusive.

In this work, we put forward simple measurement schemes of these low-order conditions by introducing multimode spin observables which act on a few replicas (*i.e.*, independent and identical copies) of the bipartite state of interest. Contrary to local canonical operators, whose low-order correlation functions have to be measured through costly tomographic routines involving homodyne measurements [115, 99, 28], such multimode spin observables can be transformed into a bunch of photon number measurements by using passive optical elements [65, 6, 50]. Following this multicopy technique, we devise measurement protocols for three of the most interesting separability criteria obtained in Ref. [141] and illustrate how they efficiently witness entanglement for the classes of Gaussian, mixed Schrödinger cat, and N00N states, respectively. In all cases, we discuss how experimental imperfections may affect the detection capability.

We begin Section 8.2 with a brief recapitulation of the Shchukin-Vogel hierarchy for entanglement witnesses (Subsection 8.2.1), followed by an overview of the multicopy method (Subsection 8.2.2) and, specifically, of the Jordan-Schwinger map used to build multimode spin observables (Subsection 8.2.3). Thereupon, we derive and evaluate multimode expressions for three important classes of entanglement criteria in Section 8.3, that is, criteria that are best suited for Gaussian states (Subsection 8.3.1), mixed Schrödinger cat states (Subsection 8.3.2), and N00N states (Subsection 8.3.3). We also discuss the influence of imperfect preparation and losses for each criterion. Finally, we summarize our findings and provide an outlook in section 8.4.

8.2 Preliminaries

In this section, we review all the important notions that we use to obtain our result. A few notations are important as well in this chapter: we write $\langle \hat{O} \rangle = \mathrm{Tr}\{\hat{\rho}\,\hat{O}\}$ and $\langle \ldots \langle \hat{O} \rangle \ldots \rangle = \mathrm{Tr}\{(\hat{\rho} \otimes \cdots \otimes \hat{\rho})\,\hat{O}\}$ for single copy and multicopy expectation values, respectively. The modes $\hat{a}$ and $\hat{b}$ are associated with Alice's and Bob's subsystems A and B, respectively, and copies are labeled by greek indices μ, ν.

8.2.1 Shchukin-Vogel hierarchy

The important separability criteria used in this chapter are the ones due to Shchukin and Vogel [141] that we already presented in Section 4.3.2. In this paper, they present a hierarchy of determinants that give necessary conditions for separability. These determinants are presented in Eq. (4.32). If a determinant is negative for a state then we can conclude that this state is entangled. We also presented the invariances of these determinants: they are invariant under rotations. However, this is not true for displacements. Indeed, many determinants vary if the state is displaced. In what follows, we will use three different criteria involving one that presents the invariance by displacement: $d_{1,2,4}$.

8.2.2 Multicopy method

All criteria obtainable by Shchukin-Vogel's approach can be expressed in terms of the non-negativity of a determinant d containing moments, which offers the possibility to write them in terms of expectation values of multimode observables. It is indeed known that any n-th degree polynomial of matrix elements of a state $\hat{\rho}$ can be accessed by defining some observable acting on a n-copy version of the state, namely $\hat{\rho}^{\otimes n}$ [18]. Inspired by this multicopy method, tight uncertainty relations [65] as well as nonclassicality witnesses [6] (see also [50]) have been formulated by devising multicopy observables from determinants similar to (4.32). The general scheme is as follows. Given the determinant d of a matrix containing expectation values of mode operators, the corresponding multicopy observable $\hat{D}$ is obtained by dropping all expectation values, assigning one copy to each row and averaging over all permutations of the copies. By construction, the multicopy expectation value $\langle \ldots \langle \hat{D} \rangle \ldots \rangle$ coincides with the determinant d.

For measuring these observables, the remaining task is to find suitable optical circuits. We start from the n-dimensional extension of mode operators describing subsystem A, which reads $[\hat{a}_\mu, \hat{a}_\nu^\dagger] = \delta_{\mu\nu}$ with $\mu, \nu \in \{1, \ldots, n\}$ and n denoting the number of copies (we will of course use a similar notation for copies of subsystem B). In order to transform the measurement of some n-mode observable $\hat{D}$ into simple photon-number measurements, we employ passive linear interferometers, which amounts to applying a unitary transformation (*i.e.*, a passive Bogoliubov transformation) to the mode operators, namely

$$(\hat{a}_1, ..., \hat{a}_n)^T \to (\hat{a}_{1'}, ..., \hat{a}_{n'})^T = M\,(\hat{a}_1, ..., \hat{a}_n)^T. \tag{8.1}$$

The unitary matrix M can be decomposed in terms of two building blocks already defined in Subsections 2.5.1 and 2.5.2, namely, the beam splitter defined as

$$\mathrm{BS}_{\mu\nu}(\tau) = \begin{pmatrix} \sqrt{\tau} & \sqrt{1-\tau} \\ \sqrt{1-\tau} & -\sqrt{\tau} \end{pmatrix}, \tag{8.2}$$

with transmittivity $\tau \in [0,1]$ and the phase shifter

$$\mathrm{PS}_\mu(\theta) = e^{-i\theta}, \tag{8.3}$$

with phase $\theta \in [0, 2\pi)$, where μ and ν designate the mode indices on which the corresponding transformations are applied.

8.2.3 Multimode spin operators

When restricting to two modes ($\mu, \nu = 1, 2$), a particularly useful set of multimode operators can be constructed from algebraic considerations. Considering again subsystem A, the fundamental representation of the Lie algebra $su(2)$, *i.e.* the Pauli matrices $G_j = \sigma_j/2$ fulfilling $[G_j, G_k] = i\,\epsilon_{jkl}\, G_l$ with $j,k,l = 1,2,3$, is realized on its two-mode extension by the quantum operators

$$\hat{L}_j = \sum_{\mu,\nu} \hat{a}_\mu^\dagger\, (G_j)_{\mu\nu}\, \hat{a}_\nu, \tag{8.4}$$

where $(G_j)_{\mu\nu}$ denotes the (μ,ν)th entry of the Pauli matrix G_j. This is known as the Jordan-Schwinger map. More generally, in the n-mode case, this leads to defining the three two-mode spin operators

$$\begin{aligned}
\hat{L}_x^{a_{\mu\nu}} &= \frac{1}{2}\left(\hat{a}_\nu^\dagger \hat{a}_\mu + \hat{a}_\mu^\dagger \hat{a}_\nu,\right), \\
\hat{L}_y^{a_{\mu\nu}} &= \frac{i}{2}\left(\hat{a}_\nu^\dagger \hat{a}_\mu - \hat{a}_\mu^\dagger \hat{a}_\nu,\right), \\
\hat{L}_z^{a_{\mu\nu}} &= \frac{1}{2}\left(\hat{a}_\mu^\dagger \hat{a}_\mu - \hat{a}_\nu^\dagger \hat{a}_\nu,\right),
\end{aligned} \tag{8.5}$$

acting on the pair of modes $(\hat{a}_\mu, \hat{a}_\nu)$. The Casimir operator commuting with all three spin operators is given by the total spin $(\hat{L}^{a_{\mu\nu}})^2 = (\hat{L}_x^{a_{\mu\nu}})^2 + (\hat{L}_y^{a_{\mu\nu}})^2 + (\hat{L}_z^{a_{\mu\nu}})^2$ and can also be expressed as $(\hat{L}^{a_{\mu\nu}})^2 = \hat{L}_0^{a_{\mu\nu}}(\hat{L}_0^{a_{\mu\nu}} + \mathbb{1})$, where the 0th spin component, defined as

$$\hat{L}_0^{a_{\mu\nu}} = \frac{1}{2}\left(\hat{a}_\mu^\dagger \hat{a}_\mu + \hat{a}_\nu^\dagger \hat{a}_\nu\right), \tag{8.6}$$

denotes (one half) the total photon number on the two modes of index μ and ν.

The 0th and z-components can be measured via photon number measurements as $\langle\langle \hat{L}_0^{a_{\mu\nu}} \rangle\rangle = (\langle \hat{n}_{a_\mu} \rangle + \langle \hat{n}_{a_\nu} \rangle)/2$ and $\langle\langle \hat{L}_z^{a_{\mu\nu}} \rangle\rangle = (\langle \hat{n}_{a_\mu} \rangle - \langle \hat{n}_{a_\nu} \rangle)/2$, where $\hat{n}_{a_\mu}$ (or $\hat{n}_{a_\nu}$) denotes the particle number operator associated with mode $\hat{a}_\mu$ (or $\hat{a}_\nu$). Note also that the 0th component can be measured simultaneously with any other spin operator and will always amount to measuring the total particle number. For the x- and y-components, simple optical circuits for transforming them into the z-component are described in [65, 50], which will be discussed below. We may of course analogously define the spin components $\hat{L}_x^{b_{\mu\nu}}$, $\hat{L}_y^{b_{\mu\nu}}$, $\hat{L}_z^{b_{\mu\nu}}$, and $\hat{L}_0^{b_{\mu\nu}}$ for any two modes $\hat{b}_\mu$ and $\hat{b}_\nu$ of subsystem B, which will be needed in subsection 8.3.1 and subsection 8.3.2. We may even define such spin operators across the two subsystems. For a single copy, this amounts to replacing $\hat{a}_\mu$ with $\hat{a}$ and $\hat{a}_\nu$ with $\hat{b}$ in Eq. (8.5), as we will need in subsection 8.3.3.

8.3 Multimode entanglement witnesses

Now we are ready to develop multicopy implementations of the separability criteria from the Shchukin-Vogel hierarchy. In a nutshell, our overall strategy is to identify physically relevant separability criteria from (4.32), rewrite them in terms of multimode observables, and then apply linear optical circuits transforming them into spin operators (8.5), which can be accessed by photon number measurements following [65, 50]. Below, we provide the resulting measurement routines for three classes of criteria that witness entanglement in Gaussian (subsection 8.3.1), mixed Schrödinger cat (subsection 8.3.2), and N00N states (subsection 8.3.3). In each case, we address two potential sources of experimental imperfections, namely imperfect copies and optical losses.

First, remark that multiple identical copies of the state are always assumed to be prepared in the multicopy method. In practice, however, the preparation process encompasses slight fluctuations, so that the prepared multicopy state will contain *imperfect* copies. Although our separability criteria are not guaranteed to remain necessarily valid from first principles in this case, we analyze whether this effect can lead to false-positive detection of entanglement, *i.e.*, can result in a negative determinant even if the imperfect copies are separable. To that end, we model the imperfect preparation by assuming a fixed form of the state – for instance a Gaussian form – for all copies but allow the parameters describing the state to differ from copy to copy. Under this assumption, we do not observe any false-positive detections for all the criteria that we have studied. Yet, imperfect copies typically weaken the detection capability of these criteria.

Second, it is clear that any optical setup will suffer from unavoidable losses, which may challenge the multicopy method. We model their effect with a pure-loss channel: each mode of interest $\hat{a}_\mu$ is coupled with the vacuum $|0\rangle$ via a beam splitter of transmittance τ_{a_μ} [159, 136]. Effectively, this amounts to multiplying each mode operator $\hat{a}_\mu$ by $\sqrt{\tau_{a_\mu}}$. As expected, it appears that the detection of entanglement is hindered by such optical losses for all the criteria we have studied. In what follows, we quantify precisely the extent to which these two sources of imperfections affect our criteria.

8.3.1 Second-order witness based on $\mathbf{D_{1,2,4}}$

Separability criterion

We start with the subdeterminant obtained from (4.32) by selecting the rows and columns 1,2, and 4 of D^{T_2}, *i.e.*,

$$d_{1,2,4} = \begin{vmatrix} 1 & \langle \hat{a} \rangle & \langle \hat{b}^\dagger \rangle \\ \langle \hat{a}^\dagger \rangle & \langle \hat{a}^\dagger \hat{a} \rangle & \langle \hat{a}^\dagger \hat{b}^\dagger \rangle \\ \langle \hat{b} \rangle & \langle \hat{a} \hat{b} \rangle & \langle \hat{b}^\dagger \hat{b} \rangle \end{vmatrix}, \tag{8.7}$$

corresponding to the operator $\hat{f} = c_1 + c_2\hat{a} + c_3\hat{b}$. As the resulting entanglement witness $d_{1,2,4} < 0$ is of second order in the mode operators, let us compare it to other prominent second-order criteria. To that end, we introduce the non-local quadrature operators [36]

$$\hat{x}_\pm = |r|\,\hat{x}_1 \pm \frac{1}{r}\,\hat{x}_2, \quad \hat{p}_\pm = |r|\,\hat{p}_1 \pm \frac{1}{r}\,\hat{p}_2, \tag{8.8}$$

with some real $r \neq 0$. For any separable state, the sums of the variances of these operators are constrained by the criterion of Duan, Giedke, Cirac and Zoller [34]

$$d_{\text{Duan}} = \sigma^2_{x_\pm} + \sigma^2_{p_\mp} - \left(r^2 + \frac{1}{r^2}\right) \geq 0, \tag{8.9}$$

where $\sigma_x^2 = \langle \hat{x}^2\rangle - \langle \hat{x}\rangle^2$ denotes the variance of the operator $\hat{x}$. Interestingly, the optimized (over r) version of condition (8.9) is implied by the non-negativity of $d_{1,2,4}$.

Indeed, one can show that $d_{1,2,4}$ reduces to

$$d_{1,2,4} = \sigma_{a^\dagger a}\sigma_{b^\dagger b} - \sigma_{a^\dagger b^\dagger}\sigma_{ab}, \tag{8.10}$$

where

$$\sigma_{yz} = \langle \hat{y}\hat{z}\rangle - \langle \hat{y}\rangle \langle \hat{z}\rangle \tag{8.11}$$

denotes the covariance of the two observables $\hat{y}, \hat{z}$. By employing the identities

$$\begin{aligned}
\sigma_{a^\dagger a} &= \frac{1}{2}\left(\sigma^2_{x_1} + \sigma^2_{p_1} - 1\right), \\
\sigma_{b^\dagger b} &= \frac{1}{2}\left(\sigma^2_{x_2} + \sigma^2_{p_2} - 1\right), \\
\sigma_{ab} &= \frac{1}{2}\left(\sigma_{x_1x_1} + i\sigma_{x_1p_2} + i\sigma_{x_2p_1} - \sigma_{p_1p_1}\right), \\
\sigma_{a^\dagger b^\dagger} &= \sigma^\dagger_{ab},
\end{aligned} \tag{8.12}$$

the condition $d_{1,2,4} \geq 0$ can be translated into a condition on the local quadratures and their correlations

$$0 \leq \left(\sigma^2_{x_1} + \sigma^2_{p_1} - 1\right)\left(\sigma^2_{x_2} + \sigma^2_{p_2} - 1\right) - \left(\sigma_{x_1x_1} - \sigma_{p_1p_1}\right)^2 - \left(\sigma_{x_1p_2} + \sigma_{x_2p_1}\right)^2. \tag{8.13}$$

Similarly, rewriting the criterion (8.9) in terms of local quadratures using

$$\begin{aligned}
\sigma^2_{x_\pm} &= r^2\sigma^2_{x_1} + \frac{1}{r^2}\sigma^2_{x_2} \pm 2\sigma_{x_1x_2}, \\
\sigma^2_{p_\pm} &= r^2\sigma^2_{p_1} + \frac{1}{r^2}\sigma^2_{p_2} \pm 2\sigma_{p_1p_2},
\end{aligned} \tag{8.14}$$

allows to optimize over r by searching for a global minimum. One finds

$$r^2 = \sqrt{\frac{\sigma^2_{x_2} + \sigma^2_{p_2} - 1}{\sigma^2_{x_1} + \sigma^2_{p_1} - 1}}, \tag{8.15}$$

such that the optimal Duan criterion in local variables reads

$$d_{\mathrm{Duan}} = 2\sqrt{\left(\sigma_{x_1}^2 + \sigma_{p_1}^2 - 1\right)\left(\sigma_{x_2}^2 + \sigma_{p_2}^2 - 1\right)} \pm 2\left(\sigma_{x_1x_2} - \sigma_{p_1p_2}\right). \tag{8.16}$$

The non-negativity of the latter is equivalent to the condition

$$0 \leq \left(\sigma_{x_1}^2 + \sigma_{p_1}^2 - 1\right)\left(\sigma_{x_2}^2 + \sigma_{p_2}^2 - 1\right) - \left(\sigma_{x_1x_1} - \sigma_{p_1p_1}\right)^2. \tag{8.17}$$

By comparing (8.13) and (8.17) it becomes apparent that $d_{1,2,4} \geq 0$ implies $d_{\mathrm{Duan}} \geq 0$ since $\left(\sigma_{x_1p_2} + \sigma_{x_2p_1}\right)^2 \geq 0$. Therefore, $d_{1,2,4} \geq 0$ is stronger than $d_{\mathrm{Duan}} \geq 0$ in the sense that the former condition contains additional information about the correlations between quadratures of different types. Hence, the witness $d_{1,2,4} < 0$ is strictly stronger than the criterion of Duan *et al.* for detecting entanglement.

Application to Gaussian states

It is well known that the criterion (8.9) is a necessary and sufficient condition for separability (after optimization over r) in the case of Gaussian states as considered here (when Alice and Bob hold one mode each) [74]. By the latter considerations, the same holds true for the determinant $d_{1,2,4}$. As a particular example, we evaluate this determinant for the archetypal entangled Gaussian state, the two-mode squeezed vacuum state (which was presented in Subsection 2.4.1)

$$|\psi\rangle = \sqrt{1-\lambda^2}\sum_{n=0}^{\infty} \lambda^n |n,n\rangle, \tag{8.18}$$

where $\lambda \in (-1,1)$.

To evaluate the determinant $d_{1,2,4}$ (Eq. (8.7)) for the two-mode squeezed vacuum state (8.18), we use the lowering/raising property of the annihilation/creation operator

$$\begin{aligned} \hat{a}\,|n,n\rangle &= \sqrt{n}\,|n-1,n\rangle, \\ \hat{a}^\dagger\,|n,n\rangle &= \sqrt{n+1}\,|n+1,n\rangle, \end{aligned} \tag{8.19}$$

and similarly for the b-creation and annihilation operators acting on mode B. Then follows for the first non-trivial matrix element of $d_{1,2,4}$

$$\begin{aligned} \langle \hat{a}^\dagger \hat{a}\rangle &= (1-\lambda^2)\sum_{n,n'=0}^{\infty} \lambda^n\lambda^{n'}\,\langle n',n'|\,\hat{a}^\dagger\hat{a}\,|n,n\rangle \\ &= (1-\lambda^2)\sum_{n,n'=0}^{\infty} \lambda^n\lambda^{n'}\sqrt{nn'}\,\delta_{nn'} \\ &= (1-\lambda^2)\sum_{n=0}^{\infty}\lambda^{2n} n \\ &= \frac{\lambda^2}{1-\lambda^2}, \end{aligned} \tag{8.20}$$

where we used the orthonormality of Fock states $\langle n|n'\rangle = \delta_{nn'}$. The remaining matrix elements are found analogously, leading to the expression (8.21) for the determinant

$$d_{1,2,4} = \begin{vmatrix} 1 & 0 & 0 \\ 0 & \frac{\lambda^2}{1-\lambda^2} & \frac{\lambda}{1-\lambda^2} \\ 0 & \frac{\lambda}{1-\lambda^2} & \frac{\lambda^2}{1-\lambda^2} \end{vmatrix} = -\frac{\lambda^2}{1-\lambda^2}, \tag{8.21}$$

which is indeed negative for any value of the parameter $\lambda \in (-1, 1)$.

Multicopy implementation

We apply the multicopy measurement method, *i.e.*, assign one copy to each row of the matrix and sum over all permutations, yielding

$$\hat{D}_{1,2,4} = \frac{1}{|S_{123}|} \sum_{\sigma \in S_{123}} \begin{vmatrix} 1 & \hat{a}_{\sigma(1)} & \hat{b}^\dagger_{\sigma(1)} \\ \hat{a}^\dagger_{\sigma(2)} & \hat{a}^\dagger_{\sigma(2)}\hat{a}_{\sigma(2)} & \hat{a}^\dagger_{\sigma(2)}\hat{b}^\dagger_{\sigma(2)} \\ \hat{b}_{\sigma(3)} & \hat{a}_{\sigma(3)}\hat{b}_{\sigma(3)} & \hat{b}^\dagger_{\sigma(3)}\hat{b}_{\sigma(3)} \end{vmatrix}, \tag{8.22}$$

where S_{123} denotes the group of permutations over the index set $\{1, 2, 3\}$ with dimension $|S_{123}| = 3!$. By construction, the multicopy expectation value of this observable gives the determinant (8.7), *i.e.*, $\langle\langle\langle \hat{D}_{1,2,4} \rangle\rangle\rangle = d_{1,2,4}$.

Indeed, we write out (8.22), giving the 36 terms

$$\begin{aligned} \hat{D}_{1,2,4} = \frac{1}{6}\Big(& \hat{a}^\dagger_1\hat{a}_1\hat{b}^\dagger_2\hat{b}_2 + \hat{a}^\dagger_1\hat{a}_1\hat{b}^\dagger_3\hat{b}_3 + \hat{a}^\dagger_2\hat{a}_2\hat{b}^\dagger_1\hat{b}_1 + \hat{a}^\dagger_2\hat{a}_2\hat{b}^\dagger_3\hat{b}_3 + \hat{a}^\dagger_3\hat{a}_3\hat{b}^\dagger_1\hat{b}_1 + \hat{a}^\dagger_3\hat{a}_3\hat{b}^\dagger_2\hat{b}_2 \\ & + \hat{a}^\dagger_2\hat{a}_1\hat{b}^\dagger_2\hat{b}_3 + \hat{a}^\dagger_3\hat{a}_1\hat{b}^\dagger_3\hat{b}_2 + \hat{a}^\dagger_3\hat{a}_2\hat{b}^\dagger_3\hat{b}_1 + \hat{a}^\dagger_2\hat{a}_3\hat{b}^\dagger_2\hat{b}_1 + \hat{a}^\dagger_1\hat{a}_2\hat{b}^\dagger_1\hat{b}_3 + \hat{a}^\dagger_1\hat{a}_3\hat{b}^\dagger_1\hat{b}_2 \\ & + \hat{a}^\dagger_2\hat{a}_3\hat{b}^\dagger_1\hat{b}_3 + \hat{a}^\dagger_3\hat{a}_2\hat{b}^\dagger_1\hat{b}_2 + \hat{a}^\dagger_1\hat{a}_3\hat{b}^\dagger_2\hat{b}_3 + \hat{a}^\dagger_1\hat{a}_2\hat{b}^\dagger_3\hat{b}_2 + \hat{a}^\dagger_2\hat{a}_1\hat{b}^\dagger_3\hat{b}_1 + \hat{a}^\dagger_3\hat{a}_1\hat{b}^\dagger_2\hat{b}_1 \\ & - \hat{a}^\dagger_2\hat{a}_2\hat{b}^\dagger_1\hat{b}_3 - \hat{a}^\dagger_3\hat{a}_3\hat{b}^\dagger_1\hat{b}_2 - \hat{a}^\dagger_1\hat{a}_1\hat{b}^\dagger_2\hat{b}_3 - \hat{a}^\dagger_1\hat{a}_1\hat{b}^\dagger_3\hat{b}_2 - \hat{a}^\dagger_2\hat{a}_2\hat{b}^\dagger_3\hat{b}_1 - \hat{a}^\dagger_3\hat{a}_3\hat{b}^\dagger_2\hat{b}_1 \\ & - \hat{a}^\dagger_1\hat{a}_2\hat{b}^\dagger_1\hat{b}_2 - \hat{a}^\dagger_1\hat{a}_3\hat{b}^\dagger_1\hat{b}_3 - \hat{a}^\dagger_2\hat{a}_3\hat{b}^\dagger_2\hat{b}_3 - \hat{a}^\dagger_2\hat{a}_1\hat{b}^\dagger_2\hat{b}_1 - \hat{a}^\dagger_3\hat{a}_1\hat{b}^\dagger_3\hat{b}_1 - \hat{a}^\dagger_3\hat{a}_2\hat{b}^\dagger_3\hat{b}_2 \\ & - \hat{a}^\dagger_2\hat{a}_1\hat{b}^\dagger_3\hat{b}_3 - \hat{a}^\dagger_3\hat{a}_1\hat{b}^\dagger_2\hat{b}_2 - \hat{a}^\dagger_1\hat{a}_3\hat{b}^\dagger_2\hat{b}_2 - \hat{a}^\dagger_1\hat{a}_2\hat{b}^\dagger_3\hat{b}_3 - \hat{a}^\dagger_3\hat{a}_2\hat{b}^\dagger_1\hat{b}_1 - \hat{a}^\dagger_2\hat{a}_3\hat{b}^\dagger_1\hat{b}_1\Big). \end{aligned} \tag{8.23}$$

When computing the multicopy expectation value of this expression on three copies of the state $\hat{\rho}$, every term appears six times, resulting in

$$\begin{aligned} \langle\langle\langle \hat{D}_{1,2,4} \rangle\rangle\rangle &= \langle \hat{a}^\dagger\hat{a} \rangle \langle \hat{b}^\dagger\hat{b} \rangle + \langle \hat{a} \rangle \langle \hat{a}^\dagger\hat{b}^\dagger \rangle \langle \hat{b} \rangle \\ &\quad + \langle \hat{b}^\dagger \rangle \langle \hat{a}^\dagger \rangle \langle \hat{a}\hat{b} \rangle - \langle \hat{b}^\dagger \rangle \langle \hat{a}^\dagger\hat{a} \rangle \langle \hat{b} \rangle \\ &\quad - \langle \hat{a} \rangle \langle \hat{a}^\dagger \rangle \langle \hat{b}^\dagger\hat{b} \rangle - \langle \hat{a}^\dagger\hat{b}^\dagger \rangle \langle \hat{a}\hat{b} \rangle \\ &= d_{1,2,4}, \end{aligned} \tag{8.24}$$

as desired.

We prove that applying an arbitrary displacement $\hat{D}(\alpha)\hat{D}(\beta)$ on the bipartite state $\hat{\rho}$ does not change the value of the determinant $d_{1,2,4}$. The annihilation operators $\hat{a}$ and $\hat{b}$ of the two subsystems transform as

$$\begin{aligned} \hat{a} &\to \hat{a}' = \hat{a} + \alpha, \\ \hat{b} &\to \hat{b}' = \hat{b} + \beta, \end{aligned} \tag{8.25}$$

with complex phases $\alpha, \beta \in \mathbb{C}$. Then, the determinant transforms as

$$\begin{aligned} d_{1,2,4} \to d'_{1,2,4} &= \begin{vmatrix} 1 & \langle \hat{a}' \rangle & \langle \hat{b}'^{\dagger} \rangle \\ \langle \hat{a}'^{\dagger} \rangle & \langle \hat{a}'^{\dagger}\hat{a}' \rangle & \langle \hat{a}'^{\dagger}\hat{b}'^{\dagger} \rangle \\ \langle \hat{b}' \rangle & \langle \hat{a}'\hat{b}' \rangle & \langle \hat{b}'^{\dagger}\hat{b}' \rangle \end{vmatrix} \\ &= \begin{vmatrix} 1 & \langle \hat{a} + \alpha \rangle & \langle \hat{b}^{\dagger} + \beta^* \rangle \\ \langle \hat{a}^{\dagger} + \alpha^* \rangle & \langle (\hat{a}^{\dagger} + \alpha^*)(\hat{a} + \alpha) \rangle & \langle (\hat{a}^{\dagger} + \alpha^*)(\hat{b}^{\dagger} + \beta^*) \rangle \\ \langle \hat{b} + \beta \rangle & \langle (\hat{a} + \alpha)(\hat{b} + \beta) \rangle & \langle (\hat{b}^{\dagger} + \beta^*)(\hat{b} + \beta) \rangle \end{vmatrix} \\ &= \begin{vmatrix} 1 & \langle \hat{a} \rangle + \alpha & \langle \hat{b}^{\dagger} \rangle + \beta^* \\ \langle \hat{a}^{\dagger} \rangle + \alpha^* & \langle \hat{a}^{\dagger}\hat{a} \rangle + \alpha \langle \hat{a}^{\dagger} \rangle + \alpha^*(\langle \hat{a} \rangle + \alpha) & \langle \hat{a}^{\dagger}\hat{b}^{\dagger} \rangle + \beta^* \langle \hat{a}^{\dagger} \rangle + \alpha^*(\langle \hat{b}^{\dagger} \rangle + \beta^*) \\ \langle \hat{b} \rangle + \beta & \langle \hat{a}\hat{b} \rangle + \alpha \langle \hat{b} \rangle + \beta(\langle \hat{a} \rangle + \alpha) & \langle \hat{b}^{\dagger}\hat{b} \rangle + \beta^* \langle \hat{b} \rangle + \beta(\langle \hat{b}^{\dagger} \rangle + \beta^*) \end{vmatrix} \\ &= \begin{vmatrix} 1 & \langle \hat{a} \rangle + \alpha & \langle \hat{b}^{\dagger} \rangle + \beta^* \\ \langle \hat{a}^{\dagger} \rangle & \langle \hat{a}^{\dagger}\hat{a} \rangle + \alpha \langle \hat{a}^{\dagger} \rangle & \langle \hat{a}^{\dagger}\hat{b}^{\dagger} \rangle + \beta^* \langle \hat{a}^{\dagger} \rangle \\ \langle \hat{b} \rangle & \langle \hat{a}\hat{b} \rangle + \alpha \langle \hat{b} \rangle & \langle \hat{b}^{\dagger}\hat{b} \rangle + \beta^* \langle \hat{b} \rangle \end{vmatrix} \\ &= d_{1,2,4}, \end{aligned} \tag{8.26}$$

where we used that the determinant remains invariant when adding to a column/row another column/row multiplied by some complex number in the two last equations. Since $d_{1,2,4}$ is invariant under displacements, we may access $\hat{D}_{1,2,4}$ by first applying a linear optics transformation on Alice's and Bob's subsystems that has the effect of concentrating the mean field on one mode of each subsystem ($\hat{a}_1$ and $\hat{b}_1$) and canceling it on the other two modes ($\hat{a}_2$ and $\hat{a}_3$, on Alice's side, and $\hat{b}_2$ and $\hat{b}_3$ on Bob's side). To that end, as shown in Refs. [65, 50], we may apply the transformation

$$\begin{aligned} M &= \left[\mathrm{BS}_{a_1 a_3}(2/3) \otimes \mathrm{I}_{a_2} \right] \left[\mathrm{BS}_{a_1 a_2}(1/2) \otimes \mathrm{I}_{a_3} \right] \\ &= \frac{1}{\sqrt{6}} \begin{pmatrix} \sqrt{2} & \sqrt{2} & \sqrt{2} \\ \sqrt{3} & -\sqrt{3} & 0 \\ 1 & 1 & -2 \end{pmatrix} \end{aligned} \tag{8.27}$$

to the $\hat{a}$-modes and similarly to the $\hat{b}$-modes as shown in Figure 8.1a. Denoting with a prime all output modes of this transformation, this results in

$$
\begin{aligned}
\hat{D}_{1,2,4} &= \frac{1}{2}\Big(\hat{a}^\dagger_{2'}\hat{a}_{2'}\hat{b}^\dagger_{3'}\hat{b}_{3'} + \hat{a}^\dagger_{3'}\hat{a}_{3'}\hat{b}^\dagger_{2'}\hat{b}_{2'} \\
&\quad - \hat{a}^\dagger_{2'}\hat{a}_{3'}\hat{b}^\dagger_{2'}\hat{b}_{3'} - \hat{a}^\dagger_{3'}\hat{a}_{2'}\hat{b}^\dagger_{3'}\hat{b}_{2'}\Big) \\
&= \frac{1}{|S_{2'3'}|}\sum_{\sigma\in S_{2'3'}} \begin{vmatrix} \hat{a}^\dagger_{\sigma(1)}\hat{a}_{\sigma(1)} & \hat{a}^\dagger_{\sigma(1)}\hat{b}^\dagger_{\sigma(1)} \\ \hat{a}_{\sigma(2)}\hat{b}_{\sigma(2)} & \hat{b}^\dagger_{\sigma(2)}\hat{b}_{\sigma(2)} \end{vmatrix} \\
&= \hat{D}_{2,4},
\end{aligned}
\tag{8.28}
$$

with $S_{2'3'}$ denoting the group of permutations over the index set $\{2',3'\}$ with dimension $|S_{2'3'}| = 2!$. Note that the dependence on mode $\hat{a}_{1'}$ and $\hat{b}_{1'}$ has disappeared, as expected. Interestingly, the latter expression corresponds to the multicopy implementation of the subdeterminant

$$
d_{2,4} = \begin{vmatrix} \langle\hat{a}^\dagger\hat{a}\rangle & \langle\hat{a}^\dagger\hat{b}^\dagger\rangle \\ \langle\hat{a}\hat{b}\rangle & \langle\hat{b}^\dagger\hat{b}\rangle \end{vmatrix},
\tag{8.29}
$$

as $\langle\langle\hat{D}_{2,4}\rangle\rangle = d_{2,4}$.

Let us now consider the experimental measurement of the multimode observable $\hat{D}_{2,4}$. To that end, we define three operators $\hat{C}_j$ based on the spin operators (8.5) and (8.6) applied onto modes $2'$ and $3'$ on Alice's and Bob's side, namely

$$
\begin{aligned}
\hat{C}_1 &= \hat{L}_0^{a_{2'3'}}\hat{L}_0^{b_{2'3'}} - \hat{L}_x^{a_{2'3'}}\hat{L}_x^{b_{2'3'}}, \\
\hat{C}_2 &= \hat{L}_0^{a_{2'3'}}\hat{L}_0^{b_{2'3'}} - \hat{L}_y^{a_{2'3'}}\hat{L}_y^{b_{2'3'}}, \\
\hat{C}_3 &= \hat{L}_0^{a_{2'3'}}\hat{L}_0^{b_{2'3'}} - \hat{L}_z^{a_{2'3'}}\hat{L}_z^{b_{2'3'}},
\end{aligned}
\tag{8.30}
$$

leading to the simple decomposition

$$
\hat{D}_{2,4} = \hat{C}_1 - \hat{C}_2 + \hat{C}_3.
\tag{8.31}
$$

Indeed, we start from the four products $\hat{L}_j^{a_{2'3'}}\hat{L}_j^{b_{2'3'}}$ for $j \in \{x,y,z,0\}$ applied to the modes $2'$ and $3'$, which read

$$
\begin{aligned}
\hat{L}_x^{a_{2'3'}}\hat{L}_x^{b_{2'3'}} &= \frac{1}{4}\Big(\hat{a}^\dagger_{3'}\hat{a}_{2'}\hat{b}^\dagger_{3'}\hat{b}_{2'} + \hat{a}^\dagger_{2'}\hat{a}_{3'}\hat{b}^\dagger_{2'}\hat{b}_{3'} + \hat{a}^\dagger_{2'}\hat{a}_{3'}\hat{b}^\dagger_{3'}\hat{b}_{2'} + \hat{a}^\dagger_{3'}\hat{a}_{2'}\hat{b}^\dagger_{2'}\hat{b}_{3'}\Big), \\
\hat{L}_y^{a_{2'3'}}\hat{L}_y^{b_{2'3'}} &= -\frac{1}{4}\Big(\hat{a}^\dagger_{3'}\hat{a}_{2'}\hat{b}^\dagger_{3'}\hat{b}_{2'} + \hat{a}^\dagger_{2'}\hat{a}_{3'}\hat{b}^\dagger_{2'}\hat{b}_{3'} - \hat{a}^\dagger_{2'}\hat{a}_{3'}\hat{b}^\dagger_{3'}\hat{b}_{2'} - \hat{a}^\dagger_{3'}\hat{a}_{2'}\hat{b}^\dagger_{2'}\hat{b}_{3'}\Big), \\
\hat{L}_z^{a_{2'3'}}\hat{L}_z^{b_{2'3'}} &= \frac{1}{4}\Big(\hat{a}^\dagger_{2'}\hat{a}_{2'}\hat{b}^\dagger_{2'}\hat{b}_{2'} + \hat{a}^\dagger_{3'}\hat{a}_{3'}\hat{b}^\dagger_{3'}\hat{b}_{3'} - \hat{a}^\dagger_{2'}\hat{a}_{2'}\hat{b}^\dagger_{3'}\hat{b}_{3'} - \hat{a}^\dagger_{3'}\hat{a}_{3'}\hat{b}^\dagger_{2'}\hat{b}_{2'}\Big), \\
\hat{L}_0^{a_{2'3'}}\hat{L}_0^{b_{2'3'}} &= \frac{1}{4}\Big(\hat{a}^\dagger_{2'}\hat{a}_{2'}\hat{b}^\dagger_{2'}\hat{b}_{2'} + \hat{a}^\dagger_{3'}\hat{a}_{3'}\hat{b}^\dagger_{3'}\hat{b}_{3'} + \hat{a}^\dagger_{2'}\hat{a}_{2'}\hat{b}^\dagger_{3'}\hat{b}_{3'} + \hat{a}^\dagger_{3'}\hat{a}_{3'}\hat{b}^\dagger_{2'}\hat{b}_{2'}\Big).
\end{aligned}
\tag{8.32}
$$

Then, following the definitions of the operators $\hat{C}_j$ given in (8.30) we find

$$\begin{aligned}
\hat{C}_1 &= \frac{1}{4}\Big(\hat{a}^\dagger_{2'}\hat{a}_{2'}\hat{b}^\dagger_{2'}\hat{b}_{2'} + \hat{a}^\dagger_{3'}\hat{a}_{3'}\hat{b}^\dagger_{3'}\hat{b}_{3'} + \hat{a}^\dagger_{2'}\hat{a}_{2'}\hat{b}^\dagger_{3'}\hat{b}_{3'} + \hat{a}^\dagger_{3'}\hat{a}_{3'}\hat{b}^\dagger_{2'}\hat{b}_{2'} \\
&\quad - \hat{a}^\dagger_{3'}\hat{a}_{2'}\hat{b}^\dagger_{3'}\hat{b}_{2'} - \hat{a}^\dagger_{2'}\hat{a}_{3'}\hat{b}^\dagger_{2'}\hat{b}_{3'} - \hat{a}^\dagger_{2'}\hat{a}_{3'}\hat{b}^\dagger_{3'}\hat{b}_{2'} - \hat{a}^\dagger_{3'}\hat{a}_{2'}\hat{b}^\dagger_{2'}\hat{b}_{3'}\Big), \\
\hat{C}_2 &= \frac{1}{4}\Big(\hat{a}^\dagger_{2'}\hat{a}_{2'}\hat{b}^\dagger_{2'}\hat{b}_{2'} + \hat{a}^\dagger_{3'}\hat{a}_{3'}\hat{b}^\dagger_{3'}\hat{b}_{3'} + \hat{a}^\dagger_{2'}\hat{a}_{2'}\hat{b}^\dagger_{3'}\hat{b}_{3'} + \hat{a}^\dagger_{3'}\hat{a}_{3'}\hat{b}^\dagger_{2'}\hat{b}_{2'} \\
&\quad + \hat{a}^\dagger_{3'}\hat{a}_{2'}\hat{b}^\dagger_{3'}\hat{b}_{2'} + \hat{a}^\dagger_{2'}\hat{a}_{3'}\hat{b}^\dagger_{2'}\hat{b}_{3'} - \hat{a}^\dagger_{2'}\hat{a}_{3'}\hat{b}^\dagger_{3'}\hat{b}_{2'} - \hat{a}^\dagger_{3'}\hat{a}_{2'}\hat{b}^\dagger_{2'}\hat{b}_{3'}\Big), \\
\hat{C}_3 &= \frac{1}{2}\Big(\hat{a}^\dagger_{2'}\hat{a}_{2'}\hat{b}^\dagger_{3'}\hat{b}_{3'} + \hat{a}^\dagger_{3'}\hat{a}_{3'}\hat{b}^\dagger_{2'}\hat{b}_{2'}\Big),
\end{aligned} \tag{8.33}$$

such that

$$\begin{aligned}
\hat{C}_1 - \hat{C}_2 + \hat{C}_3 &= \frac{1}{2}\Big(\hat{a}^\dagger_{2'}\hat{a}_{2'}\hat{b}^\dagger_{3'}\hat{b}_{3'} + \hat{a}^\dagger_{3'}\hat{a}_{3'}\hat{b}^\dagger_{2'}\hat{b}_{2'} - \hat{a}^\dagger_{2'}\hat{a}_{3'}\hat{b}^\dagger_{2'}\hat{b}_{3'} - \hat{a}^\dagger_{3'}\hat{a}_{2'}\hat{b}^\dagger_{3'}\hat{b}_{2'}\Big) \\
&= \hat{D}_{2,4},
\end{aligned} \tag{8.34}$$

as expected. Therefore, $d_{1,2,4}$ can be accessed by measuring separately the expectation value of each operator $\hat{C}_j$, resulting in

$$d_{1,2,4} = \langle\langle \hat{C}_1 \rangle\rangle - \langle\langle \hat{C}_2 \rangle\rangle + \langle\langle \hat{C}_3 \rangle\rangle \,. \tag{8.35}$$

This is achieved by applying the three linear optical circuits depicted in Figure 8.1b-d on the $\hat{a}$ modes, namely

$$\begin{aligned}
M_1 &= \mathrm{BS}_{a_{2'}a_{3'}}(1/2)\,, \\
M_2 &= \mathrm{BS}_{a_{2'}a_{3'}}(1/2)\,\mathrm{PS}_{a_{3'}}(\pi/2)\,, \\
M_3 &= \mathrm{I}_{a_{2'}a_{3'}}\,,
\end{aligned} \tag{8.36}$$

and analogously for the $\hat{b}$ modes. Afterwards, all three operators $\hat{C}_j$ are of the same form

$$\hat{C}_j = \frac{1}{2}\left(\hat{n}_{a_{2''}}\hat{n}_{b_{3''}} + \hat{n}_{a_{3''}}\hat{n}_{b_{2''}}\right), \tag{8.37}$$

which is positive semi-definite and only contains photon number operators (the double primes denote the output modes of the M_j transformations). Thus, the resulting observable $\hat{D}_{2,4}$ (hence also $\hat{D}_{1,2,4}$) depends on cross correlations between the particle numbers on two modes on Alice's and Bob's sides, so it can easily be accessed (provided we have detectors with photon number resolution).

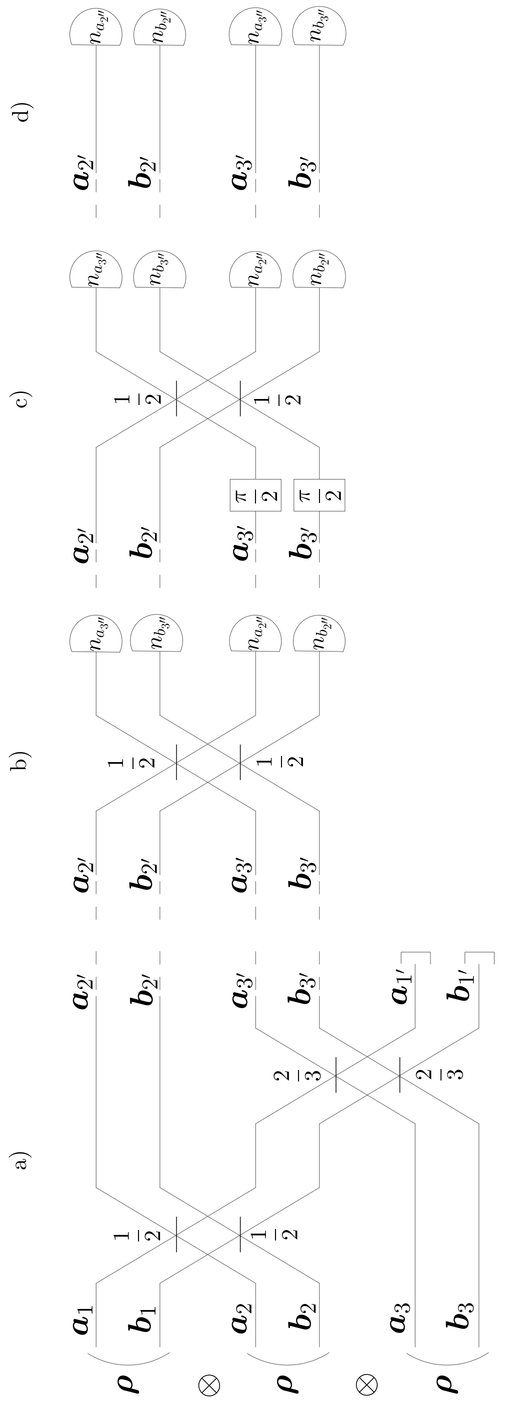

Figure 8.1: a) Optical circuit implementing the transformation M on three identical copies of the bipartite state $\hat{\rho}$, where Alice holds modes $\hat{a}_{1,2,3}$ and Bob holds modes $\hat{b}_{1,2,3}$. The displacement of the state $\hat{\rho}$ is removed by a sequence of two beam splitters of transmittances $\frac{1}{2}$ and $\frac{2}{3}$, implemented locally by Alice and Bob, and leading to modes $\hat{a}_{1',2',3'}$ and $\hat{b}_{1',2',3'}$. The mean field is concentrated on one mode of each subsystem ($\hat{a}_{1'}$ and $\hat{b}_{1'}$), which is traced over. b-d) Three optical circuits applied locally by Alice and Bob in order to access the expectation values of the three operators $\hat{C}_j$, which are needed to evaluate the entanglement witness $d_{1,2,4}$. While measuring $\hat{C}_3$ (see d) requires photon number detectors without any additional optical circuit, a beam splitter of transmittance $\frac{1}{2}$ must be added by Alice and Bob for measuring $\hat{C}_1$ (see b), preceded by a phase shift of $\frac{\pi}{2}$ for measuring $\hat{C}_2$ (see c).

Imperfect copies and optical losses

We analyze the influence of imperfect copies and optical losses when applying this witness to the two-mode squeezed vacuum state (8.18) by using two "toy" models. To that end, we allow for distinct squeezing parameters $\lambda_\mu \in (-1,1)$ for the two copies $\mu = 1,2$. Thus, we consider the state $|\psi\rangle\langle\psi|_1 \otimes |\psi\rangle\langle\psi|_2$ and insert beam splitters with transmittances $\tau_{a_\mu}, \tau_{b_\mu} \leq 1$ on the four modes $(\hat{a}_1, \hat{a}_2)$ and $(\hat{b}_1, \hat{b}_2)$ in order to model losses. Then, we obtain for the expectation value of our multicopy observable $\hat{D}_{2,4}$

$$\langle\langle\hat{D}_{2,4}\rangle\rangle = \frac{\lambda_1^2\lambda_2^2(\tau_{a_1}\tau_{b_2} + \tau_{a_2}\tau_{b_1}) - 2\lambda_1\lambda_2\sqrt{\tau_{a_1}\tau_{a_2}\tau_{b_1}\tau_{b_2}}}{2(1-\lambda_1^2)(1-\lambda_2^2)}, \tag{8.38}$$

with a slight abuse of notation (we use double brackets although the two copies are not identical). We note first that, without losses, the multicopy expectation value

$$\langle\langle\hat{D}_{2,4}\rangle\rangle^{\text{no-loss}} = \frac{\lambda_1\lambda_2(\lambda_1\lambda_2 - 1)}{(1-\lambda_1^2)(1-\lambda_2^2)} \tag{8.39}$$

is always negative provided λ_1 and λ_2 have the same sign. Otherwise, if λ_1 and λ_2 have opposite signs, entanglement is not detected anymore (this corresponds to false negatives, *i.e.*, the determinant fails to be negative even if the imperfect copies are both entangled). We also see that $\langle\langle\hat{D}_{2,4}\rangle\rangle^{\text{no-loss}} = 0$ if $\lambda_1 = 0$ or $\lambda_2 = 0$, in which case the state $|\psi\rangle_1$ or $|\psi\rangle_2$ becomes trivially separable and hence, we do not get a false-positive detection of entanglement.

Now adding losses but assuming that $\tau_{a_1} = \tau_{a_2} = \tau_{b_1} = \tau_{b_2} \equiv \tau$, we get the expectation value

$$\langle\langle\hat{D}_{2,4}\rangle\rangle = \tau^2 \langle\langle\hat{D}_{2,4}\rangle\rangle^{\text{no-loss}}. \tag{8.40}$$

Thus, in the interesting case where λ_1 and λ_2 have the same sign, the no-loss negative value is multiplied by a positive factor τ^2 smaller than or equal to unity. This implies that losses can only deteriorate the detection capabilities but, at the same time, the entanglement of the two-mode squeezed vacuum state remains detected for any non-vanishing transmittances $\tau > 0$. More generally, using $(\sqrt{\tau_{a_1}\tau_{b_2}} \pm \sqrt{\tau_{a_2}\tau_{b_1}})^2 \geq 0$, we obtain upper and lower bounds on the expectation value of $\hat{D}_{2,4}$ with arbitrary losses, namely

$$\frac{\tau_{a_1}\tau_{b_2} + \tau_{a_2}\tau_{b_1}}{2} \langle\langle\hat{D}_{2,4}\rangle\rangle^{\text{no-loss}} \geq \langle\langle\hat{D}_{2,4}\rangle\rangle \geq \sqrt{\tau_{a_1}\tau_{a_2}\tau_{b_1}\tau_{b_2}} \langle\langle\hat{D}_{2,4}\rangle\rangle^{\text{no-loss}}, \tag{8.41}$$

where we have assumed again that λ_1 and λ_2 have the same sign, so that $\langle\langle\hat{D}_{2,4}\rangle\rangle^{\text{no-loss}}$ is negative. Both bounds simply collapse to $\tau^2 \langle\langle\hat{D}_{2,4}\rangle\rangle^{\text{no-loss}}$ in the case where $\tau_{a_1}\tau_{b_2} = \tau_{a_2}\tau_{b_1} \equiv \tau^2$, from which we draw the same conclusions. Otherwise, for arbitrary transmittances, it is clear that losses always bring the (negative) lower bound on $\langle\langle\hat{D}_{2,4}\rangle\rangle$ closer to zero, corroborating the idea that losses deteriorate the witness. Yet, the entanglement of the two-mode squeezed vacuum state remains detected for any non-vanishing transmittance $\tau_{a_\mu}, \tau_{b_\mu} > 0$ as the upper bound on $\langle\langle\hat{D}_{2,4}\rangle\rangle$ always remains negative. In short, although the condition

$\langle\langle \hat{D}_{2,4} \rangle\rangle^{\text{no-loss}} < 0$ only constitutes a valid entanglement witness for $\lambda_1 = \lambda_2$, we observe that $\langle\langle \hat{D}_{2,4} \rangle\rangle$ is negative for all $\lambda_1, \lambda_2 > 0$ or $\lambda_1, \lambda_2 < 0$ and for arbitrary losses.

We can further illustrate the fact that the false-positive detection of entanglement is excluded by considering a finite set of separable states. For example, for two imperfect copies of a product of two single-mode squeezed states, the expectation value is given by

$$\langle\langle \hat{D}_{2,4} \rangle\rangle = \frac{1}{2}\Big(\tau_{a_1}\tau_{b_2} \sinh^2 r_{a_1} \sinh^2 r_{b_2} + \tau_{b_1}\tau_{a_2} \sinh^2 r_{a_2} \sinh^2 r_{b_1}\Big), \tag{8.42}$$

where r_{a_μ}, $r_{b_\mu} \in [0, \infty)$ are the squeezing parameters of the four single-mode squeezed states injected in the circuit. This expression is always non-negative and hence, we cannot obtain a false positive.

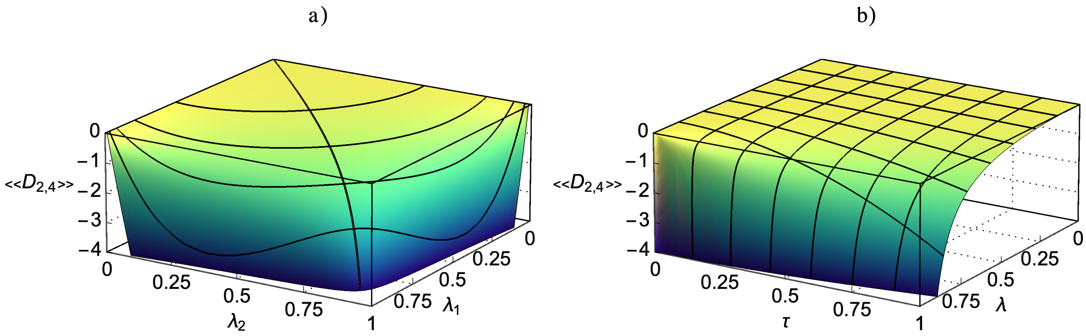

Figure 8.2: a) Expectation value of the multicopy observable $\hat{D}_{2,4}$ as a function of the squeezing parameters λ_1, λ_2 describing two different two-mode squeezed vacuum states, with contour lines of equal total entanglement entropy. The diagonal line corresponds to $\lambda_1 = \lambda_2$. We observe that $\langle\langle \hat{D}_{2,4} \rangle\rangle$ is negative for all $\lambda_1, \lambda_2 > 0$, but identical copies do not minimize $\langle\langle \hat{D}_{2,4} \rangle\rangle$ for a given amount of entanglement. b) Dependence of $\langle\langle \hat{D}_{2,4} \rangle\rangle$ on losses for given squeezing λ. As expected, decreasing the transmittance τ makes the value of $\langle\langle \hat{D}_{2,4} \rangle\rangle$ approach zero, but it remains negative for all $\tau > 0$.

We have plotted the dependence of the muticopy expectation value $\langle\langle \hat{D}_{2,4} \rangle\rangle$ on the two squeezing parameters λ_1 and λ_2 in the no-loss case in Figure 8.2a, together with contour lines of equal total entanglement entropy and a diagonal line along $\lambda_1 = \lambda_2$ indicating identical copies. Although false-positive detection is excluded, we observe that the observable is *not* jointly convex in λ_1 and λ_2 for a fixed amount of entanglement as the case $\lambda_1 = \lambda_2$ corresponds to a local maximum (instead of a global minimum) along every contour line of fixed total entanglement entropy. However, since the non-negativity of $\langle\langle \hat{D}_{2,4} \rangle\rangle$ does only constitute a separability criterion if the two copies are perfect, the possibility that its value decreases (becomes more negative) for imperfect copies is acceptable as long as both states remain entangled.

The effect of losses is illustrated for $\tau \equiv \tau_{a_1} = \tau_{a_2} = \tau_{b_1} = \tau_{b_2}$ and perfect copies $\lambda \equiv \lambda_1 = \lambda_2$ in Figure 8.2b, together with contours of equal τ and equal λ. For decreasing τ, the value of $\langle\langle \hat{D}_{2,4} \rangle\rangle$ falls off quadratically and attains zero for $\tau = 0$, *i.e.*, when the input signal is fully lost. This detrimental effect of losses is clearly stronger when the state is more entangled.

8.3.2 Fourth-order witness based on $\mathbf{D_{1,4,9}}$

Separability criterion

We now consider the criterion obtained from the operator $\hat{f} = c_1 + c_2\hat{b} + c_3\hat{a}\hat{b}$, corresponding to the determinant (see [141] for the ordering convention of moments)

$$d_{1,4,9} = \begin{vmatrix} 1 & \langle \hat{b}^\dagger \rangle & \langle \hat{a}\hat{b}^\dagger \rangle \\ \langle \hat{b} \rangle & \langle \hat{b}^\dagger \hat{b} \rangle & \langle \hat{a}\hat{b}^\dagger \hat{b} \rangle \\ \langle \hat{a}^\dagger \hat{b} \rangle & \langle \hat{a}^\dagger \hat{b}^\dagger \hat{b} \rangle & \langle \hat{a}^\dagger \hat{a} \hat{b}^\dagger \hat{b} \rangle \end{vmatrix}. \tag{8.43}$$

This determinant is of fourth order in the mode operators and thus the corresponding witness $d_{1,4,9} < 0$ is of particular interest for detecting non-Gaussian entanglement.

Application to mixed Schrödinger cat states

We use here the general family of two-mode Schrödinger cat states obtained by superposing two pairs of coherent states presented in Eq.(2.71). The state (2.71) is pure if and only if $z = 0$, in which case it reduces to the cat state considered in Ref. [141], while for $z > 0$ it corresponds to a mixed cat state. The special case $\alpha = \beta$ has been considered in Refs. [156, 130, 41]. Further, state (2.71) is separable if and only if $z = 1$ or $\alpha = \beta = 0$ (in which case it corresponds to the vacuum provided $z \neq 0$; it is ill-defined for $z = 0$ in this case). While second-moment criteria can not certify entanglement at all, sophisticated entropic criteria witness entanglement only for sufficiently large $|\alpha| = |\beta| \gtrsim 3/2$ [156, 130, 56], in which case (2.71) corresponds to two well separated coherent states.

We calculate the value of the determinant $d_{1,4,9}$ [Eq. (8.43)] for general entangled Schrödinger cat states defined in Eq. (2.71) by using that canonical coherent states are eigenstates of the annihilation operator

$$\begin{aligned} \hat{a} \left|\alpha, \beta\right\rangle &= \alpha \left|\alpha, \beta\right\rangle, \\ \left\langle\alpha, \beta\right| \hat{a}^\dagger &= \left\langle\alpha, \beta\right| \alpha^*, \end{aligned} \tag{8.44}$$

and similarly for mode B. We start with the matrix element $\langle \hat{b}^\dagger \rangle$, which evaluates to

$$\begin{aligned} \langle \hat{b}^\dagger \rangle \propto &\mathrm{Tr}\Big[\left|\alpha, \beta\right\rangle \left\langle\alpha, \beta\right| \hat{b}^\dagger + \left|-\alpha, -\beta\right\rangle \left\langle -\alpha, -\beta\right| \hat{b}^\dagger \\ &- (1-z) \Big(\left|\alpha, \beta\right\rangle \left\langle -\alpha, -\beta\right| \hat{b}^\dagger + \left|-\alpha, -\beta\right\rangle \left\langle \alpha, \beta\right| \hat{b}^\dagger \Big) \Big], \\ =&\mathrm{Tr}\Big[\left|\alpha, \beta\right\rangle \left\langle\alpha, \beta\right| \beta^* + \left|-\alpha, -\beta\right\rangle \left\langle -\alpha, -\beta\right| (-\beta^*) \\ &+ (1-z) \left(\left|\alpha, \beta\right\rangle \left\langle -\alpha, -\beta\right| \beta^* - \left|-\alpha, -\beta\right\rangle \left\langle \alpha, \beta\right| \beta^* \right) \Big], \\ =&0. \end{aligned} \tag{8.45}$$

Analogously, we find for the remaining matrix elements

$$\begin{aligned}
\langle\hat{b}\rangle &= \langle\hat{b}^\dagger\rangle = 0,\\
\langle\hat{a}\hat{b}^\dagger\rangle &= 2\alpha\beta^* N(\alpha,\beta,z)(1+(1-z)e^{-2|\alpha|^2-2|\beta|^2}),\\
\langle\hat{a}^\dagger\hat{b}\rangle &= 2\alpha^*\beta N(\alpha,\beta,z)(1+(1-z)e^{-2|\alpha|^2-2|\beta|^2}),\\
\langle\hat{b}^\dagger\hat{b}\rangle &= 2|\beta|^2 N(\alpha,\beta,z)(1+(1-z)e^{-2|\alpha|^2-2|\beta|^2}),\\
\langle\hat{a}\hat{b}^\dagger\hat{b}\rangle &= \langle\hat{a}^\dagger\hat{b}^\dagger\hat{b}\rangle = 0,\\
\langle\hat{a}^\dagger\hat{a}\hat{b}^\dagger\hat{b}\rangle &= |\alpha|^2|\beta|^2.
\end{aligned} \tag{8.46}$$

The full determinant of $d_{1,4,9}$ follows then after identifying the hyperbolic functions

$$\coth\left[|\alpha|^2+|\beta|^2-\frac{1}{2}\ln(1-z)\right] = 2N(\alpha,\beta,z)\left[1+(1-z)e^{-2\left(|\alpha|^2+|\beta|^2\right)}\right], \tag{8.47}$$

and

$$\sinh^{-2}\left[|\alpha|^2+|\beta|^2-\frac{1}{2}\ln(1-z)\right] = 4N^2(\alpha,\beta,z)\left[1+(1-z)e^{-2\left(|\alpha|^2+|\beta|^2\right)}\right]^2-1. \tag{8.48}$$

The determinant (8.43) evaluates to

$$d_{1,4,9} = -|\alpha|^2|\beta|^4\frac{\coth\left[|\alpha|^2+|\beta|^2-\frac{1}{2}\ln(1-z)\right]}{\sinh^2\left[|\alpha|^2+|\beta|^2-\frac{1}{2}\ln(1-z)\right]}. \tag{8.49}$$

As hyperbolic functions map positive numbers to positive numbers, entanglement is certified for the full parameter range, *i.e.* all $z\in[0,1)$ and $\alpha,\beta\in\mathbb{C}\setminus\{0\}$ and thus the witness $d_{1,4,9}<0$ strongly outperforms all known entropic witnesses in the case of cat-like entanglement.

Multicopy implementation

To efficiently access $d_{1,4,9}$, we again exploit the multicopy method and define the corresponding multicopy observable as

$$\hat{D}_{1,4,9} = \frac{1}{|S_{123}|}\sum_{\sigma\in S_{123}}\begin{vmatrix} 1 & \hat{b}^\dagger_{\sigma(1)} & \hat{a}_{\sigma(1)}\hat{b}^\dagger_{\sigma(1)}\\ \hat{b}_{\sigma(2)} & \hat{b}^\dagger_{\sigma(2)}\hat{b}_{\sigma(2)} & \hat{a}_{\sigma(2)}\hat{b}^\dagger_{\sigma(2)}\hat{b}_{\sigma(2)}\\ \hat{a}^\dagger_{\sigma(3)}\hat{b}_{\sigma(3)} & \hat{a}^\dagger_{\sigma(3)}\hat{b}^\dagger_{\sigma(3)}\hat{b}_{\sigma(3)} & \hat{a}^\dagger_{\sigma(3)}\hat{a}_{\sigma(3)}\hat{b}^\dagger_{\sigma(3)}\hat{b}_{\sigma(3)}\end{vmatrix}, \tag{8.50}$$

such that $d_{1,4,9}=\langle\langle\langle\hat{D}_{1,4,9}\rangle\rangle\rangle$. Equation (8.50) consists of 36 terms and can be rewritten as

$$\hat{D}_{1,4,9} = \hat{F}_1-\hat{F}_2+\hat{F}_3-\hat{F}_4-\hat{F}_5, \tag{8.51}$$

after defining the five operators

$$
\begin{aligned}
\hat{F}_1 &= \frac{1}{|P_{123}|} \sum_{\sigma \in P_{123}} \left(\hat{L}_x^{a_{\sigma(1)\sigma(2)}} + \hat{L}_x^{a_{\sigma(3)\sigma(1)}} \right) \hat{n}_{b_\sigma(1)} \hat{L}_x^{b_{\sigma(2)\sigma(3)}}, \\
\hat{F}_2 &= \frac{1}{|P_{123}|} \sum_{\sigma \in P_{123}} \left(\hat{L}_x^{a_{\sigma(2)\sigma(3)}} + \hat{n}_{a_{\sigma(1)}} \right) \hat{n}_{b_\sigma(1)} \hat{L}_x^{b_{\sigma(2)\sigma(3)}}, \\
\hat{F}_3 &= \frac{1}{|P_{123}|} \sum_{\sigma \in P_{123}} \left(\hat{L}_0^{a_{\sigma(1)\sigma(2)}} - \hat{L}_x^{a_{\sigma(1)\sigma(2)}} \right) \hat{n}_{b_{\sigma(1)}} \hat{n}_{b_{\sigma(2)}}, \\
\hat{F}_4 &= \frac{1}{|P_{123}|} \sum_{\sigma \in P_{123}} \left(\hat{L}_y^{a_{\sigma(1)\sigma(2)}} + \hat{L}_y^{a_{\sigma(3)\sigma(1)}} \right) \hat{n}_{b_{\sigma(1)}} \hat{L}_y^{b_{\sigma(2)\sigma(3)}}, \\
\hat{F}_5 &= \frac{1}{|P_{123}|} \sum_{\sigma \in P_{123}} \hat{L}_y^{a_{\sigma(2)\sigma(3)}} \hat{n}_{b_{\sigma(1)}} \hat{L}_y^{b_{\sigma(2)\sigma(3)}},
\end{aligned}
\tag{8.52}
$$

where P_{123} denotes the group of *cyclic* permutations over the index set $\{1,2,3\}$. Thus, the determinant $d_{1,4,9}$ can be accessed by measuring separately the expectation value of each of the five operators $\hat{F}_j$, that is,

$$
d_{1,4,9} = \langle\langle\langle \hat{F}_1 \rangle\rangle\rangle - \langle\langle\langle \hat{F}_2 \rangle\rangle\rangle + \langle\langle\langle \hat{F}_3 \rangle\rangle\rangle - \langle\langle\langle \hat{F}_4 \rangle\rangle\rangle - \langle\langle\langle \hat{F}_5 \rangle\rangle\rangle . \tag{8.53}
$$

Fortunately, the multicopy expectation values $\langle\langle\langle \hat{F}_j \rangle\rangle\rangle$ simplify by using the symmetry under permutations for the three summands in every operator $\hat{F}_j$ as well as for the spin operators themselves. This leads to

$$
\begin{aligned}
\langle\langle\langle \hat{F}_1 \rangle\rangle\rangle &= 2 \, \langle\langle\langle \hat{L}_x^{a_{12}} \hat{n}_{b_1} \hat{L}_x^{b_{23}} \rangle\rangle\rangle , \\
\langle\langle\langle \hat{F}_2 \rangle\rangle\rangle &= \langle\langle\langle \left(\hat{L}_x^{a_{23}} + \hat{n}_{a_1} \right) \hat{n}_{b_1} \hat{L}_x^{b_{23}} \rangle\rangle\rangle , \\
\langle\langle\langle \hat{F}_3 \rangle\rangle\rangle &= \langle\langle\langle \left(\hat{L}_0^{a_{12}} - \hat{L}_x^{a_{12}} \right) \hat{n}_{b_1} \hat{n}_{b_2} \rangle\rangle\rangle , \\
\langle\langle\langle \hat{F}_4 \rangle\rangle\rangle &= 2 \, \langle\langle\langle \hat{L}_y^{a_{12}} \hat{n}_{b_1} \hat{L}_y^{b_{23}} \rangle\rangle\rangle , \\
\langle\langle\langle \hat{F}_5 \rangle\rangle\rangle &= \langle\langle\langle \hat{L}_y^{a_{23}} \hat{n}_{b_1} \hat{L}_y^{b_{23}} \rangle\rangle\rangle .
\end{aligned}
\tag{8.54}
$$

These five multicopy expectation values can be expressed in terms of photon number measurements by applying the five respective transformations shown in Figure 8.3a-e, namely

$$
\begin{aligned}
M_1 &= \mathrm{BS}_{a_1 a_2}(1/2)\, \mathrm{BS}_{b_2 b_3}(1/2) \otimes I_{b_1 a_3}, \\
M_2 &= \mathrm{BS}_{a_2 a_3}(1/2)\, \mathrm{BS}_{b_2 b_3}(1/2) \otimes I_{a_1 b_1}, \\
M_3 &= \mathrm{BS}_{a_1 a_2}(1/2) \otimes I_{b_1 b_2 a_3 b_3}, \\
M_4 &= \mathrm{BS}_{a_1 a_2}(1/2)\, \mathrm{BS}_{b_2 b_3}(1/2)\, \mathrm{PS}_{a_2}(\pi/2)\, \mathrm{PS}_{b_3}(\pi/2) \otimes I_{b_1 a_3}, \\
M_5 &= \mathrm{BS}_{a_2 a_3}(1/2)\, \mathrm{BS}_{b_2 b_3}(1/2)\, \mathrm{PS}_{a_3}(\pi/2)\, \mathrm{PS}_{b_3}(\pi/2) \otimes I_{a_1 b_1}.
\end{aligned}
\tag{8.55}
$$

Incidentally, we note that the measurement of $\hat{F}_3$, implemented via M_3 (see Figure 8.3 c), only requires two copies, while the other four multicopy observables $\hat{F}_j$ are read out on three copies. Then, we finally obtain

$$
\begin{aligned}
\langle\langle\langle \hat{F}_1 \rangle\rangle\rangle &= \frac{1}{2} \left\langle \left(\hat{n}_{a_{1'}} - \hat{n}_{a_{2'}} \right) \hat{n}_{b_{1'}} \left(\hat{n}_{b_{2'}} - \hat{n}_{b_{3'}} \right) \right\rangle , \\
\langle\langle\langle \hat{F}_2 \rangle\rangle\rangle &= \frac{1}{2} \left\langle \left(\frac{1}{2} \left(\hat{n}_{a_{2'}} - \hat{n}_{a_{3'}} \right) + \hat{n}_{a_{1'}} \right) \hat{n}_{b_{1'}} \left(\hat{n}_{b_{2'}} - \hat{n}_{b_{3'}} \right) \right\rangle , \\
\langle\langle\langle \hat{F}_3 \rangle\rangle\rangle &= \left\langle \hat{n}_{a_{2'}} \hat{n}_{b_{1'}} \hat{n}_{b_{2'}} \right\rangle , \\
\langle\langle\langle \hat{F}_4 \rangle\rangle\rangle &= \frac{1}{2} \left\langle \left(\hat{n}_{a_{1'}} - \hat{n}_{a_{2'}} \right) \hat{n}_{b_{1'}} \left(\hat{n}_{b_{2'}} - \hat{n}_{b_{3'}} \right) \right\rangle , \\
\langle\langle\langle \hat{F}_5 \rangle\rangle\rangle &= \frac{1}{4} \left\langle \left(\hat{n}_{a_{2'}} - \hat{n}_{a_{3'}} \right) \hat{n}_{b_{1'}} \left(\hat{n}_{b_{2'}} - \hat{n}_{b_{3'}} \right) \right\rangle .
\end{aligned}
\tag{8.56}
$$

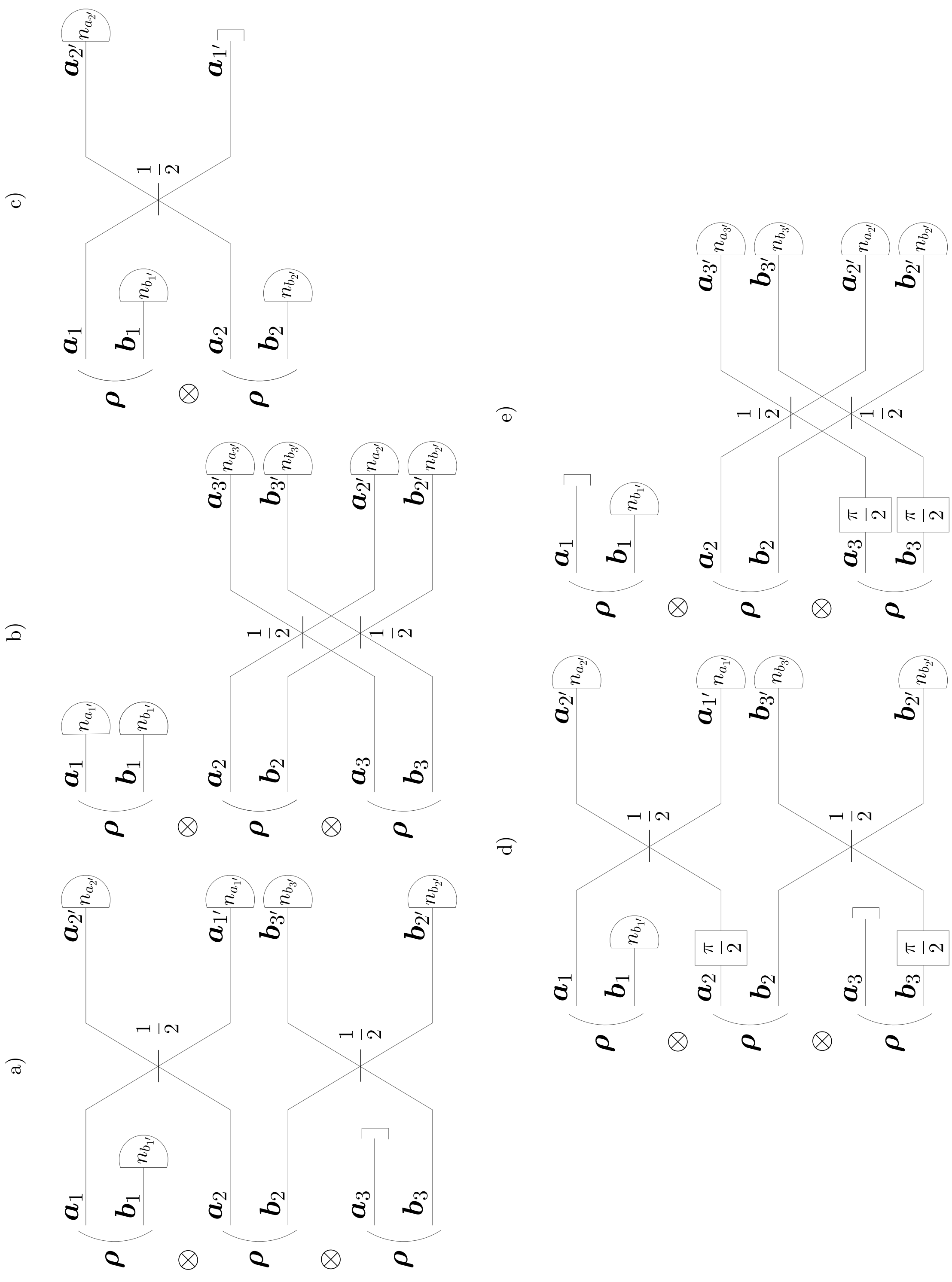

Figure 8.3: Optical circuits implementing the five transformations M_j that are needed for translating the measurements of the five multicopy observables $\hat{F}_j$ into photon number measurements. The expectation value $\langle\langle\langle\hat{F}_j\rangle\rangle\rangle$ is accessed after applying M_j from a) to e), respectively. In all cases, Alice and Bob must apply local transformations to their respective subsystems (Alice holds modes $\hat{a}_{1,2,3}$ and Bob holds modes $\hat{b}_{1,2,3}$). Note that the third copy is not needed for the measurement of $\langle\langle\langle\hat{F}_3\rangle\rangle\rangle$ (see c).

Imperfect copies and optical losses

For three distinct copies of a mixed Schrödinger cat state (2.71) at the input and with losses incorporated, we find for the corresponding multicopy expectation value

$$
\begin{aligned}
\langle\langle\langle \hat{D}_{1,4,9} \rangle\rangle\rangle = \frac{1}{3} \sum_{\sigma \in P_{123}} & \tau_{b_{\sigma(1)}} |\beta_{\sigma(1)}|^2 N(\alpha_{\sigma(1)}, \beta_{\sigma(1)}, z_{\sigma(1)}) \left(1 + (1 - z_{\sigma(1)}) e^{-2|\alpha_{\sigma(1)}|^2 - 2|\beta_{\sigma(1)}|^2}\right) \\
& \Big[\tau_{a_{\sigma(2)}} \tau_{b_{\sigma(2)}} |\alpha_{\sigma(2)}|^2 |\beta_{\sigma(2)}|^2 + \tau_{a_{\sigma(3)}} \tau_{b_{\sigma(3)}} |\alpha_{\sigma(3)}|^2 |\beta_{\sigma(3)}|^2 - 4 \sqrt{\tau_{a_{\sigma(2)}} \tau_{b_{\sigma(2)}} \tau_{a_{\sigma(3)}} \tau_{b_{\sigma(3)}}} \\
& N(\alpha_{\sigma(2)}, \beta_{\sigma(2)}, z_{\sigma(2)}) N(\alpha_{\sigma(3)}, \beta_{\sigma(3)}, z_{\sigma(3)}) \left(1 + (1 - z_{\sigma(2)}) e^{-2|\alpha_{\sigma(2)}|^2 - 2|\beta_{\sigma(2)}|^2}\right) \\
& \left(1 + (1 - z_{\sigma(3)}) e^{-2|\alpha_{\sigma(3)}|^2 - 2|\beta_{\sigma(3)}|^2}\right) \left(\alpha_{\sigma(2)} \beta^*_{\sigma(2)} \alpha^*_{\sigma(3)} \beta_{\sigma(3)} + \alpha^*_{\sigma(2)} \beta_{\sigma(2)} \alpha_{\sigma(3)} \beta^*_{\sigma(3)}\right) \Big].
\end{aligned}
\tag{8.57}
$$

Here, we restrict our analysis to the special case where all states are equally mixed $z_\mu = 1/2$ and comprise equal pairs of real amplitudes $\alpha_\mu \equiv \beta_\mu \in \mathbb{R}$, and where all modes undergo equal losses $\tau \equiv \tau_{a_\mu} = \tau_{b_\mu}$, for $\mu = 1, 2, 3$. We analyze the behavior of $\langle\langle\langle \hat{D}_{1,4,9} \rangle\rangle\rangle$ for *two* different input states (we take copies 2 and 3 to be equal but distinct from copy 1) without losses in Figure 8.4a. We observe that if α_1 and α_2 are too distinct, $\langle\langle\langle \hat{D}_{1,4,9} \rangle\rangle\rangle$ becomes positive, hence entanglement is undetected. This sensitivity to $|\alpha_1 - \alpha_2|$ is very strong for $\alpha_{1,2} \gtrsim 3/2$. Yet, false-positive detection is excluded since $\langle\langle\langle \hat{D}_{1,4,9} \rangle\rangle\rangle \geq 0$ if $\alpha_1 = 0$ or $\alpha_2 = 0$.

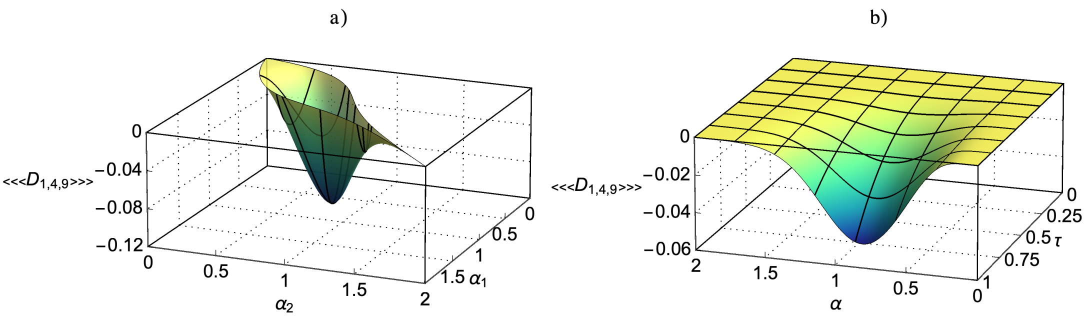

Figure 8.4: a) Negative regions of the expectation value of the multicopy observable $\hat{D}_{1,4,9}$ for the mixed Schrödinger cat state with real $\alpha_\mu = \beta_\mu$, $z_\mu = 1/2$, for $\mu = 1, 2, 3$, and unequal first and second copies ($\alpha_1 \neq \alpha_2$) while the third copy is equal to the second one ($\alpha_3 = \alpha_2$). The expectation value $\langle\langle\langle \hat{D}_{1,4,9} \rangle\rangle\rangle$ remains negative only in a small region around $\alpha_1 \approx \alpha_2$. b) Multicopy expectation value $\langle\langle\langle \hat{D}_{1,4,9} \rangle\rangle\rangle$ as a function of transmittance τ and amplitude α. Entanglement detection works best around $\alpha \approx 1$ and increasing losses also increase the (negative) value of $\langle\langle\langle \hat{D}_{1,4,9} \rangle\rangle\rangle$ without breaking its negativity.

The case of perfect copies with equal losses in all modes is considered in Figure 8.4b, where we plot the dependence of $\langle\langle\langle \hat{D}_{1,4,9} \rangle\rangle\rangle$ on the transmittance τ for a given α. As expected, losses make the value of $\langle\langle\langle \hat{D}_{1,4,9} \rangle\rangle\rangle$ approach zero from below for all α, but $\langle\langle\langle \hat{D}_{1,4,9} \rangle\rangle\rangle$ remains negative for all $\tau > 0$ (of course, we have $\langle\langle\langle \hat{D}_{1,4,9} \rangle\rangle\rangle = 0$ for $\tau = 0$). Also, we observe that the witness $d_{1,4,9} < 0$ works best around $\alpha \approx 1$, *i.e.*, if the two coherent states partially overlap. Note here that $\langle\langle\langle \hat{D}_{1,4,9} \rangle\rangle\rangle$ approaches zero exponentially (from below) for $\alpha \to \infty$, so that entanglement is indeed witnessed for all $\alpha > 0$.

8.3.3 Fourth-order witness based on $\mathbf{D_{1,9,13}}$

Separability criterion

We finally consider the separability criterion corresponding to the operator $\hat{f} = c_1 + c_2\hat{a}\hat{b} + c_3\hat{a}^\dagger\hat{b}^\dagger$, *i.e.*, selecting the rows and columns 1, 9, and 13 in (4.32), leading to the determinant

$$d_{1,9,13} = \begin{vmatrix} 1 & \langle\hat{a}\hat{b}^\dagger\rangle & \langle\hat{a}^\dagger\hat{b}\rangle \\ \langle\hat{a}^\dagger\hat{b}\rangle & \langle\hat{a}^\dagger\hat{a}\hat{b}^\dagger\hat{b}\rangle & \langle\hat{a}^{\dagger 2}\hat{b}^2\rangle \\ \langle\hat{a}\hat{b}^\dagger\rangle & \langle\hat{a}^2\hat{b}^{\dagger 2}\rangle & \langle\hat{a}\hat{a}^\dagger\hat{b}\hat{b}^\dagger\rangle \end{vmatrix}. \tag{8.58}$$

The resulting entanglement witness $d_{1,9,13} < 0$ is again of fourth order in the mode operators. However, when expanding the determinant $d_{1,9,13}$, several products of fourth-order expectation values appear, which gives an overall expression of higher order when compared to $d_{1,4,9}$ in Eq. (8.43). As we may anticipate, the corresponding multicopy observable will therefore be quite complex.

Application to N00N states

In order to illustrate this entanglement witness, we consider the class of pure N00N states with arbitrary complex amplitudes defined in Subsection 2.4.2 (Eq. (2.79)).

The state (2.79) is entangled for all allowed parameter values except when α or β is equal to 0. However, entanglement can not be witnessed by any second-order nor entropic criterion that is valid for mixed states. Pure state entropic criteria flag entanglement for low excitations, *i.e.* small n, see *e.g.* [156, 130, 56], while the Wehrl mutual information fully detects entanglement as it corresponds to a perfect witness for pure states [42]. In this sense, detecting the entanglement of the N00N states (2.79) is known to be particularly challenging, even for small n.

In order to evaluate $d_{1,9,13}$ [Eq. (8.58)], we will use again the properties of the creation and annihilation operators given in (8.19). Exemplary, for the matrix element $\langle\hat{a}\hat{b}^\dagger\rangle$ we find

$$\begin{aligned} \langle\hat{a}\hat{b}^\dagger\rangle &= \Big(\alpha^* \langle n,0| + \beta^* \langle 0,n|\Big)\hat{a}\hat{b}^\dagger\Big(\alpha\,|n,0\rangle + \beta\,|0,n\rangle\Big), \\ &= \Big(\alpha^* \langle n,0| + \beta^* \langle 0,n|\Big)\sqrt{n}\alpha\,|n-1,1\rangle\,, \\ &= \beta^*\sqrt{n}\alpha\delta_{n1}, \\ &= \alpha\beta^*\delta_{n1}. \end{aligned} \tag{8.59}$$

Repeating this strategy for the other matrix elements leads to the determinant

$$d_{1,9,13} = \begin{vmatrix} 1 & \alpha\beta^*\delta_{n1} & \alpha^*\beta\delta_{n1} \\ \alpha^*\beta\delta_{n1} & 0 & 2\alpha^*\beta\delta_{n2} \\ \alpha\beta^*\delta_{n1} & 2\alpha\beta^*\delta_{n2} & n+1 \end{vmatrix}. \tag{8.60}$$

Thus, when evaluating the determinant (8.58) for state (2.79), we find

$$d_{1,9,13} = -2\,|\alpha|^2|\beta|^2\,(\delta_{n1} + 2\delta_{n2})\,. \tag{8.61}$$

Thus, the witness $d_{1,9,13} < 0$ flags entanglement for all N00N states with $\alpha, \beta \in \mathbb{C}$ (except when $\alpha = 0$ or $\beta = 0$) when $n = 1, 2$.

The standard route to access $d_{1,9,13}$ is to define the multicopy observable

$$\hat{D}_{1,9,13} = \frac{1}{|S_{123}|} \sum_{\sigma \in S_{123}} \begin{vmatrix} 1 & \hat{a}_{\sigma(1)}\hat{b}^{\dagger}_{\sigma(1)} & \hat{a}^{\dagger}_{\sigma(1)}\hat{b}_{\sigma(1)} \\ \hat{a}^{\dagger}_{\sigma(2)}\hat{b}_{\sigma(2)} & \hat{a}^{\dagger}_{\sigma(2)}\hat{a}_{\sigma(2)}\hat{b}^{\dagger}_{\sigma(2)}\hat{b}_{\sigma(2)} & \hat{a}^{\dagger 2}_{\sigma(2)}\hat{b}^{2}_{\sigma(2)} \\ \hat{a}_{\sigma(3)}\hat{b}^{\dagger}_{\sigma(3)} & \hat{a}^{2}_{\sigma(3)}\hat{b}^{\dagger 2}_{\sigma(3)} & \hat{a}_{\sigma(3)}\hat{a}^{\dagger}_{\sigma(3)}\hat{b}_{\sigma(3)}\hat{b}^{\dagger} \end{vmatrix}, \tag{8.62}$$

with $d_{1,9,13} = \langle\langle\langle \hat{D}_{1,9,13} \rangle\rangle\rangle$. Writing this operator in terms of spin operators leads to

$$\begin{aligned}
\hat{D}_{1,9,13} =& \frac{1}{|P_{123}|} \sum_{\sigma \in P_{123}} \Bigg\{ -\left((\hat{L}_x^{a_{\sigma(1)\sigma(2)}})^2 - (\hat{L}_y^{a_{\sigma(1)\sigma(2)}})^2 \right) \left((\hat{L}_x^{b_{\sigma(1)\sigma(2)}})^2 - (\hat{L}_y^{b_{\sigma(1)\sigma(2)}})^2 \right) \\
& - \left\{ \hat{L}_x^{a_{\sigma(1)\sigma(2)}}, \hat{L}_y^{a_{\sigma(1)\sigma(2)}} \right\} \left\{ \hat{L}_x^{b_{\sigma(1)\sigma(2)}}, \hat{L}_y^{b_{\sigma(1)\sigma(2)}} \right\} \\
& + 2 \left[\left(\hat{L}_x^{a_{\sigma(1)\sigma(2)}} \hat{L}_x^{a_{\sigma(3)\sigma(1)}} + \hat{L}_y^{a_{\sigma(1)\sigma(2)}} \hat{L}_y^{a_{\sigma(3)\sigma(1)}} \right) \left(\hat{L}_x^{b_{\sigma(1)\sigma(2)}} \hat{L}_x^{b_{\sigma(3)\sigma(1)}} + \hat{L}_y^{b_{\sigma(1)\sigma(2)}} \hat{L}_y^{b_{\sigma(3)\sigma(1)}} \right) \right] \\
& + 2 \left[\left(\hat{L}_y^{a_{\sigma(1)\sigma(2)}} \hat{L}_x^{a_{\sigma(3)\sigma(1)}} - \hat{L}_x^{a_{\sigma(1)\sigma(2)}} \hat{L}_y^{a_{\sigma(3)\sigma(1)}} \right) \left(\hat{L}_y^{b_{\sigma(1)\sigma(2)}} \hat{L}_x^{b_{\sigma(3)\sigma(1)}} - \hat{L}_x^{b_{\sigma(1)\sigma(2)}} \hat{L}_y^{b_{\sigma(3)\sigma(1)}} \right) \right] \\
& - 2 \left[\hat{n}_{a_{\sigma(1)}} \hat{n}_{b_{\sigma(1)}} \left(\hat{L}_x^{a_{\sigma(2)\sigma(3)}} \hat{L}_x^{b_{\sigma(2)\sigma(3)}} + \hat{L}_y^{a_{\sigma(2)\sigma(3)}} \hat{L}_y^{b_{\sigma(2)\sigma(3)}} \right) \right] \\
& + \left(\hat{n}_{a_{\sigma(1)}} \hat{n}_{a_{\sigma(2)}} \hat{n}_{b_{\sigma(1)}} \hat{n}_{b_{\sigma(2)}} + \hat{n}_{a_{\sigma(1)}} \hat{n}_{b_{\sigma(1)}} \right) \\
& + \frac{1}{2} \left(\hat{n}_{a_{\sigma(1)}} \hat{n}_{a_{\sigma(2)}} \hat{n}_{b_{\sigma(1)}} + \hat{n}_{a_{\sigma(1)}} \hat{n}_{a_{\sigma(3)}} \hat{n}_{b_{\sigma(1)}} + \hat{n}_{a_{\sigma(1)}} \hat{n}_{b_{\sigma(1)}} \hat{n}_{b_{\sigma(2)}} + \hat{n}_{a_{\sigma(1)}} \hat{n}_{b_{\sigma(1)}} \hat{n}_{b_{\sigma(3)}} \right) \\
& - \frac{1}{2} \left[\left(\hat{n}_{a_{\sigma(3)}} + \hat{n}_{b_{\sigma(3)}} + 1 \right) \left(\left(\hat{L}_x^{a_{\sigma(1)\sigma(2)}} - i\hat{L}_y^{a_{\sigma(1)\sigma(2)}} \right) + \left(\hat{L}_x^{b_{\sigma(1)\sigma(2)}} + i\hat{L}_y^{b_{\sigma(1)\sigma(2)}} \right) \right) \right] \\
& - \frac{1}{2} \left[\left(\hat{n}_{a_{\sigma(3)}} + \hat{n}_{b_{\sigma(3)}} + 1 \right) \left(\left(\hat{L}_x^{a_{\sigma(1)\sigma(2)}} + i\hat{L}_y^{a_{\sigma(1)\sigma(2)}} \right) + \left(\hat{L}_x^{b_{\sigma(1)\sigma(2)}} - i\hat{L}_y^{b_{\sigma(1)\sigma(2)}} \right) \right) \right] \Bigg\}.
\end{aligned} \tag{8.63}$$

However, this expression is *not* directly measurable due to all terms of the form

$$\hat{L}_x^{a_{\sigma(1)\sigma(2)}} \hat{L}_x^{a_{\sigma(3)\sigma(1)}}, \tag{8.64}$$

which involve one and the same mode for several different spin operators. Passive interferometers can only simplify one of the two spin operators while complicating the other, thereby hindering the measurement of such observables when restricting to photon number measurements.

Thus, unfortunately, the straightforward application of the multicopy method leads to an observable $\hat{D}_{1,9,13}$ which cannot be accessed by using linear interferometers and photon number measurements. Therefore, we instead consider the weaker criterion $d'_{1,9,13} \geq d_{1,9,13}$, which has been put forward in Ref. [3] and reads

$$\begin{aligned} d'_{1,9,13} = &\Big(\langle \hat{a}^\dagger \hat{a} \hat{b}^\dagger \hat{b} \rangle + \langle \hat{a} \hat{a}^\dagger \hat{b} \hat{b}^\dagger \rangle + \langle \hat{a}^{\dagger 2} \hat{b}^2 \rangle + \langle \hat{a}^2 \hat{b}^{\dagger 2} \rangle - \langle \hat{a}^\dagger \hat{b} + \hat{a} \hat{b}^\dagger \rangle^2 \Big) \\ &\Big(\langle \hat{a}^\dagger \hat{a} \hat{b}^\dagger \hat{b} \rangle + \langle \hat{a} \hat{a}^\dagger \hat{b} \hat{b}^\dagger \rangle - \langle \hat{a}^{\dagger 2} \hat{b}^2 \rangle - \langle \hat{a}^2 \hat{b}^{\dagger 2} \rangle + \langle \hat{a}^\dagger \hat{b} - \hat{a} \hat{b}^\dagger \rangle^2 \Big) \\ &- \langle \hat{a}^\dagger \hat{a} + \hat{b}^\dagger \hat{b} + 1 \rangle^2 . \end{aligned} \tag{8.65}$$

For the family of N00N states (2.79), we find (since the criterion contains the same moments as the determinant $d_{1,9,13}$, the calculation is completely analogous to the one presented for the calculation of $d_{1,9,13}$)

$$d'_{1,9,13} = \left[16\, \mathrm{Re}^2(\alpha^* \beta)\, \mathrm{Im}^2(\alpha^* \beta) - 8\, |\alpha^* \beta|^2 \right] \delta_{n1} - 16\, \mathrm{Re}^2(\alpha^* \beta)\, \delta_{n2}. \tag{8.66}$$

Clearly, $d'_{1,9,13}$ is negative for $n = 2$ and all $\alpha, \beta \in \mathbb{C}$ (which includes the aforementioned example of the Hong-Ou-Mandel state), while it is also negative for $n = 1$ provided both amplitudes are for example pure real or imaginary (which includes the aforementioned example of the first Bell state). Therefore, we may equally proceed with $d'_{1,9,13}$ instead of $d_{1,9,13}$.

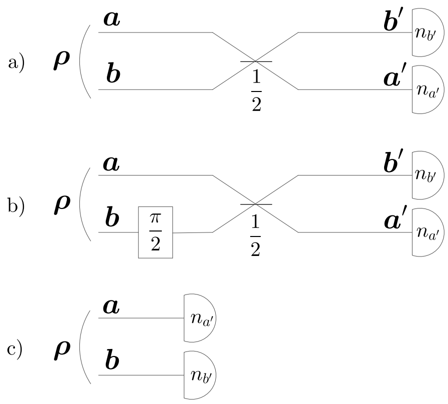

Figure 8.5: Optical circuits implementing the transformations M_1, M_2, and M_3. a) We measure $\hat{L}_x^{ab}$ by applying a balanced beam splitter between the two local modes before using photon number measurements. b) To measure $\hat{L}_y^{ab}$, we add a phase of $\frac{\pi}{2}$ on the second mode before the balanced beam splitter, followed by photon number detectors. c) $\hat{L}_z^{ab}$ directly follows from photon number measurements.

Multimode implementation

Interestingly, Eq. (8.65) can be expressed in terms of spin operators across the bipartition AB without the need for several copies, namely

$$d'_{1,9,13} = 16\, \sigma^2_{L_x^{ab}} \sigma^2_{L_y^{ab}} + 4\, \sigma^2_{L_0^{ab}} - 4\, \sigma^2_{L_z^{ab}} - 4\, \langle \hat{L}_x^{ab} \rangle^2 - 4\, \langle \hat{L}_y^{ab} \rangle^2 - 4\, \langle \hat{L}_z^{ab} \rangle^2 . \tag{8.67}$$

To access $d'_{1,9,13}$, we need three independent measurement schemes for the three spin observables $\hat{L}_x^{ab}, \hat{L}_y^{ab}, \hat{L}_z^{ab}$ (note again that $\hat{L}_0^{ab}$ can be measured simultaneously with $\hat{L}_z^{ab}$). The three

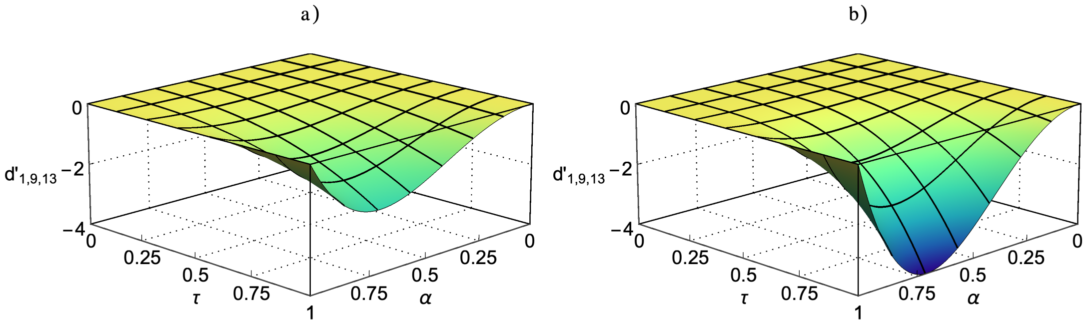

Figure 8.6: Entanglement witness $d'_{1,9,13}$ for N00N states as a function of transmittance τ and real amplitude α for $n = 1$ and $n = 2$ in a) and b), respectively. Entanglement is detected for arbitrarily small but finite losses since $d'_{1,9,13} < 0$.

corresponding transformations

$$\begin{aligned} M_1 &= \mathrm{BS}_{ab}\left(1/2\right), \\ M_2 &= \mathrm{BS}_{ab}\left(1/2\right)\mathrm{PS}_b\left(\pi/2\right), \\ M_3 &= \mathrm{I}_{ab}, \end{aligned} \tag{8.68}$$

can be respectively implemented by the three optical circuits shown in Figure 8.5. These circuits transform each spin operator into $\hat{L}_z^{ab}$, whose relevant expectation values are given by

$$\begin{aligned} \langle \left(\hat{L}_z^{a'b'}\right)^2 \rangle &= \frac{1}{4}\left(\langle \hat{n}_{a'}^2\rangle - 2\langle \hat{n}_{a'}\hat{n}_{b'}\rangle + \langle \hat{n}_{b'}^2\rangle\right), \\ \langle \hat{L}_z^{a'b'}\rangle^2 &= \frac{1}{4}\left(\langle \hat{n}_{a'}\rangle^2 - 2\langle \hat{n}_{a'}\rangle\langle \hat{n}_{b'}\rangle + \langle \hat{n}_{b'}\rangle^2\right). \end{aligned} \tag{8.69}$$

Thus, applying these circuits and measuring the photon numbers yields the needed mean values and variances, so we obtain $d'_{1,9,13}$ using Eq. (8.67).

Let us remark that, compared to the other two entanglement witnesses discussed in subsection 8.3.1 and subsection 8.3.2 where Alice and Bob had to count photons locally on their copies, $d'_{1,9,13} < 0$ is a non-local condition in the sense that Alice and Bob have to perform interferometric measurements on their joint system AB.

Imperfect copies and optical losses

We do not need to analyze the effect of imperfect copies and losses on $d_{1,9,13}$ since we have not developed a multicopy implementation of it. Nevertheless, it is worth illustrating the fact that this criterion does not suffer from false positives by considering the value of $d_{1,9,13}$ when inputting three different product states consisting each of two Fock states. For such states, all off-diagonal elements of the matrix vanish, so that the determinant is simply the product of the diagonal elements, which are all positive. The determinant is thus always positive and there are no false-positive detections.

Now coming to the criterion based on $d'_{1,9,13}$, analyzing imperfect copies is meaningless since there is no need to use more than one copy to measure it. We can only analyze the effect of losses. Adding losses to the two inputs of the optical circuit leads to the expression

$$\begin{aligned} d'_{1,9,13} =& \Big(16\,\mathrm{Re}^2(\alpha^*\beta)\,\mathrm{Im}^2(\alpha^*\beta)\,\tau_a^2\tau_b^2 - 4\left(|\alpha|^2\tau_a + |\beta|^2\tau_b + 1\right)\tau_a\tau_b|\alpha^*\beta|^2\Big)\delta_{n1} \\ & - 16\,\mathrm{Re}^2(\alpha^*\beta)\tau_a^2\tau_b^2\delta_{n2}. \end{aligned} \tag{8.70}$$

We exemplify the dependence on the transmittance $\tau \equiv \tau_a = \tau_b$ for the special case where α and β are real in Figure 8.6a and Figure 8.6b for $n = 1$ and $n = 2$, respectively. In the former case, the value of $d'_{1,9,13}$ increases cubically with τ, while in the latter case it increases quartically with τ. In both cases, entanglement is detected for all amplitudes $\alpha \neq 0, 1$, and non-zero transmittance $\tau > 0$, with the violation of the separability criterion being the largest around $\alpha \approx 3/4$.

8.4 Conclusion and outlook

To summarize, we have put forward schemes to efficiently access three continuous-variable separability criteria based on multimode operators, which are read out via linear interferometers and photon number measurements. The implementation of these schemes thus requires interferometric stability over the few replicas of the state of interest as well as photon-number resolving detectors. The benefit is that the separability criteria are directly accessed, implying that state tomography is not needed. Our schemes encompass optical circuits for second-moment criteria to detect entanglement of Gaussian states, as well as two types of fourth-order criteria suitable for witnessing entanglement in case of mixed Schrödinger cat states (for full parameter ranges) and N00N states (for low-energetic excitations), respectively.

While we focused on three specific separability criteria, our approach is in no way limited to those. Hence, it is of particular interest to identify other sets of relevant criteria and devise suitable multimode observables and corresponding measurement schemes. For example, one may investigate other prominent second-order criteria such as the Simon criterion [143], which is equivalent to the condition $d_{1,2,3,4,5} \geq 0$ [141], such that a multicopy implementation would require five replicas. Alternatively, one may try to implement the second-order criteria due to Mancini *et al.* [98, 45], which constrain the product of the variances appearing in (8.9) instead of their sum. Both criteria are interesting as they are stronger than the criteria by Duan *et al.* [34] as well as the condition $d_{1,2,4} \geq 0$ (all are equivalent in the Gaussian case).

Furthermore, given that our method is generic and based on the algebraic properties of spin operators, a more systematic approach, especially for more than three copies, would be eligible. This may lead to feasible multicopy observables beyond three copies, which could allow us to formulate multicopy versions of entanglement witnesses beyond fourth-order moments. In addition, the method should be equally applicable to other bosonic systems characterized by the pair $\hat{a}, \hat{a}^\dagger$ satisfying $[\hat{a}, \hat{a}^\dagger] = 1$, going beyond quantum optics.

At last, let us remark that the experimental application of our schemes is within reach of current technologies. As a matter of fact, the multicopy nonclassicality observable presented in Ref. [50] has been successfully accessed on a quantum computer in a recent experiment [49], thereby suggesting the general feasibility of the multicopy method. As we have shown here using two very simple models, the typical experimental imperfections should have a modest influence on the detection of entanglement. All multimode observables that we have analyzed are robust against losses in the sense that finite losses decrease the chances for entanglement detection but never completely prevent it. In all cases, false-positive detection of entanglement could be excluded by our small analysis. However, a more realistic analysis of the effect of losses and imperfect copies is needed in order to assert with certainty that the effect of imperfections is not too large. Moreover, a deeper analysis of other experimental imperfections, for instance noise effects, would be valuable towards an experimental implementation of our method.

Chapter 9

Multicopy entanglement witness for the EPR-covariance matrix

This chapter is based on an unpublished work realized together with Tobias Haas and Nicolas Cerf.

In the previous chapters presenting the main results obtained during this thesis, the logic was always the same. Indeed, we always started from existing witnesses to detect nonclassicality or entanglement. We usually analyzed the properties of these criteria like for example its invariances as this was useful for the following steps. Then, we formulated the multicopy observables that gave back the witnesses when taking their mean values on multiple copies of a state. Finally, we searched for implementations of these observables.

One question that arose was then "Is it possible to do the reverse process?". By reverse process, we mean starting from a multicopy observable that we define to obtain a valid nonclassicality or entanglement witness. This is what we do in this chapter, we define a two-copy observable based on EPR-like quadratures and we verify which entanglement witness can be obtained by applying the PPT criterion. Then, we will improve our results by using a three-copy observable to retain invariance by displacements. We will end up with a new entanglement witness which we will compare to other known criteria. This whole approach is inspired by the one presented in Hertz *et al.* paper, Ref. [65] which we presented in Section 5.2.2.

9.1 Two-copy observable

Before defining our observables, we need to define non-local quadrature operators which are a generalization of the EPR-like operators already used in Eq. (4.15).

$$\begin{aligned} \hat{x}_{\pm} &= a_1\hat{x}_1 \pm a_2\hat{x}_2, \\ \hat{p}_{\pm} &= b_1\hat{p}_1 \pm b_2\hat{p}_2, \end{aligned} \tag{9.1}$$

where a_1, a_2, b_1, and b_2 are reals. In the particular case $a_1 = a_2 = |r|$ and $b_1 = b_2 = \frac{1}{r}$, these generalized operators reduce to the ones presented in Eq. (4.15) which are the ones used in entanglement criteria by Duan *et al.* and MGVT. It can be proved that the new operators that we constructed are up to a constant conjugated pairs by calculating their commutators:

$$\begin{aligned} [\hat{x}_{\pm}, \hat{p}_{\pm}] &= i(a_1b_1 + a_2b_2), \\ [\hat{x}_{\pm}, \hat{p}_{\mp}] &= i(a_1b_1 - a_2b_2). \end{aligned} \tag{9.2}$$

Note that the $\pm$ variables are independent if and only if $a_1b_1 = a_2b_2$, in which case the second commutator vanishes.

9.1.1 Two-copy uncertainty observable

Based on the quadratures defined in Eq. (9.1), we define the two copy operator

$$\hat{L}_y^{\pm} = \frac{1}{2}(\hat{x}_{\pm} \otimes \hat{p}_{\pm} - \hat{p}_{\pm} \otimes \hat{x}_{\pm}). \tag{9.3}$$

This observable can be interpreted as the y-component of an angular momentum obtained by using the Jordan-Schwinger map on the Pauli matrices. We start with analyzing the mean and the variance of this observable in order to see if we can extract a separability criterion from it.

We start by calculating the mean of the operator presented in Eq. (9.3) for two identical bipartite states $\hat{\rho}$:

$$\begin{aligned} \langle\langle \hat{L}_y^{\pm} \rangle\rangle &= \mathrm{Tr}\left(\hat{L}_y^{\pm}\left(\hat{\rho}\otimes\hat{\rho}\right)\right), \\ &= \frac{1}{2}(\langle\hat{x}_{\pm}\rangle\langle\hat{p}_{\pm}\rangle - \langle\hat{p}_{\pm}\rangle\langle\hat{x}_{\pm}\rangle) \\ &= 0. \end{aligned} \tag{9.4}$$

As the mean value of the observable is equal to zero, to calculate its variance, we just need to compute its second moment:

$$\begin{aligned} \langle\langle \hat{L}_y^{\pm 2} \rangle\rangle &= \mathrm{Tr}\left(\hat{L}_y^{\pm 2}\left(\hat{\rho}\otimes\hat{\rho}\right)\right), \\ &= \frac{1}{4}\mathrm{Tr}\left(\left(\hat{x}_{\pm}^2\otimes\hat{p}_{\pm}^2 + \hat{p}_{\pm}^2\otimes\hat{x}_{\pm}^2 - \hat{x}_{\pm}\hat{p}_{\pm}\otimes\hat{p}_{\pm}\hat{x}_{\pm} - \hat{p}_{\pm}\hat{x}_{\pm}\otimes\hat{x}_{\pm}\hat{p}_{\pm}\right)\hat{\rho}\otimes\hat{\rho}\right), \\ &= \frac{1}{4}\left(\langle\hat{x}_{\pm}^2\rangle\langle\hat{p}_{\pm}^2\rangle + \langle\hat{p}_{\pm}^2\rangle\langle\hat{x}_{\pm}^2\rangle - \langle\hat{x}_{\pm}\hat{p}_{\pm}\rangle\langle\hat{p}_{\pm}\hat{x}_{\pm}\rangle - \langle\hat{p}_{\pm}\hat{x}_{\pm}\rangle\langle\hat{x}_{\pm}\hat{p}_{\pm}\rangle\right), \\ &= \frac{1}{2}\left(\langle\hat{x}_{\pm}^2\rangle\langle\hat{p}_{\pm}^2\rangle - \langle\hat{x}_{\pm}\hat{p}_{\pm}\rangle\langle\hat{p}_{\pm}\hat{x}_{\pm}\rangle\right). \end{aligned} \tag{9.5}$$

In order to reexpress this expression under a reduced form, we will introduce a covariance matrix for the EPR-like quadratures:

$$\gamma_\pm = \begin{pmatrix} \sigma^2_{x_\pm} & \sigma_{x_\pm p_\pm} \\ \sigma_{x_\pm p_\pm} & \sigma^2_{p_\pm} \end{pmatrix}, \tag{9.6}$$

where

$$\begin{aligned} \sigma^2_{x_\pm} &= \mathrm{Tr}\left(\hat\rho \hat x^2_\pm\right) - \mathrm{Tr}\left(\hat\rho \hat x_\pm\right)^2, \\ \sigma^2_{p_\pm} &= \mathrm{Tr}\left(\hat\rho \hat p^2_\pm\right) - \mathrm{Tr}\left(\hat\rho \hat p_\pm\right)^2, \\ \sigma_{x_\pm p_\pm} &= \frac{1}{2}\mathrm{Tr}\left(\hat\rho\{\hat x_\pm, \hat p_\pm\}\right) - \mathrm{Tr}\left(\hat\rho \hat x_\pm\right)\mathrm{Tr}\left(\hat\rho \hat p_\pm\right). \end{aligned} \tag{9.7}$$

The main differences between these expressions and the usual ones used for a covariance matrix is that here $\hat\rho$ is a bipartite state and we consider the EPR-like quadratures defined in Eq. (9.1) instead of the usual $\hat x$ and $\hat p$. In the special case of centered states $\hat\rho$, all the mean values appearing in the covariance matrix (Eq. (9.7)) will be equal to zero and we will add the upper index c showing that the states are centered:

$$\gamma^c_\pm = \begin{pmatrix} \sigma^{c2}_{x_\pm} & \sigma^c_{x_\pm p_\pm} \\ \sigma^c_{x_\pm p_\pm} & \sigma^{c2}_{p_\pm} \end{pmatrix} = \begin{pmatrix} \mathrm{Tr}\left(\hat\rho \hat x^2_\pm\right) & \frac{1}{2}\mathrm{Tr}\left(\hat\rho\{\hat x_\pm, \hat p_\pm\}\right) \\ \frac{1}{2}\mathrm{Tr}\left(\hat\rho\{\hat x_\pm, \hat p_\pm\}\right) & \mathrm{Tr}\left(\hat\rho \hat p^2_\pm\right) \end{pmatrix}. \tag{9.8}$$

Analyzing Eq. (9.5), we see that the first term can be linked with the diagonal elements of this matrix for centered states. We still need to modify the expression of the second term. To do so, we express $\hat x_\pm \hat p_\pm$ and $\hat p_\pm \hat x_\pm$ as a function of the commutator and the anticommutator of $\hat x_\pm$ and $\hat p_\pm$:

$$\begin{aligned} \hat x_\pm \hat p_\pm &= \frac{1}{2}\left([\hat x_\pm, \hat p_\pm] + \{\hat x_\pm, \hat p_\pm\}\right), \\ \hat p_\pm \hat x_\pm &= \frac{1}{2}\left(-[\hat x_\pm, \hat p_\pm] + \{\hat x_\pm, \hat p_\pm\}\right). \end{aligned} \tag{9.9}$$

Injecting this in Eq. (9.5) leads to:

$$\begin{aligned} \langle\langle \hat L_y^{\pm 2}\rangle\rangle &= \frac{1}{2}\left(\sigma^{c2}_{x_\pm}\sigma^{c2}_{p_\pm} + \frac{1}{4}\mathrm{Tr}\left(\hat\rho[\hat x_\pm, \hat p_\pm]\right)^2 - \frac{1}{4}\mathrm{Tr}\left(\hat\rho\{\hat x_\pm, \hat p_\pm\}\right)^2\right), \\ &= \frac{1}{2}\left(\sigma^{c2}_{x_\pm}\sigma^{c2}_{p_\pm} - \sigma^{c2}_{x_\pm p_\pm} + \frac{1}{4}\mathrm{Tr}\left(\hat\rho[\hat x_\pm, \hat p_\pm]\right)^2\right), \\ &= \frac{1}{2}\left(\det(\gamma^c_\pm) + \frac{1}{4}\mathrm{Tr}\left(\hat\rho[\hat x_\pm, \hat p_\pm]\right)^2\right). \end{aligned} \tag{9.10}$$

As we know that the variance of the operator $\hat L_y^{\pm 2}$ is equal to the second order moment we just calculated and we know the value of the commutator, we obtain the wanted expression, namely,

$$\sigma^2_{L_y^\pm} = \frac{1}{2}\left(\det(\gamma^c_\pm) - \frac{1}{4}(a_1 b_1 + a_2 b_2)^2\right). \tag{9.11}$$

A variance can not be negative $\sigma^2_{L_y^\pm} \geq 0$, hence we obtain the following physical condition which is nothing else than an uncertainty relation:

$$\det(\gamma^c_\pm) \geq \frac{1}{4}(a_1 b_1 + a_2 b_2)^2. \tag{9.12}$$

In the particular case $a_1 = a_2 = b_1 = b_2 = 1$, it reduces to the simple expression

$$\det(\gamma^c_\pm) \geq 1. \tag{9.13}$$

9.1.2 Two-copy entanglement observable

Starting from Eq.(9.10), we want to obtain a separability criterion. To do so, we apply the PPT criterion that we presented in Section 4.2.2. It states that if we do a partial transposition on a separable state $\hat{\rho}$, then the state obtained should remain physical. If it is not physical, then it means that the state was entangled. Here, we will apply the partial transpose to the operator. Indeed, we can prove that:

$$\text{Tr}\left(\hat{\rho}^{T_B}\hat{A}\right) = \text{Tr}\left(\hat{\rho}\hat{A}^{T_B}\right). \tag{9.14}$$

We can easily prove this equality in the special case that interests us, *i.e.* when the observable has the form

$$\hat{A} = \sum_j a_j(\hat{A}_1^j \otimes \hat{A}_2^j), \tag{9.15}$$

where $\hat{A}_i^j$ is a local operator on the subsystem i and a_j are reals. If the operator $\hat{A}$ has this form, then we have:

$$\begin{aligned}
\text{Tr}\left(\hat{\rho}^{T_B}\hat{A}\right) &= \text{Tr}\left(\sum_{n_1,n_1',n_2,n_2'} p^{n_1,n_1'}_{n_2,n_2'}\left(|n_1\rangle\langle n_1'| \otimes (|n_2\rangle\langle n_2'|)^T\right)\sum_j a_j(\hat{A}_1^j \otimes \hat{A}_2^j)\right), \\
&= \sum_{n_1,n_1',n_2,n_2'} p^{n_1,n_1'}_{n_2,n_2'} \sum_j a_j \text{Tr}\left(|n_1\rangle\langle n_1'|\,\hat{A}_1^j\right)\text{Tr}\left((|n_2\rangle\langle n_2'|)^T\hat{A}_2^j\right), \\
&= \sum_{n_1,n_1',n_2,n_2'} p^{n_1,n_1'}_{n_2,n_2'} \sum_j a_j \text{Tr}\left(|n_1\rangle\langle n_1'|\,\hat{A}_1^j\right)\text{Tr}\left(|n_2\rangle\langle n_2'|\,(\hat{A}_2^j)^T\right), \\
&= \text{Tr}\left(\sum_{n_1,n_1',n_2,n_2'} p^{n_1,n_1'}_{n_2,n_2'}\left(|n_1\rangle\langle n_1'| \otimes (|n_2\rangle\langle n_2'|)^T\right)\sum_j a_j(\hat{A}_1^j \otimes (\hat{A}_2^j)^T)\right), \\
&= \text{Tr}\left(\hat{\rho}\hat{A}^{T_B}\right).
\end{aligned} \tag{9.16}$$

As a reminder, doing a partial transposition in continuous variable reduces to a mirror reflection of the p-quadrature for the second mode $\hat{p}_2 \longrightarrow -\hat{p}_2$. We thus need to see how this transforms the different operators that are involved in the uncertainty relation: $\hat{x}_\pm$, $\hat{p}_\pm$, $\hat{x}^2_\pm$, $\hat{p}^2_\pm$, $[\hat{x}_\pm, \hat{p}_\pm]$, and $\{\hat{x}_\pm, \hat{p}_\pm\}$. We present here the detailed calculations for all of them by starting with $\hat{x}_\pm$ and $\hat{p}_\pm$:

$$\begin{aligned}
\hat{x}_\pm^{T_B} &= (a_1\hat{x}_1 \pm a_2\hat{x}_2)^{T_B}, \\
&= a_1\,(\hat{x}_1 \otimes \hat{\mathbb{1}}_2^T) \pm a_2\,(\hat{\mathbb{1}}_1 \otimes \hat{x}_2^T), \\
&= a_1\,(\hat{x}_1 \otimes \hat{\mathbb{1}}_2) \pm a_2\,(\hat{\mathbb{1}}_1 \otimes \hat{x}_2), \\
&= a_1\hat{x}_1 \pm a_2\hat{x}_2, \\
&= \hat{x}_\pm.
\end{aligned} \tag{9.17}$$

The fact that $\hat{x}_\pm$ is not affected by the partial transposition is logical as the partial transposition only applies a mirror reflection to $\hat{p}_2$.

$$\begin{aligned}
\hat{p}_\pm^{T_B} &= (b_1\hat{p}_1 \pm b_2\hat{p}_2)^{T_B}, \\
&= b_1\,(\hat{p}_1 \otimes \hat{\mathbb{1}}_2^T) \pm b_2\,(\hat{\mathbb{1}}_1 \otimes \hat{p}_2^T), \\
&= b_1\hat{p}_1 \mp b_2\hat{p}_2, \\
&= \hat{p}_\mp.
\end{aligned} \tag{9.18}$$

Next, we calculate the partial transpose of the square of the same operators. To do so, we start by developing the square and then we apply on each term the partial transpose:

$$\begin{aligned}
(\hat{x}_\pm^2)^{T_B} &= (a_1\hat{x}_1 \pm a_2\hat{x}_2)^{2T_B}, \\
&= a_1^2\,(\hat{x}_1^2 \otimes \hat{\mathbb{1}}_2^T) + a_2^2\,(\hat{\mathbb{1}}_1 \otimes \hat{x}_2^{2T}) \pm 2a_1a_2\,(\hat{x}_1 \otimes \hat{x}_2^T), \\
&= (a_1\hat{x}_1 \pm a_2\hat{x}_2)^2, \\
&= \hat{x}_\pm^2.
\end{aligned} \tag{9.19}$$

$$\begin{aligned}
(\hat{p}_\pm^2)^{T_B} &= b_1^2\,(\hat{p}_1^2 \otimes \hat{\mathbb{1}}_2^T) + b_2^2\,(\hat{\mathbb{1}}_1 \otimes \hat{p}_2^{2T}) \pm 2b_1b_2\,(\hat{p}_1 \otimes \hat{p}_2^T), \\
&= b_1^2\,(\hat{p}_1^2 \otimes \hat{\mathbb{1}}_2) + b_2^2\,(\hat{\mathbb{1}}_1 \otimes \hat{p}_2^2) \mp 2b_1b_2\,(\hat{p}_1 \otimes \hat{p}_2), \\
&= (b_1\hat{p}_1 \mp b_2\hat{p}_2)^2, \\
&= \hat{p}_\mp^2,
\end{aligned} \tag{9.20}$$

which is the same as in the linear case, *i.e.*, $\hat{x}_\pm^2$ is not affected by the partial transposition while there is a sign flip for $\hat{p}_\pm^2$. Finally, we need to calculate the partial transposition of the commutator and of the anticommutator of $\hat{x}_\pm$ and $\hat{p}_\pm$. We first analyze $\hat{x}_\pm\hat{p}_\pm$ and $\hat{p}_\pm\hat{x}_\pm$:

$$\begin{aligned}
(\hat{x}_\pm\hat{p}_\pm)^{T_B} &= \left((a_1\hat{x}_1 \pm a_2\hat{x}_2)(b_1\hat{p}_1 \pm b_2\hat{p}_2)\right)^{T_B}, \\
&= a_1b_1\,(\hat{x}_1\hat{p}_1 \otimes \hat{\mathbb{1}}_2^T) + a_2b_2\,(\hat{\mathbb{1}}_1 \otimes (\hat{x}_2\hat{p}_2)^T) \pm a_1b_2\,(\hat{x}_1 \otimes \hat{p}_2^T) \pm a_2b_1\,(\hat{p}_1 \otimes \hat{x}_2^T), \\
&= a_1b_1\,(\hat{x}_1\hat{p}_1 \otimes \hat{\mathbb{1}}_2) - a_2b_2\,(\hat{\mathbb{1}}_1 \otimes \hat{p}_2\hat{x}_2) \mp a_1b_2\,(\hat{x}_1 \otimes \hat{p}_2) \pm a_2b_1\,(\hat{p}_1 \otimes \hat{x}_2), \\
&= a_1b_1\,(\hat{p}_1\hat{x}_1 \otimes \hat{\mathbb{1}}_2) + ia_1b_1 - a_2b_2\,(\hat{\mathbb{1}}_1 \otimes \hat{p}_2\hat{x}_2) \mp a_1b_2\,(\hat{x}_1 \otimes \hat{p}_2) \pm a_2b_1\,(\hat{p}_1 \otimes \hat{x}_2), \\
&= \hat{p}_\mp\hat{x}_\pm + ia_1b_1,
\end{aligned} \tag{9.21}$$

where we used $(\hat{A}\hat{B})^T = \hat{B}^T\hat{A}^T$ between the second and the third line and the commutator

$[\hat{x}_1, \hat{p}_1] = i$ between the third and fourth line. Following the same reasoning, we have:

$$\begin{aligned}
(\hat{p}_\pm \hat{x}_\pm)^{T_B} &= ((b_1\hat{p}_1 \pm b_2\hat{p}_2)(a_1\hat{x}_1 \pm a_2\hat{x}_2))^{T_B}, \\
&= a_1b_1\,(\hat{p}_1\hat{x}_1 \otimes \hat{\mathbb{1}}_2^T) + a_2b_2\,(\hat{\mathbb{1}}_1 \otimes (\hat{p}_2\hat{x}_2)^T) \pm a_1b_2\,(\hat{x}_1 \otimes \hat{p}_2^T) \pm a_2b_1\,(\hat{p}_1 \otimes \hat{x}_2^T), \\
&= a_1b_1\,(\hat{p}_1\hat{x}_1 \otimes \hat{\mathbb{1}}_2) - a_2b_2\,(\hat{\mathbb{1}}_1 \otimes \hat{x}_2\hat{p}_2) \mp a_1b_2\,(\hat{x}_1 \otimes \hat{p}_2) \pm a_2b_1\,(\hat{p}_1 \otimes \hat{x}_2), \\
&= a_1b_1\,(\hat{x}_1\hat{p}_1 \otimes \hat{\mathbb{1}}_2) - ia_1b_1 - a_2b_2\,(\hat{\mathbb{1}}_1 \otimes \hat{x}_2\hat{p}_2) \mp a_1b_2\,(\hat{x}_1 \otimes \hat{p}_2) \pm a_2b_1\,(\hat{p}_1 \otimes \hat{x}_2), \\
&= \hat{x}_\pm\hat{p}_\mp - ia_1b_1.
\end{aligned} \tag{9.22}$$

Now that we have the expressions for these two elements, we can calculate the commutator and the anticommutator as:

$$\begin{aligned}
[\hat{x}_\pm, \hat{p}_\pm]^{T_B} &= (\hat{x}_\pm\hat{p}_\pm)^{T_B} - (\hat{p}_\pm\hat{x}_\pm)^{T_B}, \\
&= \hat{p}_\mp\hat{x}_\pm - \hat{x}_\pm\hat{p}_\mp + 2ia_1b_1, \\
&= [\hat{p}_\mp, \hat{x}_\pm] + 2ia_1b_1, \\
&= -i(a_1b_1 - a_2b_2) + 2ia_1b_1, \\
&= i(a_1b_1 + a_2b_2), \\
&= [\hat{x}_\pm, \hat{p}_\pm].
\end{aligned} \tag{9.23}$$

$$\begin{aligned}
\{\hat{x}_\pm, \hat{p}_\pm\}^{T_B} &= (\hat{x}_\pm\hat{p}_\pm)^{T_B} + (\hat{p}_\pm\hat{x}_\pm)^{T_B}, \\
&= \hat{p}_\mp\hat{x}_\pm + \hat{x}_\pm\hat{p}_\mp, \\
&= \{\hat{x}_\pm, \hat{p}_\mp\}.
\end{aligned} \tag{9.24}$$

With all these expressions, we can then apply the PPT criterion to Eq. (9.10). First, we define a new momentum operator where we flip the signs of the $\hat{p}_\pm$-operators:

$$\hat{L}_y'^{\pm} = \frac{1}{2}(\hat{x}_\pm \otimes \hat{p}_\mp - \hat{p}_\mp \otimes \hat{x}_\pm). \tag{9.25}$$

This expression is nothing else than $\hat{L}_y^{\pm T_B}$. We then want to show that applying the partial transpose on the two copies of the state $\hat{\rho} \otimes \hat{\rho}$ and measuring on this new state the mean value of $(\hat{L}_y^{\pm})^n$ gives up to a given constant the same as measuring the mean value for the initial state of $(\hat{L}_y'^{\pm})^n$:

$$\mathrm{Tr}\left(\left(\hat{\rho}^{T_B} \otimes \hat{\rho}^{T_B}\right)(\hat{L}_y^{\pm})^n\right) = \mathrm{Tr}\left((\hat{\rho} \otimes \hat{\rho})\,(\hat{L}_y'^{\pm})^n\right) + C, \tag{9.26}$$

where C is a constant. For $n = 1$, this relation is obvious. Indeed, $\mathrm{Tr}\left(\hat{\rho}^{T_B} \otimes \hat{\rho}^{T_B}(\hat{L}_y^{\pm})\right) = \mathrm{Tr}\left(\hat{\rho} \otimes \hat{\rho}(\hat{L}_y'^{\pm})^{T_B}\right) = 0$ as these two observables are designed to have a mean equal to zero for two identical copies. For $n = 2$, this relation is not obvious anymore. In order to prove that it is true, we will develop $\mathrm{Tr}\left(\hat{\rho}^{T_B}\otimes\hat{\rho}^{T_B}(\hat{L}_y^{\pm})^2\right)$ by using the Eqs. (9.14), (9.17)-(9.24).

$$\begin{aligned}
&\mathrm{Tr}\left(\hat{\rho}^{T_B}\otimes\hat{\rho}^{T_B}(\hat{L}_y^{\pm})^2\right)\\
&=\frac{1}{4}\mathrm{Tr}\left(\hat{\rho}^{T_B}\otimes\hat{\rho}^{T_B}\left(\hat{x}_\pm^2\otimes\hat{p}_\pm^2+\hat{p}_\pm^2\otimes\hat{x}_\pm^2-\hat{x}_\pm\hat{p}_\pm\otimes\hat{p}_\pm\hat{x}_\pm-\hat{p}_\pm\hat{x}_\pm\otimes\hat{x}_\pm\hat{p}_\pm\right)\right),\\
&=\frac{1}{2}\left(\mathrm{Tr}\left(\hat{\rho}^{T_B}\;\hat{x}_\pm^2\right)\mathrm{Tr}\left(\hat{\rho}^{T_B}\;\hat{p}_\pm^2\right)-\mathrm{Tr}\left(\hat{\rho}^{T_B}\;\hat{x}_\pm\hat{p}_\pm\right)\mathrm{Tr}\left(\hat{\rho}^{T_B}\;\hat{p}_\pm\hat{x}_\pm\right)\right),\\
&=\frac{1}{2}\left(\mathrm{Tr}\left(\hat{\rho}\;\hat{x}_\pm^{2T_B}\right)\mathrm{Tr}\left(\hat{\rho}\;\hat{p}_\pm^{2T_B}\right)-\mathrm{Tr}\left(\hat{\rho}\;(\hat{x}_\pm\hat{p}_\pm)^{T_B}\right)\mathrm{Tr}\left(\hat{\rho}\;(\hat{p}_\pm\hat{x}_\pm)^{T_B}\right)\right),\\
&=\frac{1}{2}\left(\mathrm{Tr}\left(\hat{\rho}\;\hat{x}_\pm^2\right)\mathrm{Tr}\left(\hat{\rho}\;\hat{p}_\mp^2\right)-\mathrm{Tr}\left(\hat{\rho}\;\hat{x}_\pm\hat{p}_\mp\right)\mathrm{Tr}\left(\hat{\rho}\;(\hat{p}_\mp\hat{x}_\pm)\right)-ia_1b_1\,\mathrm{Tr}\left(\hat{\rho}[\hat{x}_\pm,\hat{p}_\pm]\right)-a_1^2b_1^2\right),\\
&=\mathrm{Tr}\left(\hat{\rho}\otimes\hat{\rho}(\hat{L}_y'^{\pm})^2\right)-\frac{1}{2}a_1b_1a_2b_2.
\end{aligned}\tag{9.27}$$

If the initial state was separable then the PPT criterion states that $\mathrm{Tr}\left(\left(\hat{\rho}^{T_B}\otimes\hat{\rho}^{T_B}\right)(\hat{L}_y^{\pm})^2\right)\geq 0$. Hence, we end up with a necessary condition for separability:

$$\hat{\rho}\text{ separable }\Rightarrow\;\sigma^2_{L_y'^{\pm}}\geq\frac{1}{2}a_1b_1a_2b_2.\tag{9.28}$$

If this inequality is violated, then the state $\hat{\rho}$ is entangled.

In order to rewrite this criterion under a form that uses the moments of the EPR-quadratures, we use the partial transpose on Eq. (9.10) (see Eqs. (9.17)-(9.24)):

$$\sigma^2_{L_y'^{\pm}}=\frac{1}{2}\left(\det(\tilde{\gamma}^c_\pm)+\frac{1}{4}\mathrm{Tr}(\hat{\rho}[\hat{x}_\pm,\hat{p}_\mp])^2\right)=\frac{1}{2}\left(\det(\tilde{\gamma}^c_\pm)-\frac{1}{4}(a_1b_1-a_2b_2)^2\right),\tag{9.29}$$

where we defined the covariance matrix of the partially transposed state as

$$\tilde{\gamma}_\pm=\begin{pmatrix}\sigma^2_{x_\pm} & \sigma_{x_\pm p_\mp}\\ \sigma_{x_\pm p_\mp} & \sigma^2_{p_\mp}\end{pmatrix}.\tag{9.30}$$

Once again, the upper index c indicates that it is the covariance matrix in the particular case of a centered state. Finally, plugging this Eq. (9.29) in our entanglement witness (Eq. (9.28)) gives

$$\begin{aligned}\frac{1}{2}\left(\det(\tilde{\gamma}^c_\pm)-\frac{1}{4}(a_1b_1-a_2b_2)^2\right)&\geq\frac{1}{2}a_1b_1a_2b_2,\\ \det(\tilde{\gamma}^c_\pm)&\geq a_1b_1a_2b_2+\frac{1}{4}(a_1b_1-a_2b_2)^2,\end{aligned}\tag{9.31}$$

leading to the necessary condition for separability:

$$\hat{\rho}\text{ separable }\Rightarrow\;\det(\tilde{\gamma}^c_\pm)\geq\frac{1}{4}(a_1b_1+a_2b_2)^2.\tag{9.32}$$

We will compare this criterion to other known criteria in Section 9.3. However, we already notice that we restricted ourselves to centered states which is obviously not the most general case. Our previous chapters on multicopy for witnessing nonclassicality or entanglement showed us that often, when we want to obtain something invariant under any displacement, we need to add one copy. This is then what we do in the next section: we add a copy to try to obtain a criterion valid for any state, even if it is displaced.

9.2 Three-copy observable

9.2.1 Three-copy uncertainty observable

Similarly to what we did for two copies, we start by defining a new multicopy operator by using the Jordan-Schwinger map. Here, we define it based on three operators which are each involving two different copies. Moreover, each of these three operators has a similar form as the one used in the two-copy case (Eq. (9.3)):

$$\begin{aligned}\hat{M}_x^{\pm} &= \hat{\mathbb{1}}_1 \otimes \hat{x}_{\pm} \otimes \hat{p}_{\pm} - \hat{\mathbb{1}}_1 \otimes \hat{p}_{\pm} \otimes \hat{x}_{\pm},\\ \hat{M}_y^{\pm} &= \hat{p}_{\pm} \otimes \hat{\mathbb{1}}_2 \otimes \hat{x}_{\pm} - \hat{x}_{\pm} \otimes \hat{\mathbb{1}}_2 \otimes \hat{p}_{\pm},\\ \hat{M}_z^{\pm} &= \hat{x}_{\pm} \otimes \hat{p}_{\pm} \otimes \hat{\mathbb{1}}_3 - \hat{p}_{\pm} \otimes \hat{x}_{\pm} \otimes \hat{\mathbb{1}}_3.\end{aligned} \tag{9.33}$$

Using these expressions, the multicopy observable that we will analyze is the sum of the latter:

$$\hat{M}^{\pm} = \frac{1}{\sqrt{3}} \sum_i \hat{M}_i^{\pm}. \tag{9.34}$$

Now, we will perform the same kind of calculations as those we did for the two-copy observable. Hence, we will give the important steps of the calculations but not all the details. First, we calculate the first and second moment of $\hat{M}^{\pm}$. By construction of each $\hat{M}_i^{\pm}$, it appears that $\langle\langle\langle \hat{M}_i^{\pm} \rangle\rangle\rangle = 0$, and thus

$$\langle\langle\langle \hat{M}^{\pm} \rangle\rangle\rangle = 0. \tag{9.35}$$

Developing the second order moment gives:

$$\begin{aligned}\langle\langle\langle \hat{M}^{\pm 2} \rangle\rangle\rangle =& \frac{1}{3}\mathrm{Tr}\Big((\hat{\rho} \otimes \hat{\rho} \otimes \hat{\rho}) \\ & \Big(\hat{M}_x^{\pm 2} + \hat{M}_y^{\pm 2} + \hat{M}_z^{\pm 2} + \{\hat{M}_x^{\pm}, \hat{M}_y^{\pm}\} + \{\hat{M}_y^{\pm}, \hat{M}_z^{\pm}\} + \{\hat{M}_z^{\pm}, \hat{M}_x^{\pm}\}\Big)\Big).\end{aligned} \tag{9.36}$$

The three terms $\hat{M}_i^{\pm 2}$ will give three times the same contribution to this expression which is nothing else than the same terms than those appearing in Eq. (9.10):

$$\langle\langle\langle \hat{M}_i^{\pm 2} \rangle\rangle\rangle = 2\mathrm{Tr}\left(\hat{\rho}\hat{x}_{\pm}^2\right) \mathrm{Tr}\left(\hat{\rho}\hat{p}_{\pm}^2\right) + \frac{1}{2}\mathrm{Tr}\left(\hat{\rho}[\hat{x}_{\pm}, \hat{p}_{\pm}]\right)^2 - \frac{1}{2}\mathrm{Tr}\left(\hat{\rho}\{\hat{x}_{\pm}, \hat{p}_{\pm}\}\right)^2, \tag{9.37}$$

so that we just need to analyze the mean value of the anticommutators:

$$\begin{aligned}\{\hat{M}_x^{\pm}, \hat{M}_y^{\pm}\} =& \hat{M}_x^{\pm}\hat{M}_y^{\pm} + \hat{M}_y^{\pm}\hat{M}_x^{\pm}, \\ =& \hat{x}_{\pm} \otimes \hat{p}_{\pm} \otimes \{\hat{x}_{\pm}, \hat{p}_{\pm}\} + \hat{p}_{\pm} \otimes \hat{x}_{\pm} \otimes \{\hat{x}_{\pm}, \hat{p}_{\pm}\} \\ & - 2\hat{p}_{\pm} \otimes \hat{p}_{\pm} \otimes \hat{x}_{\pm}^2 - 2\hat{x}_{\pm} \otimes \hat{x}_{\pm} \otimes \hat{p}_{\pm}^2.\end{aligned} \tag{9.38}$$

This leads to:

$$\begin{aligned}\langle\langle\langle\{\hat{M}_x^{\pm}, \hat{M}_y^{\pm}\}\rangle\rangle\rangle =& 2\mathrm{Tr}\left(\hat{\rho}\hat{x}_{\pm}\right)\mathrm{Tr}\left(\hat{\rho}\hat{p}_{\pm}\right)\mathrm{Tr}\left(\hat{\rho}\{\hat{x}_{\pm}, \hat{p}_{\pm}\}\right) \\ & - 2\mathrm{Tr}\left(\hat{\rho}\hat{p}_{\pm}\right)^2\mathrm{Tr}\left(\hat{\rho}\hat{x}_{\pm}^2\right) - 2\mathrm{Tr}\left(\hat{\rho}\hat{x}_{\pm}\right)^2\mathrm{Tr}\left(\hat{\rho}\hat{p}_{\pm}^2\right),\end{aligned} \tag{9.39}$$

and we have exactly the same expression for $\langle\langle\langle\{\hat{M}_y^{\pm}, \hat{M}_z^{\pm}\}\rangle\rangle\rangle$ and $\langle\langle\langle\{\hat{M}_z^{\pm}, \hat{M}_x^{\pm}\}\rangle\rangle\rangle$. One big difference here with respect to the result for the two-copy observable is that there are terms involving the mean values of $\hat{x}_{\pm}$ and $\hat{p}_{\pm}$ which was not the case before. Due to these terms, when adding all the $\langle\langle\langle\hat{M}_i^{\pm 2}\rangle\rangle\rangle$ and $\langle\langle\langle\{\hat{M}_i^{\pm}, \hat{M}_j^{\pm}\}\rangle\rangle\rangle$, the determinant of the general covariance matrix $\gamma_{\pm}$ will appear and not only the one for centered states. We will directly give the final expression for the mean value of $\hat{M}^{\pm 2}$ which is equal to the variance of $\hat{M}^{\pm}$ because its mean value is equal to 0:

$$\sigma_{M^{\pm}}^2 = 2\left(\det\gamma_{\pm} + \frac{1}{4}\mathrm{Tr}\left(\hat{\rho}[\hat{x}_{\pm}, \hat{p}_{\pm}]\right)^2\right). \tag{9.40}$$

As this variance can not be negative, we obtain the following uncertainty relation for the state $\hat{\rho}$:

$$\sigma_{M^{\pm}}^2 \geq 0 \;\Rightarrow\; \det\gamma_{\pm} \geq \frac{1}{4}(a_1 b_1 + a_2 b_2)^2, \tag{9.41}$$

where we replaced the commutator by its value. Note that this expression is exactly the same as Eq. (9.12) but for arbitrary states. We are not restricted to centered states anymore.

9.2.2 Three-copy entanglement observable

Using the same strategy as before, we define the operators that we obtain by applying a partial transpose on the $\hat{M}_i^{\pm}$, namely,

$$\begin{aligned}\hat{M}_x'^{\pm} &= \hat{\mathbb{1}}_1 \otimes \hat{x}_{\pm} \otimes \hat{p}_{\mp} - \hat{\mathbb{1}}_1 \otimes \hat{p}_{\mp} \otimes \hat{x}_{\pm}, \\ \hat{M}_y'^{\pm} &= \hat{p}_{\mp} \otimes \hat{\mathbb{1}}_2 \otimes \hat{x}_{\pm} - \hat{x}_{\pm} \otimes \hat{\mathbb{1}}_2 \otimes \hat{p}_{\mp}, \\ \hat{M}_z'^{\pm} &= \hat{x}_{\pm} \otimes \hat{p}_{\mp} \otimes \hat{\mathbb{1}}_3 - \hat{p}_{\mp} \otimes \hat{x}_{\pm} \otimes \hat{\mathbb{1}}_3,\end{aligned} \tag{9.42}$$

such that

$$\hat{M}'^{\pm} = \frac{1}{\sqrt{3}}\sum_i \hat{M}_i'^{\pm}. \tag{9.43}$$

Then, measuring the mean value of $(\hat{M}^{\pm})^n$ for partially transposed states, $\hat{\rho}^{T_B} \otimes \hat{\rho}^{T_B} \otimes \hat{\rho}^{T_B}$, should give the same than the mean value of $(\hat{M}'^{\pm})^n$ on the initial state $\hat{\rho} \otimes \hat{\rho} \otimes \hat{\rho}$ up to a constant:

$$\mathrm{Tr}\left(\left(\hat{\rho}^{T_B}\otimes\hat{\rho}^{T_B}\otimes\hat{\rho}^{T_B}\right)(\hat{M}^{\pm})^n\right)=\mathrm{Tr}\left((\hat{\rho}\otimes\hat{\rho}\otimes\hat{\rho})\,(\hat{M}'^{\pm})^n\right)+C. \tag{9.44}$$

For $n=1$, as before, it is obvious due to the form of the operators:

$$\mathrm{Tr}\left(\left(\hat{\rho}^{T_B}\otimes\hat{\rho}^{T_B}\otimes\hat{\rho}^{T_B}\right)\hat{M}^{\pm}\right)=\mathrm{Tr}\left((\hat{\rho}\otimes\hat{\rho}\otimes\hat{\rho})\,\hat{M}'^{\pm}\right)=0. \tag{9.45}$$

For the second moment, we will explicitly prove that this also holds. To do so, we start by developing the expression by using Eqs. (9.37), (9.39) and by transferring the partial transpose to the operators:

$$\begin{aligned}\mathrm{Tr}\left(\left(\hat{\rho}^{T_B}\otimes\hat{\rho}^{T_B}\otimes\hat{\rho}^{T_B}\right)(\hat{M}^{\pm})^2\right)=&\,2\mathrm{Tr}\left(\hat{\rho}(\hat{x}_{\pm}^2)^{T_B}\right)\mathrm{Tr}\left(\hat{\rho}(\hat{p}_{\pm}^2)^{T_B}\right)+\frac{1}{2}\mathrm{Tr}\left(\hat{\rho}[\hat{x}_{\pm},\hat{p}_{\pm}]^{T_B}\right)^2\\&-\frac{1}{2}\mathrm{Tr}\left(\hat{\rho}\{\hat{x}_{\pm},\hat{p}_{\pm}\}^{T_B}\right)^2+2\mathrm{Tr}\left(\hat{\rho}\hat{x}_{\pm}^{T_B}\right)\mathrm{Tr}\left(\hat{\rho}\hat{p}_{\pm}^{T_B}\right)\mathrm{Tr}\left(\hat{\rho}\{\hat{x}_{\pm},\hat{p}_{\pm}\}^{T_B}\right)\\&-2\mathrm{Tr}\left(\hat{\rho}\hat{p}_{\pm}^{T_B}\right)^2\mathrm{Tr}\left(\hat{\rho}(\hat{x}_{\pm}^2)^{T_B}\right)-2\mathrm{Tr}\left(\hat{\rho}\hat{x}_{\pm}^{T_B}\right)^2\mathrm{Tr}\left(\hat{\rho}(\hat{p}_{\pm}^2)^{T_B}\right).\end{aligned} \tag{9.46}$$

To go further, we use Eqs. (9.17)-(9.24):

$$\begin{aligned}\mathrm{Tr}\left(\left(\hat{\rho}^{T_B}\otimes\hat{\rho}^{T_B}\otimes\hat{\rho}^{T_B}\right)(\hat{M}^{\pm})^2\right)=&2\mathrm{Tr}\left(\hat{\rho}\hat{x}_{\pm}^2\right)\mathrm{Tr}\left(\hat{\rho}\hat{p}_{\mp}^2\right)+\frac{1}{2}\mathrm{Tr}\left(\hat{\rho}[\hat{x}_{\pm},\hat{p}_{\pm}]\right)^2\\&-\frac{1}{2}\mathrm{Tr}\left(\hat{\rho}\{\hat{x}_{\pm},\hat{p}_{\mp}\}\right)^2+2\mathrm{Tr}\left(\hat{\rho}\hat{x}_{\pm}\right)\mathrm{Tr}\left(\hat{\rho}\hat{p}_{\mp}\right)\mathrm{Tr}\left(\hat{\rho}\{\hat{x}_{\pm},\hat{p}_{\mp}\}\right)\\&-2\mathrm{Tr}\left(\hat{\rho}\hat{p}_{\mp}\right)^2\mathrm{Tr}\left(\hat{\rho}(\hat{x}_{\pm}^2)\right)-2\mathrm{Tr}\left(\hat{\rho}\hat{x}_{\pm}\right)^2\mathrm{Tr}\left(\hat{\rho}\hat{p}_{\mp}^2\right),\\=&2\mathrm{Tr}\left(\hat{\rho}\hat{x}_{\pm}^2\right)\mathrm{Tr}\left(\hat{\rho}\hat{p}_{\mp}^2\right)+\frac{1}{2}\mathrm{Tr}\left(\hat{\rho}[\hat{x}_{\pm},\hat{p}_{\mp}]\right)^2\\&-\frac{1}{2}\mathrm{Tr}\left(\hat{\rho}\{\hat{x}_{\pm},\hat{p}_{\mp}\}\right)^2+2\mathrm{Tr}\left(\hat{\rho}\hat{x}_{\pm}\right)\mathrm{Tr}\left(\hat{\rho}\hat{p}_{\mp}\right)\mathrm{Tr}\left(\hat{\rho}\{\hat{x}_{\pm},\hat{p}_{\mp}\}\right)\\&-2\mathrm{Tr}\left(\hat{\rho}\hat{p}_{\mp}\right)^2\mathrm{Tr}\left(\hat{\rho}(\hat{x}_{\pm}^2)\right)-2\mathrm{Tr}\left(\hat{\rho}\hat{x}_{\pm}\right)^2\mathrm{Tr}\left(\hat{\rho}\hat{p}_{\mp}^2\right)\\&+\frac{1}{2}\mathrm{Tr}\left(\hat{\rho}[\hat{x}_{\pm},\hat{p}_{\pm}]\right)^2-\frac{1}{2}\mathrm{Tr}\left(\hat{\rho}[\hat{x}_{\pm},\hat{p}_{\mp}]\right)^2,\\=&2\mathrm{Tr}\left(\hat{\rho}\hat{x}_{\pm}^2\right)\mathrm{Tr}\left(\hat{\rho}\hat{p}_{\mp}^2\right)+\frac{1}{2}\mathrm{Tr}\left(\hat{\rho}[\hat{x}_{\pm},\hat{p}_{\mp}]\right)^2\\&-\frac{1}{2}\mathrm{Tr}\left(\hat{\rho}\{\hat{x}_{\pm},\hat{p}_{\mp}\}\right)^2+2\mathrm{Tr}\left(\hat{\rho}\hat{x}_{\pm}\right)\mathrm{Tr}\left(\hat{\rho}\hat{p}_{\mp}\right)\mathrm{Tr}\left(\hat{\rho}\{\hat{x}_{\pm},\hat{p}_{\mp}\}\right)\\&-2\mathrm{Tr}\left(\hat{\rho}\hat{p}_{\mp}\right)^2\mathrm{Tr}\left(\hat{\rho}(\hat{x}_{\pm}^2)\right)-2\mathrm{Tr}\left(\hat{\rho}\hat{x}_{\pm}\right)^2\mathrm{Tr}\left(\hat{\rho}\hat{p}_{\mp}^2\right)\\&-\frac{1}{2}(a_1b_1+a_2b_2)^2+\frac{1}{2}(a_1b_1-a_2b_2)^2,\\=&\mathrm{Tr}\left((\hat{\rho}\otimes\hat{\rho}\otimes\hat{\rho})\,(\hat{M}'^{\pm})^2\right)-2a_1b_1a_2b_2,\end{aligned} \tag{9.47}$$

where we had to add the mean value of the commutator between $\hat{x}_{\pm}$ and $\hat{p}_{\mp}$ and we used the known values for the two commutators.

The PPT criterion implies that for a separable state $\mathrm{Tr}\left(\left(\hat{\rho}^{T_B}\otimes\hat{\rho}^{T_B}\otimes\hat{\rho}^{T_B}\right)(\hat{M}^{\pm})^2\right)\geq 0$

leading to the following necessary criterion for separability:

$$\hat{\rho} \text{ separable } \Rightarrow \sigma^2_{M'\pm} \geq 2a_1b_1a_2b_2. \tag{9.48}$$

Expressing this in terms of the covariance matrix $\tilde{\gamma}_\pm$ of the partially transposed state (Eq. (9.30)) can be done by using Eq. (9.40) where we replace all the $\hat{p}_\pm$ by $\hat{p}_\mp$:

$$\sigma^2_{M'\pm} = 2\left(\det\tilde{\gamma}_\pm + \frac{1}{4}\mathrm{Tr}\left(\hat{\rho}[\hat{x}_\pm, \hat{p}_\mp]\right)^2\right), \tag{9.49}$$

leading to

$$2\left(\det\tilde{\gamma}_\pm + \frac{1}{4}\mathrm{Tr}\left(\hat{\rho}[\hat{x}_\pm, \hat{p}_\mp]\right)^2\right) \geq 2a_1b_1a_2b_2. \tag{9.50}$$

We obtain our necessary criterion by isolating the determinant:

$$\hat{\rho} \text{ separable } \Rightarrow \det\tilde{\gamma}_\pm \geq \frac{1}{4}(a_1b_1 + a_2b_2)^2. \tag{9.51}$$

This criterion is the same than the one for two copies but generalized to arbitrary states. In the next section, we will compare it to other known criteria.

9.3 Comparison with well-known entanglement criteria

In the previous sections, we demonstrated two necessary criteria for separability given in Eq. (9.32) and Eq. (9.51). These two criteria reduce to the same one when the state is centered. However, for a displaced state, Eq. (9.32) is not valid. This shows that the criterion presented in Eq. (9.51) is stronger which is the reason why we will concentrate ourselves on that one.

As our criterion involves moments of order two in the quadratures, we will compare it to the ones of Duan *et al.*, MGVT and Simon that were presented in detail in Subsection 4.3.1. Here, we used generalized EPR-like operators defined with four parameters a_1, b_1, a_2, and b_2 (Eq. (9.1)) but the witnesses that we want to compare to are based on the usual EPR-like operators (Eq. (4.15)) which only depends on one real parameter r. The generalized quadratures are equal to the usual ones when taking $a_1 = b_1 = r$ and $a_2 = b_2 = \frac{1}{|r|}$. In this particular case, our criterion reduces to:

$$\hat{\rho} \text{ separable } \Rightarrow \det\tilde{\gamma}_\pm \geq \frac{1}{4}(r^2 + \frac{1}{|r|^2})^2. \tag{9.52}$$

Developing the determinant leads to

$$\sigma^2_{x_\pm}\sigma^2_{p_\mp} \geq \frac{1}{4}(r^2 + \frac{1}{|r|^2})^2 + \sigma^2_{x_\pm p_\mp}. \tag{9.53}$$

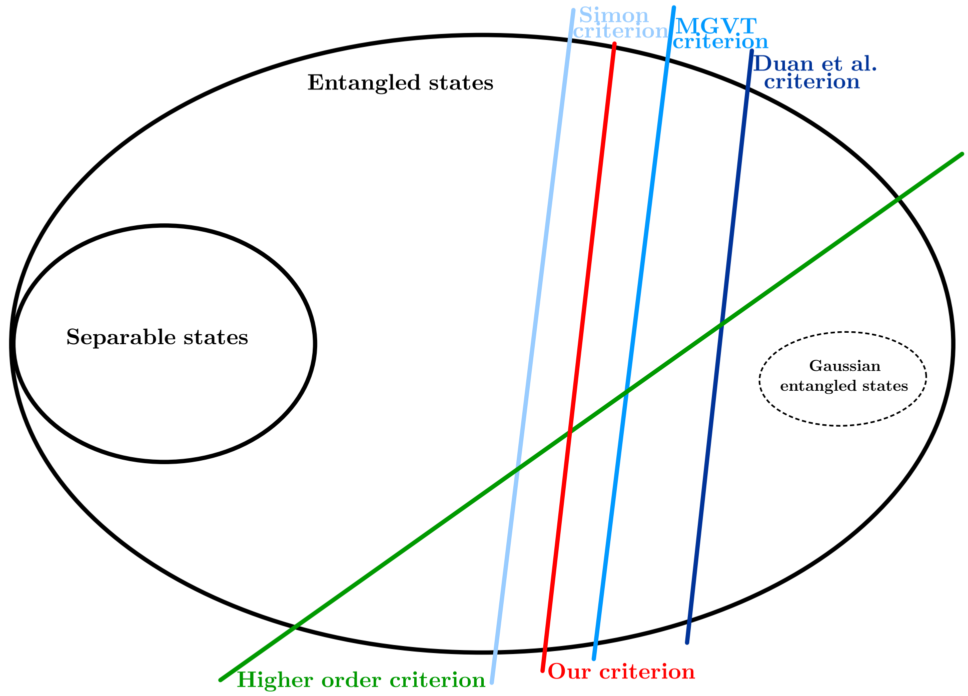

Figure 9.1: Continuous-variable witnesses for the detection of entanglement compared to our new criterion (in red).

As $\sigma^2_{x_\pm p_\mp}$ is always positive, this implies

$$\sigma^2_{x_\pm}\sigma^2_{p_\mp} \geq \frac{1}{4}(r^2 + \frac{1}{|r|^2})^2, \tag{9.54}$$

which is exactly the MGVT criterion (Eq. (4.22)). Moreover, we already proved that the criterion of MGVT is stronger than the one of Duan *et al.* Hence, our criterion also implies the one of Duan *et al.* However, Simon's criterion is the more general criterion that can be written using only second order moments which means that it is still stronger than ours. Furthermore, as Duan's criterion is necessary and sufficient for the detection of Gaussian bipartite entangled states, the same holds true for our witness. A comparison similar to Fig. 4.1 is shown in Fig. 9.1 with our criterion highlighted in red.

9.4 Conclusion and outlook

In this chapter, we have been studying the problem from another perspective: we started by defining a multicopy observable that has a symmetrical form. We then calculated its mean value and variances which lead us to an uncertainty relation based on the covariance matrix for EPR-like quadratures. Then, we applied the PPT criterion in order to obtain a separability criterion. However, our result was only valid for centered states. Hence, we added a copy and defined a new observable for three copies. Redoing the same calculation, we ended up with a new entanglement witness which is true for arbitrary states and not only the centered ones. Finally, we compared our criterion to criteria known in the literature and we proved that it implies MGVT criterion and thus that it is necessary and sufficient for Gaussian bipartite entangled states.

One question remains about our entanglement three copy witness: how can we measure it? Indeed, when translating its expression in terms of quadratures into an expression based on the creation and annihilation operators, we can prove that it can not be measured by using only photon number detectors. This appears because in the expression, there are terms that do not contain the same number of creation and annihilation operators and it is thus impossible to obtain only number operators. One possible way of avoiding such problem could be to consider homodyne or heterodyne detectors but this is left as an open problem for future work.

Chapter 10

Conclusion of this thesis and future perspectives

The aim of this thesis was to design quantum optical circuits in order to efficiently detect the nonclassicality of single-mode states or entanglement of bipartite states of the electromagnetic field. Detecting these two uniquely quantum features is usually done by resorting to so-called witnesses, whose measurement often relies on full tomography of the state, involving a very costly operation in terms of experimental runs. Hence, the main objective of this thesis was to find simpler ways of accessing important nonclassicality and entanglement witnesses. To that end, we exploited Brun's multicopy technique, which gives direct access to nonlinear quantities via the expectation value of joint observables, corresponding physically to the application of a linear interferometer on several independent and identical copies of the state.

The first nonclassicality witnesses we studied in Chapter 6 belong to a hierarchy of nonclassicality witnesses due to Shchukin, Richter, and Vogel. This hierarchy is based on a matrix of normally-ordered moments of the mode operator: if the determinant of any (principal) submatrix is negative, then the state is nonclassical. We started by identifying the most interesting low-dimension submatrices to see which states can be detected as nonclassical. To do so, we considered different examples of test states, namely, the cat states, squeezed states, and Fock states. We proved that each of these classes of pure nonclassical states can be detected when considering suitable subdeterminants. We also analyzed the nonclassicality of mixed Gaussian states and we proved that all nonclassical Gaussian states can be detected. After having analyzed these criteria in detail, we then turned to their implementation, starting with the simplest case of 2x2 determinants. Using the multicopy technique, we managed to find several interesting interferometric circuits using two identical copies, a passive interferometer, and photon number detectors. However, the measurable witnesses with our technique appeared not to be invariant under displacements (by construction, the invariance under phase rotations is guaranteed), and could not detect the nonclassicality of the entirety of sample states mentioned above. In order to overcome this difficulty, we investigated the implementation of 3-copy witnesses. This led to an improvement as we could then design circuits detecting the nonclassicality for some displaced states, *e.g.*, all displaced squeezed states, but not for all the above-mentioned nonclassical states after displacement. Finally, we identified an "ideal" witness in this hierarchy, which can detect the nonclassicality of all our example states, including displaced ones. This witness involves four copies of the state of interest and exhibits a strong detection capability. Unfortunately, we could not find an efficient implementation to measure it with linear optics and photon number measurements, even though we could simplify its expression by using a four-copy interferometer. Thus, one possible direction for future work would be to find a more systematic procedure to design circuits based on determinants. One may also consider to use active elements such as squeezers and/or homodyne/heterodyne detection.

In Chapter 7, we studied another possible method to witness the nonclassicality of a state based on a recently introduced quantity, namely the quadrature coherence scale (QCS). If its value exceeds one, the state is necessary nonclassical. However, before this thesis, no simple experimental implementation was known and its measurement seemed to require a full tomography of the state. Here, we applied the multicopy method and designed a simple circuit to measure the QCS. We separated the problem into two independent steps: the measurement of the numerator and denominator of the QCS, which are both written as quadratic expressions of the density operator, meaning that they are accessible using only two copies. After finding the 2-copy observables associated with the numerator and denominator, we managed to find a simple and unique optical implementation for measuring the QCS (it is just the classical postprocessing that differs for the numerator and denominator). We also simulated the corresponding experiment for some specific classes of nonclassical states, and analyzed how the photon number obtained after the interferometric measurement gives some indication on the nonclassicality of the state. We also reformulated our results in terms of the Wigner function of the output state, which allowed us to reinterpret some known results. Finally, we generalized our circuit to multimode states.

Then, in Chapter 8, we turned to the measurement of entanglement witnesses. We used the hierarchy of Shchukin and Vogel and isolated three most promising low-order witnesses of bipartite entanglement based on three corresponding determinants. Each of these three witnesses allows ones to detect an interesting class of entangled states: Gaussian entangled states, generalized Schrödinger cat states, and low-order N00N states. We exploited again the multicopy method in order to find the multimode observables that can be measured to yield the above three witnesses. In the two first cases, we could design appropriate circuits, using a local passive interferometer supplemented with photon number measurement by each party. For the third witness, we could not find an implementation using only passive interferometry and photon-number resolving detectors. However, we could find the linear-optics implementation of a weaker form of the criterion, which still detects the entanglement of low-order N00N states. This implementation is different in its spirit as it does not need several copies but requires non-local measurements, *i.e.*, the interferometer extends across the two parties. Finally, for the three circuits, we studied the effect of two practical imperfections: optical losses and the fact that the different copies are imperfect due to source flucutations.

Finally, in Chapter 9, we followed a completely different approach. We started by defining a two-copy observable in terms of EPR-type quadratures that has the desired rotation invariance. By expressing the condition that its variance must be non-negative, we obtained a condition that turned out to be equivalent to an uncertainty relation (but is only valid for centered states). Once this was done, we applied the positive-partial-transpose (PPT) criterion at the level of the two-copy observable in order to translate the uncertainty relation into a separability criterion. This gave us a new separability criterion (valid for centered states) involving second-order moments but going beyond all known second-order criteria. We could then relax the fact that it is valid for centered states only by using the same methodology as before, namely we increased the number of copies and defined a three-copy observable. Doing the same kind of calculations as for the two-copy case, we managed to prove that it leads to the same separability criterion but is valid, this time, for arbitrary states. Finally, we compared our criterion to the known second-order criteria and proved that it implies the criterion of MGVT, which is a necessary and sufficient condition for the separability of Gaussian bipartite states, proving that our criterion is necessary and sufficient for Gaussian states as well. However, we are still lacking an implementation to measure our three-copy observable which is probably only possible by using homodyne and heterodyne detectors.

Bibliography

[1] J. Aasi et al. Enhanced sensitivity of the LIGO gravitational wave detector by using squeezed states of light. *Nature Photonics*, 7:613–619, 2013.

[2] G. S. Agarwal. *Quantum optics*. Cambridge University Press, 2013.

[3] G. S. Agarwal and A. Biswas. Inseparability inequalities for higher order moments for bipartite systems. *New Journal of Physics*, 7(1):211, 2005.

[4] G. S. Agarwal and K. Tara. Nonclassical character of states exhibiting no squeezing or sub-Poissonian statistics. *Physical Review A*, 46(1):485–488, 1992.

[5] M. Alexanian. Non-classicality criteria: Glauber–Sudarshan P function and Mandel parameter. *Journal of Modern Optics*, 65(1):16–22, 2018.

[6] M. Arnhem, C. Griffet, and N. J. Cerf. Multicopy observables for the detection of optically nonclassical states. *Physical Review A*, 106(4):043705, 2022.

[7] W. Asavanant, Y. Shiozawa, S. Yokoyama, B. Charoensombutamon, H. Emura, R. Alexander, S. Takeda, J.-i. Yoshikawa, N. Menicucci, H. Yonezawa, and A. Furusawa. Generation of time-domain-multiplexed two-dimensional cluster state. *Science*, 366:373–376, October 2019.

[8] J. K. Asbóth, J. Calsamiglia, and H. Ritsch. Computable Measure of Nonclassicality for Light. *Physical Review Letters*, 94(17):173602, 2005.

[9] A. Aspect, P. Grangier, and G. Roger. Experimental Realization of Einstein-Podolsky-Rosen-Bohm *Gedankenexperiment* : A New Violation of Bell's Inequalities. *Physical Review Letters*, 49(2):91–94, 1982.

[10] M. Avenhaus, K. Laiho, M. V. Chekhova, and C. Silberhorn. Accessing Higher Order Correlations in Quantum Optical States by Time Multiplexing. *Physical Review Letters*, 104(6):063602, 2010.

[11] A. Bach and U. Lüxmann-Ellinghaus. The simplex structure of the classical states of the quantum harmonic oscillator. *Communications in Mathematical Physics*, 107(4):553–560, 1986.

[12] J. S. Bell. On the Einstein Podolsky Rosen paradox. *Physics Physique Fizika*, 1(3):195–200, 1964.

[13] C. H. Bennett and G. Brassard. Quantum cryptography: public key distribution and coin tossing. *Theoretical Computer Science*, 560:7– 11, 2014.

[14] C. H. Bennett, G. Brassard, C. Crépeau, R. Jozsa, A. Peres, and W. K. Wootters. Teleporting an unknown quantum state via dual classical and Einstein-Podolsky-Rosen channels. *Physical Review Letters*, 70(13):1895–1899, 1993.

[15] M. Bohmann, E. Agudelo, and J. Sperling. Probing nonclassicality with matrices of phase-space distributions. *Quantum*, 4:343, 2020.

[16] F. A. Bovino, G. Castagnoli, A. Ekert, P. Horodecki, C. Moura Alves, and A. V. Sergienko. Direct Measurement of Nonlinear Properties of Bipartite Quantum States. *Physical Review Letters*, 95(24):240407, 2005.

[17] S. L. Braunstein and P. van Loock. Quantum information with continuous variables. *Reviews of Modern Physics*, 77(2):513–577, 2005.

[18] T. A. Brun. Measuring polynomial functions of states. *Quantum Information and Computation*, 4:401–408, 2004.

[19] K. E. Cahill and R. J. Glauber. Density Operators and Quasiprobability Distributions. *Physical Review*, 177(5):1882–1902, 1969.

[20] K. E. Cahill and R. J. Glauber. Ordered Expansions in Boson Amplitude Operators. *Physical Review*, 177(5):1857–1881, 1969.

[21] N. J. Cerf and C. Adami. Negative Entropy and Information in Quantum Mechanics. *Physical Review Letters*, 79(26):5194–5197, 1997.

[22] N. J. Cerf, C. Adami, and R. M. Gingrich. Reduction criterion for separability. *Physical Review A*, 60(2):898–909, 1999.

[23] U. Chabaud, P.-E. Emeriau, and F. Grosshans. Witnessing Wigner Negativity. *Quantum*, 5:471, 2021.

[24] U. Chabaud, G. Ferrini, F. Grosshans, and D. Markham. Classical simulation of Gaussian quantum circuits with non-Gaussian input states. *Physical Review Research*, 3(3):033018, 2021.

[25] K. Chen and L-A. Wu. A matrix realignment method for recognizing entanglement (arXiv:quant-ph/0205017), 2003.

[26] S. S. Y. Chua, B. J. J. Slagmolen, D. A. Shaddock, and D. E. McClelland. Quantum squeezed light in gravitational-wave detectors. *Classical and Quantum Gravity*, 31:183001, 2014.

[27] J. F. Clauser and M. A. Horne. Experimental consequences of objective local theories. *Physical Review D*, 10(2):526–535, 1974.

[28] M. Cramer, M. B. Plenio, S. T. Flammia, R. Somma, D. Gross, S. D. Bartlett, O. Landon-Cardinal, D. Poulin, and Y-K. Liu. Efficient quantum state tomography. *Nature Communications*, 1(1):149, 2010. Number: 1 Publisher: Nature Publishing Group.

[29] A. J. Daley, H. Pichler, J. Schachenmayer, and P. Zoller. Measuring Entanglement Growth in Quench Dynamics of Bosons in an Optical Lattice. *Physical Review Letters*, 109(2):020505, 2012.

[30] S. De Bièvre, D. B. Horoshko, G. Patera, and Mikhail I. Kolobov. Measuring Nonclassicality of Bosonic Field Quantum States via Operator Ordering Sensitivity. *Physical Review Letters*, 122(8):080402, 2019.

[31] S. Deside, M. Arnhem, C. Griffet, and N. J. Cerf. Probabilistic pure state conversion on the majorization lattice (arXiv:2303.10086), 2023.

[32] V. V. Dodonov, O. V. Man'ko, V. I. Man'ko, and A. Wünsche. Hilbert-Schmidt distance and non-classicality of states in quantum optics. *Journal of Modern Optics*, 47(4):633–654, 2000.

[33] R. Dong, M. Lassen, J. Heersink, C. Marquardt, R. Filip, G. Leuchs, and U. L. Andersen. Experimental entanglement distillation of mesoscopic quantum states. *Nature Physics*, 4(12):919–923, 2008.

[34] L.-M. Duan, G. Giedke, J. I. Cirac, and P. Zoller. Inseparability Criterion for Continuous Variable Systems. *Physical Review Letters*, 84(12):2722–2725, 2000.

[35] A. Einstein. Über einen die Erzeugung und Verwandlung des Lichtes betreffenden heuristischen Gesichtspunkt,. *Annalen der Physik*, 322(6):132–148, 1905.

[36] A. Einstein, B. Podolsky, and N. Rosen. Can Quantum-Mechanical Description of Physical Reality Be Considered Complete? *Physical Review*, 47(10):777–780, 1935.

[37] A. K. Ekert. Quantum cryptography based on Bell's theorem. *Physical Review Letters*, 67(6):661–663, 1991.

[38] A. K. Ekert, C. Moura Alves, D. K. L. Oi, M. Horodecki, P. Horodecki, and L. C. Kwek. Direct Estimations of Linear and Nonlinear Functionals of a Quantum State. *Physical Review Letters*, 88(21):217901, 2002.

[39] M. Fadel, T. Zibold, B. Décamps, and P. Treutlein. Spatial entanglement patterns and Einstein-Podolsky-Rosen steering in Bose-Einstein condensates. *Science*, 360(6387):409–413, 2018.

[40] R. Filip. Overlap and entanglement-witness measurements. *Physical Review A*, 65(6):062320, 2002.

[41] S. Floerchinger, M. Gärttner, T. Haas, and O. R. Stockdale. Entropic entanglement criteria in phase space. *Physical Review A*, 105(1):012409, 2022.

[42] S. Floerchinger, T. Haas, and H. Müller-Groeling. Wehrl entropy, entropic uncertainty relations, and entanglement. *Physical Review A*, 103(6):062222, 2021.

[43] M. Fox. *Quantum optics: an introduction*. Number 15 in Oxford master series in physics. Oxford University Press, 2006.

[44] W. Ge, K. Jacobs, S. Asiri, M. Foss-Feig, and M. S. Zubairy. Operational resource theory of nonclassicality via quantum metrology. *Physical Review Research*, 2(2):023400, 2020.

[45] V. Giovannetti, S. Mancini, D. Vitali, and P. Tombesi. Characterizing the entanglement of bipartite quantum systems. *Physical Review A*, 67(2):022320, 2003.

[46] R. J. Glauber. Coherent and Incoherent States of the Radiation Field. *Physical Review*, 131(6):2766–2788, 1963.

[47] R. J. Glauber. The Quantum Theory of Optical Coherence. *Physical Review*, 130(6):2529–2539, 1963.

[48] A. Z. Goldberg and D. F. V. James. Nonclassical mixed states that generate zero entanglement with a beam splitter. *Journal of Physics A: Mathematical and Theoretical*, 51(38):385303, 2018.

[49] A. Z. Goldberg, G. S. Thekkadath, and K. Heshami. Measuring the quadrature coherence scale on a cloud quantum computer. *Physical Review A*, 107(4):042610, 2023.

[50] C. Griffet, M. Arnhem, S. De Bièvre, and N. J. Cerf. Interferometric measurement of the quadrature coherence scale using two replicas of a quantum optical state. *Physical Review A*, 108(2):023730, 2023. Publisher: American Physical Society.

[51] C. Griffet, T. Haas, and N. J. Cerf. Accessing continuous-variable entanglement witnesses with multimode spin observables. *Physical Review A*, 108(2):022421, 2023.

[52] C. Gross, H. Strobel, E. Nicklas, T. Zibold, N. Bar-Gill, G. Kurizki, and M. K. Oberthaler. Atomic homodyne detection of continuous-variable entangled twin-atom states. *Nature*, 480(7376):219–223, 2011.

[53] F. Grosshans and P. Grangier. Continuous Variable Quantum Cryptography Using Coherent States. *Physical Review Letters*, 88(5):057902, 2002.

[54] M. Gärttner, T. Haas, and J. Noll. Detecting continuous variable entanglement in phase space with the Q-distribution (arXiv:2211.17165), 2022.

[55] M. Gärttner, T. Haas, and J. Noll. General class of continuous variable entanglement criteria (arXiv:2211.17160), 2022.

[56] M. Gärttner, T. Haas, and J. Noll. Optimizing detection of continuous variable entanglement for limited data (arXiv:2211.17168), 2022.

[57] O. Gühne, Y. Mao, and X.-D. Yu. Geometry of Faithful Entanglement. *Physical Review Letters*, 126(14):140503, 2021.

[58] O. Gühne and G. Tóth. Entanglement detection. *Physics Reports*, 474(1):1–75, 2009.

[59] W. Heisenberg. Über den anschaulichen Inhalt der quantentheoretischen Kinematik und Mechanik. *Zeitschrift für Physik*, 43(3):172–198, 1927.

[60] A. Hertz, M. Arnhem, A. Asadian, and N. J. Cerf. Realignment separability criterion assisted with filtration for detecting continuous-variable entanglement. *Physical Review A*, 104(2):022427, August 2021.

[61] A. Hertz, N. J. Cerf, and S. De Bièvre. Relating the Entanglement and Optical Nonclassicality of Multimode States of a Bosonic Quantum Field. *Physical Review A*, 102(3):032413, 2020.

[62] A. Hertz and S. De Bièvre. Quadrature Coherence Scale Driven Fast Decoherence of Bosonic Quantum Field States. *Physical Review Letters*, 124(9):090402, 2020.

[63] A. Hertz and S. De Bièvre. Decoherence and nonclassicality of photon-added and photon-subtracted multimode Gaussian states. *Physical Review A*, 107(4):043713, 2023.

[64] A. Hertz, E. Karpov, A. Mandilara, and N. J. Cerf. Detection of non-Gaussian entangled states with an improved continuous-variable separability criterion. *Physical Review A*, 93(3):032330, 2016.

[65] A. Hertz, O. Oreshkov, and N. J. Cerf. Multicopy uncertainty observable inducing a symplectic-invariant uncertainty relation in position and momentum phase space. *Physical Review A*, 100(5):052112, 2019.

[66] M. Hillery. Classical pure states are coherent states. *Physics Letters A*, 111(8-9):409–411, 1985.

[67] M. Hillery. Nonclassical distance in quantum optics. *Physical Review A*, 35(2):725–732, 1987.

[68] M. Hillery. Total noise and nonclassical states. *Physical Review A*, 39(6):2994–3002, 1989.

[69] C. K. Hong, Z. Y. Ou, and L. Mandel. Measurement of subpicosecond time intervals between two photons by interference. *Physical Review Letters*, 59(18):2044–2046, 1987.

[70] M. Horodecki and P. Horodecki. Reduction criterion of separability and limits for a class of distillation protocols. *Physical Review A*, 59(6):4206–4216, 1999.

[71] M. Horodecki, P. Horodecki, and R. Horodecki. Separability of mixed states: necessary and sufficient conditions. *Physical Letters A*, 223(1):1–8, 1996.

[72] M. Horodecki, P. Horodecki, and R. Horodecki. Mixed-State Entanglement and Distillation: Is there a “Bound” Entanglement in Nature? *Physical Review Letters*, 80(24):5239–5242, 1998.

[73] P. Horodecki and A. Ekert. Method for Direct Detection of Quantum Entanglement. *Physical Review Letters*, 89(12):127902, 2002.

[74] R. Horodecki, P. Horodecki, M. Horodecki, and K. Horodecki. Quantum entanglement. *Reviews of Modern Physics*, 81(2):865–942, 2009.

[75] D. B. Horoshko, S. De Bièvre, G. Patera, and M. I. Kolobov. Thermal-difference states of light: Quantum states of heralded photons. *Physical Review A*, 100(5):053831, 2019.

[76] H. Huang and G. S. Agarwal. General linear transformations and entangled states. *Physical Review A*, 49(1):52–60, January 1994.

[77] K. Husimi. Some Formal Properties of the Density Matrix. *Proceedings of the Physico-Mathematical Society of Japan. 3rd Series*, 22(4):264–314, 1940.

[78] R. Islam, R. Ma, P. M. Preiss, M. Eric Tai, A. Lukin, M. Rispoli, and M. Greiner. Measuring entanglement entropy in a quantum many-body system. *Nature*, 528:77–83, 2015.

[79] A. Kenfack and K. Życzkowski. Negativity of the Wigner function as an indicator of non-classicality. *Journal of Optics B: Quantum and Semiclassical Optics*, 6(10):396–404, 2004.

[80] E. H. Kennard. Zur Quantenmechanik einfacher Bewegungstypen. *Zeitschrift für Physik*, 44(4):326–352, 1927.

[81] N. Killoran, F. E. S. Steinhoff, and M. B. Plenio. Converting Nonclassicality into Entanglement. *Physical Review Letters*, 116(8):080402, 2016.

[82] M. S. Kim, F. A. M. de Oliveira, and P. L. Knight. Properties of squeezed number states and squeezed thermal states. *Physical Review A*, 40(5):2494–2503, 1989.

[83] M. S. Kim, W. Son, V. Bužek, and P. L. Knight. Entanglement by a beam splitter: nonclassicality as a prerequisite for entanglement. *Physical Review A*, 65(3):032323, 2002.

[84] J. R. Klauder. Improved Version of Optical Equivalence Theorem. *Physical Review Letters*, 16(12):534–536, 1966.

[85] E. Knill, R. Laflamme, and G. J. Milburn. A scheme for efficient quantum computation with linear optics. *Nature*, 409:18, 2001.

[86] P. Kunkel, M. Prüfer, S. Lannig, R. Strohmaier, M. Gärttner, H. Strobel, and M. K. Oberthaler. Detecting Entanglement Structure in Continuous Many-Body Quantum Systems. *Physical Review Letters*, 128(2):020402, 2022.

[87] P. Kunkel, M. Prüfer, H. Strobel, D. Linnemann, A. Frölian, T. Gasenzer, M. Gärttner, and M. K. Oberthaler. Spatially distributed multipartite entanglement enables EPR steering of atomic clouds. *Science*, 360(6387):413–416, 2018.

[88] H. Kwon, Kok C. Tan, T. Volkoff, and H. Jeong. Nonclassicality as a Quantifiable Resource for Quantum Metrology. *Physical Review Letters*, 122(4):040503, 2019.

[89] K. Lange, J. Peise, B. Lücke, I. Kruse, G. Vitagliano, I. Apellaniz, M. Kleinmann, G. Tóth, and C. Klempt. Entanglement between two spatially separated atomic modes. *Science*, 360(6387):416–418, 2018.

[90] C. T. Lee. Measure of the nonclassicality of nonclassical states. *Physical Review A*, 44(5):R2775–R2778, 1991.

[91] C. T. Lee. Theorem on nonclassical states. *Physical Review A*, 52(4):3374–3376, 1995.

[92] U. Leonhardt. Quantum physics of simple optical instruments. *Reports on Progress in Physics*, 66(7):1207, 2003.

[93] U. Leonhardt. *Essential Quantum Optics: From Quantum Measurements to Black Holes*. Cambridge University Press, 1 edition, 2010.

[94] R. Loudon. *The Quantum Theory of Light*. Oxford Science Publications, 3rd edition, 2000.

[95] S. Luo and Y. Zhang. Quantifying nonclassicality via Wigner-Yanase skew information. *Physical Review A*, 100(3):032116, 2019.

[96] A. I. Lvovsky and J. H. Shapiro. Nonclassical character of statistical mixtures of the single-photon and vacuum optical states. *Physical Review A*, 65(3):033830, 2002.

[97] N. Lütkenhaus and S. M. Barnett. Nonclassical effects in phase space. *Physical Review A*, 51(4):3340–3342, 1995.

[98] S. Mancini, V. Giovannetti, D. Vitali, and P. Tombesi. Entangling Macroscopic Oscillators Exploiting Radiation Pressure. *Physical Review Letters*, 88(12):120401, 2002.

[99] S. Mancini, P. Tombesi, and V. I. Man'ko. Density matrix from photon number tomography. *EPL*, 37(2):79, 1997.

[100] L Mandel. Sub-Poissonian photon statistics in resonance fluorescence. *Optics Letters*, 4:205–207, 1979.

[101] L. Mandel and E. Wolf. *Optical Coherence and Quantum Optics*. Cambridge University Press, 1st edition, 1995.

[102] P. Marian and T. A. Marian. Uhlmann fidelity between two-mode Gaussian states. *Physical Review A*, 86(2):022340, 2012.

[103] P. Marian, T. A. Marian, and H. Scutaru. Quantifying Nonclassicality of One-Mode Gaussian States of the Radiation Field. *Physical Review Letters*, 88(15):153601, 2002.

[104] A. W. Marshall, I. Olkin, and B. C. Arnold. *Inequalities: Theory of Majorization and Its Applications*. Springer Series in Statistics. Springer, 2011.

[105] A. Miranowicz, M. Bartkowiak, X. Wang, Y. Liu, and F. Nori. Testing nonclassicality in multimode fields: A unified derivation of classical inequalities. *Physical Review A*, 82(1):013824, 2010.

[106] A. Miranowicz and M. Piani. Comment on "Inseparability Criteria for Continuous Bipartite Quantum States". *Physical Review Letters*, 97(5):058901, 2006.

[107] A. Miranowicz, M. Piani, P. Horodecki, and R. Horodecki. Inseparability criteria based on matrices of moments. *Physical Review A*, 80(5):052303, 2009.

[108] G. Moody et al. 2022 Roadmap on integrated quantum photonics. *JPhys Photonics*, 4(1):012501, 2022.

[109] C. Moura Alves, P. Horodecki, D. K. L. Oi, L. C. Kwek, and A. K. Ekert. Direct estimation of functionals of density operators by local operations and classical communication. *Physical Review A*, 68(3):032306, 2003.

[110] C. Moura Alves and D. Jaksch. Multipartite Entanglement Detection in Bosons. *Physical Review Letters*, 93(11):110501, 2004.

[111] R. Nair. Nonclassical distance in multimode bosonic systems. *Physical Review A*, 95(6):063835, 2017.

[112] M. A. Nielsen and I. L. Chuang. *Quantum Computation and Quantum Information*. Cambridge University Press, 1 edition, 2012.

[113] M. A. Nielsen and J. Kempe. Separable States Are More Disordered Globally than Locally. *Physical Review Letters*, 86(22):5184–5187, 2001.

[114] J. L. O'Brien, A. Furusawa, and J. Vuckovic. Photonic quantum technologies. *Nature Photonics*, 3:687–695, 2009.

[115] T. Opatrný and D.-G. Welsch. Density-matrix reconstruction by unbalanced homodyning. *Physical Review A*, 55(2):1462–1465, 1997.

[116] R. N. Palmer, C. Moura Alves, and D. Jaksch. Detection and characterization of multipartite entanglement in optical lattices. *Physical Review A*, 72(4):042335, 2005.

[117] M. G. A. Paris. Entanglement and visibility at the output of a Mach-Zehnder interferometer. *Physical Review A*, 59(2):1615–1621, 1999.

[118] J. Peise, I. Kruse, K. Lange, B. Lücke, L. Pezzè, J. Arlt, W. Ertmer, K. Hammerer, L. Santos, A. Smerzi, and C. Klempt. Satisfying the Einstein-Podolsky-Rosen criterion with massive particles. *Nature Communications*, 6:8984, 2015.

[119] A. Peres. Separability Criterion for Density Matrices. *Physical Review Letters*, 77(8):1413–1415, 1996.

[120] M. Planck. Ueber das Gesetz der Energieverteilung im Normalspectrum. *Annalen der Physik*, 4(3):553–563, 1901.

[121] M. B. Plenio and S. Virmani. An Introduction to Entanglement Measures. *Quantum Information & Computation*, 7(1):1–51, 2007.

[122] Z. Qin, M. Gessner, Z. Ren, X. Deng, D. Han, W. Li, X. Su, A. Smerzi, and K. Peng. Characterizing the multipartite continuous-variable entanglement structure from squeezing coefficients and the Fisher information. *npj Quantum Information*, 5(1):3, 2019.

[123] T. C. Ralph and P. K. Lam. A bright future for quantum communications. *Nature Photonics*, 3:671–673, 2009.

[124] Th. Richter and W. Vogel. Nonclassicality of Quantum States: A Hierarchy of Observable Conditions. *Physical Review Letters*, 89(28):283601, 2002.

[125] A. Rivas and A. Luis. Nonclassicality of states and measurements by breaking classical bounds on statistics. *Physical Review A*, 79(4):042105, 2009.

[126] H. P. Robertson. The Uncertainty Principle. *Physical Review*, 34(1):163–164, 1929.

[127] O. Rudolph. Further Results on the Cross Norm Criterion for Separability. *Quantum Information Processing*, 4(3):219–239, 2005.

[128] S. Ryl, J. Sperling, E. Agudelo, M. Mraz, S. Köhnke, B. Hage, and W. Vogel. Unified nonclassicality criteria. *Physical Review A*, 92(1):011801, 2015.

[129] S. Ryl, J. Sperling, and W. Vogel. Quantifying nonclassicality by characteristic functions. *Physical Review A*, 95(5):053825, 2017.

[130] A. Saboia, F. Toscano, and S. P. Walborn. Family of continuous-variable entanglement criteria using general entropy functions. *Physical Review A*, 83(3):032307, 2011.

[131] B. C. Sanders. Quantum dynamics of the nonlinear rotator and the effects of continual spin measurement. *Physical Review A*, 40(5):2417–2427, 1989.

[132] J. Schneeloch and G. A. Howland. Quantifying high-dimensional entanglement with Einstein-Podolsky-Rosen correlations. *Physical Review A*, 97(4):042338, 2018.

[133] J. Schneeloch, C. C. Tison, M. L. Fanto, P. M. Alsing, and G. A. Howland. Quantifying entanglement in a 68-billion-dimensional quantum state space. *Nature Communications*, 10(2785):1–7, 2019.

[134] E. Schrödinger. Zum Heisenbergschen Unschärfeprinzip. *Sitzungsberichte der Preussischen Akademie der Wissenschaften*, 14:296–303, 1930.

[135] E. Schrödinger. Die gegenwärtige Situation in der Quantenmechanik. *Naturwissenschaften*, 23(48):807–812, 1935.

[136] A. Serafini. *Quantum Continuous Variables: A Primer of Theoretical Methods*. CRC Press, 2017.

[137] A. Serafini, G. Adesso, and F. Illuminati. Unitarily localizable entanglement of Gaussian states. *Physical Review A*, 71(3):032349, 2005.

[138] F. Shahandeh, A. P. Lund, and T. C. Ralph. Quantum Correlations in Nonlocal Boson Sampling. *Physical Review Letters*, 119(12):120502, 2017.

[139] F. Shahandeh, A. P. Lund, and T. C. Ralph. Quantum correlations and global coherence in distributed quantum computing. *Physical Review A*, 99(5):052303, 2019.

[140] E. Shchukin, Th. Richter, and W. Vogel. Nonclassicality criteria in terms of moments. *Physical Review A*, 71(1):011802(R), 2005.

[141] E. Shchukin and W. Vogel. Inseparability Criteria for Continuous Bipartite Quantum States. *Physical Review Letters*, 95(23):230502, 2005.

[142] E. V. Shchukin and W. Vogel. Nonclassical Moments and their Measurement. *Physical Review A*, 72(4):043808, 2005.

[143] R. Simon. Peres-Horodecki Separability Criterion for Continuous Variable Systems. *Physical Review Letters*, 84(12):2726–2729, 2000.

[144] R. Simon, E. C. G. Sudarshan, and N. Mukunda. Gaussian-Wigner distributions in quantum mechanics and optics. *Physical Review A*, 36(8):3868–3880, October 1987.

[145] S. Slussarenko and G. J. Pryde. Photonic quantum information processing: A concise review. *Applied Physics Reviews*, 6:041303, 2019.

[146] J. Sperling, M. Bohmann, W. Vogel, G. Harder, B. Brecht, V. Ansari, and C. Silberhorn. Uncovering Quantum Correlations with Time-Multiplexed Click Detection. *Physical Review Letters*, 115(2):023601, 2015.

[147] J. Sperling and W. Vogel. Convex ordering and quantification of quantumness. *Physica Scripta*, 90(7):074024, 2015.

[148] H. Strobel, W. Muessel, D. Linnemann, T. Zibold, D. B. Hume, L. Pezzè, A. Smerzi, and M. K. Oberthaler. Fisher information and entanglement of non-Gaussian spin states. *Science*, 345(6195):424–427, 2014.

[149] E. C. G. Sudarshan. Equivalence of Semiclassical and Quantum Mechanical Descriptions of Statistical Light Beams. *Physical Review Letters*, 10(7):277–279, 1963.

[150] D. S. Tasca, Ł Rudnicki, R. M. Gomes, F. Toscano, and S. P. Walborn. Reliable Entanglement Detection under Coarse-Grained Measurements. *Physical Review Letters*, 110(21):210502, 2013.

[151] U. M. Titulaer and R. J. Glauber. Correlation Functions for Coherent Fields. *Physical Review*, 140(3B):B676–B682, 1965.

[152] Z. Van Herstraeten and N. J. Cerf. Quantum Wigner entropy. *Physical Review A*, 104(4):042211, 2021.

[153] K. Vogel and H. Risken. Determination of quasiprobability distributions in terms of probability distributions for the rotated quadrature phase. *Physical Review A*, 40(5):2847–2849, 1989.

[154] J. von Neumann. *Mathematical Foundations of Quantum Mechanics*. Springer, 1932.

[155] S. P. Walborn, A. Salles, R. M. Gomes, F. Toscano, and P. H. Souto Ribeiro. Revealing Hidden Einstein-Podolsky-Rosen Nonlocality. *Physical Review Letters*, 106(13):130402, 2011.

[156] S. P. Walborn, B. G. Taketani, A. Salles, F. Toscano, and R. L. de Matos Filho. Entropic Entanglement Criteria for Continuous Variables. *Physical Review Letters*, 103(16):160505, 2009.

[157] D.F. Walls and G. J. Milburn. *Quantum Optics*. Springer Berlin Heidelberg, 2008.

[158] M. Walschaers. Non-Gaussian Quantum States and Where to Find Them. *PRX Quantum*, 2(3):030204, 2021.

[159] C. Weedbrook, S. Pirandola, R. García-Patrón, N. J. Cerf, T. C. Ralph, J. H. Shapiro, and S. Lloyd. Gaussian quantum information. *Reviews of Modern Physics*, 84(2):621–669, 2012.

[160] R. F. Werner and M. M. Wolf. Bound Entangled Gaussian States. *Physical Review Letters*, 86(16):3658–3661, 2001.

[161] E. Wigner. On the Quantum Correction For Thermodynamic Equilibrium. *Physical Review*, 40(5):749–759, 1932.

[162] B. Yadin, F. C. Binder, J. Thompson, V. Narasimhachar, M. Gu, and M. S. Kim. Operational Resource Theory of Continuous-Variable Nonclassicality. *Physical Review X*, 8(4):041038, 2018.

[163] B. Yadin and V. Vedral. General framework for quantum macroscopicity in terms of coherence. *Physical Review A*, 93(2):022122, 2016.

[164] C. Zhang, S. Yu, Q. Chen, and C. H. Oh. Detecting and Estimating Continuous-Variable Entanglement by Local Orthogonal Observables. *Physical Review Letters*, 111(19):190501, 2013.